Trapped Modes of the Helmholtz Equation

A thesis presented for the degree of

Doctor of Philosophy of Imperial College

by

Cristina Vasilica Sargent

Department of Mathematics

Imperial College

180 Queen's Gate, London SW7 2BZ

20TH FEBRUARY 2013

I certify that this thesis, and the research to which it refers, are the product of my own work, and that any ideas or quotations from the work of other people, published or otherwise, are fully acknowledged in accordance with the standard referencing practices of the discipline.

Signed:

Copyright

To Elena, Cristofor, Tanti, Nenea and Howard.

Abstract

In the framework of the classical theory of linearised water waves in unbounded domains, trapped modes consist of non-propagating, localised oscillation modes of finite energy occurring at some well-defined frequency and which, in the absence of dissipation, persist in time even in the absence of external forcing.

Jones (1953) proved the existence of trapped modes for problems governed by the Helmholtz equation in semi-infinite domains. Trapped modes have been studied in quantum mechanics, elasticity and acoustics and are known, depending on the context, as bound states, acoustic resonances, Rayleigh-Bloch waves, sloshing modes and motion trapped modes.

We consider trapped modes in two dimensional infinite waveguides with either Neumann or Dirichlet boundary conditions. Such problems arise when considering obstacles in acoustic waveguides or bound states in quantum wires for example. The mathematical model is a boundary value problem for the Helmholtz equation. Under the usual assumptions of potential theory, the solution is written in terms of a boundary integral equation. We develop a Boundary Element Method (BEM) program which we use to obtain approximate numerical solutions. We extend existing results by identifying additional trapped modes for geometries already studied and investigate new structures. We also carry out a detailed investigation of trapped modes, using the planewave spectrum representation developed for various characteristic problems from the classical theories of radiation, diffraction and propagation. We use simple planewaves travelling in diverse directions to build a more elaborate solution, which satisfies certain conditions required for a trapped mode. Our approach is fairly flexible so that the general procedure is independent of the shape of the trapping obstacle and could be adapted to other geometries. We apply this method to

the case of a disc on the centreline of an infinite Dirichlet acoustic waveguide and obtain a simple mathematical approximation of a trapped mode, which satisfies a set of criteria characteristic of trapped modes. Asymptotically, the solution obtained is similar to a nearly trapped mode, which is a perturbation of a genuine trapped mode.

Acknowledgements

Firstly, I would like to thank my supervisor, Professor Jonathan Mestel for the support, direction and insight he has given me over the past four years.

This work was funded by the Engineering and Physical Sciences Research Council and the Defence Science and Technology Laboratory, and I thank Dr Duncan Williams of Dstl for his involvement in the project.

I thank my friends and colleagues from the mathematics department, especially Florencia, Sophie and Ani, for providing such a stimulating environment in which to work, and for making the last four years so much fun.

Finally, I would like to thank Professor Jeroen Lamb for his support, encouragement, advice, and belief in me.

Cristina Vasilica Sargent

Contents

List of Tables

List of Figures

Chapter 1

Introduction

Within the framework of classical wave theory, trapped modes are time-harmonic oscillations at some well-defined frequency, localised to the vicinity of a boundary or trapping structure in unbounded domains, and decaying exponentially with distance away from the trapping feature.

In 1951 Ursell showed that a water-wave system bounded by a surface of infinite extent, may have decaying eigenmodes corresponding to point eigenvalues embedded in the continuous spectrum of propagating modes [73]. Ursell constructed two trapped modes: (1) a mode on a sloping beach in a semi-infinite canal and (2) a mode near a submerged circular cylinder in an infinite canal of finite width. In a subsequent study Jones (1953), using the theory of unbounded operators, investigated the spectrum of the Laplacian and established that semi-infinite domains which are cylindrical at infinity have a continuous spectrum with a discrete spectrum embedded in it [37]. Jones' work established the Helmholtz equation, with suitable boundary conditions as a mathematical model for the study of trapped modes. This formulation applies to the trapped modes studied in this thesis. Similar confinement properties were predicted for the solutions of analogous acoustic or electromagnetic problems. He also investigated cases where trapped modes occur in surface wave problems, governed by the Laplace's equation plus certain boundary conditions. Thus the two main governing equations for the study of trapped modes were established. Lately however, new mathematical models for this topic have emerged, to account for the diversity of contexts in which they are studied. For example (Maksimov 2006) uses the linear Navier-Cauchy

equation, which models the vectorial vibrations in elastic plates, to reveal the bound states appearing in X, T and L-shaped elastic waveguides [46].

Over the past 60 years the study of trapped modes has intensified and diversified. Depending on the context, trapped modes are known as acoustic resonances, Rayleigh-Bloch waves, edge waves, array guided surface waves, sloshing modes, motion trapped modes and bound states. There is an immense amount of literature on trapped mode problems, covering analytical, numerical and physical aspects to which it is hard to do justice. We mention here a few trends, results and relevant topics, with our list of references being far from exhaustive.

1.1 Non-uniqueness of solutions

For a specified geometry, uniqueness of the solution to a forcing problem at a particular frequency is equivalent to the non-existence of a trapped mode at that frequency. A trapped mode is a solution of the corresponding homogeneous problem and represents a free oscillation with finite energy (see section 1.2) of the fluid surrounding the fixed structure. For a given structure, trapped modes may exist only at discrete frequencies. Mathematically, a trapped mode corresponds to an eigenvalue of the relevant operator but not all eigenvalues give rise to trapped mode solutions. Principally, a condition preventing any dissipation of energy in the far field, must be satisfied by an eigenfunction to be a trapped mode solution.

The uniqueness of solutions in the frequency-domain to the scattering and radiation problems has been a subject of research since at least the early 1950's (uniqueness at a particular frequency is equivalent to the absence of trapped modes). In 1950 John [36] established uniqueness for a particular class of single, surface-piercing bodies, which have the property that any vertical line emanating from the free surface does not intersect the body and Ursell (1950) proved uniqueness for a circular cylinder submerged in fluid of infinite depth [72]. Since then many other partial results have been obtained (see, for example, Simon and Ursell 1984 [68]). A detailed review of the literature is provided by Kuznetsov *et al.* [39] and by Linton & McIver [43]. Despite a growing number of results, a general proof of uniqueness for all bodies at all frequencies was not found. The reason for the absence of a general uniqueness proof became clear when M. McIver (1996), showed how to construct an explicit example of two surface-piercing bodies for which the potential is non-unique at a specific frequency [49]. Hence there can be no general uniqueness proof because trapped

modes can be constructed for given structures meaning that non-trivial solutions of the homogeneous problem exist for particular frequencies.

1.2 Finite energy

Ursell (1951) established the correspondence between the finite energy of a trapped mode and the type of eigenvalue which gives rise to it [73]. If a fluid is bounded by fixed surfaces and by a free surface of finite extent on which the pressure is constant, there is an enumerable infinity (or discrete spectrum) of characteristic modes. But if the free surface extends to infinity, the modes of vibration will be expected to form a continuous spectrum, with an infinite amount of energy in each mode. As an illustration, consider the zeroth order Bessel equation

$$\frac{d^2y}{dx^2} + \frac{1}{x}\frac{dy}{dx} + \lambda^2 y = 0 \tag{1.1}$$

where the solution has to be bounded and to vanish at $x = L$. When L is finite, an eigenmode is $y = J_0(\lambda x)$ where λ is a root of $J_0(\lambda L) = 0$. But when L is infinite, every positive value of λ^2 is an eigenvalue and the energy $\int_0^\infty x[J_0'(\lambda x)]^2 dx$ is infinite. These eigenvalues form a non-countable set, a complete, continuous spectrum. But, as Ursell points out [73], if there are also modes of oscillation with finite total energy, i.e. with amplitude falling rapidly to zero, the previous modes, with infinite energy, do not by themselves form a complete set. Any motion possessing finite total energy may then be expanded in an integral over the infinite modes (continuous spectrum), together with a sum over the modes of finite energy (discrete spectrum). An analogue of the Riemann-Lebesgue lemma, applied to the time and space dependent solutions, shows that at any point the energy in the continuous spectrum is ultimately transferred to infinity whereas the energy in the discrete spectrum remains trapped near the origin. Ursell presented two problems from the theory of surface waves with a discrete as well as a continuous spectrum. The first is that of an infinite sloping beach and the second describes motion round a submerged circular cylinder with the axis normal to the walls of a deep tank. Hence he showed that if the free surface extends to infinity in some direction there may be eigenmodes with finite total energy as well as modes with infinite total energy. The eigenmodes corresponding to frequencies in the point spectrum retain their energy whereas the latter radiate towards infinity.

More details on the notion of embedded eigenvalues are given in Chapter 2.

1.3 Classes of trapped modes

The classification of trapped modes is not straightforward as they depend on the governing equations, type of eigenvalue, propagation medium, geometry and symmetries. We now present a brief synopsis of trapped modes in waveguides and periodic media, governed by the 2-D Helmholtz equation. We also include a brief section on trapped modes in water waves, governed by the Laplace equation. This classification is not definitive as some water waves problems are governed by the Helmholtz equation. For example the mathematical formulation for an infinite array of vertical cylinders in water waves is similar to that for one cylinder in a waveguide, with appropriate boundary conditions, and this is a classical trapped mode problem governed by the reduced wave equation.

1.3.1 Waveguides

In an important paper by Jones (1953) the spectrum of the Laplacian is investigated when the boundary conditions are given on surfaces which extend to infinity [37]. Infinite or semi-infinite waveguides have a continuous spectrum with a discrete spectrum embedded in it. Jones' work proved the existence of trapped modes for problems governed by the Helmholtz equation in infinite waveguides, indicating that such bound states could occur in other contexts, e.g. acoustics and electromagnetic waves. Details of the governing equations and boundary conditions, for the trapped mode problem in acoustic, water-wave and quantum waveguides are included in Chapter 2.

A class of geometries frequently studied is that of waveguides with simple geometric indentations or protrusions out of the waveguide walls. Such configurations permit decomposition into subdomains on which the eigenfunctions of the relevant operator are known and connection formulae between regions are used to determine the trapped mode frequencies. In this manner Evans & Linton (1991) identified the modes trapped in a guide containing a symmetrically placed rectangular rigid block extending throughout the water depth [21]. The modes, which are antisymmetric about the centreline of the guide, may be either symmetric or antisymmetric about a line through the middle of the block perpendicular to the channel walls.

Another area of research receiving interest recently is that of Neumann and Dirichlet waveguides with a smooth arbitrarily shaped cross-section and a single slowly varying distention. Using WKBJ theory, Biggs (2012) derived an approximate expression for the oscillating and evanescent modes which can be present in the guide. Using established results in perturbation theory, a turning point is found in the geometry such that the solution is oscillatory in the enlarged part of the guide and decaying towards infinity. Asymptotic expansions in the two regions are matched and a uniform expansion in Airy functions is determined for the trapped modes [6]. Gaulter & Biggs (2012) extended this scheme to three-dimensional waveguides with arbitrary cross-section, again with either sound soft or sound hard boundary conditions. Countably many trapped modes, symmetric and antisymmetric and increasing in number with the distention amplitude, are computed for guides with circular and elliptic cross-sections [7].

Waveguides with one or more obstacles of various shapes, placed either symmetrically with respect to the centreline or off-centre, have been studied in various contexts as the problem has been shown to have some important applications. The configuration is equivalent mathematically to that of an infinite array of vertical cylinders. It was discovered that finite counterpart structures may exhibit 'nearly' trapped modes, which consist of large amplitude oscillations that appear at frequencies near those of trapped modes - see section 1.3.1.2.

The existence of a trapped mode in an infinitely long Neumann acoustic waveguide containing an obstacle of a fairly general shape, symmetric about the centreline was proved by Evans *et al.* [22]. The proof makes use of the Rayleigh quotient idea to characterise the lowest eigenvalue of the Laplacian on an infinite domain. Calculations of associated eigenvalues for embedded and non-embedded trapped modes for one or more circular obstacles followed. Callan *et al* (1991) established that a non-embedded trapped mode, antisymmetric with respect to the centreline, is supported by a circular obstacle of any radius, placed on the centre of a Neumann guide [10]. Above the first cut-off only one such mode exists for a precise ratio of the radius of the obstacle to the guide width. Please note that the definition and a detailed discussion on the notion of cut-off frequency are included in Chapter 2, section 2.2. The geometry and associated frequencies are discussed in detail in this thesis in Chapter 4. We reproduce these results, using our numerical method, and find that as the disc radius approaches the width of the guide two modes exist, the second is antisymmetric

with respect to both axes of symmetry of the guide - see Chapter 4, section (4.2.1.3). For the Dirichlet problem (soft walls) a non-embedded mode, antisymmetric with respect to the guide centreline, can be found for circular obstacles with radii such that the ratio between the disc and half the waveguide width is less than 0.6788. In contrast, between the first and the second cut-off, only one embedded mode exists for a particular frequency and disc radius. These embedded modes are unstable in that varying only one parameter destroys them. It was shown by McIver (2001) that embedded modes do not exist for arbitrary symmetric bodies but if an obstacle is defined by two geometrical parameters then branches of trapped modes may be obtained by varying both of these parameters simultaneously [51]. A family of embedded trapped modes was computed for ellipses of varying aspect ratio and size, placed on the centreline of a Neumann waveguide. Thus the circle is just one point on a continuous curve of shapes which support embedded modes, ranging from a plate laying on the centreline of the guide to a plate perpendicular to the guide walls. Evans and Porter (1997) extended these results to include any number of cylinders symmetrically placed on the centreplane of a channel and established that there are at most N non-embedded trapped modes for any configuration of N cylinders, the precise number depending critically on the geometry. We extend this result by establishing the behaviour of the modes for two discs of either equal or different radius as they progressively approach and intersect each other, up to the point where they are concentric. We also investigate the existence of embedded trapped modes for two similar cylinders and find that by varying the separation distance, a mode can be found for obstacles of continuous radius below a certain limit, depending on the boundary condition on the waveguide walls.

For symmetric perturbations many authors employed the general same strategy: if the essential spectrum of the operator is bounded away from zero, say $[k_c^2, \infty)$ then the search for point eigenvalues is carried out in the interval $(0, k_c^2)$. If the essential spectrum is $[0, \infty)$ then the problem is decomposed into a symmetric and antisymmetric part and the latter will have $[k_a^2, \infty)$ as its essential spectrum for some k_a specific for the antisymmetric problem. A simple variation principle applied to the linear operator in question means that any solutions found for the antisymmetric problem below the first cut-off are also valid for the whole problem.

This strategy is not applicable to cases without symmetry about the centre line of the guide. Linton *et al.* [51] using a variety of techniques (variational methods, boundary integral

equations, slender-body theory, modified residue calculus theory) established a host of results for two dimensional Dirichlet and Neumann waveguides, with one obstacle placed asymmetrically with respect to the centreline. For the Dirichlet problem below the first cut-off a geometric condition is derived to predict whether it is likely for an obstacle to support a trapped mode. In general, the closer a body is to the centreline, the less likely it is for a trapped mode to exist. An exception to this is a thin plate aligned with the guide walls for which modes exist for any offset greater than zero. Trapped modes are also possible for the Dirichlet problem between the first and second cut-offs and for the Neumann problem below the first cut-off. For the Neumann problem between the first and second cut-offs the problem is solved for a thin plate aligned with the guide walls and it is shown that modes exist for discrete pairs of the two parameters which define the geometry (the size and the position of the plate). Another notable rigorous treatment for this class of geometries is that of Davies & Parnovski [17]. The authors established general results for existence and non-existence of embedded eigenvalues for a pair of identical obstacles of general shape, reflections of each other and located symmetrically with respect to the guide centreline.

In this thesis we consider some cases without symmetry with respect to the centreline of the guide. We investigate the existence of embedded and non-embedded trapped modes in Dirichlet and Neumann waveguides with rectangular and smooth cavities. In addition we consider these configurations with a circular obstacle placed in the centre and off the centre of the guide. The cases are presented in detail in Chapter 5 and full numerical results are given in Appendix B.

The waves described by the Helmholtz equation subject to Dirichlet boundary conditions apply to analogous electromagnetic problems. Following Ursell's important article [73], in 1965 Weinstein reported resonant modes in open laser systems [74] and the question of bound states in special quantum waveguides was raised by Sakaki in 1984 [65]. The mathematical setup is equivalent to that of electrons in open configurations described by the steady Schrodinger equation and these studies suggested that confinement is also a feature of the two-dimensional transport of charge carriers in ultra-fine metal and semiconductor devices [11]. The study of bound states in quantum guides is in general linked to any local enlargement in a smooth waveguide. The simplest waveguide that supports a bound state is a curved waveguide. Exner and Seba (1987) established that for a free quantum particle on a curved planar strip with Dirichlet boundary conditions, bound states,

with energy below the first transversal mode, exist for sufficiently fast decaying curvatures of the guide [29]. Goldstone and Jaffe [32] proved that at least one bound state exists for all twisted two-dimensional tubes, subject to Dirichlet boundary conditions, except in waveguides of constant curvature, which have no bound states. A series of theoretical and experimental studies followed for more complicated structures showing that generally, by bending and crossing waveguides and quantum wires, bound states can be obtained with energies below the continuous spectrum. Bound states were found in the cross-terminal structure (the X-shaped waveguide) by Schult *et al.* [66] and in the T and L-shaped waveguide by Lin *et al.* [40] and Maksimov [46]. Amore *et al.* [3] considered the behaviour of bound states in asymmetric cross, T- and L-shaped configurations. For different values of the ratio of the widths Amore *et al.* proved the existence, or non-existence under certain conditions, of bound states in each symmetry class. Moreover, many similar quantum wire systems have been found with bound states embedded in the continuous spectrum [8]. A full mathematical treatment of the spectra of open quantum waveguides is contained in chapter 16 of the book by Blank *et al.* [8]. Also recently Linton & Ratcliffe (2003) using a mode-matching technique computed the bound-state energies in two and three-dimensional coupled waveguides [45], [44]. A number of computed examples (using the method of particular solutions) of eigenmodes of L- and zig-zag shaped finite and infinite plates are presented together with a discussion of their implication concerning bound and continuum states, symmetry and resonances by Trefethen & Betcke [71].

1.3.1.1 Empirical /Observed trapped modes

Trapped modes are ubiquitous in nature, appearing in oscillating systems at mesoscopic scale in quantum waveguides, at macroscopic scale in built systems and at planetary scale in oceans and continental shelves. They have even been reported on astrophysical scale where for example trapped oscillating modes of pulsating white dwarf stars (pure hydrogen atmosphere) correspond to certain eigenvalues of the frequency spectrum [75], [57]. We present now a few specific examples of trapped modes experiments together with relevant references.

Acoustic resonances are observed in axial flow compressors and this has led to many detailed investigations into the conditions for their existence. In particular, Parker [59] observed such resonances experimentally, in two-dimensional (2D) channels that contain ar-

rays of parallel plates - see section 1.3.2. Careful experiments by C. H. Retzler* have confirmed the predicted trapped mode frequencies of Callan *et al.* [10] for three different-sized circular cylinders. Field observations of edge waves have been reported by Huntley & Bowen [34]. Trapped modes played an important role in the impedance budget of the Large Hadron Collider (LHC) [12]. Casper (1995) showed that they occur very close to the waveguide cutoff frequency of the LHC liner and are linked to the perforations in the tube.

Cobelli *et al.* [16] carried out an experiment which provides evidence for the occurrence the trapped modes around a vertical surface-piercing circular cylinder of radius a placed symmetrically between the parallel walls of a long but finite water waveguide of width $2d$. A wavemaker placed obliquely near the entrance of the waveguide was used to force an asymmetric perturbation into the guide, and the free-surface deformation field was measured using a global single-shot optical profilometric technique. Using the optical profilometric technique the authors were able to measure the space-time evolution of the free-surface deformation within the guide. A series of measurements showing the time evolution of the free surface deformation, for the aspect ratio $a/d = 0.5$ is shown in Fig. 1.1. A harmonic decomposition in terms of the driving angular frequency $\omega = 2\pi f$ of the surface deformation, allowed the dominant linear contribution to be isolated from the higher order time harmonics (the nonlinear part of the free surface deformation). The $f = 2.5$Hz is the incident wave frequency and it corresponds to an angular frequency $\omega = 15.7080$ rad/s. Further separation of the free-surface linear deformation into symmetric and antisymmetric parts with respect to the centerplane of the channel, led to the recovery of the detailed structure of the trapped mode. An example showing the first linear deformation field and its decomposition into even and odd parts is shown in Fig. 1.2. For each of the aspect ratios considered, the spatial structure of the trapped mode was obtained and compared to the theoretical predictions of Callan *et al.* [10] by the multipole expansion method.

At least one trapped mode was observed for each aspect ratio a/d below the first cut-off (of the antisymmetric problem). A second trapped mode was found for radii $a/d = 0.85, 0.90$ and 0.95, a result which is also consistent with our findings for this case, see section 4.2.1.3.

*Private communication (1996) to D. V. Evans [26]

Figure 1.1: Cobelli *et. al.* [16] Experimental measurements of the instantaneous total free-surface deformation fields. The figure shows a time-sequence of the evolution of the free surface deformation fields for a particular case of the aspect ratio explored, namely $a/d = 0.5$. The incident wave frequency is $f = 2.5$Hz. Frames are separated by $\Delta t = 0.04$s.

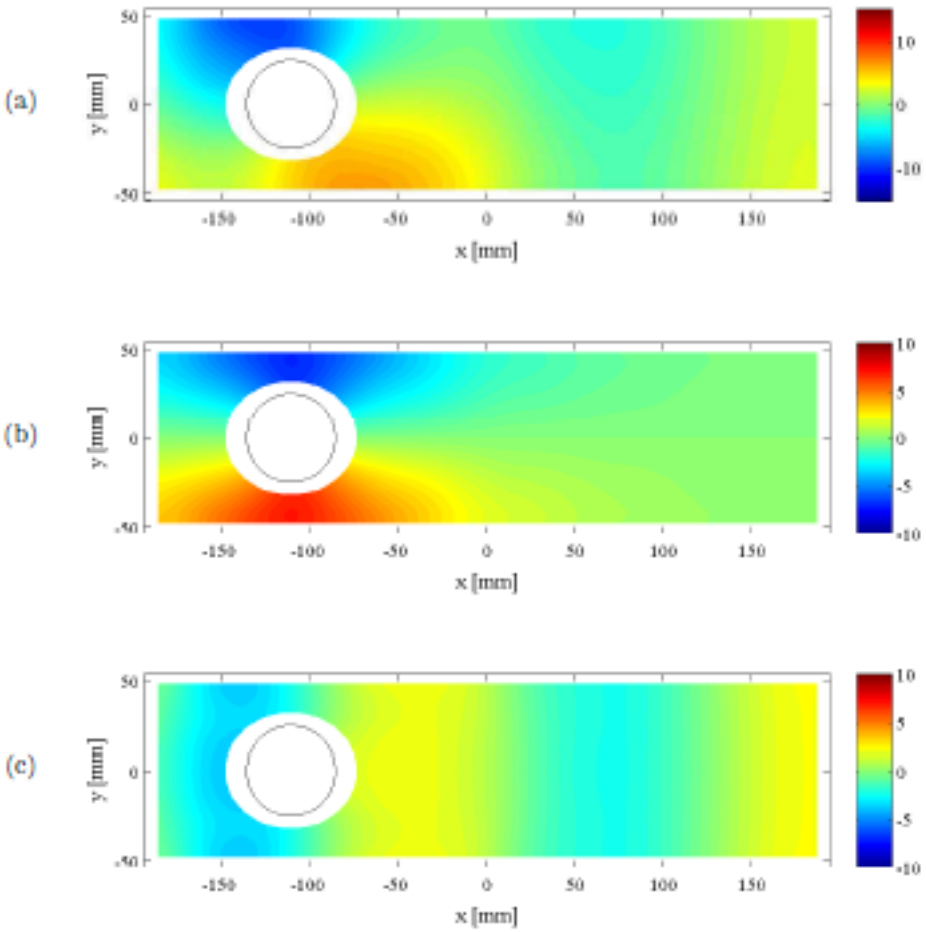

Figure 1.2: [16]Linear part of the experimentally measured free-surface deformation for $a/d = 0.5$. Panel (a) shows the linear deformation field . Panels (b) and (c) show the symmetric and antisymmetric parts of the linear mode respectively. The position of the obstacle within the waveguide is indicated by the black circle.

1.3.1.2 Nearly trapped modes

A related and relevant topic is that of nearly trapped modes, which are resonances with very small radiation. Trapped modes are characterised by zero radiation. Nearly trapped modes become important especially when considering the real implications of trapped modes. They are generally perturbations of trapped modes and there are two main ways in which they appear in this problem.

Firstly, some of the geometric specification for trapped modes may be idealised and not likely to occur in physical situations. For example, an infinite or doubly infinite periodic array of vertical cylinders is known to support pure trapped waves. In finite arrays near-

trapping occurs in the form of large resonances which appear at the incident wave frequency which corresponds to the trapped mode frequency for the infinite array [24]. Predicting near-trapping is important as this phenomenon arises because of the existence of standing waves trapped between cylinders whose energy leaks away to infinity but critically more slowly than it is being supplied. Maniar and Newman calculated the distribution of forces along a finite array of 100 cylinders at the 'near-trapping' frequency and shown that the force on the middle cylinder is approximately 34 times higher than that on an isolated cylinder [47]. This is obviously relevant to the wave forces on the supporting columns of an offshore platform and undoubtedly to other industrial applications governed by the Helmholtz equation in a domain exterior to a periodic array of obstacles.

Nearly trapped modes also appear consistently throughout our numerical and analytical investigations. We found that in general the specific set of parameters which corresponds to an embedded trapped mode is a discrete point in a small continuous band of parameters which all support nearly trapped modes. What this means is that a geometry which approximates that required for a trapped mode will give rise to a nearly trapped mode, which in a physical system might be indistinguishable from an exact resonant mode. We refer to Table 4.3 in Chapter 4 for the problem of a Neumann waveguide with a sound-hard disc and a rectangular cavity of varying width w and depth h. The energy dissipation calculated for a range of h and w sharply decreases as it approaches the geometric parameters required for the formation of a trapped mode but we can see that slightly perturbed configurations have low radiation loss, corresponding to a nearly trapped mode.

We also find that in embedded regimes, there are some configurations which only support nearly trapped modes and despite intense investigation we are not able to identify a set of parameters providing a purely trapped mode.

1.3.2 Periodic structures

Acoustic resonances were observed in axial flow compressors and this has led to many detailed investigations into the conditions for their existence. In particular, Parker [59] observed such resonances experimentally, in two-dimensional (2D) channels that contain arrays of parallel plates. He subsequently made numerical calculations of the frequencies of the oscillations [60] and this has led to them being referred to as Parker modes. Over the next two decades, he and several of his co-workers made both theoretical and experimental

investigations into the types of resonances that can exist and a review of the work in this area is given by Parker and Stoneman [61]. Many more examples have been studied since then, using both analytical and numerical techniques. Acoustic resonances are also found when quasi-periodic boundary conditions are applied on the channel walls. In this case, they are known as Rayleigh - Bloch waves and represent waves that propagate along, and are confined to the vicinity of, an infinite, periodic array of rigid structures. If the grating has periodicity $2d$ (in the y-direction, for example) we can search for a quasi-periodic solution ϕ which satisfies

$$\phi(x, y + 2md) = e^{2im\beta d}\phi(x, y), \tag{1.2}$$

for some $m \in \mathbb{Z}$ and some real parameter β (the propagation or Bloch constant). For a given β we can search for values of k for which the solution decays to zero as $|x| \to \infty$. Standard techniques are used to search for Rayleigh-Bloch modes below this cut-off and Porter and Evans (1999) discovered such surface waves along a variety of periodic structures [25]. Just as for the waveguide problem, for each given k there are a number of possible propagating modes in the region, away from the array, and increasing by one every time one of the cut-off lines) $k = m\pi/d \pm \beta$ is crossed. See section 2.2 for a discussion on the notion of cut-off frequencies. The existence of embedded modes, in which $\beta < k < \pi/d - \beta$, has been established by Porter and Evans for comb-like gratings [27] and for arrays of rectangular blocks [28], the former being a special case of the latter. More theoretical investigations into the conditions under which such modes exist for arrays of structures have been made by Evans [20], Bonnet-Bendhia and Starling [5], Linton and McIver [41] and McIver [50].

1.3.3 Water waves

The modes in this case are the result of interaction of water waves with a structure that is either fixed or free to move within a fluid that extends to infinity in at least one horizontal direction. The problem considered is the linearised frequency domain problem with the implied $e^{-i\omega t}$ dependence. In this context trapped modes correspond to solutions for the velocity potential ϕ of the Laplace equation $\nabla^2\phi = 0$ subject to appropriate boundary conditions on the surface of the trapping structure and the sea bed, a radiation condition that requires that any disturbance created by the structure must propagate outwards and the

linearised condition

$$\frac{\partial \phi}{\partial z} = K\phi \tag{1.3}$$

on the undisturbed free surface [43], [52]. Here z is the vertical coordinate and $K = \omega^2/g$. The main mathematical distinction between the water-wave and the waveguide problem is that the eigenvalue parameter K appears in the boundary condition (1.3) rather than the field equation. The first example of decaying solutions to this problem was discovered by Stokes [70] and consists of waves which are periodic in one direction, travel in the long-shore direction over a uniformly sloping beach and decay to zero in the seaward direction. Such trapped modes are called edge waves and they have been the subject of intense research over the past 50 years. A discussion of mathematical results obtained for edge waves, modes trapped by submerged obstacles and surface piercing structures, is provided by Kuznetsov *et al.* [39] and a review by Linton & McIver [43].

In the last fifteen years, the study of trapped modes has developed and diversified widely. For more information regarding recent developments in the study of trapped modes, we refer to the comprehensive review given by Linton & McIver [43]. Other notable trapped modes results from various domains of physics, such as quantum mechanics, elasticity, acoustics are those of Zernov *et al.* [76], Pagneux [58] and Postnova & Craster (2008) [63].

1.3.4 Elastic plates

A well known example of an elastic trapped mode is the so-called edge resonance, when the elastic energy is localized near the edge of a semi-infinite stress-free plate. The phenomenon was first observed by Shaw (1956) in his experiments on vibration of circular discs [67]. When excited at a particular frequency, vibration tended to localize near the disc edge. However, the observed vibration frequency lay below the first cut-off frequency of the corresponding infinite layer and could not therefore be related to thickness vibration modes [38]. A first explanation was provided by Mindlin & Onoe in 1957 [54]. They noted that at every particular frequency, in addition to a finite number of propagating Rayleigh - Lamb modes (modes along a solid plate, constrained by the elastic properties of the surface that guide them), an unbounded plate possesses an infinite family of non-propagating

modes associated with complex wavenumbers. These exponentially decaying modes form an infinite system of standing waves, which can be used to satisfy the boundary conditions at the edge of a semi-infinite plate. It has recently been shown that trapped modes exist in elastic waveguides that have either curvature or width variations [33], [38] and [62].

The solution for the elastic problem in 2-D waveguides, the displacement field, is presented in terms of two scalar potentials that completely determine the displacement components. Each of these potentials satisfies the Helmholtz equations.

1.4 Overview of thesis

The literature on trapped modes is extensive, however establishing whether a given arbitrary geometry can support trapped modes is extremely difficult and requires a large suite of mathematical methods. The aim of this research is to develop a flexible, accurate and reliable method of investigating trapped modes for complex configurations.

In this thesis we study a few examples of trapped modes of the Helmholtz equation in waveguides, with either Dirichlet or Neumann boundary conditions. The trapping features are either cavities, smooth or rectangular, sound hard circular obstacles on the centre of the guide or a combination of both.

In Chapter One - Introduction, trapped modes as a physical phenomenon and as a mathematical object are introduced. The development of the mathematical context and of associated notions, including non-uniqueness and the energy associated with this type of solution are presented, in a quasi-chronological manner. A brief review of the main classes of trapped modes, areas of research and relevant results is given in an attempt to cover some main points without being exhaustive.

In Chapter Two, details of the governing equations and associated notions relevant to the study of trapped modes, cut off frequencies and embedded eigenvalues of the problem, are presented.

In Chapter Three, the mathematical model used and adapted for this problem is discussed. Under the usual assumptions of potential theory, the solution is derived in terms of a boundary integral equation. We also present the Boundary Element Method (BEM) written in Matlab, in order to obtain approximate numerical solutions. The program identifies the

eigenmodes which depend on a finite set of parameters including wave frequency and the domain configuration.

In Chapter Four, to validate our approach and test the accuracy of the program, test cases are considered and compared with known analytical solutions obtained by other authors using different methods (modified multipole potentials, finite element and perfectly matched layer methods). We present details of five such cases alongside with published results.

In Chapter Five, additional trapped modes found using our BEM program are presented in detail. The findings extend results for some geometries already studied, for higher frequency bands, and for more complex, new configurations.

In Chapter Six, guided by the numerical results obtained we carry out a detailed investigation of one set of results (antisymmetric modes in Dirichlet waveguide with a sound hard disc on the centreline) and discuss characteristics which are common to all the modes. We superpose simple planewaves travelling in diverse directions to build a more elaborate approximate solution, which satisfies certain conditions required for a trapped mode. Our approach is fairly flexible so that the general procedure is independent of the shape of the trapping obstacle and could be adapted to other geometries. We apply this method to the case of a disc on the centreline of an infinite Dirichlet acoustic waveguide and obtain a simple mathematical approximation of a mode which satisfies a set of criteria which is also satisfied by the corresponding trapped mode. Asymptotically, the solution obtained is similar to a nearly trapped mode, which is a perturbation of a genuine trapped mode.

Finally, in Chapter Seven the main results of the thesis are summarised annd discussed and proposed extensions to the research are described. We also included a short discussion on practical applications of trapped modes.

Appendix A and B contain details of trapped modes for two identical discs and for two disc of different radii, placed on the centreline of either a Dirichlet or Neumann waveguide.

Appendix C presents mathematical details of solving the disc integral derived in Chapter 6.

Appendix D contains the mathematical details of approximating the waveguide integral derived in Chapter 6.

Appendix E contains the code for the BEM program used to identify trapped mode in an

infinite Dirichlet acoustic waveguide with a rectangular cavity and a sound hard disc on its centre.

Chapter 2

Basic Concepts

2.1 Formulation of the problem for infinite waveguides

Throughout the thesis we will refer to the trapped mode problem in terms of spectral terminology applied to acoustic problems, but a comparison can be made with associated trapped mode problems in water-waves and in quantum waveguides.

The domain is an infinite waveguide, W, consisting of a pair of two-dimensional parallel walls ($\Gamma_{\pm}$), separated by a distance $2d$. The walls are at $y = \pm d$ and the guide is parallel to the x-axis. Cartesian axes are chosen so that both x and y axes coincide with the horizontal and vertical guide centerlines respectively. Depending on the case to be studied, cavities or circular obstacles will be added to the guide to act as trapping features. In those cases where one or more discs are added to the domain, the assumption is that they are sound hard discs, i.e. the Neumann condition applies on their boundaries.

2.1.1 Acoustic waveguides

We consider the propagation of acoustic waves in two dimensions, described by the linear wave equation:

$$\nabla^2 U = \frac{1}{c^2}\frac{\partial^2 U}{\partial t^2}. \tag{2.1}$$

where c is the speed of sound in still air and $U = U(\mathbf{x}, t)$ is the velocity potential. If the motion is assumed to be time-harmonic, with ω the angular frequency, the function U may

be written in the form:

$$U(\mathbf{x}, t) = \phi(\mathbf{x})e^{-i\omega t}. \tag{2.2}$$

Here ϕ is the reduced velocity potential which is only space dependent. With the elimination of the time coordinate, equation (2.1) reduces to the Helmholtz equation (2.4) and we have the dispersion relation

$$k^2 = \frac{\omega^2}{c^2}. \tag{2.3}$$

Boundary conditions on $\Gamma_\pm$ are either Neumann or Dirichlet, depending on the nature of the guide. We now write explicitly the Neumann ($\mathbb{N}$) and the Dirichlet ($\mathbb{D}$) boundary value problems for the potential $\phi(x, y)$, in acoustic context. Let D be a trapping feature placed inside the guide and bounded away from infinity with boundary ∂D. The symbol $\partial/\partial n$ refers to the directional derivative considered at a point on a boundary, along the normal vector to that surface at that point.

$$(\nabla^2 + k^2)\phi = 0 \quad \text{for} \quad (x, y) \in W \backslash D \tag{2.4}$$

$$\lim_{x \to \pm\infty} \left[\phi \mp ik\frac{\partial \phi}{\partial x}\right] = 0 \quad \text{for} \quad |y| \leq d \tag{2.5}$$

$$\frac{\partial \phi}{\partial n} = 0 \quad \text{for} \quad (x, y) \in \partial D \tag{2.6}$$

$$\text{Dirichlet problem:} \quad \phi = 0 \quad \text{for} \quad (x, y) \in \Gamma_\pm \quad \text{or} \tag{2.7}$$

$$\text{Neumann problem:} \quad \frac{\partial \phi}{\partial y} = 0 \quad \text{for} \quad (x, y) \in \Gamma_\pm \tag{2.8}$$

A number $\lambda = k^2$ is an eigenvalue of either the Dirichlet or Neumann problem if it corresponds to a non-trivial solution ϕ which satisfies either eqns. (2.4) - (2.7) or eqns. (2.4) - (2.6) and (2.8) respectively. In terms of spectral theory of operators, the eigenvalues k^2 make up the point spectrum of the problem. Potentials relating to the values of k^2 in the continuous spectrum are known as propagating modes.

The condition (2.6) is the Sommerfeld radiation condition which prohibits any incoming waves from infinity. This condition leads to the following decay condition for a trapped mode:

$$\phi \to 0 \quad \text{for} \quad |x| \to \infty, \quad |y| \leq d. \tag{2.9}$$

To show the similarity between the two expressions, (2.6) and (2.9) consider the waveguide W, bounded at infinity by the segments $y = \pm d, x = \pm L, L \to \infty$. Let ϕ_R and ϕ_I be the real and the imaginary parts of the potential ϕ respectively. Assuming that ϕ is twice continuously differentiable in W we apply Green's second identity as follows:

$$\int_W \phi_R \nabla^2 \phi_I - \phi_I \nabla^2 \phi_R \, d\mathbf{x} = \int_{\partial W} \frac{\partial \phi_I}{\partial n} \phi_R - \frac{\partial \phi_R}{\partial n} \phi_I \, ds. \tag{2.10}$$

Both the real and imaginary parts of ϕ must satisfy the Helmholtz equation hence the left side of (2.10) is zero. Given either Dirichlet or Neumann boundary conditions for a problem, the terms in the right side of (2.10) are zero on $\Gamma_\pm$. We apply (2.6) to the real and imaginary parts of ϕ and we get the following relations

$$\begin{aligned} \frac{\partial \phi_R}{\partial x} \pm k\phi_I = 0, \\ \frac{\partial \phi_I}{\partial x} \mp k\phi_R = 0, \end{aligned} \tag{2.11}$$

for a point in W at $x \to \pm\infty$ respectively. There are two remaining contributions to the integral from the boundary segments $y = \pm d, x = \pm L, L \to \infty$. Using (2.11) for each respective case, the contributions are

$$k \int_{-d}^{d} \left[\phi_R^2(x,y) + \phi_I^2(x,y)\right] dy = 0, \quad x = \pm L, L \to \infty. \tag{2.12}$$

This is possible only if $\phi_R \to 0$, $\phi_I \to 0$ as $x \to \pm\infty$, as stated in (2.9).

2.1.2 Quantum waveguides

The same set of equations can also be used to study bound states in mesoscopic semiconductor structures. In this context trapped modes are known as bound states in quantum wires or quantum waveguides [11], [29]. The narrow two dimensional quantum waveguides are composed of tiny strips of very pure semiconductor material, that allow electrons to propagate but require the wave function to vanish on the surface. If in the Schrodinger equation, describing a system with piecewise constant potential V, we denote $k^2 = 2mE/\hbar^2$, where m is the mass of an electron, E is its total energy and $\hbar$ is the reduced Planck constant, we reduce the problem to finding trapped modes of the Helmholtz

equation, subject to the Dirichlet boundary condition.

2.1.3 Water waveguides

The problems of acoustic resonances in an infinite waveguide with circular 2-D obstacles and that of trapped modes in a 3-D long narrow channel with standing cylinders are identical, from a mathematical viewpoint [43]. Under the usual assumptions of linear water-wave theory, the problem is formulated as follows: the origin is placed in the undisturbed free surface $z = 0$ midway between the parallel channel walls situated at $y = \pm d$. The $z-$ axis is measured vertically upwards with the channel bottom at $z = -h$, with h constant. Let a three-dimensional fluid flow be characterised by the fluid velocity **u** such that

$$\mathbf{u} = [u(x, y, z, t), v(x, y, z, t), w(x, y, z, t)], \tag{2.13}$$

and suppose that the fluid is irrotational, so that there exists a velocity potential $\Phi(x, y, z, t)$, which we assume has a separable depth dependence so that

$$\Phi(x, y, z, t) = Re\{\phi(x, y)f(z)e^{-i\omega t}\}, \tag{2.14}$$

The fluid motion arises from a deformation of the water surface. We denote the equation of this surface

$$z = \eta(x, t) \tag{2.15}$$

By Acheson, the linearised kinematic condition on the free surface [2] is

$$\frac{\partial \Phi}{\partial z} = \frac{\partial \eta}{\partial t} \quad \text{on} \quad z = 0. \tag{2.16}$$

Also, from the Bernoulli's linearised equation for unsteady irrotational flow, the linearised condition on the free surface [2], can be derived as

$$\frac{\partial \Phi}{\partial t} + g\eta = 0 \quad \text{on} \quad z = 0. \tag{2.17}$$

A fixed vertical cylinder is placed on the centreplane of the channel and extends uniformly throughout the depth. If we assume a travelling wave solution, the free surface is

$$\eta = Re\{\phi(x,y)e^{-i\omega t}\}, \tag{2.18}$$

where ω is the angular frequency. If the fluid is bounded by a rigid plane on the bottom of the channel so that

$$\frac{\partial \Phi}{\partial z} = 0 \quad \text{at} \quad z = -h \tag{2.19}$$

By virtue of the incompressibility equation $\nabla \cdot \mathbf{u} = 0$, Φ satisfies the Laplace's equation and this gives for $f(z)$

$$f''\phi + \nabla^2\phi f = 0, \tag{2.20}$$

Let k^2 be the separation constant for the (2.20) above. Then ϕ satisfies the Helmholtz equation (2.4). We also can write the general solution for

$$f(z) = Ce^{kz} + De^{-kz}, \tag{2.21}$$

and applying the condition on the bottom of the guide (2.19) we obtain

$$\Phi = Re\{\phi(x,y)[C(e^{kz} - e^{-k(2h+z)})]e^{-i\omega t}\}, \tag{2.22}$$

Substituting this form of Φ into (2.16) and (2.17), keeping in mind that they are valid at $z = 0$, we have

$$Ck(1 + e^{-2kh}) = -i\omega, \quad C(1 - e^{-2kh})(-i\omega) + g = 0. \tag{2.23}$$

and thus we obtain the dispersion relation for this problem

$$\omega^2 = gk\tanh(kh). \tag{2.24}$$

A similar formulation for the deep water problem results in the dispersion relation

$$\omega^2 = gk, \tag{2.25}$$

with the phase velocity

$$c^2 = \frac{g}{k}. \tag{2.26}$$

Thus we found that the time independent potential ϕ satisfies the Helmholtz equation (2.4) and the problem has again been reduced to finding those solutions which satisfy the required boundary conditions, including condition (2.9). The depth dependence has been removed and the wavenumber k is now the positive root of the dispersion relation (2.24).

Trapped modes in channels with one or more cylinders on the centreline, have already been extensively studied, [22], [10], [23], [47], [43] and references therein, using different techniques. These studies are motivated by the fact that it is possible to remove the channel walls and regard the solutions as oscillations between adjacent cylinders in an infinite row. The Neumann modes then have an antinode at each mid-plane between cylinders while the Dirichlet modes a node. It is important to predict the trapped mode frequencies in view of the fact that such periodic arrays have practical applications, for example to floating bridges, floating airports, off-shore oil platforms and other structures supported by bottom mounted cylinders [47].

2.2 Cut-off frequencies

One of the characteristic properties of waveguides is the occurrence of cut-off frequencies. Studies of trapped modes are associated with cut-off frequencies, which partition the frequency domain, depending on the number of associated travelling modes. In physics and electrical engineering, a cutoff frequency is a boundary in a system's frequency response at which energy flowing through the system is reduced (attenuated or reflected) rather than passing through. The cut-off frequency of an acoustic, or electromagnetic, waveguide is the lowest frequency which allows a mode to propagate.

In our problem cut-off values are mainly used to differentiate between two important types of trapped mode namely embedded and non-embedded, defined in section (2.3). They provide a delineation between the frequency bands to be investigated.

The cut-off frequencies for our problem are found by solving the Helmholtz equation in an unobstructed waveguide. Any exciting frequency lower than the cut-off frequency will

attenuate, rather than propagate. To illustrate this we consider the Helmholtz equation in a Dirichlet guide. If we seek y-antisymmetric solutions in an unobstructed channel, the potential ϕ should be similar to a superposition of solutions of the form:

$$\phi \approx \exp\left\{ i\left[k^2 - \left(\frac{n\pi}{d}\right)^2\right]^{\frac{1}{2}} x \right\} \sin\left(\frac{n\pi y}{d}\right) \tag{2.27}$$

where n is any positive integer. If we are looking for y-symmetric solutions we just replace $\sin(n\pi y/d)$ with $\cos[(2n-1)\pi y/2d]$.

The first cut-off for the Dirichlet anti-symmetric case is $k_1 = \pi/d > 0$, and is so defined because for k in the range $0 < k < k_1 = \frac{\pi}{d}$, the corresponding solution decays exponentially; propagation down the guide is not possible, hence any mode for this k is trapped. Subsequent cut-off frequencies, integer multiples of the first one, $k_n = n\pi/d$, $n = 1, 2\ldots$, act similarly, as barriers to all the modes with frequencies below them. On the other hand for a frequency k such that $k_1 < k < k_2$ the x component of the solution in (4.15) for $n = 1$ propagates rather than decays and we say that a travelling mode is present in that frequency range. For a given frequency k with $k \leq k_{n+1}$ there are n y-antisymmetric travelling modes present which we need to bear in mind when seeking trapped modes. For the Neumann problem, a solution of the form e^{ikx}, i.e. with $n = 0$, satisfies the boundary conditions for all values of k hence zero is the first cutoff for this case. For a given frequency $k < k_n$ there are n y-antisymmetric travelling modes. It is much more difficult to establish the existence of trapped modes in regions of parameter space which permit energy to travel away from the trapping structure.

2.3 Embedded trapped modes

In this section we discuss the notion of an *embedded eigenvalue*, which appears in the context of spectral analysis of an operator, and establish the connection with the trapped mode problem.

Trapped modes can be classified as embedded or non-embedded, depending on whether their frequency is either above or below the first cut-off respectively. It is important to distinguish between the two types as this determines the stability of the modes. The non-embedded modes are stable in the sense that if a geometric parameter is modified, the

mode persists up to some limit, with only a slight variation of the frequency. In contrast, embedded modes may only exist for a specific combination of the geometric parameters and are destroyed by an infinitesimal perturbation of the configuration. This is because they exist in regions of the k- space where travelling modes are present. Therefore for each additional propagating mode that is introduced, an extra geometric parameter is required to satisfy side conditions, which force the amplitude of these travelling modes to zero. A slight change in geometry modifies the relation between the coefficients of these modes and the resulting mode is a combination of an exponentially decaying mode and travelling modes. This means that often, a given configuration may not support any embedded modes at any frequency or there may be only a few discrete sets of geometric parameters which support such a mode.

An important physical aspect of embedded modes is that since they exist at frequencies which also support travelling modes they can be excited by appropriate external forcing. In contrast, non-embedded trapped modes can only be excited by internal, local pulsating sources as they can not be accessed via any propagating waves. Although the definition of trapped modes assumes total trapping of energy in practice some radiation occurs, but at a slower rate than it is being put into the system, and this allows for a large concentration of energy around the trapping structure. Depending on the geometry, these resonances lead to increase of forces in response of the incident wavefield which correspond to the trapped modes. For example, Neumann and Maniar (1996) analysed the pressure forces on a finite array of bottom-mounted, identical, equally spaced circular cylinders [47] and established that the force on the middle cylinder at the centre of an array of 100 cylinders is cca. 35 times larger than that on an isolated cylinder. Evans and Porter [26] showed that the peak force on an arrangement of four standing cylinders placed at the corner of a square is 54 times higher than that on an isolated cylinder, under the effect of an incoming wave at the trapped mode frequency.

Formally, an eigenvalue λ of a differential operator $\mathcal{L}$ is called an embedded eigenvalue if it is a point spectrum in the continuous spectrum of $\mathcal{L}$. A point spectrum is a complex value λ such that $\lambda I - \mathcal{L}$ does not have an inverse. The equation $(\lambda I - \mathcal{L})\mathbf{y} = 0$ then has a non trivial solution called an *eigensolution* and λ is an *eigenvalue* of $\mathcal{L}$. We shall say that a number λ is an eigenvalue of either the Dirichlet ($\mathbb{D}$) or the Neumann ($\mathbb{N}$) boundary value problems, in other words, λ belongs to the point spectrum of the problem ($\mathbb{D}$) or ($\mathbb{N}$) if for

this λ there exists a non-trivial potential ϕ which satisfies (2.4) - (2.7) or (2.4) - (2.6) and (2.8) respectively.

We will refer to the notions of point and continuous spectra *of the problem*, rather than of the operator, as defined by Evans *et al.* [22] as follows:

A point λ belongs to the continuous spectrum of the problem if for this value there exists a non-trivial potential ϕ, which satisfies the Neumann or Dirichlet condition above with the exception of $\phi \to 0$ as $|x| \to \infty$. The solution ϕ may propagate or grow algebraically, $\sim |x|^n$, $n \in \mathbb{Z}$, but not exponentially [22]. The potentials corresponding to frequencies in the continuous spectrum are eigenfunctions of the operator but not solutions of the full Dirichlet or Neumann problems. As they are propagating modes rather than trapped modes, they do not satisfy the decay condition (2.9). However, consideration of such non-decaying solutions is important for the understanding of our problems in terms of spectral theory of operators. From the physical point of view, modes corresponding to point eigenvalues neither receive from nor radiate energy to $x = \pm\infty$ whereas radiation occurs in modes corresponding to points of the continuous spectrum. From a computational perspective the distinction is important because embedded trapped modes require higher detection accuracy than non-embedded modes as an eigenvalue in the continuous spectrum of an operator disappears under very small perturbations.

The notions of embedded eigenvalues and cut-off frequencies are connected as follows: the first-cut off is the square root of the lower bound of the essential spectrum (i.e. the continuous spectrum plus any embedded eigenvalue) of the problem. If the lower bound of the continuous spectrum is not zero and if an eigenvalue of the problem can be found below the first cut-off then the corresponding trapped mode is non-embedded. All other trapped modes, corresponding to point spectrum eigenvalues, above the first cut-off, are embedded.

The continuous spectrum of the Neumann problem is the semi-interval $[0, +\infty)$ [21], [37]. If the problem is symmetric about the centreline of the guide then it can be decomposed into its symmetric and anti-symmetric parts and the latter will have $[(\pi/2d)^2, \infty)$ as its essential spectrum [22]. The Neumann problem then has an additional Dirichlet condition on the centre-plane, $\phi = 0$. With this modification the problem reduces to finding eigenvalues in the range $0 < k < \pi/2d$. This is a valid approach because if λ is an eigenvalue of the anti-symmetric problem then it is also an eigenvalue to the full problem. Also, since the

continuous spectrum of the problem occupies the entire non-negative half line $[0, \infty)$, any eigenvalues that are found are embedded in the continuous spectrum. A rigorous proof for the existence of a minimum eigenvalue for the Neumann anti-symmetric problem an infinite waveguide with an obstruction of a fairly general shape, symmetric about the centreline was provided by Evans *et al.* [22].

The first cut-off for the full Dirichlet problem, without any symmetry considerations, is $\pi/2d$. However, if the trapped modes sought are anti-symmetric about the centreline of the guide then the continuous spectrum of the problem is the semi-interval $[\pi^2, +\infty)$. Eigenvalues below this range correspond to non-embedded trapped modes. It follows that an eigenvalue λ regarded as an eigenvalue of the *full* Dirichlet or especially the Neumann boundary value problem could be seen as embedded in the continuous spectrum but when regarded as an eigenvalue of the *anti-symmetric* problem could be below the first cut-off value, hence non-embedded. This convention which places the eigenvalues outside the embedded regime, is not applicable to cases where the geometry is not symmetric about the centreline of the guide as the problem can not be decomposed into two parts, symmetric and antisymmetric.

Aslanyan *et. al* [4] showed that if the symmetry is broken then real eigenvalues transform into complex resonances of so called *leaky modes* with radiation losses. Evans *et al.* (1993) proved the existence of trapped modes for an off-centre plate of finite length placed parallel to the waveguide walls, showing that symmetry is not a necessary requirement for the existence of trapped modes [19]. Linton *et al.* (2001) considered a non-symmetric obstacle as part of an infinite array of obstacles symmetric about the sound-hard waveguide wall or antisymmetric about the soft wall and were able to compute embedded trapped modes above the first cut-off frequency [42].

Chapter 3

Investigation method

We use basic concepts of potential theory to derive an integral equation representation of the problem. Integral equation methods are often used to solve boundary-value problems. The essential feature and the main advantage of the method is that it transfers a problem over the whole domain of interest to one involving only its boundary, so that the dimension over which computation is carried out is reduced by one. We formulate the problem indirectly, starting from Green's second identity and regarding the potential function and its normal derivative on the domain boundary as main variables. We develop a numerical method which we use to identify any existing trapped modes.

The domain W is two dimensional, bounded, with boundary ∂W. We denote a point in the field $\mathbf{x} = (x, y) \in W$ and a source point $\mathbf{x}' = (x', y') \in W$. The fundamental solution $G(\mathbf{x}, \mathbf{x}')$ has a singularity at $\mathbf{x} = \mathbf{x}'$. Let $\mathcal{L}$ be the Helmholtz operator $\nabla^2 + k^2$ and consider the following integral over the whole domain W

$$\int_W \left[\mathcal{L}\phi(\mathbf{x})\, G(\mathbf{x}, \mathbf{x}') - \mathcal{L}G(\mathbf{x}, \mathbf{x}')\, \phi(\mathbf{x})\right] d\mathbf{x} \tag{3.1}$$

We exclude the source point from the domain W by removal of a disc D_ϵ , of radius $\epsilon \to 0$, centered at $\mathbf{x}'$ hence the integral in (3.1 above) is equal to

$$\lim_{\epsilon \to 0} \left\{ \int_{W \setminus D_\epsilon} \left[\mathcal{L}\phi(\mathbf{x})\, G(\mathbf{x}, \mathbf{x}') - \mathcal{L}G(\mathbf{x}, \mathbf{x}')\, \phi(\mathbf{x})\right] d\mathbf{x} \right\} \tag{3.2}$$

On $W \setminus D_\epsilon$, both $\mathcal{L}\phi$ and $\mathcal{L}G$ are zero. Since we removed the singularity at $\mathbf{x}'$, both ϕ and G

are differentiable and we can Green's second identity on $W\backslash D_\epsilon$. Eqn. (3.2) can be written

$$\begin{aligned}
&\lim_{\epsilon\to 0}\left\{\int_{W\backslash D_\epsilon}\left[\nabla^2\phi(\mathbf{x})\,G(\mathbf{x},\mathbf{x}')-\nabla^2 G(\mathbf{x},\mathbf{x}')\,\phi(\mathbf{x})\right]d\mathbf{x}\right\}\\
&=\int_{\Gamma_\pm}\left[\frac{\partial\phi}{\partial n}(\mathbf{x})\,G(\mathbf{x},\mathbf{x}')-\frac{\partial G}{\partial n}(\mathbf{x},\mathbf{x}')\,\phi(\mathbf{x})\right]\,ds(\mathbf{x})\\
&+\lim_{\epsilon\to 0}\left\{\int_{\partial D_\epsilon}\left[\frac{\partial\phi}{\partial n}(\mathbf{x})\,G(\mathbf{x},\mathbf{x}')-\frac{\partial G}{\partial n}(\mathbf{x},\mathbf{x}')\,\phi(\mathbf{x})\right]ds(\mathbf{x})\right\}. \qquad (3.3)
\end{aligned}$$

Adding and subtracting $\phi(\mathbf{x}')\cdot\frac{\partial G}{\partial n}(\mathbf{x},\mathbf{x}')$ from the integrand in expression (3.3), we obtain

$$\begin{aligned}
&\lim_{\epsilon\to 0}\left\{\int_{\partial D_\epsilon}\left[\phi(\mathbf{x}')-\phi(\mathbf{x})\right]\frac{\partial G}{\partial n}(\mathbf{x},\mathbf{x}')-\frac{\partial\phi}{\partial n}(\mathbf{x})\,G(\mathbf{x},\mathbf{x}')\,ds(\mathbf{x})\right\}\\
&\qquad -\phi(\mathbf{x}')\int_{\partial D_\epsilon}\frac{\partial G}{\partial n}(\mathbf{x},\mathbf{x}')\,ds(\mathbf{x}). \qquad (3.4)
\end{aligned}$$

As $\epsilon\to 0$, the potential and its derivative approaching the source point are such that $\phi(\mathbf{x}')\to\phi(\mathbf{x})$ and $\int_{\partial D_\epsilon}\frac{\partial\phi}{\partial n}(\mathbf{x})\,G(\mathbf{x},\mathbf{x}')\,ds(\mathbf{x})\to 0$. The only non-zero term left to estimate in equation (3.4) is $-\phi(\mathbf{x}')\int_{\partial D_\epsilon}\frac{\partial G}{\partial n}(\mathbf{x},\mathbf{x}')ds(\mathbf{x})$. In two dimensions the fundamental free-space Green function is the Hankel function of zeroth order, of either first or second kind, depending on the radiation condition we impose. For our problem we only allow outgoing waves, towards infinity, therefore the suitable Green function is the Hankel function of first kind.

$$G(\mathbf{x},\mathbf{x}')=\frac{-i}{4}H_0^1(k|\mathbf{x}-\mathbf{x}'|)=\frac{-i}{4}H_0^1(kr),\quad r=|\mathbf{x}-\mathbf{x}'|. \qquad (3.5)$$

Its normal derivative is:

$$\frac{\partial G}{\partial n}(\mathbf{x},\mathbf{x}')=\frac{-i}{4}\frac{\partial H_0^1(kr)}{\partial n}=\frac{ikH_1^1(kr)}{4}\frac{\partial r}{\partial n}, \qquad (3.6)$$

and when $r\to 0$, according to Abramovitz and Stegun [1], the Hankel function is approximately

$$H_1^1(kr)\approx\frac{2}{i\pi kr}. \qquad (3.7)$$

Using polar coordinates, integral (3.4) reduces to:

$$-\phi(\mathbf{x}')\left\{\int_{D_\epsilon}\frac{\partial G}{\partial n}(\mathbf{x},\mathbf{x}')ds(\mathbf{x})\right\}=-\phi(\mathbf{x}')\left\{\frac{1}{2\pi}\int_0^{2\pi}d\theta\right\}=-\phi(\mathbf{x}'). \qquad (3.8)$$

Combining equations (3.4 - 3.8) we get an expression for the potential $\phi(\mathbf{x}')$, in terms of integrals defined on the domain boundary

$$\phi(\mathbf{x}') = \int_{\partial W} \left[\phi(\mathbf{x}) \frac{\partial G(\mathbf{x}, \mathbf{x}')}{\partial n} - G(\mathbf{x}, \mathbf{x}') \frac{\partial \phi(\mathbf{x})}{\partial n} \right] ds(\mathbf{x}). \tag{3.9}$$

For any point $\mathbf{x}'$ on the boundary ∂W, the boundary integral equation (3.9) can be generalised in the form

$$c(\mathbf{x}')\, \phi(\mathbf{x}') = \int_{\partial W} \left[\phi(\mathbf{x}) \frac{\partial G(\mathbf{x}, \mathbf{x}')}{\partial n} - G(\mathbf{x}, \mathbf{x}') \frac{\partial \phi(\mathbf{x})}{\partial n} \right] ds(\mathbf{x}), \tag{3.10}$$

since the previous idea of excluding the source point is still valid, the only change being on the upper limit of the integrals in (3.8) which is now the angle α subtended at point $\mathbf{x}'$. The free coefficient $c(\mathbf{x}')$ is then given by:

$$c(\mathbf{x}') = \frac{\alpha}{2\pi}, \quad 0 \leq c(\mathbf{x}') \leq 1. \tag{3.11}$$

Thus we converted the domain integrals to an expression for ϕ involving only boundary integrals.

3.0.1 Boundary element method

We now develop a general numerical method which we apply to the solution obtained in (3.10) and can be used to solve problems with arbitrary geometry and boundary conditions. The Boundary element method (BEM) is a well-known method of solving boundary integral equations, based on a discretisation procedure. First we approximate the boundary by dividing it into N small boundary elements S_m such that:

$$\sum_{m=1}^{N} S_m \approx \partial D. \tag{3.12}$$

Taking this into account, equation (3.10) can be written in the form:

$$c(\mathbf{x}')\phi(\mathbf{x}') = \sum_{m=1}^{N} \left\{ \int_{S_m} \left[\phi(\mathbf{x}) \frac{\partial G(\mathbf{x}, \mathbf{x}')}{\partial n} - G(\mathbf{x}, \mathbf{x}') \frac{\partial \phi(\mathbf{x})}{\partial n} \right] ds(\mathbf{x}) \right\}, \quad \mathbf{x}' \in S_m, \tag{3.13}$$

so that the integration along the entire boundary has been reduced to a summation of integrals over each boundary element. Thus we can, within a certain level of approximation, model a general boundary using polygons.

At each point on the boundary either ϕ or $\partial\phi/\partial n$ is known from boundary conditions but not both. Along each boundary element S_m we write the unknown ϕ or $\partial\phi/\partial n$, as a linear function of their values taken at the end points. As the potential (or its derivative) is considered at each of these points, the singularity of the Green function dictates that they are excluded from the domain, one by one, following the procedure outlined in section 3, hence they are referred to as source points. We introduce the fairly standard notation: let ϕ_p be the potential and $q_p = \partial\phi/\partial n$ the flux at the source point p. Consider the boundary element $S_m$with extremities, $\mathbf{x}'_m = (x_m, y_m)$ and $\mathbf{x}'_{m+1} = (x_{m+1}, y_{m+1})$ respectively. We introduce a local coordinate $-1 \leq \xi \leq 1$ along each boundary element so that general Cartesian coordinates (x, y) become:

$$x = \frac{1-\xi}{2}x_m + \frac{1+\xi}{2}x_{m+1},$$

$$y = \frac{1-\xi}{2}y_m + \frac{1+\xi}{2}y_{m+1}, \quad 1 \leq m \leq N. \tag{3.14}$$

On the boundary element S_m either ϕ_m or q_m and ϕ_{m+1} or q_{m+1}, at its extremities, are unknown. We assume that these quantities, potential and flux, vary linearly between the endpoints so that at a general location $\mathbf{x} \in S_m$ we can write:

$$\phi(\mathbf{x}) = \frac{1-\xi}{2}\phi_m + \frac{1+\xi}{2}\phi_{m+1}, \quad \mathbf{x} \in S_m,$$

and

$$q(\mathbf{x}) = \frac{1-\xi}{2}q_m + \frac{1+\xi}{2}q_{m+1}, \quad \mathbf{x} \in S_m. \tag{3.15}$$

Let l_m be the length of each boundary element S_m. Then in local coordinate we have that:

$$ds = \left[\left(\frac{dx}{d\xi}\right)^2 + \left(\frac{dy}{d\xi}\right)^2\right]^{\frac{1}{2}} d\xi = \frac{l_m}{2}d\xi. \tag{3.16}$$

For each node $p = 1, \ldots, N$, we apply equation (3.13) and obtain N equations of the form:

$$c_p\phi_p = \sum_{j=1}^{N} \left\{ \int_{S_m} \left[\left(\frac{1-\xi}{2}\phi_m + \frac{1+\xi}{2}\phi_{m+1} \right) \frac{\partial}{\partial n} \left(\frac{-iH_0^1(kr)}{4} \right) \Big|_{r=r_{pm}} \right.\right.$$
$$\left.\left. - \left(\frac{1-\xi}{2}q_m + \frac{1+\xi}{2}q_{m+1} \right) \left(\frac{-iH_0^1(kr_{pm})}{4} \right) \right] \frac{l_m}{2} d\xi \right\}, \tag{3.17}$$

where

$$r_{pm} = r_{pm}(\xi) = |\mathbf{x_p} - \mathbf{x}|, \quad \mathbf{x} \in S_m. \tag{3.18}$$

The derivative of the Green function, with respect to the normal alongside the boundary element S_m is of the form:

$$\frac{\partial}{\partial n} \left[\frac{-i}{4} H_0^1(kr) \right]_{r=r_{pm}} = \frac{ik}{4} H_1^1(kr_{pm}) \left. \frac{\partial r}{\partial n} \right|_{r=r_{pm}} = \frac{ik}{4} H_1^1(kr_{pm}) \frac{d_{pm}}{l_m r_{pm}}, \tag{3.19}$$

The quantities d_{ij} depend on the coordinates of the nodal point i, (x_i, y_i) and the extremities of the boundary element S_j, i.e. the points (x_j, y_j) and (x_{j+1}, y_{j+1}), as follows:

$$d_{pm} = d\left[x_m y_{m+1} - x_{m+1} y_m - x_p(y_{m+1} - y_m) + y_p(x_{m+1} - x_m) \right]. \tag{3.20}$$

The coefficient $d = \pm 1$, depending on the orientation of the contour under integration. We denote

$$\begin{aligned}
\widehat{A}_{pm} &= \frac{ikd_{pm}}{16} \int_{S_m} (1-\xi) \frac{H_1^1(kr_{pm})}{r} d\xi, \\
\widehat{B}_{pm} &= \frac{ikd_{pm}}{16} \int_{S_m} (1+\xi) \frac{H_1^1(kr_{pm})}{r} d\xi, \\
C_{pm} &= \frac{-il_m}{16} \int_{S_m} (1-\xi) H_0^1(kr_{pm}) d\xi, \\
D_{pm} &= \frac{-il_m}{16} \int_{S_m} (1+\xi) H_0^1(kr_{pm}) d\xi.
\end{aligned} \tag{3.21}$$

and

$$\begin{aligned}
A_{pm} &= \widehat{A}_{pm} - c_p \delta_{pm}, \\
B_{pm} &= \widehat{B}_{pm} - c_p \delta_{pm}.
\end{aligned} \tag{3.22}$$

Here δ_{pm} is the Kronecker delta symbol. The c_p terms result from integrating (3.18) around each source point and are given by the formula in (3.11). Now we re-write equation (3.17) in the form:

$$\sum_{m=1}^{N} \left(A_{pm}\phi_m + B_{pm}\phi_{m+1} \right) = \sum_{m=1}^{N} \left(C_{pm}q_m + D_{pm}q_{m+1} \right), \tag{3.23}$$

for all nodal points $p = 1, \ldots, N$. Once the boundary conditions are applied we have a system of N equations in N unknowns, which are either ϕ_m or q_m, at each nodal point $m = 1, \ldots, N$. The system is written in matrix form as:

$$M\mathbf{X} = 0. \tag{3.24}$$

where the matrix $M = M(k)$ is obtained by combining the entries in matrices A, B, C and D and $\mathbf{X}$ is a vector storing the unknowns. Trapped modes, i.e. non-unique, non-trivial solutions of the problem correspond to those values of k where the Laplacian operator has an eigenvalue. M is a complex matrix, which we can write explicitely as

$$M = M_R + iM_I. \tag{3.25}$$

The physical problem must have real solutions for ϕ meaning that the eigenvector $\mathbf{X}$ must be real or have a small imaginary part. Hence solutions to our problem correspond to those frequencies for which both the real and the imaginary parts of the matrix $M(k)$ are singular

$$|M_R| = 0 \quad \& \quad |M_I| = 0. \tag{3.26}$$

We use these two conditions in our program to verify the accuracy of the calculations.

3.0.2 Singularities

The coefficients A_{pm}, B_{pm}, C_{pm} and D_{pm}, for $p \neq j$ are evaluated using standard numerical integrations schemes. For those cases where the source point is on the element under integration ($p = m$, or $p = m - 1$), due to the singularity of the fundamental solution we have to carry out a more accurate integration. The Hankel function of zeroth order has a singularity of the form $\ln(kr/2)$ which poses a problem as we approach the source point (p), $(r \to 0)$. To solve this, when evaluating the coefficients $A_{pp}, A_{pp-1}, B_{pp}, B_{pp-1}$, which

involve integration on elements collinear with node (p), we subtract the singularity and resolve it analytically. The integral left after subtracting the singularity is then evaluated using standard numerical methods (we used the Simpson composite method).

The coefficients $C_{pm}, C_{pp-1}, D_{pp}, D_{pp-1}$, that involve evaluation of $\partial G/\partial n$ on boundary elements that are colinear with the source located at $\mathbf{x_p}$, are all zero since on elements S_p and S_{p-1} the radial unit vector $\hat{\mathbf{r}}$ and the normal $\hat{\mathbf{n}}$ to the boundary element are perpendicular to each other, therefore we have that $\partial r/\partial n = 0$.

3.0.3 Trapped-mode solutions

To detect trapped modes for a particular configuration, in a particular frequency range, we look for non-trivial solutions of eqn. (3.24). The necessary condition for the existence of such non-trivial solutions translates into finding values of k which satisfy equations (3.26).

The trapped mode problem is formulated for an infinite domain. To carry out computations on a finite domain we must impose conditions which mimic the infinity at the point where we truncate the waveguide - for details see eq. (4.9) in section 4.2. The truncation of the domain leads to the appearance of spurious eigenvalues which appear at values of k which although satisfy eqn. (4.9) they do not satisfy the trapped mode problem. Plotting the determinant of the matrix M against values of k, for increasing number of discretisation points N, can help differentiate between pure, genuine trapped modes and fictitious solutions. A typical situation is that (3.26) may have a solution for a certain N but if we shorten the length of the boundary element, the solution will disappear. Another typical situation is that with each increase in N the curve $\det[M(k)]$ will cross the axis at different points, at distances large enough to suggest that they will fail to converge to a limit.

Below we illustrate these situations for the case of a cavity (of depth $h = 2.2$ and width $w = 5.8$) in a Dirichlet waveguide (of width $2d$ and for ease of notation let $d = 1$) . This geometry has two trapped modes, at two different frequencies, $k_1 \approx 2.7361 = 0.8709\,\pi$ and $k_2 \approx 3.03302 = 0.9654\,\pi$. In Fig. 3.1 we show plots of the $\det[M_R(k)]$ for k in the vicinity of the real trapped modes. The plots are drawn for two discretisation rates, $N = 280$ (boundary element = 0.2) and $N = 560$ (boundary element = 0.1). In each plot we show the real trapped mode and a spurious eigenvalue. In the first plot we see a variation of cca. 0.005 between the solutions given by the two discretisations, which in our experience is

too large to consider it a candidate for a genuine trapped mode. A true eigenvalue also varies with the number of points used to discretise the boundary, however the change is of order 10^{-6}, which is consistent with errors predicted by the Simpson rule which we use to estimate the entries in matrix M. The second plot illustrates the case where with the doubling of the number of discretisation points the spurious mode disappears altogether.

Once a genuine eigenvalue of the problem is identified, the values of either ϕ or $q = \frac{\partial \phi}{\partial n}$ around the domain boundary are given by the eigenvector of M corresponding to the zero matrix eigenvalue. The system (3.24) is solved and the values of ϕ and q obtained along the boundary, are substituted back in equation (3.13), with position coefficient $c(\mathbf{x}') = 1$, to calculate the potential ϕ at points inside the domain W.

We implemented this numerical method using Matlab software. The flexible design of the program allows analysis of any two dimensional geometry, for which coordinates can be calculated, and can be applied to both internal and external problems.

More details of how the boundary element program is used to detect trapped modes, including the methods we use to differentiate between pure, genuine trapped modes and fictitious solutions are included in Chapter 4, section 4.2.1.1.

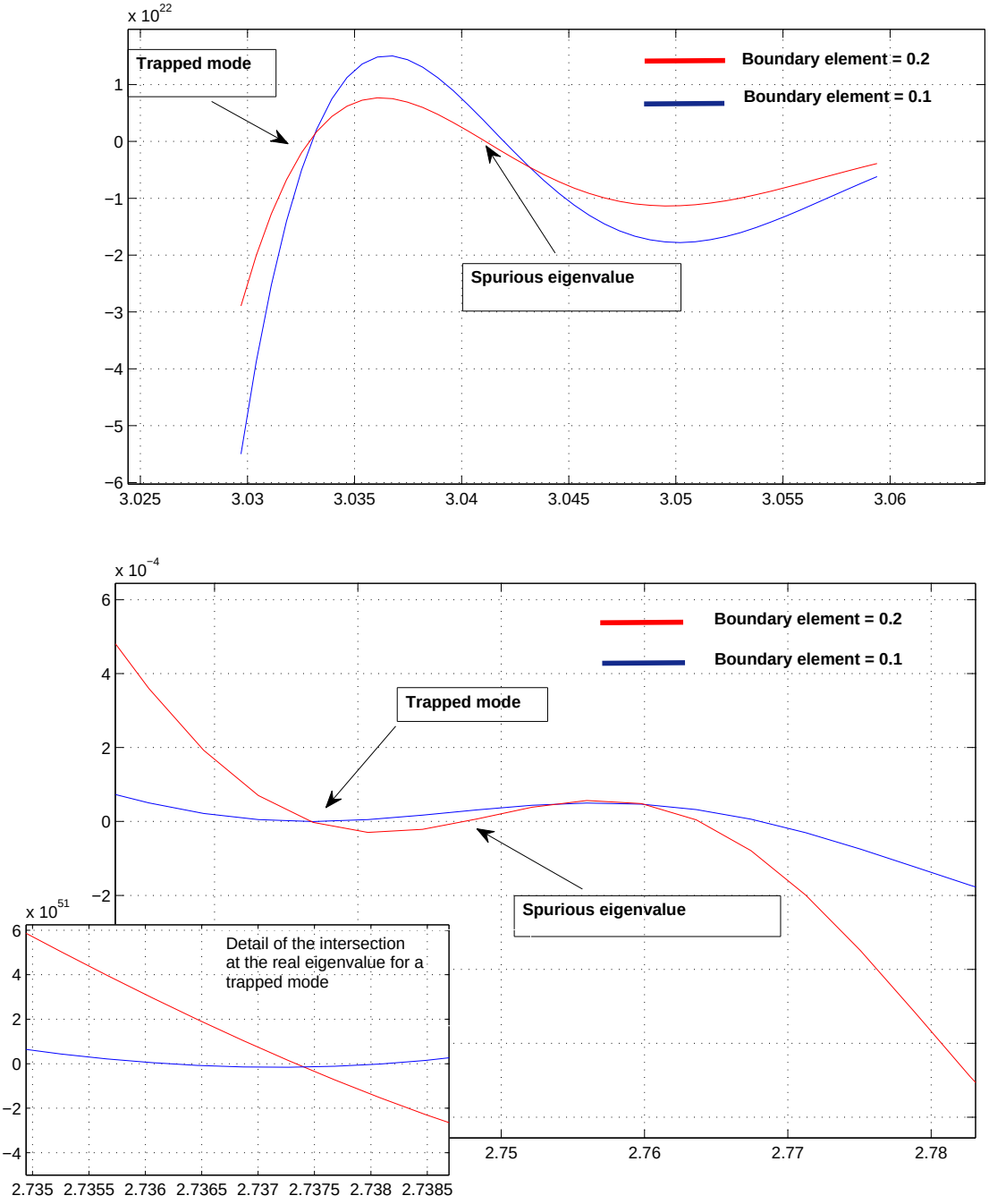

Figure 3.1: Plots of the det$[M_R(k)]$ variation with kd, for different discretisation rates, help separate genuine trapped modes from spurious eigenvalues.

Chapter 4

Test Cases

Trapped modes correspond to discrete eigenvalues in the spectrum of an operator. Some of these values are unstable and can easily be destroyed by any small perturbation to the geometry. To ensure that our method yields correct results we initially applied it to cases where solutions are either already known or can be calculated analytically. In this chapter we present some known trapped modes we replicated with our program in order to confirm our method's validity. New results, where we extended the range of frequencies investigated for geometries already studied and for new configurations are presented in Chapter 5. To confirm the accuracy of the program we also checked the convergence rate of frequencies to known results.

4.1 Closed domains

Although trapped modes are only defined on unbounded domains we first considered simple closed shapes for which solutions to the Helmholtz equation are known analytically. Using our numerical method we sought eigenvalues for internal problems, defined on circular and rectangular domains and a combination of both, with either Dirichlet or Neumann boundary conditions. For all these problems, the eigenvalues are well-known and can be precisely computed.

4.1.0.1 Disc with Dirichlet boundary conditions

For example, consider the problem of the Helmholtz equation on a circular domain with radius $r = a$, with Dirichlet boundary conditions. In polar coordinates the Helmholtz equation is

$$\frac{\partial^2\phi}{\partial r^2} + \frac{1}{r}\frac{\partial\phi}{\partial r} + \frac{1}{r^2}\frac{\partial^2\phi}{\partial^2\theta} + k^2\phi = 0. \tag{4.1}$$

Assuming solutions of the form $\phi(r,\theta) = R(r)\Theta(\theta)$ we obtain two equations, one for $\Theta(\theta)$, which yields solutions of the form $a_n e^{in\theta} + b_n e^{-in\theta}$ and one for $R(r)$. It follows from the periodicity condition (Θ must be periodic of period 2π) that $\Theta(\theta) = \alpha_n \cos n\theta$ where n must be an integer.

Making the substitution $rk = \rho$ in the equation for $R(r)$, we obtain the Bessel equation

$$\rho^2 R'' + \rho R' + (\rho^2 - n^2)R = 0. \tag{4.2}$$

Hence, the general solution for our problem takes the form of an infinite sum of terms involving products of $\sin(n\theta)$ or $\cos(n\theta)$ and Bessel functions of the first kind of order n, denoted J_n.

To satisfy the Dirichlet boundary condition it is required that $J_n(ka) = 0$. The Bessel function of order n, J_n, has infinitely many roots, denoted $\rho_{m,n}$ with m signifying the m'th root, in ascending order. Our program correctly identifies the non-trivial, non-unique solutions of this problem occuring for precisely those frequencies $k = \frac{1}{a}\rho_{m,n}$.

To illustrate, in Table (4.1), we show the first five values of k, obtained with our method presented in Chapter 3, corresponding to the first zeros of the Bessel functions J_0, J_1, J_2, J_3 and J_4. As the number of points N, used to discretise the boundary progressively increases, k converges to the Bessel function's roots (values listed in the last column):

N	30	60	120	240	480	∞
k_1	2.405781	2.405183	2.405046	2.404946	2.404869	$J_{0,1} = 2.404825$
k_2	3.832370	3.832210	3.832041	3.831887	3.831805	$J_{1,1} = 3.831705$
k_3	5.140863	5.136209	5.136068	5.135894	5.135696	$J_{2,1} = 5.135622$
k_4	6.385247	6.380649	6.380690	6.380471	6.380326	$J_{3,1} = 6.380161$
k_5	7.591930	7.588619	7.588954	7.588729	7.588542	$J_{4,1} = 7.588342$

Table 4.1: As N increases, the values of k converge to zeros of Bessel functions.

4.1.0.2 Rectangle with Neumann boundary conditions

Another case where we can easily compute the eigenvalues is the Helmholtz equation on on a rectangular domain. Consider a rectangle with sides $-a \leq x \leq a$ and $-b \leq y \leq b$. Then the eigenfunctions

$$\begin{aligned}
\phi_{nm} &= \cos\left(\frac{m\pi x}{a}\right)\cos\left(\frac{n\pi y}{b}\right), \\
\phi_{nm} &= \cos\left(\frac{m\pi x}{a}\right)\sin\left(\frac{n\pi y}{b}\right), \\
\phi_{nm} &= \sin\left(\frac{m\pi x}{a}\right)\cos\left(\frac{n\pi y}{b}\right), \\
\phi_{nm} &= \sin\left(\frac{m\pi x}{a}\right)\sin\left(\frac{n\pi y}{b}\right).
\end{aligned} \tag{4.3}$$

are all solutions to the problem for the appropriate values of $m, n = 0, \frac{1}{2}, 1, \frac{3}{2}, ...$ chosen to satisfy the Neumann condition at $x = 1$ and $y = b$. Possible eigenvalues for this problem satisfy

$$\lambda_{nm} = \pi^2\left(\frac{n^2}{a^2} + \frac{m^2}{b^2}\right). \tag{4.4}$$

for couples of (m, n) chosen appropriately, to satisfy the boundary conditions.

The first five solutions for a configuration with $a = a$, and $b = 1$, calculated using our program, taking increasing number of discretising points N around the boundary and the corresponding exact values, computed using equation (4.4) are presented in the table (4.2).

N	40	80	160	320	640	$1,280$	∞	(m, n)
k_1*	1.5766	1.5723	1.5712	1.5709	1.5708	1.5707	1.5707	$\left(\frac{1}{2}, 0\right)$
k_2	2.2342	2.2247	2.2222	2.2216	2.2214	2.2214	2.2214	$\left(\frac{1}{2}, \frac{1}{2}\right)$
k_3	3.1650	3.1479	3.1432	3.1420	3.1416	3.1416	3.1416	$(1, 0)$
k_4	3.5146	3.5141	3.5136	3.5130	3.5125	3.5120	3.5120	$\left(\frac{1}{2}, 1\right)$
k_5	4.5497	4.4684	4.4488	4.4443	4.4432	4.4429	4.4428	$(1, 1)$

Table 4.2: As N increases, the values of k converge to exact eigenvalues of the Helmholtz equation on a rectangular domain, with Neumann boundary conditions.

*Note: as we have chosen $a = b = 1$, both $\left(\frac{1}{2}, 0\right)$ and $\left(0, \frac{1}{2}\right)$ are eigenfunctions for this problem, hence k_1 is a double eigenvalue. Figure 4.1 shows a plot of det$[M_R(k)]$ and we see that the curve behaves like $(k - \pi/2)^2$. The equation det$([M_R(k)] = 0$ has a double solution indicating that the problem has a degeneracy at $\pi/2$.

The matrix $M(k_1)$ has two eigenvalues equal to zero and their respective eigenvectors cor-

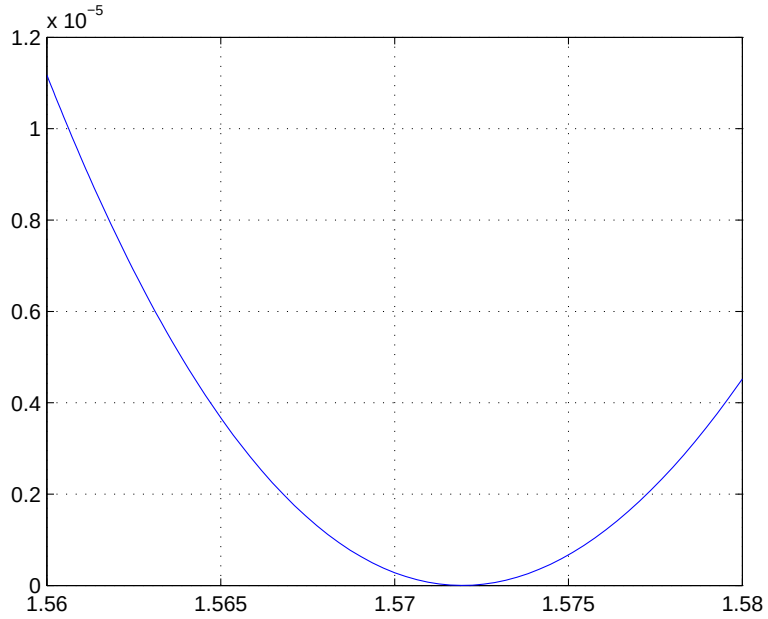

Figure 4.1: The equation $\det[M_R(k)] = 0$ has a double solution at $\pi/2$.

respond to the eigenfunctions of the problem.

A simple error analysis confirms the precision of our method as follows: let N_1 be the number of points taken around the boundary, k_{N_1} the value of k obtained for this discretisation and k_∞ the exact value of an eigenvalue k (calculated analytically). The error corresponding to this discretisation is

$$e_1 = k_{N_1} - k_\infty \approx \frac{\alpha}{N_1^2} \tag{4.5}$$

for some constant α. Doubling the number of points, $N_2 = 2N_1$, the error is

$$e_2 \approx \frac{\alpha}{N_2} \approx \frac{e_1}{2^2}, \tag{4.6}$$

and if we continue doubling the discretisation rate, for a number of points $N_p = 2^{p-1}N_1$, the error should be

$$e_p \approx \frac{\alpha}{\left(2^{p-1}N_1\right)^2} \approx \frac{1}{2^{2p-2}} e_1. \tag{4.7}$$

Equation (4.7) predicts that the logarithm of the error decreases linearly with the discret-

isation rate p

$$E_p = \log e_p = -2p \log 2 + 2 \log 2 + \log e_1. \tag{4.8}$$

$E_p = \log(e_p)$ for k_1 to k_5 listed in Table (4.2) are plotted in Fig. (4.2) to illustrate the agreement between the error prediction and the accuracy of results obtained using our method. The values of $E_p = \log(e_p)$ obtained using our program are in fact exactly the same values predicted by Eq. (4.8).

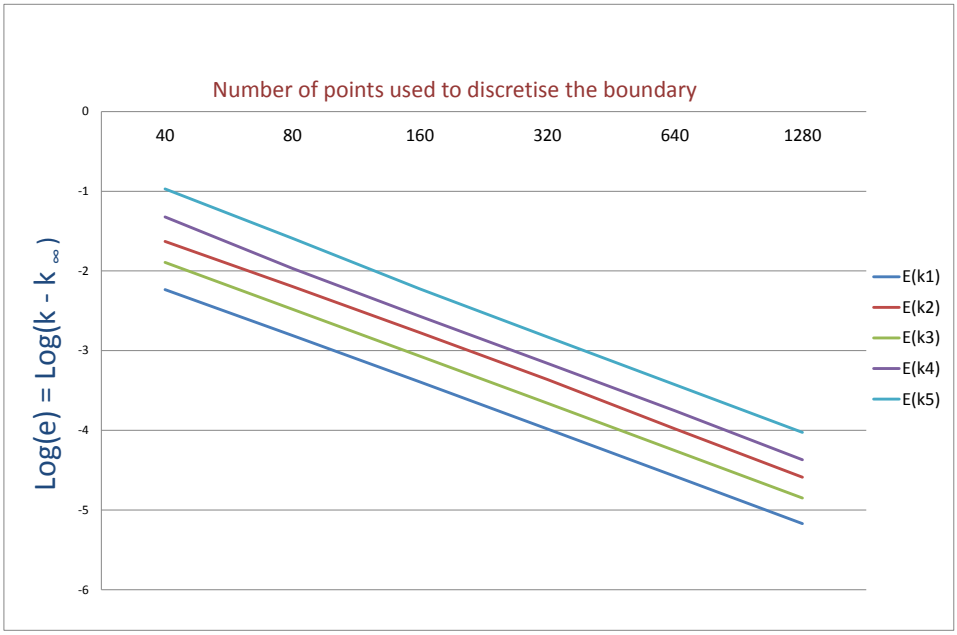

Figure 4.2: Log-error plot for the first five eigenvalues; the logarithm of error decreases linearly with the discretisation rate, as predicted by Eq.(4.8).

4.1.0.3 Multiply connected domain

In this section we consider the problem on a multiply connected domain, composed of an inner square boundary and outer circular boundary. The eigenvalues for this problem were computed by Chen *et. al* [35] using a finite element method. We computed the eigenvalues for this problem, and in this section we present the results for the case with Dirichlet boundary conditions on all boundaries. Our results are very similar to those already published. The first four eigenvalues, together with the corresponding eigenmodes, are shown

in Figure (4.3). The process of reduction of the Helmholtz eigenvalue problem from the

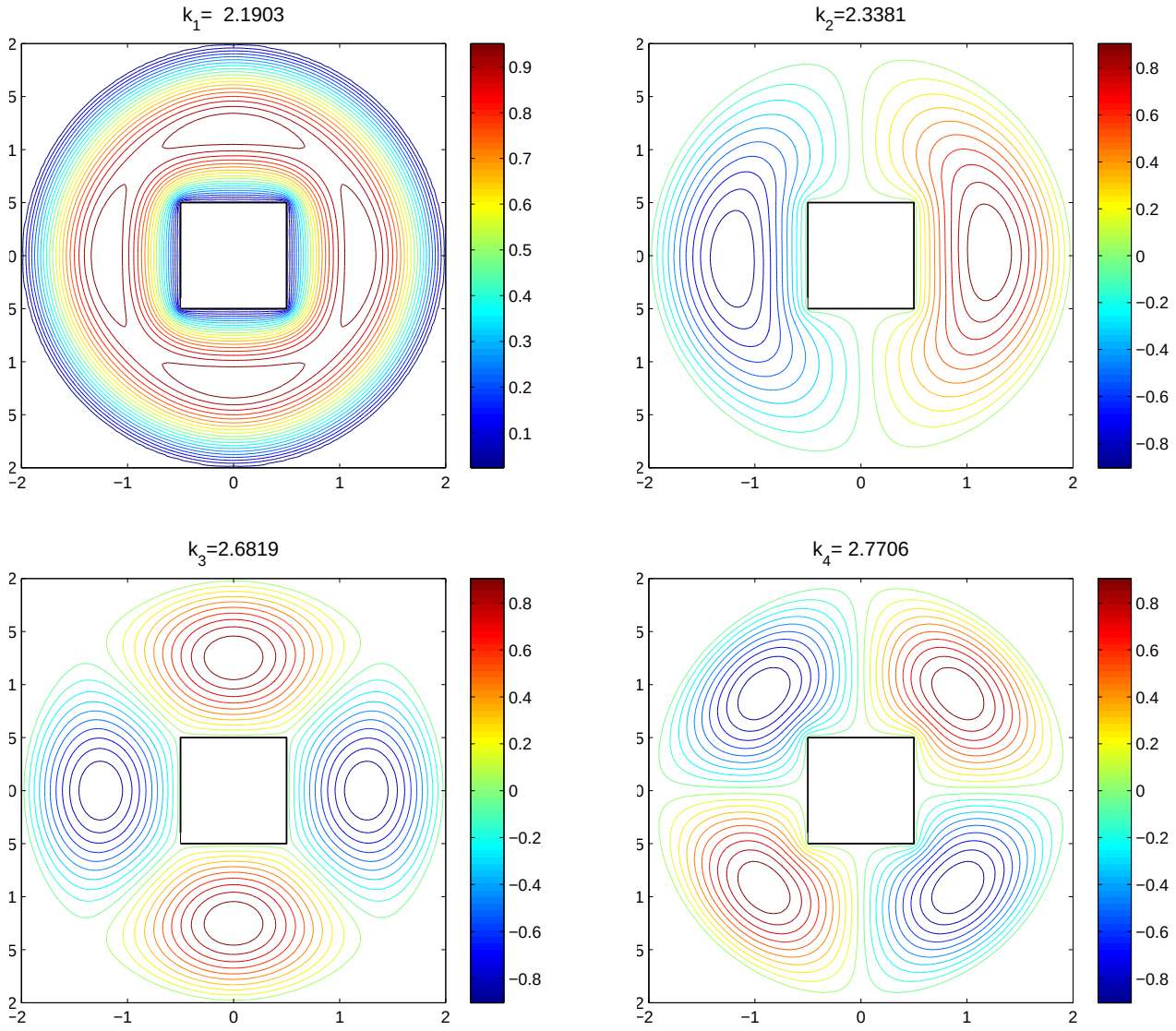

Figure 4.3: Four eigensolutions corresponding to four different eigenvalues of the Dirichlet problem on a closed multiply connected domain.

exterior domain to the boundary gives rise to difficulties of non-uniqueness which are not inherent in the original problem [9], [31]. These irregular values embedded in the singular integral equations are found to be the associated eigenvalues for the corresponding interior problem with either Dirichlet or Neumann boundary conditions [9], [48]. For our problem, the boundary-element method yields spurious eigenvalues which depend on the geometry of the inner domain [14]. For this case, the first predicted fictitious eigenvalue is $\pi\sqrt{2} = 4.4428$, corresponding to the inner square solution $\sin \pi x \sin \pi y$. Our program also

yields this spurious eigenvalue, however, as the number of points N around the boundary is increased, this false solution disappears. In the next section we will relate a few more techniques we apply to distinguish between real and fictitious eigenvalues, which often appear in problems for infinite domains and can be computationally very costly.

4.2 Infinite domains

4.2.1 Waveguide with circular obstacle

This case is as formulated in Chapter 2, Eqn.(2.4-2.7) for the Dirichlet problem and Eqn.(2.4-2.6) and Eqn.(2.8) for the Neumann problem, including one circular obstacle D placed on the centerline of the waveguide with $x^2 + y^2 = a^2$ and its radius $a \leq d$.

This is the first case where we verify that our program can detect actual trapped modes, rather than eigensolutions, as they are found in an *infinite* or *semi-infinite* domain. This obviously poses the difficulty of computing over a finite area for a problem defined on an infinite domain. We also have to set an appropriate boundary condition to reflect the fact that solutions decay exponentially in the far field. To ensure that our program detects the decaying modes and filters out the propagating modes we impose, away from the obstacle, for $-d < y < d$ and $x \gg a$ a condition of the form:

$$\frac{\partial \phi}{\partial x} \sim -\mu_1 \phi, \tag{4.9}$$

The decay coefficient μ_1 depends on the problem and the range of frequencies investigated. For example, if we look for y - antisymmetric trapped modes, below the first cut-off, the decay coefficient is

$$\mu_1 = \left[\left(\frac{\pi}{2d} \right)^2 - k^2 \right]^{\frac{1}{2}}, \tag{4.10}$$

for the Neumann problem and

$$\mu_1 = \left[\left(\frac{\pi}{d} \right)^2 - k^2 \right]^{\frac{1}{2}}. \tag{4.11}$$

for the Dirichlet problem. This choice of a boundary condition is motivated as follows: for

the Neumann problem, in the far field, away from the obstacle, the solution is

$$\phi \approx \sum_{n=1}^{n=\infty} a_n e^{-\mu_n x} \sin\left[\frac{(2n-1)\pi}{2d} y\right], \quad \mu_n = \left[\left(\frac{2n-1}{2d}\pi\right)^2 - k^2\right]^{\frac{1}{2}}. \tag{4.12}$$

for large x, the solution asymptotically should behave like the dominant term

$$\phi \approx a_1 e^{-\mu_1 x} \sin\frac{\pi y}{2d}. \tag{4.13}$$

This condition, selects the solutions where the coefficients $a_n, n = 2, \ldots,$ are zero which in effect filters out solutions that do not decay exponentially, as specified by equation (4.9).

4.2.1.1 Spurious eigenvalues

Condition (4.9) enables accurate detection of any trapped modes present in the frequency ranges investigated, but it also introduces fictitious solutions. Although the convention is that the eigenvalues corresponding to the antisymmetric mode are not in the continuous spectrum of the antisymmetric problem, the actual computation is carried out for frequencies embedded in the continuous spectrum of the whole problem, therefore travelling modes are in fact present in that k-parameter space. For certain values of k, down the guide, where we truncate the domain, on the lines say $|x| = L, |y| < d$, travelling modes $\phi \sim \sin kx$ or $\phi \sim \cos kx$, satisfy the condition imposed by Eq. (4.9) but they obviously do not decay exponentially. These spurious modes are identified by our BEM program and they are false solutions to the trapped mode problem. We now discuss the strategies we adopted to identify and discard spurious modes.

One strategy to eliminate these travelling modes is to apply the decay condition (4.9) to modes $\phi \sim a \sin kx$ and $\phi \sim b \cos kx$, at distance $|x| = L$ away from the obstacle. We obtain two relations depending on k, as follows:

$$k + \left[\sqrt{\left(\frac{\pi}{2d}\right)^2 - k^2}\right] \tan kL = 0 \quad \text{and} \tag{4.14}$$

$$k \tan kL - \left[\sqrt{\left(\frac{\pi}{2d}\right)^2 - k^2}\right] = 0 \tag{4.15}$$

We plot each of these two equations above against $\det[M(k)] = 0$ and discard those values of k where the solutions coincide.

Increasing the number of points used to discretise the domain and comparing the plots for $\det[M(k)]$ is also a way to differentiate between genuine and spurious eigenvalues, and two examples are discussed in Chapter 2. However, both these strategies, although reliable, are time consuming when applied to wide ranges of frequencies and geometric parameters.

A fast method we use to distinguish between genuine trapped modes and fictitious solutions is by computing an energy radiation index (ERI) as follows:

- for a given geometry determine all frequencies such that $\det[M_R(k)] = 0$
- identify for each singular matrix $M_R(k)$ the zero eigenvalue(s) and the corresponding eigenvector(s)
- use the eigenvector to compute the solution ϕ at points in the far field, located in a rectangular mesh , of width circa one wavelength, positioned down the guide, in the farfield. For example a mesh is formed of a finite number of points in W such that $n\lambda \leq x \leq (n+1)\lambda, -d \leq y \leq d$
- compute the potential ϕ on the boundary of the truncated waveguide
- the energy radiation index is the ratio between the sums of the squares of these two values

$$\text{EDI}(k) = \frac{\sum\limits_{(x,y)\in \text{Mesh}} [\phi(k,x,y)]^2}{\sum\limits_{(x,y)\in \text{ Boundary}} [\phi(k,x,y)]^2}. \tag{4.16}$$

- a trapped mode will correspond to a local minimum of the energy dissipation index, represented as a function of geometric parameters.

This is a very effective method to detect trapped modes as the dissipation indices can be calculated and stored for all values of k in a given frequency range and corresponding to many sets of geometric parameters. These data can provide at a glance an indication of those configurations which may support a trapped mode. In Table (4.3) we show the

lowest energy dissipation indexes calculated for values of k such that $\det[M(k)] = 0$ for the problem of a Neumann waveguide with a disc of a fixed radius ($a/d = 0.6$) placed on the centre, and a rectangular cavity of depth h/d and width w/d. We vary the depth and the width of the cavity and display the lowest EDI for each geometry. Different values of minimum EDI correspond to different sets of geometric parameters (h, w) and it can be seen as the cavity approaches $h/d \to 0.6$, $w/d \to 6$ the energy dissipation reaches a minimum. An extra check to ensure that the trapped mode found is genuine is to vary the truncation of the waveguide, the length $x = L$, over which the computation is carried out. The eigenvalue corresponding to genuine trapped mode will not vary with L whereas a spurious mode will yield a different k for each length of the waveguide. The trapped modes for these cases will be discussed in detail in Chapter 5.

Energy Dissipation Index					
	Width				
Depth	5.6	5.8	6	6.2	6.4
0.3	0.008455	0.002247	0.003243	0.002444	0.00258
0.4	0.003609	0.002715	0.006771	0.003997	0.002162
0.5	0.007636	0.009425	$1.01E-05$	0.033749	0.005245
0.6	0.006043	0.020728	$4.86E-07$	0.022481	0.032897
0.7	0.006498	0.027052	$8.23E-06$	0.000752	0.000417
Corresponding k value					
	Width				
Depth	5.6	5.8	6	6.2	6.4
0.3	1.394992	1.377506	1.332086	1.331205	1.3311
0.4	1.217997	1.21766	1.211755	1.205328	1.178883
0.5	1.216767	1.216327	1.370104	1.446332	1.454928
0.6	1.21718	1.20984	1.371246	1.420508	1.419266
0.7	1.218978	1.207365	1.371073	1.286347	1.122679

Table 4.3: Energy dissipation index, and associated frequencies, for the problem of a Neumann waveguide with disc of fixed radius $a/d = 0.6$ and a rectangular cavity with varying depth h/d and width w/d.

4.2.1.2 Disc on the centre of Dirichlet waveguide, $k < k_1$

It has been established that in this range of k, a unique trapped mode exists for each a such that $0 < a/d \leq 0.6788$ [43].

Using our method we computed the eigenvalues for this problem. Our results agree to a

high level of accuracy with those of Maniar and Newman [47], obtained using a different numerical method, based on Fourier modes. The eigenvalues we obtained are presented in the table (4.4), together with the results of Maniar and Newman, for comparison.

a	kd	kd/π	Maniar & Newman results
0.1	3.129	0.996	3.129
0.2	3.056	0.969	3.055
0.3	2.990	0.951	2.989
0.4	2.998	0.954	2.999
0.5	3.071	0.977	3.071
0.6	3.132	0.999	3.132

Table 4.4: Comparison of Dirichlet trapped wavenumber obtained using our method (columns 2 and 3) with results obtained by Maniar & Newman

The absence of trapped modes for $a/d > 0.6788$ may be due to the proximity of the Dirichlet condition on the wall and the Neumann condition on the circle. Figures (4.4(a) - 4.4(b)) show contour profiles of two trapped mode solutions. For the smaller disc of radius $a/d = 0.3$, the solution decays rapidly and has a more prominent x dependence. The second profile is for the near-limit case $a/d = 0.676$, and we can see the decay rate is much smaller in comparison with the previous example.

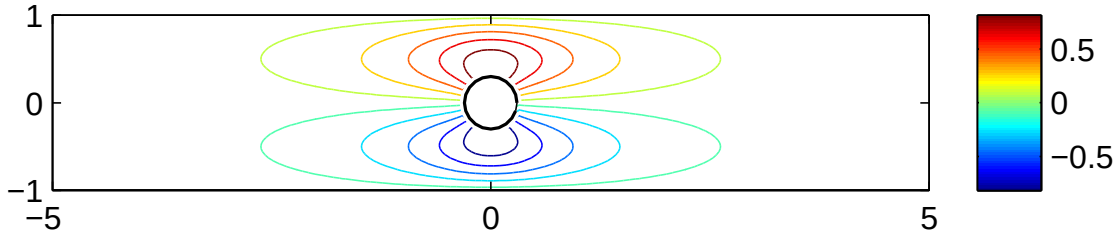

(a) Potential ϕ in a waveguide with Dirichlet BCs on the walls, $a/d = 0.3,\ kd \sim 2.990 = 0.951\pi$

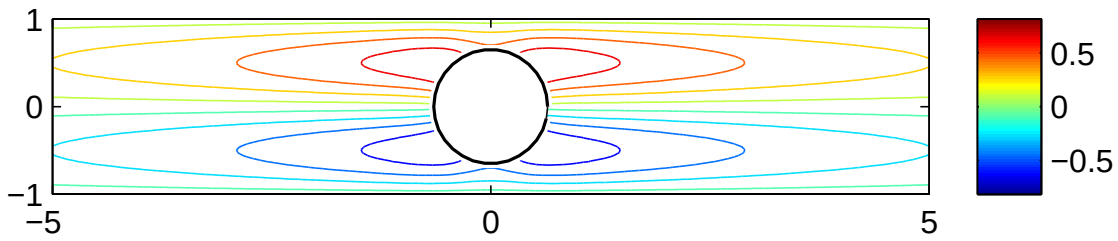

(b) Potential ϕ in a waveguide with Dirichlet BCs on the walls, $a/d = 0.676,\ kd \sim 3.1415 = 0.999\pi$

Figure 4.4: Trapped modes in a Dirichlet waveguide, obtained using our BEM program

The infinite Dirichlet waveguide with a disc on its centreline will be discussed in detail in Chapter 6.4, where we develop a mathematical representation using the plane wave spectrum analysis method.

4.2.1.3 Disc on the centre of Neumann waveguide, $k < k_1$

For every $k \geq 0$, a travelling mode of the form e^{ikx} satisfies the Neumann boundary condition on the waveguide walls, hence the continuous spectrum for this problem is $[0, \infty)$. For the $y-$antisymmetric problem the first cut-off is $\pi/2d$ and so the solutions can be considered to be non-embedded eigenvalues.

We computed the eigenvalues for the Neumann problem in the range $0 < k < k_1$. The variation of the non-dimensionalised trapped mode kd with the radius of the obstacle a/d is shown in Fig. 4.5, the minimum value being $kd \approx 1.32 \approx 0.42\pi$.

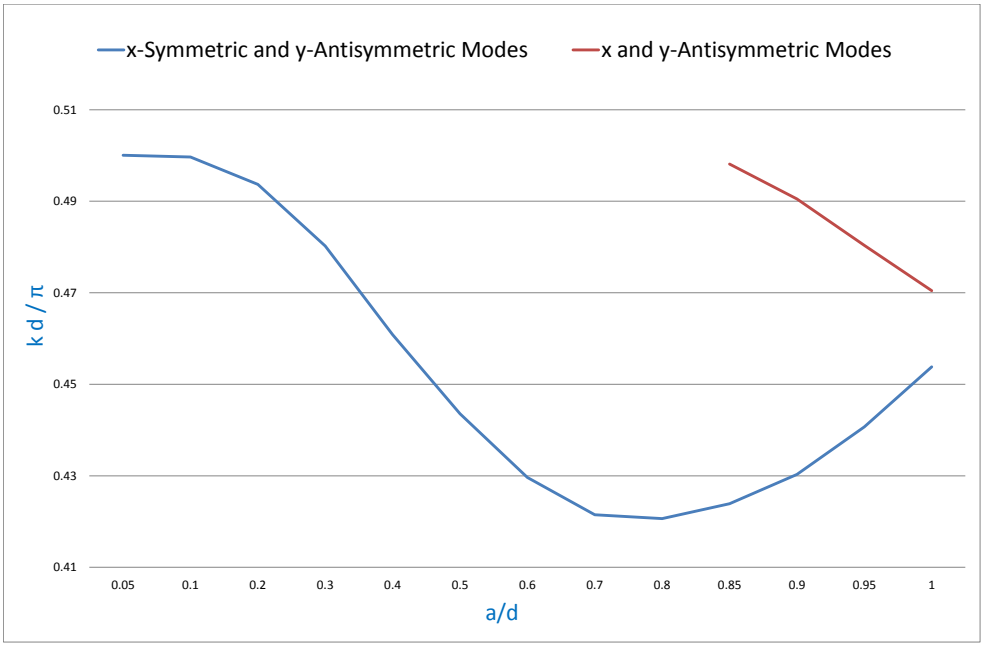

Figure 4.5: Variation of Neumann trapped-mode wavenumbers with the spacing parameter a/d. Notice the second mode, antisymmetric with respect to both x and y axes.

The solutions described above are stable in the sense that if the geometrical parameter a/d is varied continuously the trapped modes persist and the eigenvalues also vary continuously.

The limiting case $a/d \to 0$ is similar to the previous Dirichlet trapped modes case - as $a/d \to 0$, the trapped mode approaches the standing wave solution with slow decay down the guide.

For the $a/d \to 1$ we found two trapped modes, the second being anti-symmetric with respect to both axes. The first mode of this type is found for $a/d = 0.85$. We initially considered that the second modes may be due to errors which may appear due to computations carried out in the sharp region between the circle and the waveguide ($|x| \to 0$, $|y| \to d$) where the solution has a singularity. However, despite increasing the number of points N used to discretise the boundary, these second modes persisted. We subsequently found that the same modes were reported in a note by Evans and Porter [24]. They are also consistent with the results reported by Cobelli *et al.* who reproduced experimentally this case (see Chapter 1) and reported two resonance curves for discs $a/d \geq 0.85$ [16]. The variation with a/d, for the second type of modes, is also shown on Fig.(4.5). We notice that frequencies increase as $a/d \to 1$ for the first type of mode, whereas they decrease for the second mode.

These new solutions contradict the results reported by Callan [10], where all the solutions, constructed using multipole potentials, were found to be antisymmetric with respect to the x axis only. The values found using our program for both types of modes, for $a/d \geq 0.8$, are presented in Table (4.5).

	x-Symmetric y-Antisymmetric		x, y-Antisymmetric	
$\mathbf{a/d}$	$\mathbf{k_1 d}$	$\mathbf{k_1 d/\pi}$	$\mathbf{k_2 d}$	$\mathbf{k_2 d/\pi}$
0.85	1.33171	0.42389	1.56487	0.49811
0.90	1.35201	0.43034	1.54580	0.49204
0.95	1.38457	0.44070	1.51762	0.48307
1.0	1.38457	0.44070	1.51762	0.48307

Table 4.5: Two trapped modes are found for a sound-hard disc on the centre of a Neumann guide as the radius increases: $a/d \geq 0.85$.

Plots for two trapped modes found for a disc of radius $a/d = 0.85$ are presented in Fig. 4.6(a) - 4.6(b).

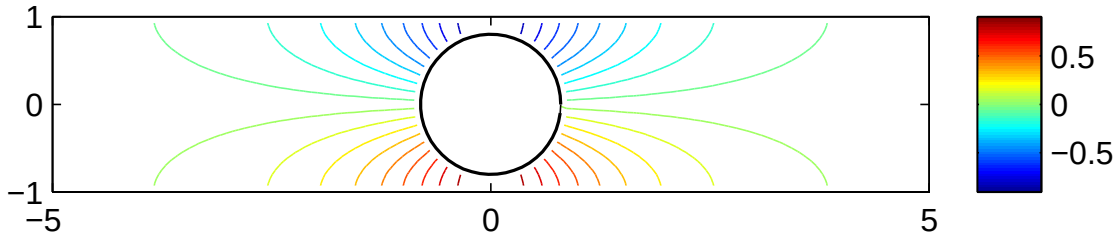

(a) Neumann trapped mode, $a/d = 0.85, kd \approx 1.33171 = 0.42389\,\pi$

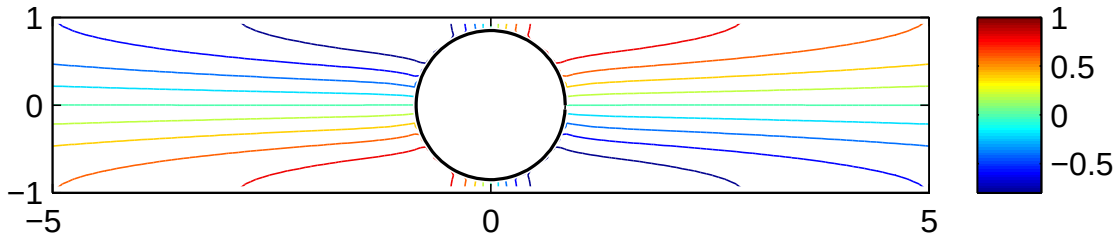

(b) Neumann trapped mode, $a/d = 0.85, kd \approx 1.56487 = 0.49811\,\pi$

Figure 4.6: Two trapped modes are found for the same case, Neumann waveguide with a disc on the centre of the guide, $a/d = 0.85$.

4.2.1.4 Disc on centre of Dirichlet waveguide, $k_1 < k < k_2$

Using the same approach we looked for eigenvalues in the range $k_1 < k < k_2$. The continuous spectrum of this problem is $[(\pi/d)^2, \infty)$, therefore any trapped mode found in this range are embedded. For this geometry only one embedded trapped mode exists in this range: $kd \approx 6.258 \approx 1.992\pi$ for $a/d \approx 0.267$. The presence of propagating waves restricts the values of a/d for which trapped mode exist. This is due to the need to satisfy a side condition which corresponds to forcing the amplitude of the travelling mode to be zero [**?**].

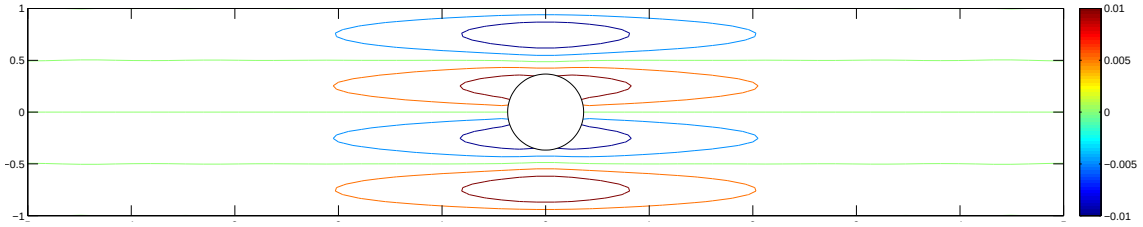

Figure 4.7: Dirichlet embedded trapped mode $kd \approx 6.258 \approx 1.992\pi$ for $a/d \approx 0.267$

This type of eigenvalue is unstable in the sense that it exists only for a particular geometry (in this case $a/d \sim 0.267$) and an arbitrary geometrical perturbation will destroy the eigenvalue. However, the mode is stable in the sense that if a geometrical parameter is varied

continuously in such a way as to maintain the validity of the operator decomposition into symmetric and anti-symmetric parts, then the eigenvalue varies continuously [4]. This principle applies to the case of a two-dimensional waveguide with a symmetric obstacle placed on the centreline. It was proved by McIver *et al.* [51] that the embedded trapped mode found for the Dirichlet waveguide with a circular obstacle on the centerline is a point on a continuous branch of modes for obstacles with shapes of the form $|x/a|^\nu + |y/a|^\nu = 1$, $1 \leq \nu < \infty$, the circle corresponding to $\nu = 2$.

4.2.2 Neumann waveguide with two rectangular symmetric indentations

Duan *et al.* [18] computed a series of trapped modes for the case of an infinite Neumann waveguide with a rectangular cavity. Acoustic resonances for a rectangular cavity and waveguide are well known and the problem allowed for a mode matching approach. The results were compared with resonances obtained numerically using a combination of the finite element method (FEM) and perfectly matched layer (PML). We were able to reproduce their results and an example of a symmetric mode found for $w/d = 5.987, h/d = 2$, $kd \approx 1.0500 = 0.334\pi$ is shown in Fig. 4.8.

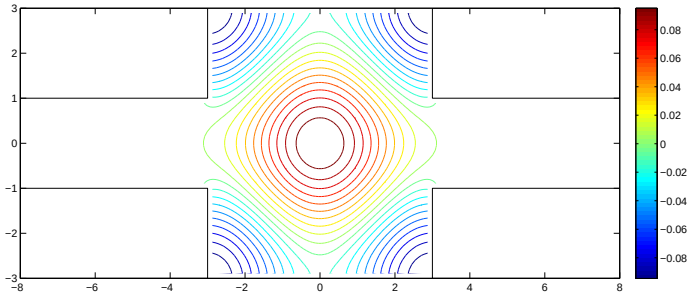

Figure 4.8: Neumann embedded trapped mode at frequency $kd = 1.0500 = 0.334\pi$ for $w/d = 5.987, h/d = 2$.

We have thus tested the boundary element program we devised to detect trapped modes for the Helmholtz equation in two dimensions. We established that it is accurate and reliable and were able to reproduce a large, varied set of published results, for a wide range of geometries, boundary conditions in both the embedded and non-embedded frequency regimes.

The results we presented in this chapter have already been obtained by other researchers using different methods and our intention was to reproduce them in order to validate and

refine our BEM program. In Chapter 5 we apply our method to extend these results and investigate new, more complex geometries.

Chapter 5

New results

The existence of the trapped modes presented in Chapter 4 has already been established [22] and associated calculations were reported in [10], [23] and [47]. All these solutions were obtained using different techniques from the one we developed and we reproduced them in order to test the validity of our approach and assess the accuracy of the boundary element program (BEM), prior to extending it to other, more complex configurations. Our method allows for easy modification of the domain and the addition of new elements so that the appearance of new modes may be investigated. In this chapter we present additional modes for geometries already studied and also some results for new structures. With one exception, for the cases presented in this chapter, to our knowledge, there are no published results neither in the context of acoustic nor water-wave problems. The exception is the case of non-embedded trapped modes for two, non-intersecting discs in an infinite waveguide. Our results are in agreement with those published by Evans and Porter [26] for the case of a long narrow wave channel containing any number of different size bottom mounted circular cylinders arbitrarily spaced along the centreline of the channel. As discussed in Chapter 2, these modes correspond to acoustic resonances, where the same governing equations and boundary conditions apply. Evans and Porter have already shown that there are no more than N trapped modes, in the range $0 < kd < \pi$, for any configuration of N cylinders, the precise number depending critically on the geometry of the configuration. We extend the existing results for this case by establishing the behaviour of these modes for intersecting discs, up to the point where they become a single disc. We also study this configuration for the next band of frequency values, $\pi < kd < 2\pi$.

All the geometries considered in this chapter include a 2-D infinite waveguide, consisting of a pair of two-dimensional parallel walls ($\Gamma_{\pm}$). Walls are such that $y = \pm d$ and the guide is parallel to the x -axis. Cartesian axes are chosen so that both x and y axes coincide with the horizontal and vertical guide centerlines respectively. A disc radius will be denoted a, with appropriate subscripts if necessary. For ease of notation, we now set $d = 1$, with the implicit assumption that all the spacing parameters in this chapter are non-dimensionalised by a factor of d. The boundary conditions on $\Gamma_{\pm}$ are either Neumann or Dirichlet. In those cases where one or more discs are added to the domain, the assumption is that they are sound hard discs, i.e. $\frac{\partial \phi}{\partial n} = 0$ on their boundaries. A disc radius will be denoted a, with appropriate subscripts if necessary. Two discs will be separated by a distance c, measured between their centres. We shall often relate c to the wavelength of the mode, which is defined, as is the usual convention, in wave theory

$$\lambda = \frac{2\pi}{k}. \tag{5.1}$$

In this chapter we present trapped mode result for the following geometries:

- Two sound-hard discs on the horizontal centreline of either a Neumann or a Dirichlet waveguide. The two discs are either similar or of different radii.
- Neuman and Dirichlet waveguides with rectangular, triangular and smooth cavities. The smooth cavity is modeled by a Gaussian function.
- A sound-hard disc on the horizontal centreline of either a Neumann or Dirichlet waveguide, with one rectangular cavity. The disc is either located on the vertical symmetry line of the cavity or removed from the centre, thus the geometry does not have any symmetry lines.

Throughout this chapter we shall refer to the trapped mode frequency for one single disc on the centreline of an infinite waveguide as the characteristic frequency and use the notation $k = k_c$.

5.1 Two discs on the centre of an infinite waveguide

In this section we present the trapped modes supported by two discs, placed on the centreline of an infinite waveguide. We consider both identical and different-sized discs and determine the trapped modes occurring in two k ranges: $0 < kd < \pi/2$ and $\pi/2 < kd < 3\pi/2$ for Neumann waveguides and $0 < kd < \pi$ and $\pi < kd < 2\pi$ for Dirichlet waveguides. The problem is either Dirichlet ($\mathbb{D}$) or Neumann ($\mathbb{N}$) as defined in Chapter 2. As mentioned in Chapter 2, the problems of acoustic resonances in an infinite waveguide with circular 2-D obstacles and of trapped modes in a 3-D long narrow channel with bottom-mounted cylinders are mathematically identical. The study of trapped modes in these configurations is motivated by the fact that it is possible to remove the channel walls and regard the solutions as oscillations between adjacent pairs of cylinders in a doubly infinite row, the Neumann modes having an antinode (the wave amplitude is a maximum) at each mid-plane between pairs of cylinders and the Dirichlet modes a node (the wave has minimal amplitude). It is then important to predict the trapped mode frequencies in view of the fact that such periodic arrays have important applications, for example to structures such as floating bridges, proposed designs for floating airports and other structures supported by bottom mounted cylinders, e.g. off-shore oil platforms [47].

For non-intersecting discs, Evans and Porter [24] already determined the trapped modes which can occur, for identical and different-sized cylinders, in both Neumann and Dirichlet waveguides, below the first cut-off. The solution obtained by Evans and Porter is based on the multipole method, in which singular solutions of the Helmholtz equation, satisfying an antisymmetry condition on the channel centreplane are modified to include the boundary condition on the channel walls. For further details we refer to [24] and references therein.

Throughout this chapter we shall refer to the trapped mode frequency characteristic to one disc on the centreline of the waveguide as $k = k_c$.

5.1.1 Two identical discs on the centreline of an infinite Neumann waveguide

5.1.1.1 $0 < k < \pi/2$

All modes are embedded since for any frequency in this range, at least one propagating mode exists. This propagating mode is a solution of the Helmholtz 2-D equation, which satisfies the boundary conditions on the waveguide walls and discs. For the case of one disc, of radius a, placed on the centre of an infinite Neuman waveguide it was established by Callan *et.al* [10] - and we were able to reproduce these results using our programme - that at least one trapped mode exists for all discs of radii $0 < a \leq 1$. All modes presented in this section are antisymmetric about the centreline of the waveguide. Henceforth, unless otherwise stated, symmetry references will apply to the x direction only.

Two discs of equal radius, placed on the centreline of the waveguide support either one or two trapped modes, depending on the distance between discs. There are some features which distinguish, qualitatively, between the modes found:

- For a small separation (see Appendix A), the value of which decreases with a, oscillations are captured between the two discs. We call these coupled modes as the two obstacles are connected by this non-decaying continuous wave.
- As c/a increases we find a lower frequency symmetric mode and a higher frequency antisymmetric mode for each configuration. The potential ϕ attains maximum/minimum values near each disc. The solution decays exponentially in the inner region and in the case of the anti-symmetric mode, the potential is zero at $x = 0$, so there is no energy transfer between the two parts of the guide.

To illustrate, we present in detail the case $a_1 = a_2 = 0.3$.

- $0 \leq c < 2a$
  For $c = 0$ we obviously have the single disc solution and $k = k_c = 1.5086 = 0.4802\pi$. As c increases, the object formed by the two intersecting discs supports a trapped mode at a frequency which decreases linearly with the spacing parameter c, up to the point where the discs separate ($c = 2a$) and $k = 1.2352 = 0.3931\pi$.

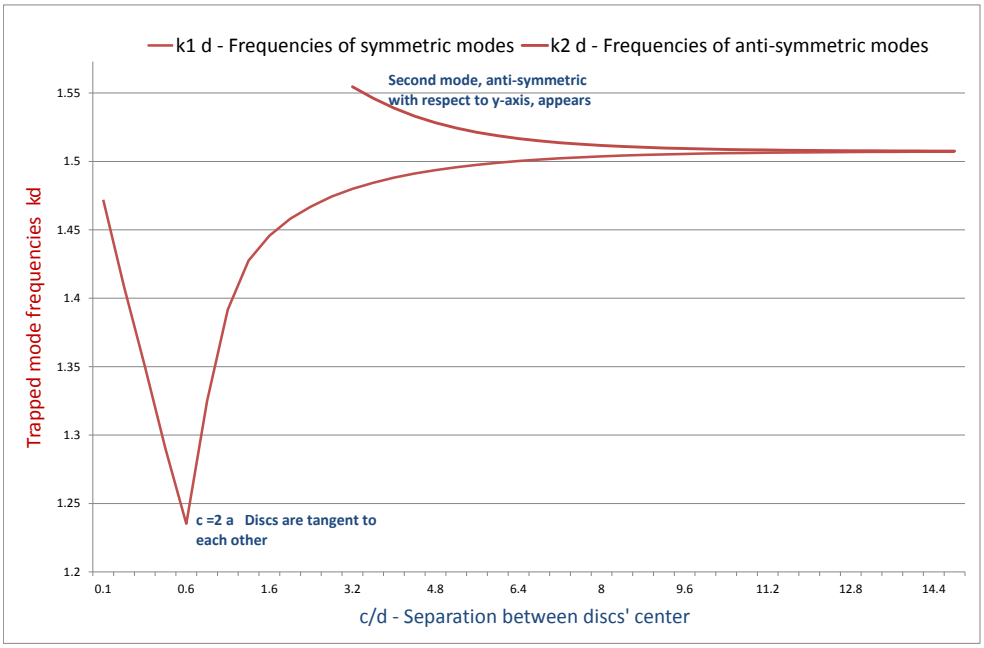

Figure 5.1: Trapped mode frequencies for two discs of equal radius, $a/d = 0.3$, placed on the centre of a Neumann waveguide

- $2a < c \lesssim \lambda$.

  A symmetric trapped mode, at a lower frequency, say $k_s < k_c$, envelopes the two discs and there is a standing wave between them. These are coupled modes as they are linked by the trapped oscillation and there is no exponential decay between discs.

- $c \approx \lambda$

  As the separation between discs increases, exponential decay appears in the inner region. There are relatively high amplitude waves localised around each disc but their interaction diminishes. At some point they become independent of each other and this new degree of freedom enables the appearance of a new, antisymmetric trapped mode, at a higher frequency ($k_c < k_a$). Figure 5.3 shows the two modes, symmetric and anti-symmetric for a disc of radius $a = 0.3$. The separation c required for the decoupling of the two oscillations is specific to the case discussed here, $a = 0.3$. As can be seen from the data in Appendix A, for other cases, the separation c required

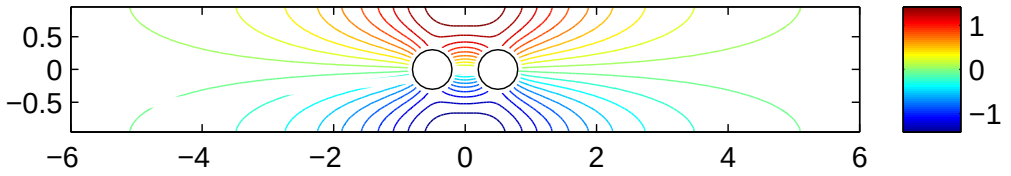

Figure 5.2: Coupled mode trapped by two discs of radius $a = 0.3$, separation distance $c = 1$. This geometry has only one trapped mode, at $kd = 1.4138 = 0.4502\pi$

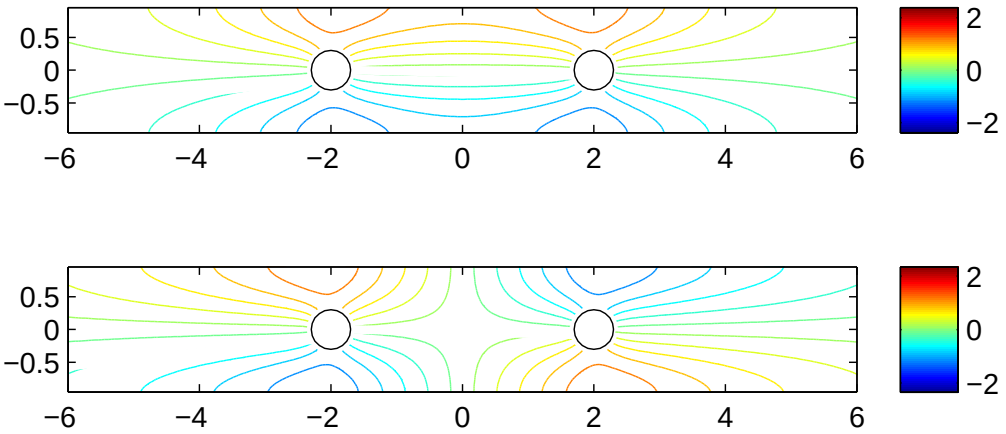

Figure 5.3: The same structure, two discs of $a = 0.3$, at distance $c = 4$ supports two trapped modes: symmetric, $kd \approx 1.4881 = 0.4739\pi$ and anti-symmetric, $kd \approx 1.5389 = 0.4901\pi$, with respect to the y - axis

for oscillations decoupling and the appearance of a second mode, decreases with the radius of the discs. For $a/d > 0.5$ the second mode will be found even for intersecting discs - see Appendix A.

- $c > \lambda$

  The two modes, symmetric and anti-symmetric persist and their frequencies converge to k_c -see Fig. 5.1.

  Figure 5.1 shows the evolution of trapped mode frequencies with the separation between discs. Each point on the computed curves corresponds to a trapped mode

and we can see that as $c \to \infty$ the trapped modes approach the single-disc results as the interaction between them diminishes. Trapped modes in this k range are stable in that varying the geometry continuously does not substantially change the whole picture. The sample presented here is sufficiently illustrative for this type of geometry. As results are similar for disc of other radii we relegate the relevant details to Appendix A .

5.1.1.2 Embedded modes, $\pi/2 < k < 3\pi/2$

As discussed in Chapter 2, section 2.3, as k increases through successive cut-off values, additional travelling modes are possible. It is likely that trapped modes exist for all frequency ranges, but for each additional propagating mode that is introduced, an extra geometrical parameter is required to satisfy side conditions which force the amplitude of these travelling modes to zero.

A single disc on the centre of a Neuman waveguide supports one embedded trapped mode, above the first cut-off ($\pi/2 < k < 3\pi/2$), [23], for $a = 0.352$ for a frequency

$$k_c d \approx 4.677 \approx 1.4896\pi.$$

The addition of another disc on the centreline of the Neumann waveguide, provides a new parameter, the separation distance c, which can be varied until a specific value will correspond to zero amplitude of the propagating modes. This rationale predicts that more than one trapped modes may exist for this geometry. Using our BEM program we established the following results for this frequency range

- Trapped modes exist for discrete couples (a, c) for small discs, $0 < a \leq 0.4$. Varying the spacing parameter in the range $0 < c < 4$, we found ten configurations which support trapped modes, both symmetric and antisymmetric. It is likely that for a given radius one might find an appropriate value of c such that a trapped mode might be detected in that geometry. These modes are difficult to detect as embedded eigenvalues are sensitive to minute changes in the geometry and can only be distinguished from the travelling modes when the exact combination of parameter values is used. The relevant parameters for these modes are presented in Table 5.1.

- All modes are y-antisymmetric. For larger separations both x-symmetric and anti-symmetric modes can be found. The x - symmetry for each mode found is specified for each case in Table 5.1.

- Each of these modes is accompanied by a large number of nearly trapped modes and they exist for all values of $0 < a < 0.4$ and slightly modified values of c. Although from a mathematical viewpoint, nearly trapped modes are not solutions to our problem, physically they are important as they would behave similarly in a domain which approximates that required for a genuine trapped mode. A list of nearly trapped modes is enclosed in Table 5.2.

- For a particular value of a more than one embedded trapped mode exists for different separations c. For example we identified a symmetric coupled mode, for $a/d = 0.25, c/d = 0.8$ at a lower frequency $kd \approx 4.4915 = 1.4296\pi$, and an antisymmetric one for $c = 1.9$ for a higher frequency, $kd \approx 4.6968 = 1.4950\pi$. Plots of both these modes are presented in Fig. 5.4.

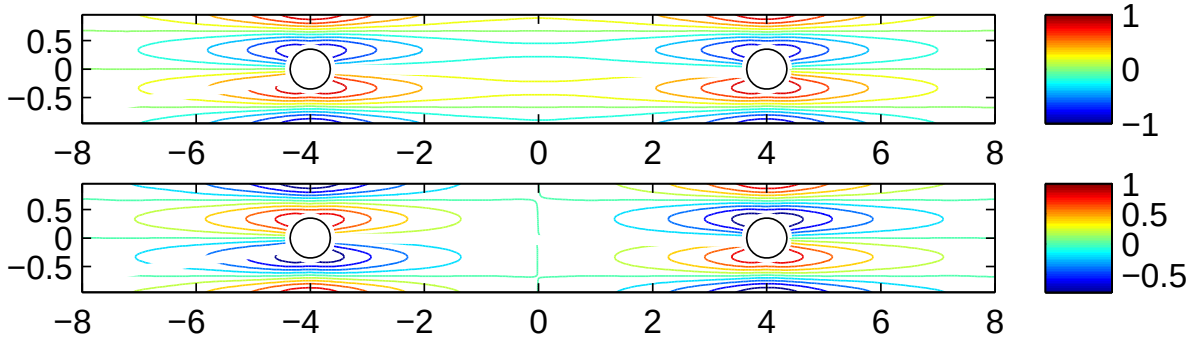

Figure 5.4: Trapped modes in a Neumann waveguide with two discs of radius $a = 0.352$ on its centreline, distance between centres $c = 8$ appear at frequencies $k_{\text{symmetric}} \approx 4.6771$ and $k_{\text{antisymmetric}} \approx 4.6792$.

- The largest radius of discs which we found to support an embedded trapped mode is $a \approx 0.4$ - a symmetric mode exists for $c = 1.9$. This exceeds the value $a \sim 0.352$ which is the only single disc case in this frequency range. The mode we found for

$a = 0.4$ is presented in Fig. 5.5.

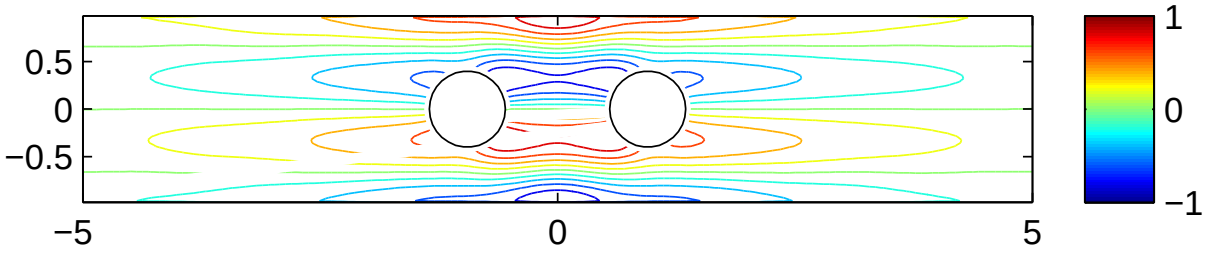

Figure 5.5: Trapped mode enveloping two discs of radius $a = 0.4$, at distance $c = 1.9$ for $kd \approx 4.6968 = 1.4950\pi$.

- Two discs with $a = 0.352$, placed on the waveguide centre do not support trapped modes but only nearly trapped modes, some with low energy radiation, which can be computed as detailed in section (4.2.1.1). For $0 < c \lesssim 1$, i.e. including intersecting discs but not fully overlapping, the geometry does not support trapped modes. For $c \approx 1$ a symmetric mode appears at a frequency lower than k_c. Increasing the separation to $c \approx 2.6$ we find an anti-symmetric mode, at a slightly higher frequency than k_c - see (5.2). The solutions feature two independent, non-interacting, high amplitude oscillations confined in regions around each disc - see Fig. 5.4. The antisymmetric mode is decoupled, in the sense discussed above, the solution decays exponentially in the inner region between discs and so there is little interaction between the waves localised around the two obstacles.

$$k_{\text{symmetric}} \approx 4.457 < k_c = 4.677 < k_{\text{antisymmetric}} \approx 4.682. \tag{5.2}$$

5.1.2 Two discs of different radii on the centre line of a Neumann waveguide

In this section the geometry consists of two discs of different radii, $a_1 = 0.3$ and $a_2 = 0.7$, with Neumann boundary conditions on all surfaces. We look for trapped modes in the range

a	c	kd	kd/π	x - Symmetry
0.125	3.60	4.656108	1.482085	Symmetric
0.250	0.80	4.491496	1.429687	Symmetric
0.250	1.20	4.692561	1.493688	Antisymmetric
0.275	2.80	4.634083	1.475074	Antisymmetric
0.300	3.60	4.625632	1.472384	Symmetric
0.325	1.00	4.457053	1.418724	Symmetric
0.325	2.60	4.682178	1.490383	Antisymmetric
0.350	2.60	4.659922	1.483299	Symmetric
0.350	3.90	4.689750	1.492793	Antisymmetric
0.400	1.90	4.696900	1.495070	Symmetric

Table 5.1: Embedded trapped modes supported by two identical discs placed on the centre of a Neumann waveguide.

$0 < k < \pi/2$ which are anti-symmetric about the centreline of the guide. As $\pi/2$ is the first cut-off value all eigenvalues which are found in this range are non-embedded. Solutions corresponding to non-embedded frequencies are stable, in that varying the geometry does not destroy the trapped mode, it only modifies the value of k.

The characteristic trapped mode frequencies are $k_{c1} = 1.5086 = 0.4802\pi$ for an isolated disc of $a = 0.3$ and $k_{c2} = 1.3241 = 0.42148\pi$ for $a = 0.7$ respectively. We present below our main findings for this case. Further details of trapped mode frequencies are enclosed in Appendix A.

Depending on the distance c between the discs, there are either one or two trapped modes for each geometry:

- Overlapping discs, $0 < c < (a_1 + a_2)$

  A single trapped mode is found for all c in this range, at a frequency near the char-

a	**c**	**kd**	**kd/π**	x **Symmetry**
0.1	0.7	4.6462	1.4789	Symmetric
0.15	0.7	4.5582	1.4340	Symmetric
0.2	0.9	4.5051	1.4509	Symmetric
0.3	0.9	4.5433	1.4462	Symmetric
0.38	1.8	4.7012	1.4964	Symmetric

Table 5.2: Nearly trapped modes supported by two identical discs placed on the centre of a Neumann waveguide.

acteristic frequency for the larger disc. As the distance between discs increases, the trapped mode frequency decreases linearly with the separation c until it reaches a minimum frequency of $kd = 1.1342 = 0.3610\pi$, for $c = 1$, i.e. the discs are tangent to each other.

- $a_1 + a_2 < c < 2.2 \sim 0.4\lambda$

  The discs are separated but the distance between them does not permit the decoupling of oscillations. In this geometry only one trapped mode is found at a frequency nearer to the frequency characteristic of the larger disc $k \to k_{c2}$. As $k_{c2} < k_{c1}$, the wavelength corresponding to the larger disc, of $a = 0.7$, is greater than that for the smaller disc. It makes geometric sense that the trapped mode is found for a frequency nearer to k_{c2} as the wavelength must accommodate both discs and satisfy the required boundary conditions. Oscillations are present around both discs with higher amplitudes near the larger disc where the potential ϕ attains its maximum and minimum. This type of solution is illustrated in Fig. 5.7.

- $2.2 \approx 0.4\lambda < c$

  Two trapped modes exist, a symmetric mode, at a lower frequency say k_s, and an antisymmetric mode, at a higher frequency k_a, for each geometry. The symmetric mode has stronger perturbations localised around the larger disc, with $k_s < k_{c1}, k_s \to k_{c1}$. The antisymmetric mode has maximum and minimum amplitudes around the

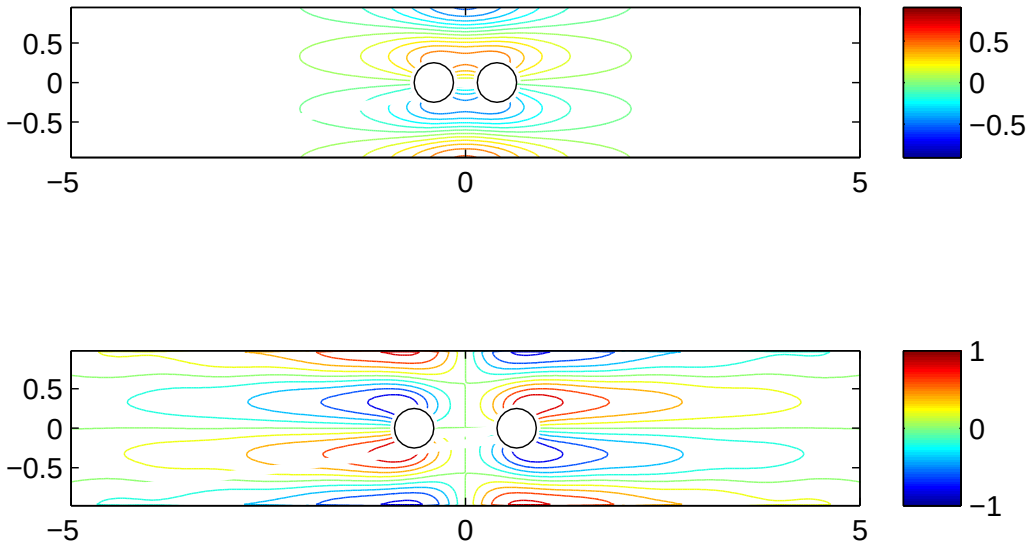

Figure 5.6: Two discs of radius $a/d = 0.25$, placed at different distances, c, support two embedded modes: symmetric, $c = 0.8$, for $kd \approx 4.4914 = 1.4296\pi$ and anti-symmetric, $c = 1.3$, $kd \approx 4.6925 = 1.4936\pi$.

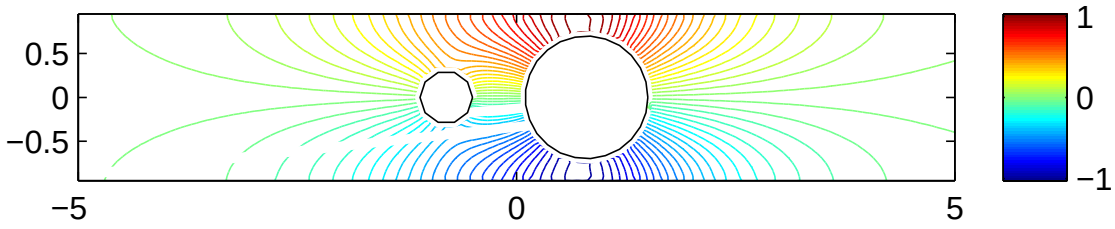

Figure 5.7: Contour plot of trapped mode enveloping two discs of radii $a_1 = 0.3, a_2 = 0.7$, separated by a distance $c = 1.6$, and at a frequency $kd \approx 1.2802 = 0.4075\pi$.

smaller disc, with frequencies $k_a < k_{c2}, k_a \to k_{c2}$.

Figure 5.8 shows the variation of k with the distance between disc centres, for the two type of modes.

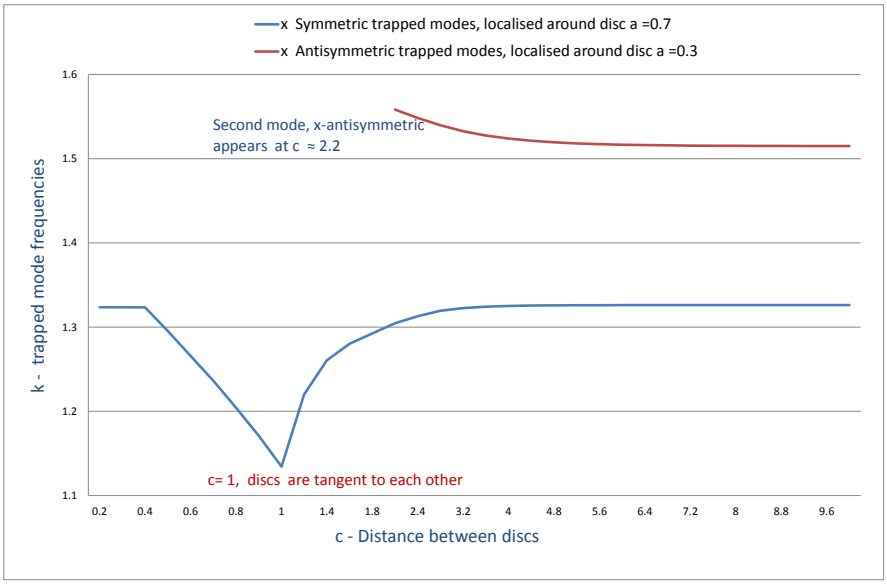

Figure 5.8: Variation of trapped mode frequencies with the distance between two discs with radii $a_1 = 0.3$ and $a_2 = 0.7$. The discs are placed on the centreline of a Neumann waveguide.

5.1.3 Two identical discs on the centreline of a Dirichlet infinite waveguide

One trapped mode, with frequency below the first cut-off, $0 < kd < \pi$, can be found for all discs on the centre of a soft (satisfying the Dirichlet boundary condition, $\phi = 0$), infinite waveguide, as long as $0 < a/d \lesssim 0.67$ as reported by Maniar et. al [47] and Callan [10]. For $\pi/d < kd < 2\pi$, a trapped mode exists only for $a \approx 0.267$, see Porter [23] and Linton [43]. Two discs, of equal radius, $0 < a \leq 0.67$, on the center of a Dirichlet waveguide, support one or two trapped modes. The second mode can be found only for discs such that $0 < a < 0.6$ and only if the separation parameter is above a certain value, depending on the disc size.

5.1.3.1 Frequency range: $0 < kd < \pi$

In this frequency range we find at least one trapped mode for every geometry, as long as $a_1, a_2 \lesssim 0.67$, irrespective of the distance between discs. The modes are stable, in the

sense that the frequency varies continuously as we increase the separation, the only abrupt change is the appearance of a second mode when the spacing parameter c reaches a certain value. We present below in detail the case $a = a_1 = a_2 = 0.3$. The frequencies for trapped modes for all other cases studied are enclosed in Appendix A.

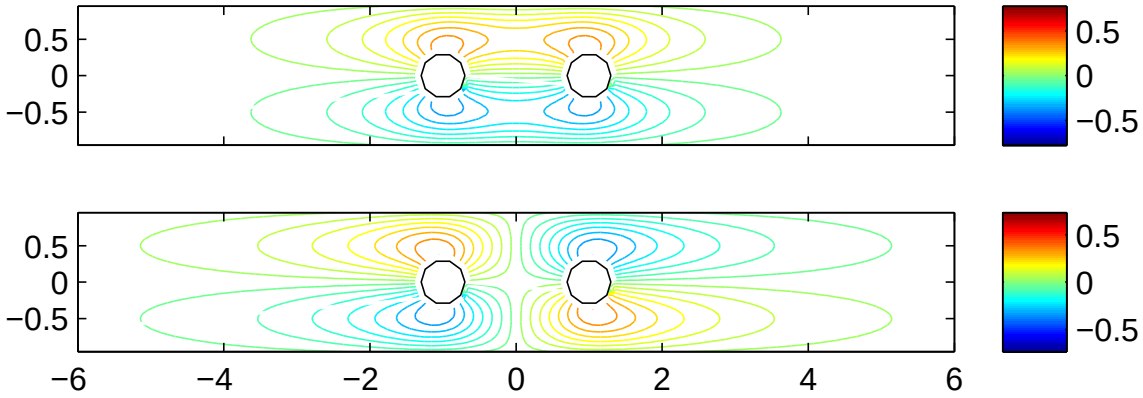

Figure 5.9: Two discs of $a = 0.3$, placed on the centreline of an infinite Dirichlet waveguide, at a distance $c = 2$ from each other, support two trapped modes: $x-$ symmetric, $kd \approx 2.9595 = 0.9420\pi$ and $x-$antisymmetric, $kd \approx 3.0670 = 0.9762\pi$.

- $0 < c \leq 2a$

  Two intersecting discs support a trapped mode at a frequency which decreases linearly with the separation, from a starting value of $k = k_c$, when $c = 0$, to $kd = 2.7852 = 0.8865\pi$, when the discs are tangent to each other.

- $2a < c < 1.2 \approx 0.55\lambda$

  A coupled, symmetric mode is supported by these geometries, its frequency increases with the separation c.

- $1.2 \approx 0.55\lambda < c$

  Two trapped modes exist in this range, with high amplitude oscillations localised around each disc. Frequencies for the symmetric and anti-symmetric modes are such that

$$k_{symmetric} < k_c < k_{antisymmetric}. \tag{5.3}$$

Plots of two such modes, for the same geometry, are enclosed in Fig. 5.9.

The second mode, antisymmetric does not exist for $0.6 \geq a$, as indeed mentioned by Evans and Porter [24]. However, for larger discs we found another type of mode which, although is not a solution to our problem, in that it does not satisfy condition (2.9), is still notable in the context of trapped modes. The maximum amplitude of oscillations in the inner area is $\approx 10^3$ higher than in outer area. Although theses are not trapped modes from a mathematical viewpoint, the high amount of energy present between the discs, in comparison with the amount that dissipates, could be of importance in predicting the exciting forces on individual cylinders within a large periodic arrangement of circular obstacles. These modes are symmetric with respect to the guide centreline and can be either symmetric or anti-symmetric in x. For large distances between circles more than one mode can be found for the same geometry. An example of such a mode, for $a = 0.7$, is presented in Fig. 5.10.

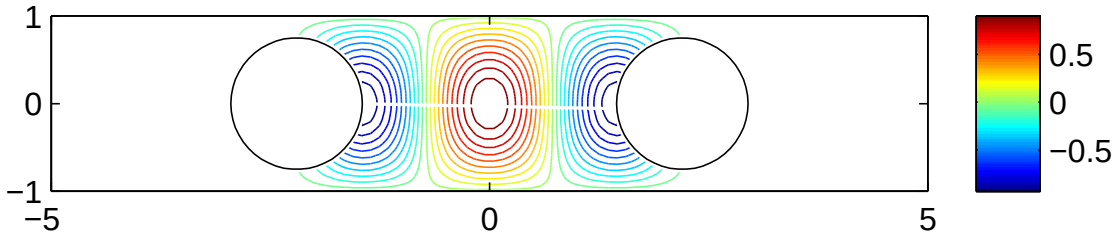

Figure 5.10: (x, y) Symmetric mode for $a = 0.7$, $c = 4.4$ and $kd \approx 2.6497 = 0.8434$.

5.1.3.2 Frequency range $\pi < kd < 2\pi$

For one disc on the centreline of an infinite Dirichlet waveguide only one embedded mode exists in this range, for a specific value of a [43].

$$kd \approx 6.258 \approx 1.992\pi, \ a/d \approx 0.267. \tag{5.4}$$

We refer to section (2.3) where we discussed that in embedded regimes the presence of propagating modes requires side conditions which force the amplitude of these travelling

modes to zero. In this k range we have one propagating mode but we also have an additional parameter, c which can be varied until a trapped mode is found. Our results show that trapped modes can be found for discs of all radii such that $a \lesssim 0.3$ at discrete values of c. Some disc sizes support more modes in this frequency range than others. For distances $0 < c < 4$, a disc with $a = 0.125$ has three trapped modes whereas for a slightly smaller disc, for $a = 0.1$, only one mode was found. The list of modes found for this geometry is given in Table 5.3. It is probable that as the distance between discs is increased more modes can be found for additional values of c for small discs but not for larger discs. In Fig. 5.11(a) - 5.11(c) we present three trapped modes for the same disc, with radius $a = 0.125$. The first plot, Fig. 5.11(a), corresponds to a small separation between discs $c = 0.6$. A second mode appears at a slightly larger separation, $c = 1.75$. Both these modes are symmetric in x and antisymmetric in y. As the distance increases, a third mode, anti-symmetric in both x and y, appears at $c = 3.35$. It is probable that more modes can be found for additional, larger c.

5.1.4 Two discs of different radius on the centreline of an infinite Dirichlet waveguide

In this section we present the results for the case of two discs, with radii $a_1 = 0.2, a_2 = 0.5$, placed on the centreline of a soft waveguide. The discs have individual characteristic trapped mode frequencies, $k_{c1}d = 3.0561 = 0.9728\pi, k_{c2}d = 3.07145 = 0.9776\pi$. This type of geometry has either one or two trapped modes, depending on the separation between the discs. The modes are stable in the sense that frequencies vary continuously with c, they are antisymmetric about the guide centreline and they can be either symmetric or anti-symmetric in x. The symmetric mode has the highest amplitude oscillations localised around the smaller disc, with $k_s < k_{c1}, k_s \to k_{c1}$ and the anti-symmetric mode is localised around the boundary of the larger disc, with $k_a > k_{c2}, k_a/d \to k_{c2}$. Fig. 5.12, shows the frequencies of the two type of trapped modes and their variation with c. As the distance between discs changes we distinguish three stages in the appearance of trapped modes and how they modify their qualitative features:

- $0 < c < a_1 + a_2$

  One symmetric trapped mode exists for all c, with frequencies decreasing linearly with c.

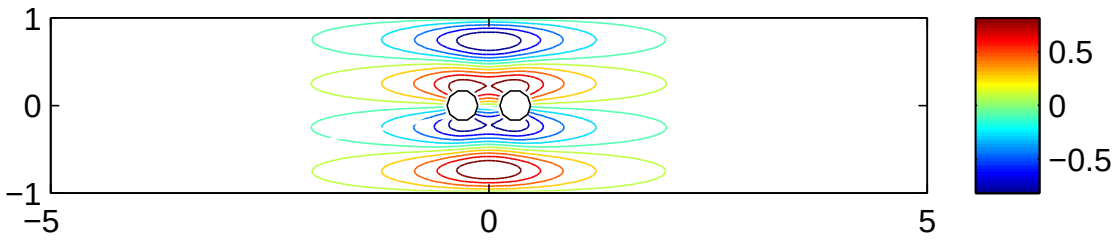

(a) First embedded trapped mode, for a disc of radius $a/d = 0.125$, at $kd \approx 6.1313 = 1.9516\,\pi$ and distance between discs $c/d = 0.6$.

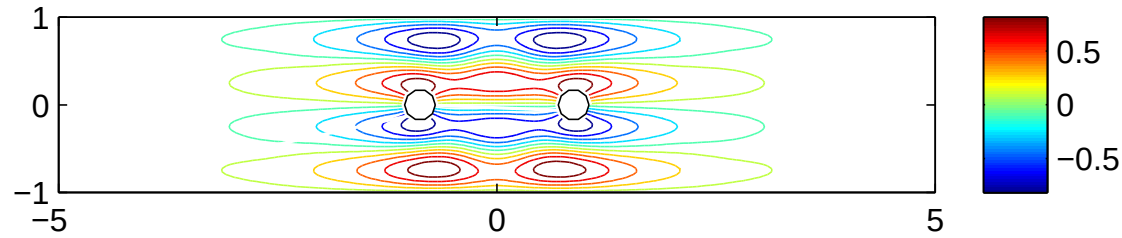

(b) Second embedded trapped mode, for a disc of radius $a/d = 0.125$, at $kd \approx 6.1897 = 1.9702\,\pi$ and distance between discs $c/d = 1.75$.

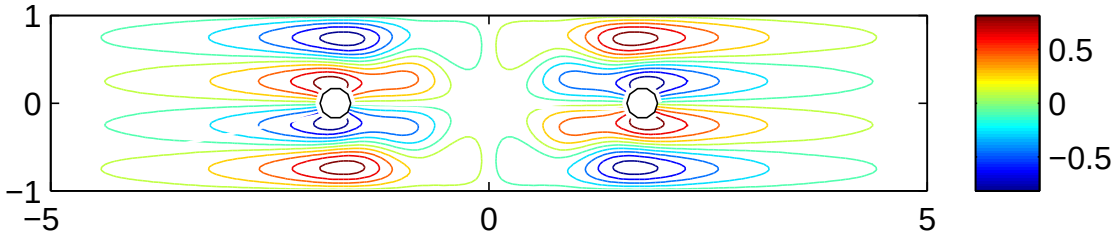

(c) Third embedded trapped mode, for a disc of radius $a/d = 0.125$, at $kd \approx 6.2188 = 1.9795\,\pi$ and distance between discs $c/d = 3.5$.

Figure 5.11: Three embedded modes, $\pi < kd < 2\pi$ for two identical discs on the centreline of a Dirichlet waveguide

- $a_1 + a_2 \leq c < \lambda$

  A second mode, antisymmetric in x appears, at a higher frequency. The symmetric mode is coupled in the sense that there is oscillation between discs. The antisymmetric mode is decoupled, as exponential decay appears in the inner area and the waves localised around each disc are almost independent of each other.

- $3\lambda < c$

  As the distance between obstacles increases, the energy distribution between the two discs becomes skewed and the trapped mode tends to be localised around only one disc: the symmetric mode has potential minimum/maximum on the boundary of the

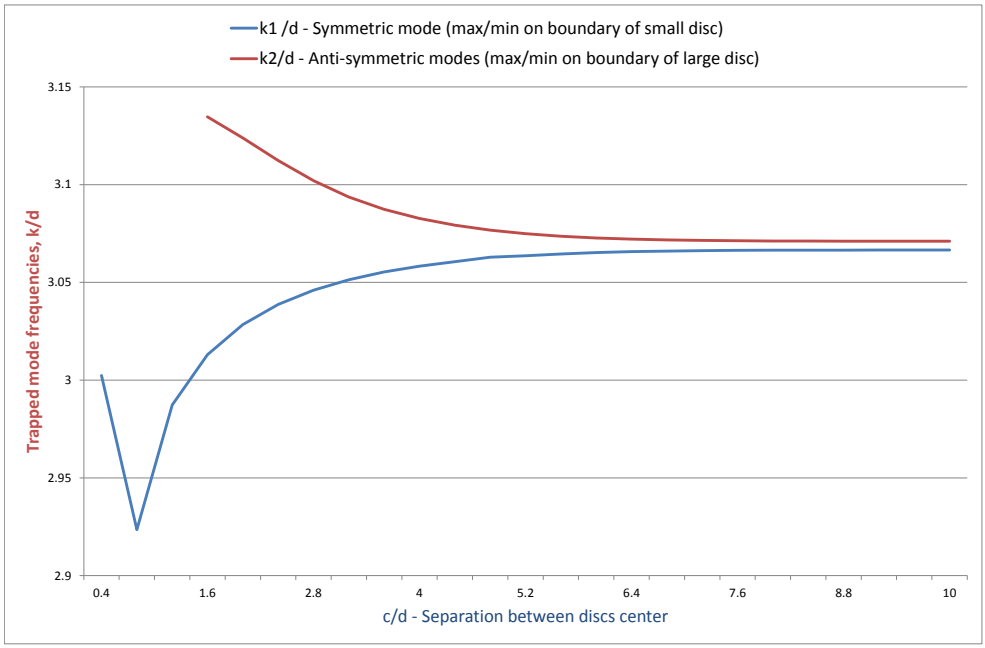

Figure 5.12: Trapped mode frequencies for two discs with radii with $a_1 = 0.2, a_2 = 0.5$, placed on centre of soft infinite waveguide

smaller disc, with $k_s < k_{c1}, k_s \to k_{c1}$ as $c \to \infty$. We also note that the anti-symmetric mode has the highest amplitude oscillations on the boundary of the larger disc, with $k_a > k_{c2}, k_a \to k_{c2}$. In Fig. 5.13 five trapped modes are plotted as follows:

- Panel 1: one trapped mode with $c = 1.6$ at $kd \approx 2.9873 = 0.9508\pi$.
- Panels 2 and 3: two trapped modes, for same geometry, one symmetric and one anti-symmetric, $c = 3.6$ at $kd = 3.0553 \approx 0.9725\pi$ and $kd \approx 3.0873 = 0.9827\pi$ respectively.
- Panels 4 and 5: two trapped modes, for same geometry, symmetric and anti-symmetric, $c = 6$, for $kd \approx 3.0652 = 0.9756\pi$ and $kd \approx 3.0727 = 0.9780\pi$. Notice the skewed distribution of velocity potential ϕ between the two discs.
- Panels 6 and 7: two trapped modes, for same geometry, symmetric and anti-symmetric, $c = 8$ for frequencies $kd \approx 3.0664 = 0.9760\pi$ and $kd = 3.0711 = 0.9775$ respectively. Notice that in each case there are strong oscillations in the

vicinity of one disc and $\phi \to 0$ in the neighbourhood of the other disc.

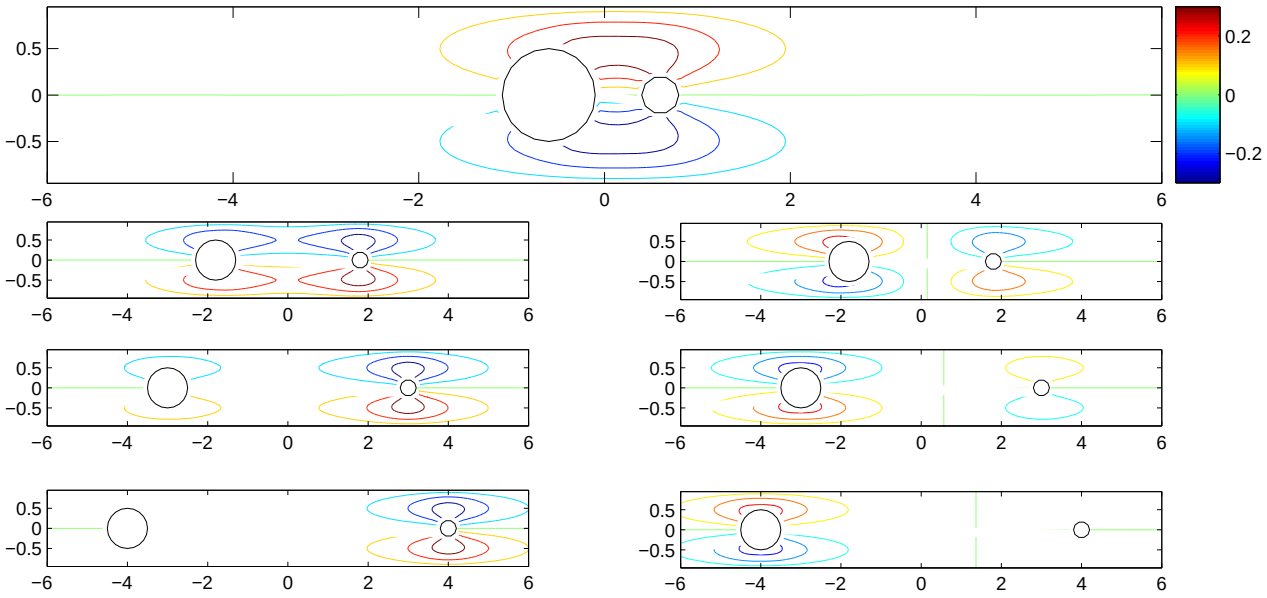

Figure 5.13: Trapped mode solutions for two discs with radii with $a_1 = 0.2, a_2 = 0.5$, placed on centre of a soft infinite waveguide for four values of the spacing parameter $c = 1.6, 3.6, 6$ and 8.

a	**c**	**kd**	**kd/π**	x **Symmetry**
0.100	0.60	6.2831	1.9999	Symmetric
0.125	0.60	6.1313	1.9516	Symmetric
0.125	1.75	6.1897	1.9702	Symmetric
0.125	3.50	6.2188	1.9795	Antisymmetric
0.175	0.62	6.0866	1.9374	Symmetric
0.175	1.75	6.1652	1.9624	Symmetric
0.175	2.30	6.2108	1.9769	Antisymmetric
0.225	0.65	6.1368	1.9534	Symmetric
0.225	1.75	6.1963	1.9723	Symmetric
0.250	0.75	6.1850	1.9687	Symmetric
0.250	1.75	6.2216	1.9804	Symmetric
0.250	1.75	6.2412	1.9843	Symmetric
0.275	1.30	6.2412	1.9866	Symmetric
0.295	1.55	6.2703	1.9959	Symmetric

Table 5.3: Embedded trapped modes supported by two identical discs on the centreline of a Dirichlet waveguide.

5.2 Infinite waveguides with cavities

In this section we present results for rectangular, triangular and smooth cavities in an infinite, 2-D infinite waveguide, consisting of a pair of two-dimensional parallel walls $(\Gamma_{\pm})$ at $y = \pm d$. The boundary conditions will be either Neumann or Dirichlet on the waveguide walls with the usual decay condition at infinity (2.9).

5.2.1 Rectangular cavity in a Dirichlet waveguide

First we consider the problem of a rectangular cavity of depth h and width $2w$ in a Dirichlet infinite waveguide. The trapped modes for this problem can be either resonances in soft acoustic waveguides or bound states in quantum waveguides [11], [29]. The latter are narrow two dimensional quantum waveguides, composed of tiny strips of a very pure semiconductor material, that allow electrons to propagate but require the wave function to vanish on the surface. We keep $h/d = 1$ fixed, vary w/d and seek trapped modes in the range $0 < kd < \pi/2$. For small widths of the cavity, the eigenmode rate of decay with distance x is small and the trapped mode frequency is close to the cut-off frequency $\pi/2d$. As $w \to 0$, the solution approaches the non-trapped standing wave solution $\phi \sim \cos \frac{\pi}{2d} y$. A simple analysis predicts the appearance of trapped modes as follows: for generality we consider both symmetric and anti-symmetric solutions, with respect to the x-axis. If we assume simple separable solutions of the Helmholtz equation in a waveguide

$$\phi = X(x) \cdot Y(y), \tag{5.5}$$

in this regime of k values, the first cut-off prescribes, far away from the cavity, solutions of the form

$$\phi \approx \exp\left\{ \pm i \left[k^2 - \left(\frac{\pi}{2d} \right)^2 \right]^{\frac{1}{2}} x \right\} \cos\left(\frac{\pi y}{2d} \right). \tag{5.6}$$

If $kd < \pi/2$, this y - symmetric oscillation cannot propagate down the guide. We now assume that w is large and consider the region of the cavity separately. In the centre of the cavity, for $|x| \to 0$, in order to satisfy the Dirichlet boundary condition on $y = d$ and

$y = -d - h$, the y component of the solution should behave like

$$Y(y) \simeq \cos\left[\frac{\pi}{2}\left(\frac{y + h/2}{d + h/2}\right)\right] = \cos\left[\mu_2(y + h/2)\right], \tag{5.7}$$

so that the wavevector is $\boldsymbol{\mu} = (\mu_1, \mu_2)$ with

$$\begin{aligned} \mu_1 &= \sqrt{k^2 - \mu_2^2}, \\ \mu_2 &= \frac{\pi}{2}\left(\frac{1}{d + h/2}\right), \end{aligned} \tag{5.8}$$

prescribing the x-dependency inside the cavity as

$$X(x) \simeq e^{(\pm i\mu_1 x)} = \exp\left[\pm i\left(k^2 - \mu_2^2\right)^{\frac{1}{2}} x\right]. \tag{5.9}$$

If k is such that

$$\frac{\pi}{2d + h} < k < \frac{\pi}{2d}, \tag{5.10}$$

oscillations are possible in both the x and y directions in the region of the cavity, but not in the rest of the guide. A wave inside the cavity would be effectively trapped there as it would not be permitted to propagate down the guide. This is obviously an over-simplification of the problem, a real trapped mode has a far more complicated structure than that assumed above. However, this is the non-embedded regime and due to the simplicity of the geometry, this argument renders the appearance of trapped modes plausible. Also, if we consider the Dirichlet boundary condition on the vertical walls of the cavity, at $x = \pm w$ we require

$$X(w) = \cos \mu_1 w = 0, \tag{5.11}$$

and this gives us an approximation for the minimum width of the cavity for a trapped mode

$$\mu_1 w = \frac{\pi}{2}. \tag{5.12}$$

This condition, together with (5.10), predicts that for $w/d \approx 1.34$ y-even modes are possible inside the cavity but not down the guide. And indeed for $1.3 \lesssim w/d$ we find an x-symmetric trapped mode for all cavities. This expression also serves as an approxima-

tion for k. These approximations for k, though not the frequencies of the mode themselves, are a useful indicator of the range of values which should be checked numerically for the actual trapped mode, saving significant computation time.

$$k \approx \sqrt{\left(\frac{\pi}{2d+h}\right)^2 + \left(\frac{k_n}{w}\right)^2}, \tag{5.13}$$

where we denote the cut-off values $k_n = \pi/2, \pi, 3\pi/2, 2\pi, ...$

For example if we look at a cavity of $h = 1, w = 2.8$, according to the above formula a trapped mode should appear for roughly $kd \approx 1.1879 = 0.3781\pi$. We find using our boundary element program the first trapped mode for this geometry has $kd = 1.1524 \approx 0.3668\pi$. We also see that (5.13) predicts that k will decrease as the width of the cavity increases, which is consistent with the values we found.

As the width of the cavity increases, additional, x-antisymmetric, modes appear for the same geometry. These new solutions appear for new values of k which satisfy approximately

$$\mu_1 w = \pi. \tag{5.14}$$

Following the same route as above, we find that the new trapped modes exist for all $w \gtrsim 2.2$. As we increase w more trapped modes are found as new eigenvalues can be found satisfying the condition

$$\mu_1 w = k_n. \tag{5.15}$$

This example and the simple analysis developed illustrates how the existence and the values of trapped modes is determined by the relationships between various geometric parameters.

We now look at trapped modes in the range $\pi/2 < kd < \pi$. These modes are embedded and exist for discrete couples (w, h). There are only a few values we found which support trapped modes in this range and they are tabulated in Table 5.4 below. To find these eigenvalues we used a boundary element step of $l = 0.1$ and $l = 0.05$ hence the spacing parameters h and w displayed in Table 5.4 have an expected error in the range $0.05 - 0.1$.

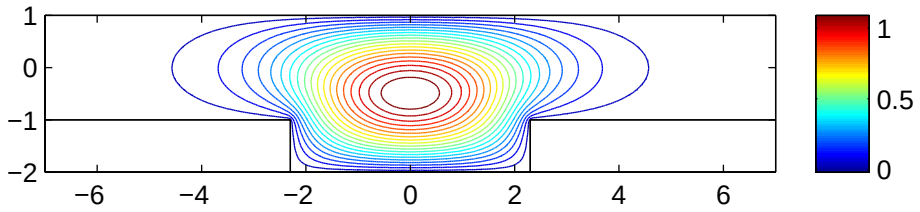

(a) Dirichlet, first trapped mode, for $w = 2.3, h = 1$ at $kd \approx 1.1943 = 0.3801\,\pi$,

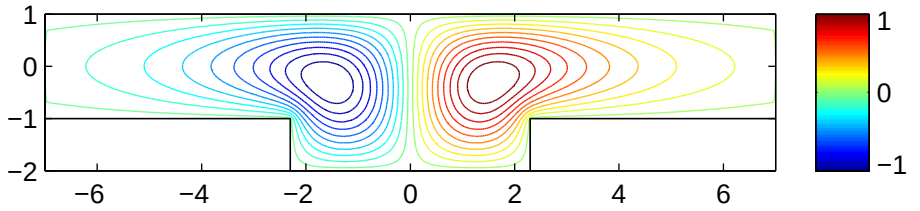

(b) Dirichlet, second trapped mode, for the same geometry, at $kd \approx 1.5028 = 0.4783\,\pi$.

Figure 5.14: Two non-embedded trapped mode for a cavity in a Dirichlet waveguide.

One notable geometry we found is the cavity with $h = 2.2, w = 2.9$ which supports two trapped modes, at two different frequencies, $k_1 d \approx 2.7361 = 0.8709\,\pi$ (see Fig. 5.15(a) for solution contour plot) and $k_2 d \approx 3.03302 = 0.9654\,\pi$ (see Fig. 5.15(b)).

5.2.2 Smooth cavity in a Dirichlet waveguide

Whilst searching for trapped modes in a rectangular cavity we found that if we smoothed slightly the sharp corners at the top of the cavity, the trapped mode would disappear. This raised the question about the role of corner singularities in the formation of trapped modes and whether a smooth cavity would support trapped modes. We considered a Dirichlet waveguide with a smooth lower boundary, modelled by a Gaussian function

$$\Gamma_-(x) = -d - h \cdot e^{\frac{-x^2}{w}}. \tag{5.16}$$

Keeping $h/d = 1$ fixed we checked the frequencies range $0 < kd < \pi/2$ and found that non-embedded trapped modes exist for all w/d and their k-values vary continuously with the geometry as illustrated in Fig. 5.16.

h/d	w/d	kd	kd/π
2	1.9	2.4819	0.7900
2.2	2.9	2.7361	0.8709
2.2	2.9	3.0330	0.9654
2.6	1.4	2.9022	0.9238
3.0	1.7	2.6566	0.8456
3.0	1.95	2.6212	0.8343
2.1	2.6	2.3726	0.7552

Table 5.4: Embedded trapped modes supported by a rectangular cavity in a Dirichlet waveguide.

Embedded modes in the higher frequency range, $\pi/2 < kd < \pi$, exist only for discrete pairs (h, w) and the details for two such modes are presented in Table 5.5.

h/d	w/d	kd	kd/π
3	1.80	2.3442	0.7461
2.6	0.80	2.7473	0.8745

Table 5.5: Embedded trapped modes supported by a cavity with a Gaussian curvature in a Dirichlet waveguide.

5.2.3 Triangular cavities in a Neumann waveguides

The case of Neumann trapped modes for rectangular cavities was discussed in section (4.2.2). The flexibility built into our program allows us to investigate trapped modes in other cavities. We looked at a triangular indentation with depth h and upper width w and found that trapped modes exist for discrete couples (h, w) and these geometric parameter values are similar to those which support trapped modes in the case of rectangular cavit-

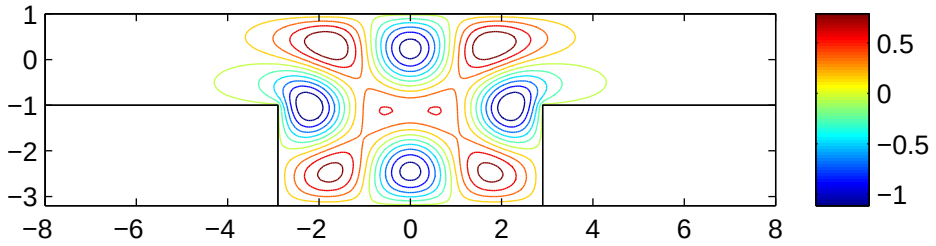

(a) Dirichlet, embedded, first trapped mode, for $w = 2.9, h = 2.2$ at $k_1 d \approx 2.7361 = 0.8709\,\pi$,

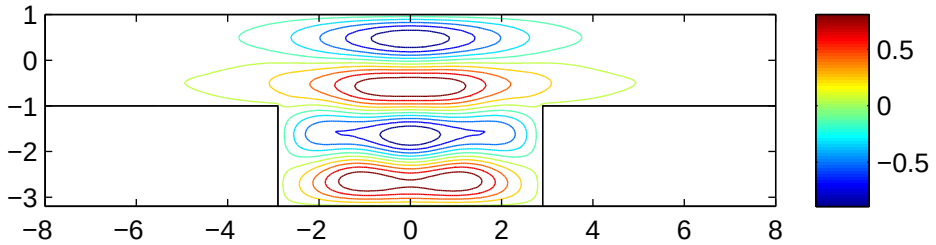

(b) Dirichlet, embedded, second trapped mode, for the same geometry, at $k_2 d \approx 3.0330 = 0.9654\,\pi$.

Figure 5.15: Two embedded trapped modes for the same rectangular cavity, in a Dirichlet waveguide.

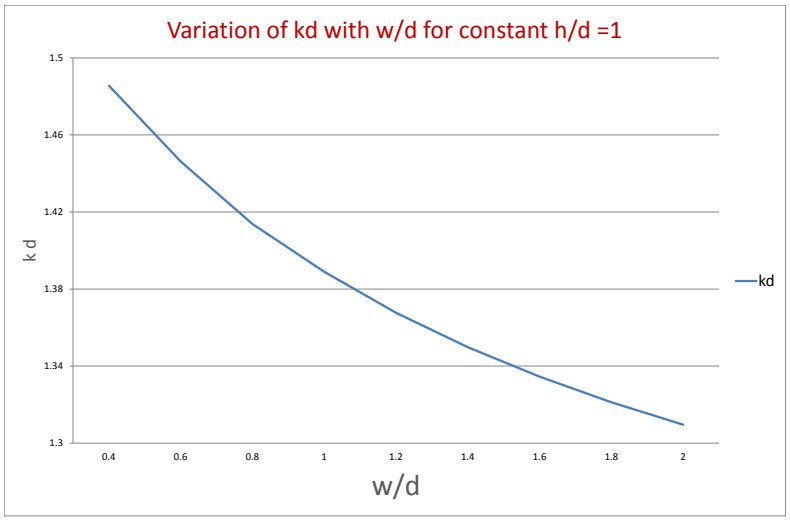

Figure 5.16: Trapped mode frequencies below the first cut-off, $0 < kd < \pi/2$, for a smooth cavity in an infinite Dirichlet waveguide.

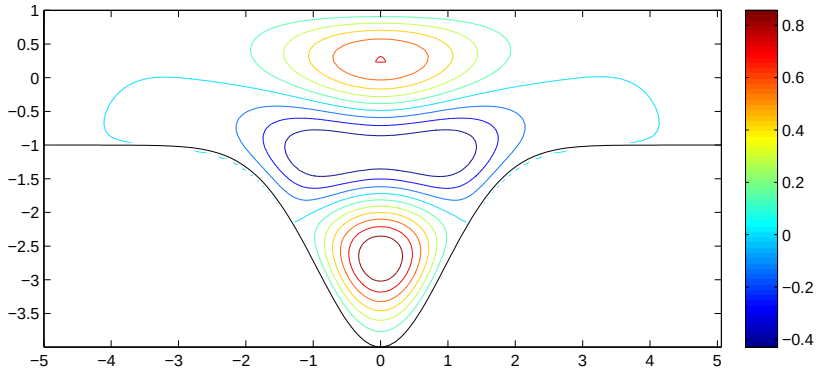

Figure 5.17: Embedded trapped mode in a smooth cavity with Gaussian profile, $h/d = 3, w/d = 1.8$ and frequency $kd \approx 2.3442 = 0.7461\pi$.

ies. The essential spectrum of the operator is $[0, \infty)$, meaning that the trapped modes are embedded. Table 5.6 lists the modes found for this case. All modes found are even in x.

h/d	**w/d**	**kd**	**kd/π**
2.9	3.8	1.45625	0.4635
3.5	5.2	1.2448	0.3962
3.9	5.8	1.1594	0.3690
5.6	4.4	1.3492	0.4294
5.9	4.8	1.2823	0.4081

Table 5.6: Trapped mode frequencies for a triangular cavity in a Neumann waveguide.

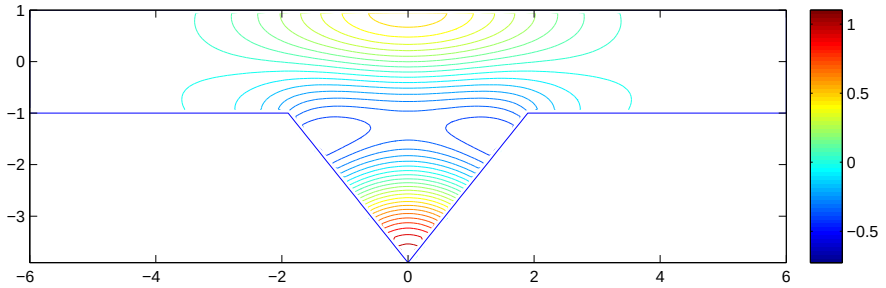

Figure 5.18: An embedded trapped mode in a triangular cavity, $h = 2.9, w = 3.8$ and frequency $kd \approx 1.4563 = 0.4635\pi$.

5.3 Rectangular cavity and disc in an infinite waveguide

A single disc, of radius a, on the centreline of an infinite waveguide may support a trapped mode, depending on its size and the type of boundary condition on the guide. A cavity, of width w and depth h, in the absence of other obstacles in the guide, may support a trapped mode for discrete (h, w). Isolated thin or shallow cavities cannot support trapped modes - the spacing parameters must exceed some threshold in order for such resonances to be found. The addition of a disc in the centre of a waveguide ($x = 0, y = 0$) changes the situation completely as the combination of these two elements greatly increases the affinity of a geometry to trapped mode type resonances.

5.3.1 Rectangular cavity and disc in a Neumann waveguide

Using our BEM program we searched for trapped modes in a Neumann waveguide with a rectangular cavity and a disc placed on its centre, in the frequency range $0 < kd < \pi/2$. Our findings for this case can be summarised as follows:

- All discs of radius $0 < a \leq 1$, placed in the centre of the guide, support trapped modes for discrete couples of (h, w). The case $a = 1$ is included because a cavity of width $w > 1$, allows the whole domain to remain connected.

- A disc of a given radius supports trapped modes for more than one cavity, for discrete, specific couples (h, w).

- The addition of a disc enables the appearance of trapped modes for cavities which

would not support trapped modes on their own.

- Trapped modes can be found for a larger range of geometric parameters than for isolated disc or cavity as the combination of both gives rise to many more resonances. For example, in the absence of a disc, shallow or narrow cavities do not support trapped modes. The minimum depth required for the appearance of a mode in a cavity is $h \geq 2$, whereas the addition of a disc will enable trapped modes, in some cases, for cavities such that $h \leq 0.4$.

- For a given cavity depth it is possible that there are no trapped modes, irrespective of its width and the disc radius.

- For a given cavity width it is possible that there are no trapped modes, irrespective of its depth and the disc radius.

- Some cavities may support modes for more than one disc. For example a cavity of depth $h = 4.6$ and width $w = 4.2$, has a trapped mode in combination with a disc of radius $a = 0.3$. If the disc diameter changes, even by a small amount, the trapped mode is perturbed but there are still a multitude of nearly trapped modes with very low radiation, which physically would probably be very difficult to distinguish from the trapped mode itself. At $a = 1$ an antisymmetric mode appears, at a frequency $kd \approx 1.5432 = 0.4912\pi$.

We also considered geometries without any (x, y) symmetry. Let the coordinates of the disc centre be (x_c, y_c). When the disc is placed in the centre of the guide the coordinates are $x_c = 0, y_c = 0$. If the disc is removed from the centre of the guide, even by a small distance, in the x direction say, so that $0 < x_c < \epsilon$, any existing trapped mode will be perturbed and become a nearly trapped mode. As the distance is increased further, at some point the nearly trapped mode also disappears. As $x_c \gtrsim \lambda$, we recover nearly trapped modes corresponding to the pure trapped modes for either a single cavity or a single disc in the waveguide. The frequencies are similar but not identical to those corresponding to the pure trapped modes. These modes are localised either around the disc or the cavity. The mode for a disc is perturbed in the region of and beyond the cavity. Also, the mode trapped in the cavity is perturbed as it approaches the disc down the guide. However, we should note that although they are perturbations of pure trapped modes, the radiation is very low.

Two such modes, for a cavity $h = 4, w = 11.9$ and a disc of radius $a = 0.4$ placed on the centreline of the guide, removed from the centre of the guide by a distance $x_c = 10$ are enclosed in Fig. 5.19. The characteristic trapped mode frequencies for the isolated disc and cavity are $k_c \approx 1.4478 = 0.4608\pi$ and $k_c \approx 0.5050 = 0.16074\pi$ respectively. We did not find any pure trapped modes for asymmetric geometries, irrespective of the disc radius and cavity size. This does not exclude the possibility that a trapped mode may exist for a specific set of values (a, h, w, x_c), however we were unable to identify such a geometry.

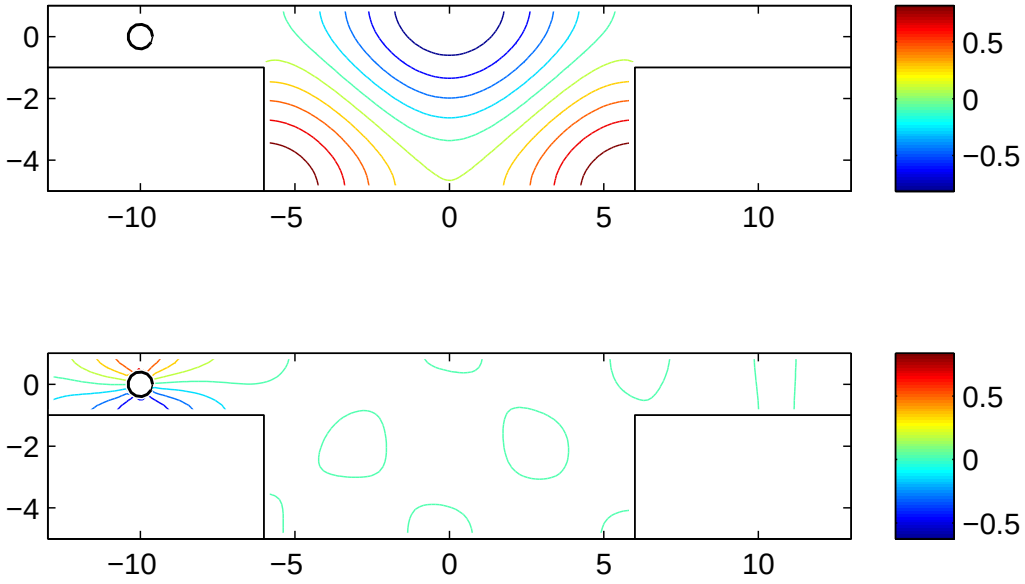

Figure 5.19: Nearly trapped modes in a rectangular cavity at $kd \approx 0.5250 = 0.1671\pi$ at and around a disc on centre of a Neumann waveguide, for $kd \approx 1.4566 = 0.4636\pi$. The characteristic trapped mode frequencies for the isolated cavity and disc are $k_c \approx 0.5050 = 0.16074\pi$ and $k_c \approx 1.4478 = 0.4608\pi$ respectively.

In Table 5.7 we present trapped mode frequencies for the case $a = 0.4$. The k values found vary noticeably from case to case in contrast to those for an isolated disc in the waveguide, which are close to the relevant cut-off. Details of trapped mode for other discs $(0 < a \leq 1)$ are given in Appendix A.

Some examples of trapped modes found for this geometry are presented in Figures 5.20 - 5.22. Further plots to illustrate the variety of trapped modes supported by this geometry are presented in Appendix A. The plots below illustrate the evolution of the trapped modes as

h/d	**w/d**	**kd**	$\mathbf{kd}/\boldsymbol{\pi}$	$\mathbf{x-}$ **Symmetry**
0.8	6	1.15662	0.36816	Symmetric
1.4	6.75	0.98842	0.31462	Symmetric
1	7	1.26435	0.40246	Anti-symmetric
3.4	6	1.14732	0.36520	Symmetric
3.8	6.2	1.09465	0.34844	Symmetric
4.8	4.4	1.36155	0.43339	Symmetric (see Fig 5.22)
4.2	7	1.02482	0.32621	Symmetric
4.6	3.4	1.40248	0.44642	Symmetric (see Fig. 5.20)
4.9	6.6	1.45577	0.46339	Anti-symmetric (see Fig. 5.22)

Table 5.7: Trapped mode frequencies found for a cavity and a sound hard disc placed on the centre of a Neumann waveguide.

the cavity size increases. As the horizontal walls of the cavity are pulled further apart, the solution develops new local critical points on the cavity walls, at $x = \pm w$ - see Fig. 5.20 below. As the cavity increases further, an antisymmetric mode appears, with a series of peaks and troughs on the cavity walls - see Fig. 5.22.

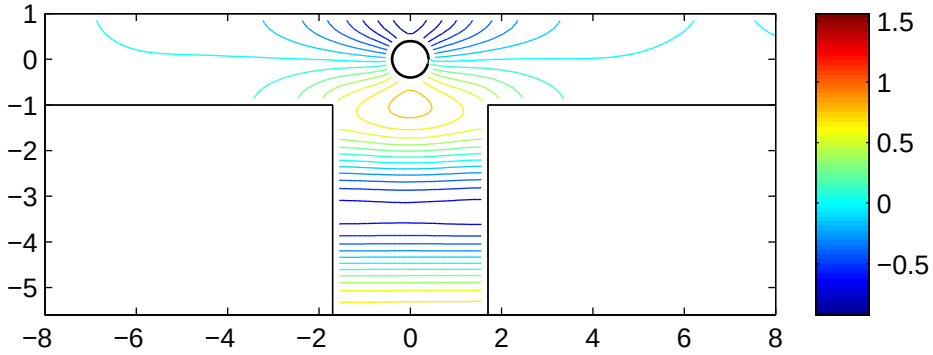

Figure 5.20: Trapped mode for a rectangular cavity and a disc on centre of a Neumann waveguide, $h/d = 4.6, w/d = 3.4$ and frequency $kd \approx 1.4024 = 0.4464\pi$.

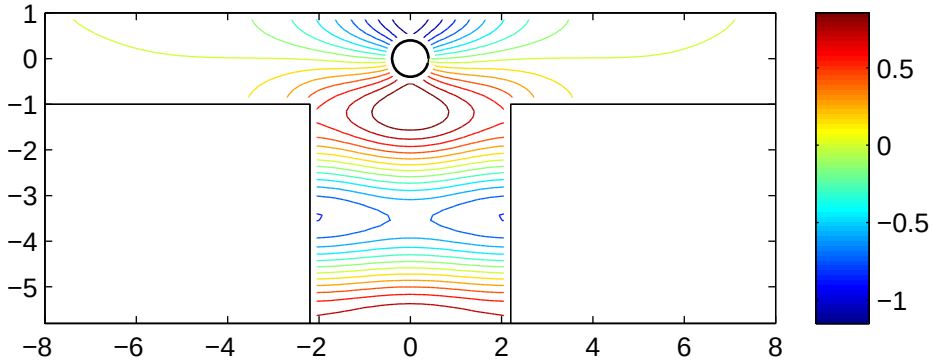

Figure 5.21: Trapped mode for a rectangular cavity and a disc at the centre of a Neumann waveguide, $h/d = 4.8, w/d = 4.4$ and frequency $kd \approx 1.3615 = 0.4334\pi$.

5.3.2 Rectangular cavity and disc in a Dirichlet waveguide

In the last section of this chapter we present our findings for a soft infinite waveguide with a rectangular cavity of depth h and width w, and a disc of radius a, positioned in the centre of the guide. A single disc with $0 < a < 0.67$, on the centreline of the guide, without cavities, supports one trapped mode with $kd < \pi, kd \to \pi$ as $a/d \to 0$ and $a/d \to 0.67$.

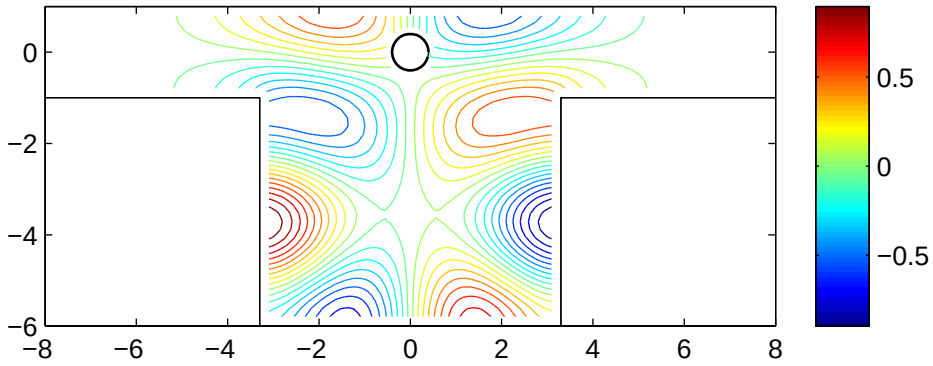

Figure 5.22: Trapped mode for a rectangular cavity and a disc at the centre of a Neumann waveguide, $h/d = 4.9, w/d = 6.6$ and frequency $kd \approx 1.4557 = 0.4634\pi$.

The addition of a cavity to the guide leads to the appearance of a large number of trapped modes as follows:

- Any disc of radius $0 < a \leq 1$, placed at the centre of a soft infinite guide, supports trapped modes for discrete couples of (h, w). We note that the presence of a cavity increases the range of possible disc sizes above the $a = 0.67$ limit for an isolated disc. The case $a = 1$ is considered with a cavity such that $w > 1$, which allows the $\pm x$ sides of the guide to remain connected.

- A disc of a given radius supports trapped modes for more than one cavity with discrete, specific values of h and w.

- For just a cavity in a soft waveguide, in the range $0 < h \leq 6$, $0 < w \leq 6$, we found only six geometries which support trapped modes - see Table5.4. We obviously did not exhaust all the possible choices of h and w and it is plausible that there are other, larger cavities which may support trapped modes. However, for the size range, with the addition of the disc to the guide, we found 84 trapped modes (see results presented in Appendix B).

- For a given depth it is possible that there are no trapped modes, irrespective of the cavity width and disc radius. For a given width it is possible that there are no trapped

modes, irrespective of cavity height and the disc radius.

- As the (a, h, w) triples are so densely distributed, we found that most geometries support at least nearly trapped modes. It is therefore possible, to find either a trapped mode or a nearly trapped mode with low radiation for most values of h and w. Although not an exact solution to our problem, nearly trapped modes would physically be very difficult to distinguish from the perfectly decaying modes.

- Some cavities may support modes for more than one disc.

- Some configurations may support more than one mode. We found two examples, where the same geometry has two trapped modes, at two different frequencies. Solution plots in Fig. 5.23(e) and Fig. 5.23(f) correspond to such a geometry with $(a = 0.4, h = 3, w = 3.8)$.

We also considered geometries without any (x, y) symmetry for this case. Using the same notation for the centre of the disc as in the previous case we are also able to recover nearly trapped modes corresponding to either a single cavity or a single disc in the waveguide for $x_c \gtrsim \lambda$. The frequencies are similar but not identical to those corresponding to the pure trapped modes. Two such modes, for a cavity $h = 2.6, w = 5.8$ and a disc of radius $a = 0.3$ placed on the centreline of the guide, removed from the centre of the guide to a distance $x_c = 6$, are enclosed in Figures 5.23(a) -5.23(b). We did not find any pure trapped modes for asymmetric geometries, irrespective of the disc radius and cavity size. This does not exclude the possibility that a trapped mode may exist for a specific set of values (a, h, w, x_c, y_c), however we were unable to identify such a geometry.

In Figure 5.22 we present ten trapped modes found for the same disc, of radius $a = 0.4$. The series of plots illustrates the manner in which the solution profile changes with the cavity size. The modes are presented in increasing order of cavity depth. A list of trapped mode frequencies for all disc sizes, with a catalogue of solution plots, to illustrate the variety of solutions found are enclosed in Appendix B. The figures enclosed map out, for each disc size, the transformations in trapped mode profiles, induced by changes of the spacing parameters (h, w).

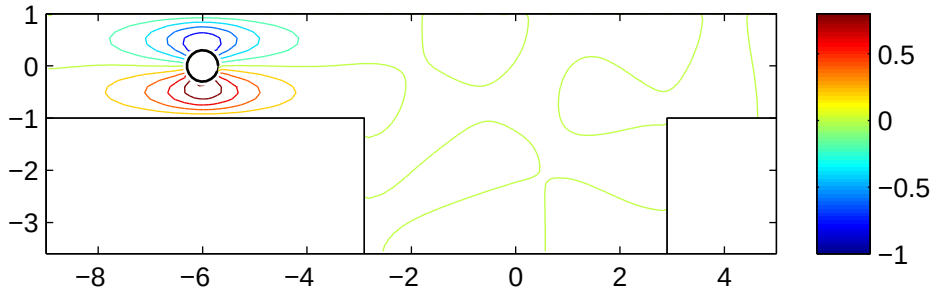

(a) Nearly trapped mode in a Dirichlet waveguide, for a disc of radius $a = 0.3$, at $k \approx 2.9931 = 0.9527\pi$. For a single disc a trapped mode appears at $k_c \approx 2.9907 = 0.9511\pi$

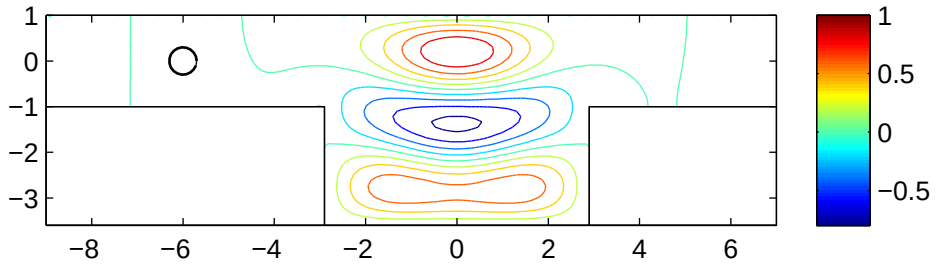

(b) Nearly trapped mode in a Dirichlet waveguide, for a cavity with $h = 2.6$, $w = 5.8$, at $k \approx 2.7037 = 0.8606$. For the same cavity a trapped mode appears at $k_c \approx 2.6566 = 0.7900$

Figure 5.23: Nearly trapped modes form around trapping features which are at a distance $x_c >> \lambda$ from each other.

5.4 Conclusion - overview of results

Two sound-hard discs placed on the centreline of an infinite acoustic waveguide were found to support either one or two non-embedded trapped modes, depending on the distance between them. Our results are in agreement with those of Evans and Porter [26] for the case of a long narrow wave channel containing any number of different size bottom mounted circular cylinders arbitrarily spaced along the centreline of the channel. Evans and Porter showed that there are no more than N trapped modes, in the range $0 < kd < \pi$, for any configuration of N cylinders, the precise number depending critically on the geometry of the configuration. We extended the existing results for this case by establishing the behaviour of these modes for intersecting discs, up to the point where they become a single disc. We also studied this configuration for the next band of frequency values $\pi < kd < 2\pi$. We also investigated similar geometries in a Neumann waveguide, for both non-embedded $(0 < kd < \pi/2)$ and embedded frequencies $(\pi/2 < kd < 3\pi/2)$.

We first considered two intersecting discs then progressively increased the distance between

them, c, up to several wavelengths. For each of these geometries we found the associated trapped modes and mapped the evolution of trapped mode frequencies with the distance separating the discs. Evans *et. al* [22] proved that a two-dimensional acoustic waveguide containing a $y-$symmetric obstruction of general shape, has at least one local oscillation which decays with distance down the waveguide, away from the obstruction. Using our program we found this type of mode for two intersecting discs. The mode found is $y-$antisymmetric and x-symmetric (symmetric mode). Interestingly, the frequency decreases linearly with the distances between the discs' centres, irrespective of the discs relative sizes. The minimum frequency value is attained for the case when the discs are tangent to each other. After separation, the two discs support at least one trapped mode. A second mode, antisymmetric with respect to both axes, appears at a specific separation distance which depends on the discs radii (antisymmetric mode). The antisymmetric mode frequency is higher than that of the symmetric mode. Both modes persist and vary continuously with the geometry. As c/d increases the frequencies of both the symmetric and antisymmetric modes approach the characteristic frequencies of the isolated discs. For the case of two discs of equal radius, as $c/d \to \infty$ we found that

$$k_{symmetric} \to k_c \leftarrow k_{antisymmetric}, \tag{5.17}$$

and for two discs of different radii, $a_1 < a_2$, with characteristic trapped mode frequencies, k_{c1}, k_{c2}

$$k_{symmetric} \to k_{c2} < k_{c1} \leftarrow k_{symmetric}, \tag{5.18}$$

as illustrated in Fig. (5.1) and (5.8).

Non-embedded modes were also computed for two sound-hard discs on the centreline of a soft waveguide. Qualitatively, these modes follow the same pattern as in the previous case. A slight variation relates to the disc sizes which support these modes. For the symmetric case we found that two identical discs of radius up to $a/d = 0.7$ support trapped modes in contrast to just a single disc in a waveguide, where the upper limit is $a/d = 0.67$. We found antisymmetric modes only with $0 < a/d < 0.6$, in accordance with Evans *et. al* [22].

Embedded Neumann trapped modes, both symmetric and antisymmetric with respect to the $y-$axis, were found for two discs of radii $0.125 \leq a_1/d = a_2/d \leq 0.400$ and specific

values of c/d. For a given radius in this range there may be more than one value of c which corresponds to a trapped mode. The addition of a second disc increased the range of geometries which support trapped modes in this frequency range. We note that for an isolated disc in a waveguide only one embedded mode occurs at $a/d = 0.352$. Details of the modes found are presented in Table 5.1. We did not exhaust the range of geometric couples $(a/d, c/d)$ which support trapped modes in this frequency range. Further computations would undoubtedly identify new trapped modes for increasing values of c. For all modes found we have that

$$k_{symmetric} < k_{antisymmetric}, \tag{5.19}$$

and that the antisymmetric mode appears at a larger separation distance than that required for the symmetric mode.

Dirichlet embedded modes were also found for two discs of identical radii in the range $0.1 \leq a_1/d = a_2/d \leq 0.295$ and specific values of c/d, in contrast to the case of one isolated disc in a soft waveguide, which supports only one mode for the discrete value $a/d = 0.267$. As for the Neumann case, the antisymmetric trapped mode frequencies are higher than those found for the symmetric modes. Details of the modes found are presented in Table 5.4.

Rectangular cavities in Dirichlet waveguides support trapped modes below the first cut-off $(0 < kd < \pi/2)$ for any cavity of depth h and width $2w$ such that

$$w \gtrapprox \frac{1}{\sqrt{1 - \frac{1}{d+h/2}}}. \tag{5.20}$$

This lower limit is obtained using a simple argument whereby an oscillation of frequency such that $\frac{\pi}{2d+h} < k < \frac{\pi}{2d}$ which satisfies a Dirichlet condition on the cavity walls, $|x| = w$, would be effectively trapped inside the cavity and decay to zero with distance away from the cavity. All these non-embedded modes are $y-$symmetric. As the cavity width is increased more modes appear, symmetric and antisymmetric in x. The first mode found is x-symmetric, for $h/d = 1$ and width $2w/d \approx 2.4$, as predicted by eqn. (5.20). Embedded modes for this problem $(\pi/2 < kd < \pi)$ only appear for discrete couples (h, w) and examples of such modes are presented in Table 5.4. Predicting the appearance of these

modes is not as straightforward as for non-embedded modes and we are only able to identify the suitable values of h and w by using our computational method to investigate a large range of geometric parameters.

Searching for trapped modes occurring in cavities in Neumann waveguides is equivalent to searching for embedded oscillations which means that they exist only for discrete parameters (h, w). The rectangular cavity has already been studied and we refer to results obtained by Duan *et. al* [18]. We extended the study of this problem by looking at triangular cavities in Neumann guides and presented five such embedded modes, which we found using our BEM program - see Table 5.6.

We also investigated a smooth cavity in a Dirichlet waveguide, and established that in the absence of sharp corners at the top of the cavity, trapped modes are still possible. Firstly, for the non-embedded frequencies, $(0 < kd < \pi/2)$, we found that trapped modes appear for any cavity such that $h/d = 1, w/d > 0.8$. Within the next band of frequencies, $(\pi/2 < kd < \pi)$ we only found trapped modes for discrete couples $(h/d, w/d)$ and examples of two such modes are presented in Table 5.5. Undoubtedly more embedded modes could be found, if we extended the range of geometric parameters investigated.

The last type of geometry investigated involves a sound-hard disc on the horizontal centreline of either a Dirichlet or a Neuman waveguide with a rectangular cavity. To our knowledge there are no known results for this geometry. The $x-$axis is not a line of symmetry for this geometry anymore, hence the problem can not be decomposed into its symmetric and antisymmetric parts. As a consequence the argument mentioned in 2.3 is not valid for this problem and this means that all the modes we found are embedded.

A symmetric combination of the two features, cavity and disc, greatly increases the affinity of the geometry to trapped mode type resonances. We first studied the case where the disc centre (x_c, y_c) is symmetrically placed above the cavity.

We found that for both cases, Dirichlet and Neumann, trapped modes exist for discrete triples $(a/d, h/d, w/d)$. If one geometric parameter is fixed, the other parameters can be varied until a mode is found. For example, for a given disc radius we varied the cavity size and found a number of trapped modes for discrete, precise values of h and w. We thus found that discs of all radii $(0 < a/d \leq 1)$ support trapped modes for many associated

cavities. A list of modes found for both Dirichlet and Neumann cases, for cavities in the range $0 < h/d < 6$, $0 < w/d < 6$, are presented in Appendix B. This contrasts with the case of a single disc in a Dirichlet waveguide, which in the absence of a cavity, has one trapped mode in the range $\pi/2 < kd < \pi$, but only if $0 < a/d < 0.67$. The presence of the disc also extends the range of cavities which support trapped modes, as in general thin or shallow cavities do not support embedded trapped modes. If more than one geometric parameter is fixed we were not always able to find a trapped mode, e.g. for a cavity of given (h, w), we were not necessarily able to find any trapped modes irrespective of the disc's size.

As with all embedded modes, changing a geometric parameter destroys the trapped mode. For this geometry, however, we found many nearly trapped modes, some with low radiation, which means that physically they would be difficult to distinguish from genuine trapped modes.

We also considered geometries without any (x, y) symmetry. As the disc is removed from the cavity's vertical symmetry line, any existing trapped mode is destroyed. We did not find any pure trapped mode for the asymmetric geometries, irrespective of the disc radius and cavity size. This does not exclude the possibility that a trapped mode may exist for a specific set of values (a, h, w, x_c, y_c), but we were unable to find such a geometry. If the disc is moved more than one wavelength from the cavity symmetry line we found nearly trapped modes, corresponding to the pure modes of either the isolated disc or cavity. The nearly trapped modes are oscillations localised around either the disc or the cavity, decaying away from the trapping feature and perturbed near the cavity or disc, respectively.

The cases studied show that symmetry is an essential condition for the formation of trapped mode type resonances. Increasing the number of trapping features, placed with a degree of symmetry, leads to the appearance of new trapped modes. The addition of a new geometric parameter to a problem which has one embedded trapped mode solution for a specific discrete geometry, leads to the appearance of a continuous set of trapped modes.

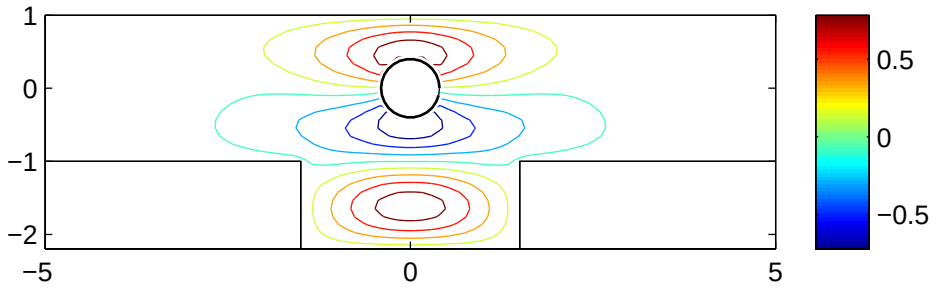

(a) Dirichlet waveguide with a cavity and a sound-hard disc, with $a = 0.4, h = 1.4, w = 2.9$ at $kd \approx 2.6463 = 0.8423\,\pi$.

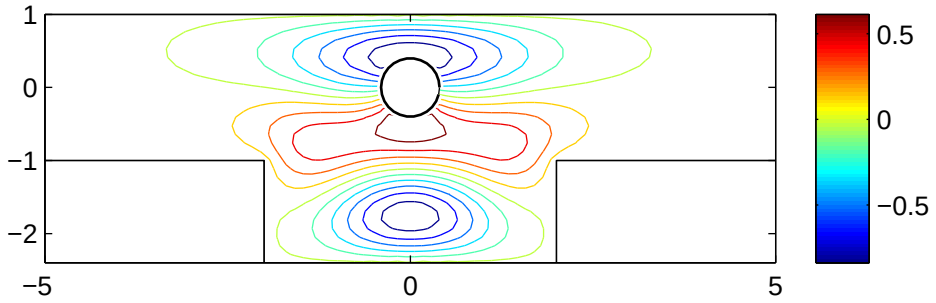

(b) Dirichlet waveguide with a cavity and a sound-hard disc, with $a = 0.4, h = 1.4, w = 4$ at $kd \approx 2.7526 = 0.8761\,\pi$

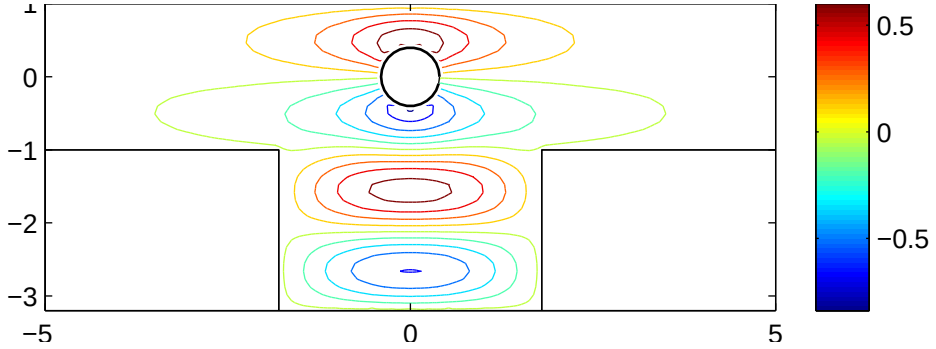

(c) Dirichlet waveguide with a cavity and a sound-hard disc, with $a = 0.4, h = 2.3, w = 3.6$ at $kd \approx 2.9913 = 0.9521\,\pi$.

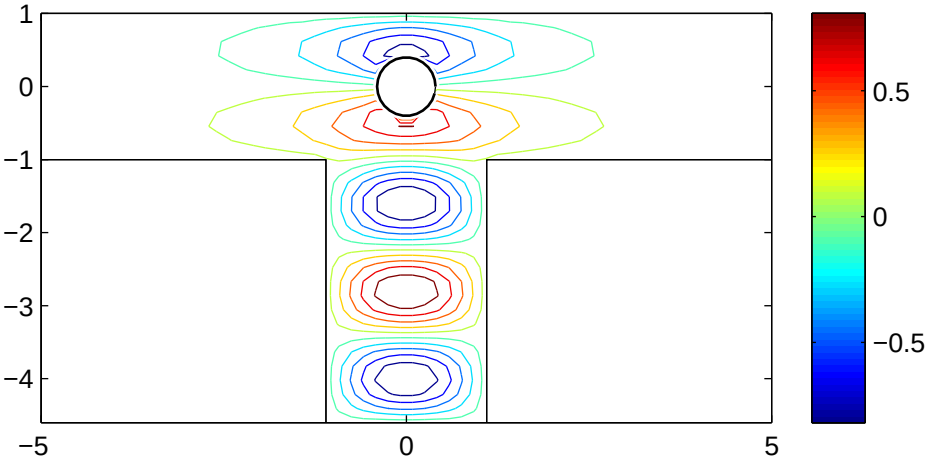

(d) Dirichlet waveguide with a cavity and a sound-hard disc, with $a = 0.4, h = 3.6, w = 2.2$ at $kd \approx 2.9854 = 0.9503\,\pi$.

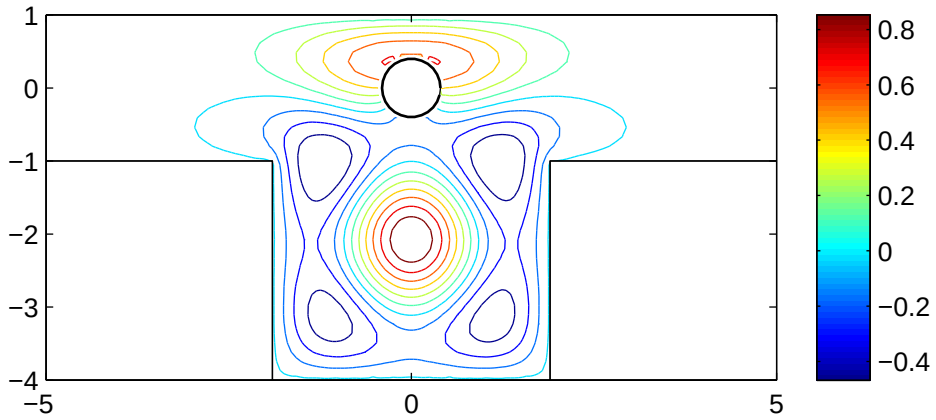

(e) Dirichlet waveguide with a cavity and a sound-hard disc, with $a = 0.4, h = 3, w = 3.8$ at $kd \approx 2.9172 = 0.9286\,\pi$.

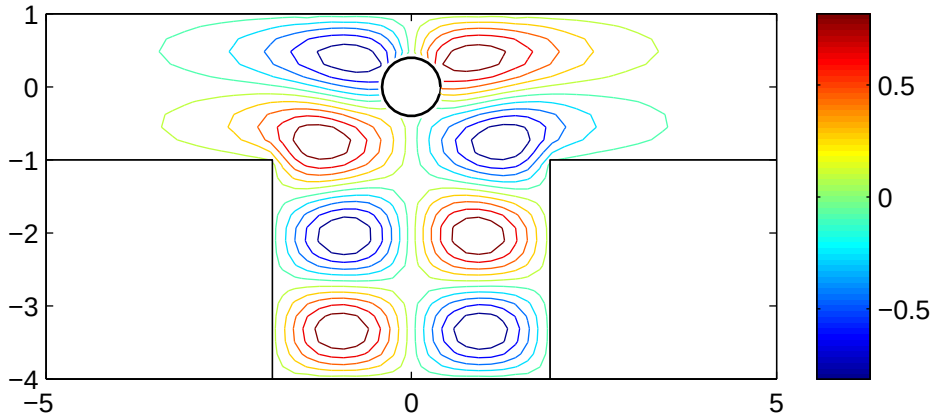

(f) Dirichlet waveguide with a cavity and a sound-hard disc, with $a = 0.4, h = 3, w = 3.8$ at $kd \approx 2.5975 = 0.8268\,\pi$.

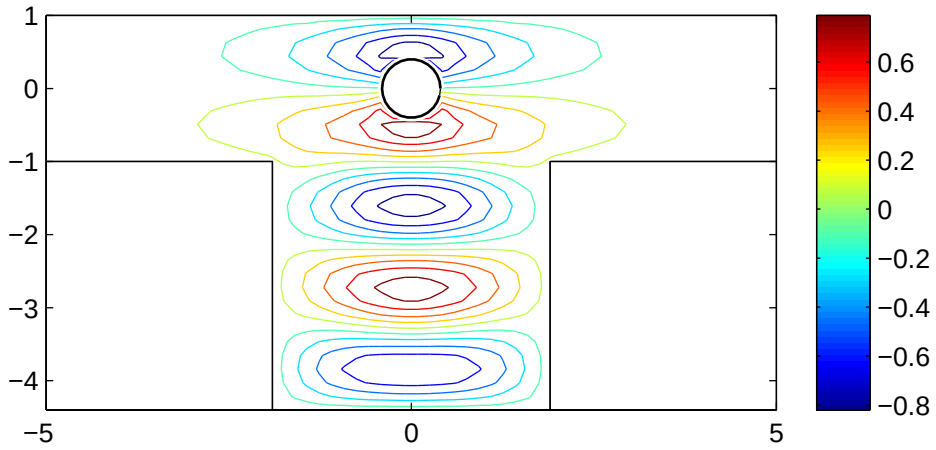

(g) Dirichlet waveguide with a cavity and a sound-hard disc, with $a = 0.4, h = 3.4, w = 3.8$ at $kd \approx 2.9302 = 0.9327\,\pi$.

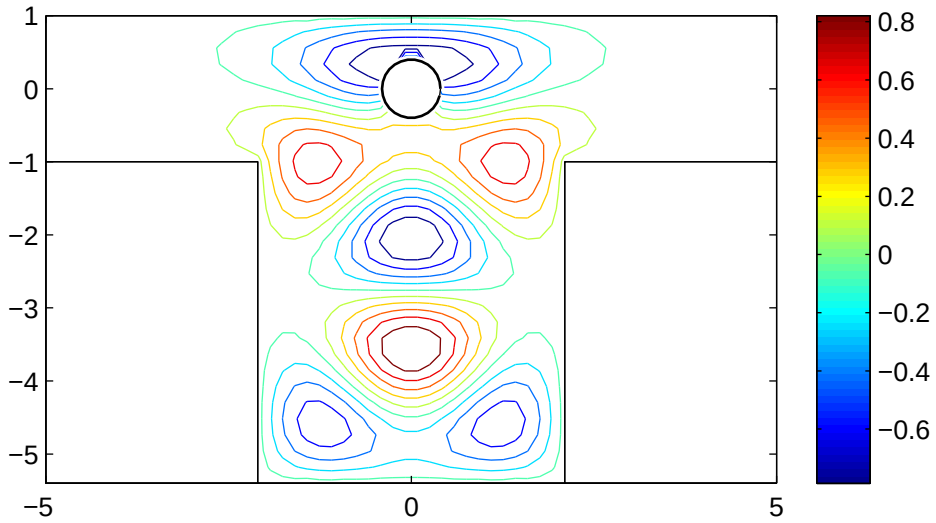

(h) Trapped mode in a Dirichlet waveguide, for $a = 0.4, h = 3.4, w = 3.8$ at $kd \approx 2.5374 = 0.8076\,\pi$.

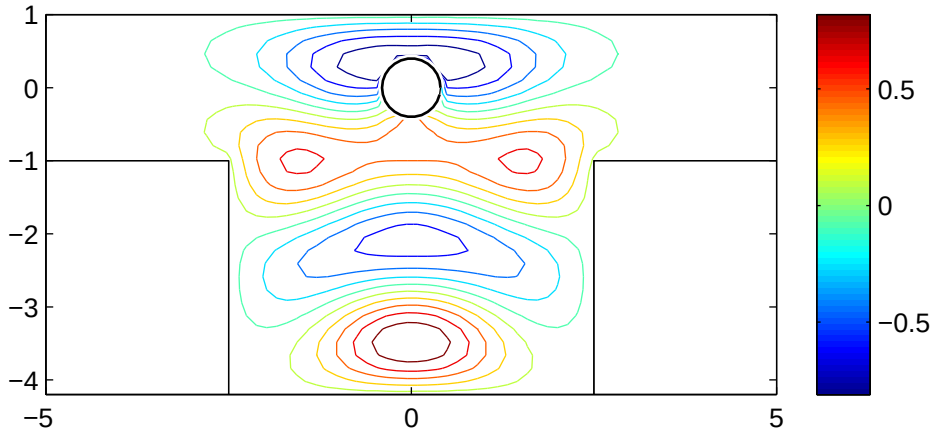

(i) Dirichlet waveguide with a cavity and a sound-hard disc, with $a = 0.4, h = 3.4, w = 3.8$ at $kd \approx 2.4679 = 0.7855\,\pi$.

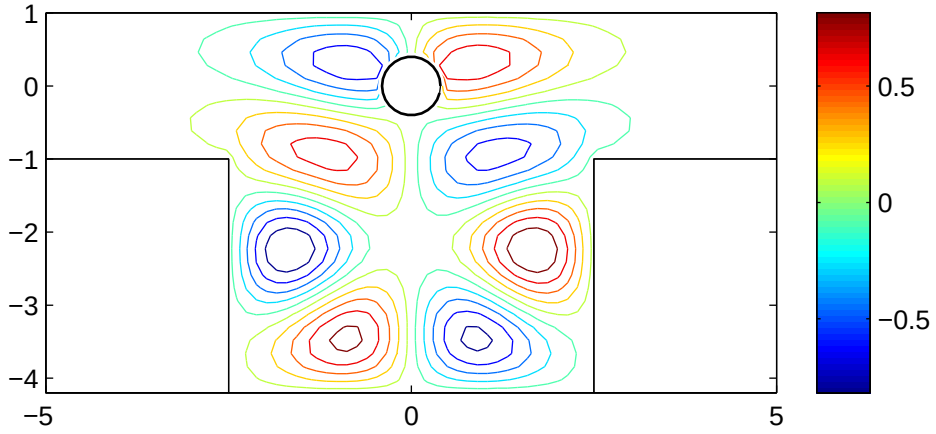

(j) Dirichlet waveguide with a cavity and a sound-hard disc, with $a = 0.4, h = 3.4, w = 3.8$ at $kd \approx 2.6968 = 0.8584\,\pi$.

Figure 5.22: Trapped modes in a Dirichlet waveguide, supported by cavities of various sizes and a disc of radius $a/d = 0.4$.

Chapter 6

Planewave spectrum analysis

6.1 Preliminaries

The catalogue of trapped modes obtained using our BEM program gives a global perspective on the structure of these solutions and reveals a series of characteristics which are common to all geometries. The numerical results indicate that on boundaries, the solution and its normal gradient could locally be approximated by a series of simple trigonometric functions, homogeneous or inhomogeneous planewaves, with wavelengths commensurate with the size of the trapping feature. In this chapter we proceed with an analysis of a trapped mode, based on a planewave spectrum representation, which was developed for various characteristic problems in the classical theories of radiation, diffraction and propagation. The idea is to employ the simplicity of plane waves travelling in diverse directions and use them to build more elaborate types of solutions which may arise in various geometries. Our approach is fairly flexible so that the general procedure is independent of the shape of the trapping obstacle and could be adapted to other geometries. Once the validity of the method is confirmed, guided by the computational results obtained and presented in Chapter 5, we will seek to apply it to other geometries.

In this chapter we consider the Dirichlet problem, defined in Chapter 4, Eq. (4.11) -(4.15) for a Neumann circular obstacle, of radius $0 < a/d < 0.67$, placed on the centreline of a two dimensional infinite soft waveguide of width $2d$, see Fig. 6.1. A solution $\phi(\mathbf{x})$ satisfies the two dimensional Helmholtz equation in the fluid region between the circle and the lines,

and the normal gradient of the potential vanishes on the circle. Existence of eigensolutions for this particular geometry satisfying conditions (4.11) - (4.15) follows from [22] and calculation of associated eigenvalues were reported in [10] and [47]. In each of these works the appropriate potential was constructed using an infinite linear combination of all possible, suitably modified multipoles, involving Hankel functions.

We now introduce the main notation and terminology used throughout this chapter. We use the usual notation for the the position vector $\mathbf{r} = (x, y)$:

$$\begin{aligned} x &= r\cos\theta, \\ y &= r\sin\theta, \quad \theta \in (0, 2\pi]. \end{aligned} \tag{6.1}$$

We consider a general plane wave which travels at angle α to the x axis, that is:

$$u(x, y) = Ue^{ik(x\cos\alpha + y\sin\alpha)} = Ue^{ikr\cos(\theta-\alpha)}. \tag{6.2}$$

The propagation vector $\mathbf{k}$ has components

$$\begin{aligned} \mathbf{k} &= (k_1, k_2), \\ k_1 &= k\cos\alpha, \\ k_2 &= k\sin\alpha. \end{aligned} \tag{6.3}$$

Vector $\mathbf{k}$ has magnitude k as defined for the acoustic problem in Chapter 2, (2.6).

The geometric domain of the problem is denoted W. The waveguide boundaries are Γ_- and Γ_+, with $y(\Gamma_-) = -d$ and $y(\Gamma_+) = d$. A disc of radius a is placed on the centre of the guide. The disc boundary is denoted ∂D so that

$$\partial W = \Gamma_- \cup \Gamma_+ \cup \partial D.$$

A point of interest in the field, $P \in W \backslash \partial W$, has position vector $\mathbf{r} = (x, y)$ with x, y as defined above (6.1). A point Q on the boundary of the domain ($Q \in \partial W$), has position vector $\mathbf{r}' = (x', y')$.

Let $\mathbf{R}$ be the vector connecting a point P inside the domain, with a point Q on the boundary

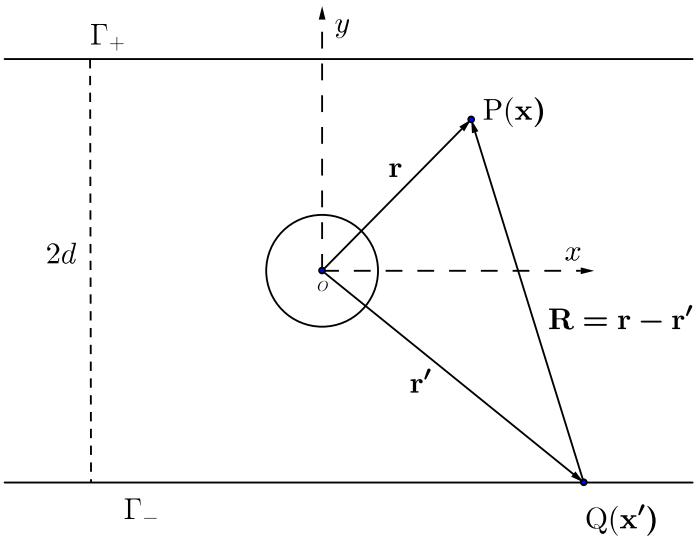

Figure 6.1: Problem domain - an infinite Dirichlet waveguide with disc on its centre.

∂W, then

$$\mathbf{R} = \mathbf{r} - \mathbf{r}', \tag{6.4}$$

with

$$\mathbf{R} \ = R(\cos\nu, \sin\nu), \quad \nu \in (0, 2\pi]. \tag{6.5}$$

In this chapter we often use the terms near and far field. The near field is in the order of the trapped mode wavelength; it is located in the centre of the guide and it extends away from the trapping structure as far as the oscillatory behaviour is detected. The far field is the part of the domain where the mode is decaying exponentially. As in optics, where we borrowed the terms from, there is not a clear boundary between the two regions, rather there is a transition zone where the two fields overlap.

6.2 Overview of method

The most general velocity potential field satisfying the Helmholtz equation is expressible as a superposition of harmonic terms, that is, as a Fourier integral. For this we require that the integration in the frequency space, must run the full range from $-\infty$ to ∞. We note

that there is no requirement that the components of $\mathbf{k}$ be restricted to real values; for full generality they must be supposed to be complex. Hence we can write our solution as an appropriate superposition of plane waves of the form (6.2) :

$$\phi(\mathbf{r}) = \int_C P(k, \sin\alpha)\, e^{ikr\cos(\theta-\alpha)}\, d\alpha = \int_C P(k, \sin\alpha)\, e^{i\mathbf{k}\cdot\mathbf{r}}\, d\alpha. \tag{6.6}$$

The contour of integration C is chosen so that two main requirements are satisfied:

- The range covered by α is such that $\sin\alpha$, hence the vertical component of the propagation vector, k_2, goes through real values from $-\infty$ to ∞,
- The sign of the imaginary part of α is determined by the requirement that the inhomogeneous waves decay *away* from the y axis.

An appropriate integration path C, in the complex α plane, is that depicted in Fig. 6.2.

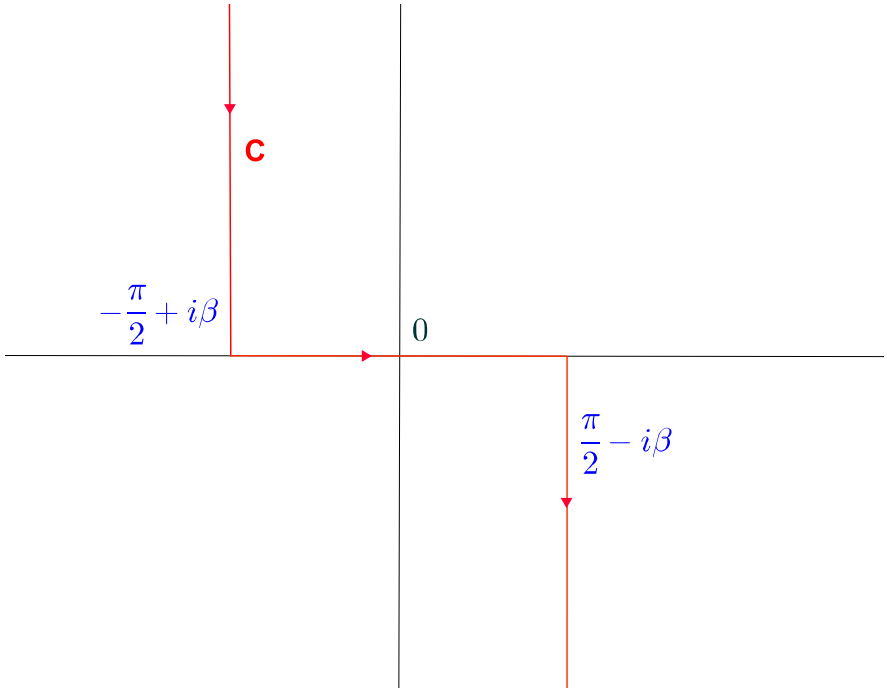

Figure 6.2: Complex α - contour.

Assume $x > 0$ and let $\beta \in \mathbb{R}^+$, then the exponent

$$\psi = ikr\cos(\theta - \alpha), \tag{6.7}$$

takes the following values along the chosen contour C:

1. $\alpha = -\frac{\pi}{2} + i\beta,\ \psi = -kx\sinh\beta - iky\cosh\beta$, decay in x - direction and oscillations in y direction,
2. $\alpha \in \left[-\frac{\pi}{2}, \frac{\pi}{2}\right],\ \psi = ikx\cos\alpha + iky\sin\alpha$, oscillations in x and y directions,
3. $\alpha = \frac{\pi}{2} - i\beta,\ \psi = -kx\sinh\beta + iky\cosh\beta$, decay in x - direction and oscillations in y direction.

In equation (6.6), $P(\sin\alpha)$ is the *spectrum function*, which specifies in terms of amplitude and phase the "weight" attached to each plane wave of the spectrum.

We now illustrate the general strategy of our approach with a simpler case, that of a two dimensional Dirichlet waveguide, without any obstacles. Although this geometry does not support a trapped mode we use this example to outline the method which will later be applied to the case of a disc on the centre of the guide, where trapped modes are known to exist.

We consider the Helmholtz equation in this domain. Following the procedure described in Chapter 3, after application of Dirichlet boundary conditions on Γ_- and Γ_+, the solution, according to (3.10), can be written as follows:

$$\phi(\mathbf{r}) = \int\limits_{\Gamma_\pm} \left(-\frac{\partial\phi(\mathbf{r}')}{\partial n}\right)\left(-\frac{i}{4}H_0^1(kR)\right)\, d\mathbf{r}', \quad \mathbf{r}' \in \Gamma_\pm. \tag{6.8}$$

An integral representation for the Hankel function of first kind, according to Morse and Feshbach [56] is

$$H_0^1(kR) = \frac{1}{\pi}\int\limits_C e^{ikR\cos(\nu-\alpha)}\, d\alpha \tag{6.9}$$

where the contour C can be modified to be the same as our chosen contour in Fig. 6.2. We also note that the result in (6.9) is independent of ν, therefore ν can be chosen so that it

coincides with the angle of the vector $\mathbf{R}$. Substituting this expression for H_0^1 in (6.8) we can write our solution as follows:

$$\begin{aligned}\phi(\mathbf{r}) &= \frac{i}{4\pi}\int\limits_{\Gamma_\pm} \frac{\partial\phi(\mathbf{r}')}{\partial n}\left(\int\limits_C e^{ikR\cos(\nu-\alpha)}\,d\alpha\right)\,d\mathbf{r}' = \frac{i}{4\pi}\int\limits_{\Gamma_\pm} \frac{\partial\phi(\mathbf{r}')}{\partial n}\left(\int\limits_C e^{i\mathbf{k}\cdot\mathbf{R}}\,d\alpha\right)\,d\mathbf{r}' \\ &= \int\limits_{\Gamma_\pm} \frac{\partial\phi(\mathbf{r}')}{\partial n}\left(\frac{i}{4\pi}\int\limits_C e^{i\mathbf{k}\cdot(\mathbf{r}-\mathbf{r}')}\,d\alpha\right)\,d\mathbf{r}' = \int\limits_C e^{i\mathbf{k}\cdot\mathbf{r}}\left(\frac{i}{4\pi}\int\limits_{\Gamma_\pm} \frac{\partial\phi(\mathbf{r}')}{\partial n}\,e^{-i\mathbf{k}\cdot\mathbf{r}'}d\mathbf{r}'\right)d\alpha \\ &= \int\limits_C P(k,\sin\alpha)\,e^{i\mathbf{k}\cdot\mathbf{r}}d\alpha \qquad (6.10)\end{aligned}$$

Comparing the expression above with that given in (6.6), we infer that

$$P(k,\sin\alpha) = \frac{i}{4\pi}\int\limits_{\Gamma_\pm} \frac{\partial\phi(\mathbf{x}')}{\partial n}\,e^{-i\mathbf{k}\cdot\mathbf{r}'}\,d\mathbf{x}'. \qquad (6.11)$$

For a Dirichlet problem we cannot specify $\partial\phi(\mathbf{r}')/\partial n$ in (6.10). However, if a suitable function for a trapped mode is found, the integral in (6.11) should decay exponentially as $x \to \pm\infty$. Suitable trial functions can be substituted for the planewave spectrum in (6.11) to verify whether they satisfy this exponential decay requirement. The results, although not exact for a trapped mode, can reveal useful properties of the spectrum function and give some useful insight of its mathematical form. Further progress can be made if the behaviour of $\phi(\mathbf{r})$ or its gradient could be known in certain regions of the domain. Let us assume that some geometric, symmetry or physical factors allows us to specify $\frac{\partial\phi(\mathbf{r})}{\partial x}$ on $x = 0$ for example. Then

$$\left.\frac{\partial\phi(\mathbf{r})}{\partial x}\right|_{x=0} = \int\limits_C ik\cos\alpha\,P(k,\sin\alpha)\,e^{iky\sin\alpha}\,d\alpha. \qquad (6.12)$$

and with the change of integration variable from α to

$$\lambda = \sin\alpha \qquad (6.13)$$

(6.12) becomes

$$\left.\frac{\partial\phi(\mathbf{r})}{\partial x}\right|_{x=0} = ik\int_{-\infty}^{\infty} P(\lambda)\, e^{iky\lambda}\, d\lambda. \tag{6.14}$$

If there is some well behaved function $f(k,y)$ which approximates the directional derivative of ϕ in the direction $+x$, at $x=0$

$$ik\int_{-\infty}^{\infty} P(\lambda)\, e^{iky\lambda}\, d\lambda \sim f(k,y) \tag{6.15}$$

then an approximation for $P(\lambda)$ is given by the Fourier inverse of Eq.(6.14), namely

$$P(\lambda) \sim -\frac{i}{2\pi}\int_{-\infty}^{\infty} f(k,y)\; e^{-iky\lambda}\; dy. \tag{6.16}$$

The remainder of this chapter is concerned with determining a suitable approximation for $P(k,\sin\alpha)$ for the Dirichlet problem ($\mathbb{D}$) as defined in Chapter 2, using these simple strategies. Broadly we proceed as follows:

- We first derive conditions on $P(k,\sin\alpha)$ motivated by the exponential decay condition at infinity. The requirement is that integration of Eq.(6.10) should result in an expression which decays exponentially as $x \to \pm\infty$. The direct application of the method above, coupled with the method of steepest descent, leads us to conclude that $P(k,\sin\alpha)$ can not be an analytical smooth function, hence we will consider functions which have two simple poles in the complex plane α.

- Guided by numeric results obtained computationally we assume a simple plane wave form for ϕ on the segment normal to the disc, on $x=0$, between the disc and the waveguide wall. This simple local approximation suggests that $P(k,\sin\alpha)$ must have two simple poles at two particular values of α which depend on $d-a$.

- Again, we use our BEM solutions to approximate the normal of the solution on the waveguide walls, in the far field. Using these simple planewave approximations we find the same contribution to $P(k,\sin\alpha)$ in the form of two simple complex poles at particular values of α.

- Using these properties and conditions on the plane wave spectrum, we finally derive a mathematical expression which satisfies certain criteria required for a trapped mode.

The asymptotic behaviour of the approximation obtained for ϕ is that of a nearly trapped mode, which is a perturbation of a genuine trapped mode solution.

6.3 Trapped mode - Case study

In this section we extend the procedure briefly introduced in the previous section, to the case of two dimensional Dirichlet acoustic waveguide described by two infinite parallel lines a distance $2d$ apart with sound hard disc (Neumann condition) of radius $a < d$, placed symmetrically between them. As discussed in Chapter (5), trapped mode exists for all discs of radius a such that $0 < a/d < 0.67$, at a frequency k satisfying $0.95\pi < kd < \pi$. For this Dirichlet problem, the velocity potential calculated at a field point $P(x, y) = P(\mathbf{x})$, not on any boundary ($P \in W \backslash \partial W$), according to Eq.(3.11), can be written as

$$\phi(\mathbf{r}) = \underbrace{\int_{\partial D} \phi(\mathbf{r}') \, \frac{\partial}{\partial n}\left(\frac{-i}{4} H_0^1(k_0 R)\right) \, d\mathbf{r}'}_{I_{\text{Disc}}} + \underbrace{\int_{\Gamma_\pm} \left(-\frac{\partial \phi(\mathbf{r}')}{\partial n}\right)\left(-\frac{i}{4} H_0^1(k_0 R)\right) \, d\mathbf{r}'}_{I_{\text{Waveguide}}} \quad (6.17)$$

where $\mathbf{r}', \Gamma_\pm, R$ are as defined in section (6.2). We shall refer throughout this chapter to $I_{\text{Disc}}, I_{\text{Waveguide}}$ as the Disc Integral and Waveguide Integral respectively.

Using the integral representation for H_0^1 (Eq.6.9) and expression (6.5) we have:

$$\begin{aligned}
\phi(\mathbf{r}) &= -\frac{i}{4\pi} \int_{\partial D} \phi(\mathbf{r}') \, \frac{\partial}{\partial n}\left(\int_C e^{i\mathbf{k}\cdot(\mathbf{r}-\mathbf{r}')} d\alpha\right) d\mathbf{r}' + \frac{i}{4\pi} \int_{\Gamma_\pm} \frac{\partial \phi(\mathbf{r}')}{\partial n}\left(\int_C e^{i\mathbf{k}\cdot(\mathbf{r}-\mathbf{r}')} \, d\alpha\right) \, d\mathbf{r}' \\
&= -\frac{i}{4\pi} \int_C e^{i\mathbf{k}\cdot\mathbf{r}} \left[\int_{\partial D} \phi(\mathbf{r}')(-i\mathbf{k}\cdot\hat{\mathbf{r}}') e^{-i\mathbf{k}\cdot\mathbf{r}'} d\mathbf{r}'\right] d\alpha + \frac{i}{4\pi} \int_C e^{i\mathbf{k}\cdot\mathbf{r}} \left(\int_{\Gamma_\pm} \frac{\partial \phi(\mathbf{r}')}{\partial n} \, e^{-i\mathbf{k}\cdot\mathbf{r}'} d\mathbf{r}'\right) d\alpha \\
&= \int_C P(k, \sin\alpha) \, e^{i\mathbf{k}\cdot\mathbf{r}} \, \mathrm{d}\alpha. \qquad (6.18)
\end{aligned}$$

where

$$P(k, \sin\alpha) = \frac{i}{4\pi} \left[\int_{\partial D} \phi(\mathbf{r}')(i\mathbf{k}\cdot\hat{\mathbf{r}}') \, e^{-i\mathbf{k}\cdot\mathbf{r}'} \mathrm{d}\mathbf{r}' + \int_{\Gamma_\pm} \frac{\partial \phi(\mathbf{x}')}{\partial n} \, e^{-i\mathbf{k}\cdot\mathbf{r}'} \mathrm{d}\mathbf{r}'\right] \quad (6.19)$$

and $\hat{\mathbf{r}}'$ is the unit position vector

$$\hat{\mathbf{r}}' = \left(\frac{x'}{\sqrt{x'^2 + y'^2}}, \frac{y'}{\sqrt{x'^2 + y'^2}} \right). \tag{6.20}$$

The integration order interchange in eqn. (6.18) is admissible as the limits of both integrals, with respect to α and $\mathbf{r}$, are $(-\infty, \infty)$. Also, the two separate integrals are convergent for a trapped mode, satisfying the theorems for reversing the order of integration [13].

We note that the plane wave spectrum $P(k, \sin\alpha)$ is determined by values of ϕ on ∂D and by its normal gradient on the waveguide walls. However, once the boundary conditions for the problem are prescribed, without fully solving the problem neither $\phi(\mathbf{r}')$ on ∂D nor its normal derivative $\partial\phi(\mathbf{r}')/\partial n$ on $\Gamma_- \cup \Gamma_+$ can not be specified.

We can however use the numeric results obtained with our BEM method and the exponential decay at infinity condition in order to obtain some suitable approximations for the solution in the far field and on $x = 0$ in the nearfield. These in turn will help us derive some properties for $P(k, \sin\alpha)$ and determine the type of function which would be suitable as a spectrum function for trapped mode.

In Fig. 6.3 we present six trapped mode plots for discs of increasing radii. An overview of solutions displayed in Fig. 6.3 reveals some common features and also some differentiating aspects, which help us determine which parameters depend on the obstacle size and which attributes are independent of a/d. For example, two main types of solution behaviour can be distinguished in each contour plot, the near field, where the dominant behaviour is oscillatory, and the far field where the potential decays exponentially. A comparison can be made between these contour plots, with respect to the extent of these fields. There is a transition between the near field, where the propagation vector in the x direction has a near zero or small imaginary part, and the far field where the solution decays to zero. There is a direct correlation between the disc size, and by extension the trapped mode frequency k, and the length of this transition region. In Table 6.1 we present computational results obtained for various a/d. Numerical results obtained with our BEM programme show that for each trapped mode, in the far field ($2\pi/k \ll |x|$), the solution is similar to a simple decaying mode in a waveguide without obstructions and the propagation vector components tend to constant values. Let these constant values be (μ_1, μ_2). We adopt the

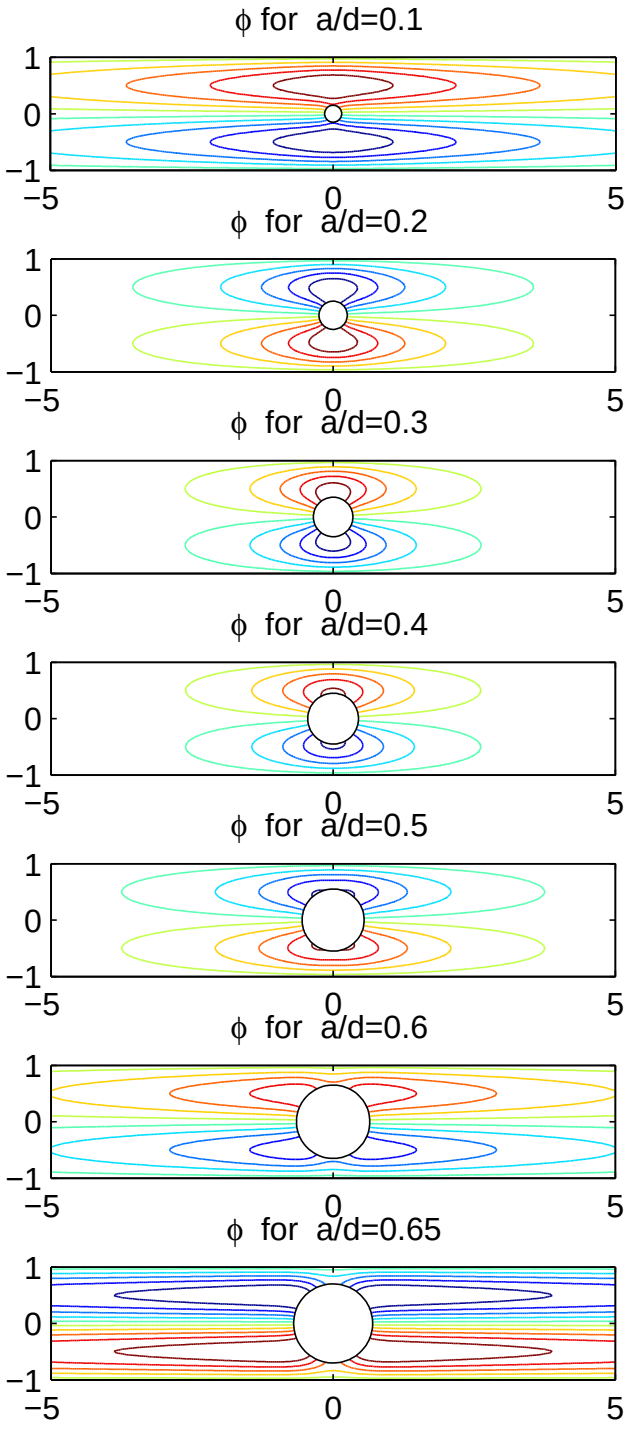

Figure 6.3: Trapped modes in a Dirichlet waveguide with a disc on the centreline.

notation

$$\mu_1 = k\cos\beta_0,$$
$$\mu_2 = k\sin\beta_0, \tag{6.21}$$

where β_0 is a particular value of α such that the constant components (μ_1, μ_2) are achieved. The horizontal component, μ_1 is imaginary hence it corresponds to the decay rate in the x direction. Using our BEM program we easily computed the decay rate for each mode and values for seven such cases are enclosed in Table 6.1. The decay rates obtained are similar to $\sqrt{k^2-(\pi/d)^2}$ for $0.2 \leq a/d \leq 0.5$. We notice that lower frequencies result in higher decay rates and oscillations vanish at short distances from the obstacle, hence determining the length of the transition region between the near field and the far field where the solution decays to zero. Going back to the contour plots in Fig. 6.3 we also notice some differentiat-

a/d	kd	μ_1	$\sqrt{k^2-(\pi/d)^2}$
0.1	3.1340	0.2028 i	0.2086 i
0.2	3.0618	0.7043 i	0.7054 i
0.3	2.9930	0.9534 i	0.9547 i
0.4	3.0001	0.9336 i	0.9342 i
0.5	3.0715	0.6547 i	0.6597 i
0.6	3.1331	0.2331 i	0.2369 i
0.65	3.1414	0.0021 i	0.00389 i

Table 6.1: Variation of solution decay rate, in the far field, with a/d . Values found computationally (μ_1) and comparison with $\sqrt{k^2-(\pi/d)^2}$.

ing aspects between modes which appear beyond certain threshold values of a/d . For discs of radius $0.5 \leq a/d < 0.67$, noticeable exponential decay appears in the region between disc and waveguide walls. This indicates that the vertical component of the propagation vector in the centre of the nearfield has a non-zero imaginary part. The behaviour of the solution in the nearfield is complicated and we could not describe it exactly using simple functions. We refer to the work of Callan *et. al* [10] and Maniar [47] where the appropriate Helmholtz potential satisfying (4.11 - 4.15) was constructed using an infinite linear com-

bination of all possible suitable modified multipoles. The wave vector components in the near field vary with x and y, in contrast to those in the far field, where the solution settled to an asymptotic decaying form.

We will now use these observations to approximate the solution in the far field, $x \to \infty$ and on the segments $x = 0,\ a < |y| < d$.

6.3.1 Far field

The cartesian and polar coordinates for a point in the far field are such that

$$\begin{aligned} r \to x,\ \theta \to 0, \\ y \ll x. \end{aligned} \tag{6.22}$$

and the potential in Eq. (6.18)

$$\phi(\mathbf{r}) \to \int_C P(k, \sin\alpha)\ e^{ikx\cos\alpha}\, \mathrm{d}\alpha. \tag{6.23}$$

The large x in the exponential term means that (6.23) is suitable for the application of the method of steepest descent, a classical procedure for approximating integrals in the complex plane. As this is a well known method for estimating integrals we only outline the main ideas, necessary for its application to our problem. A preliminary heuristic argument is based on the method of *stationary phase*. As $x \to \infty$ the amplitudes of the inhomogeneous waves are very small and such waves may be neglected. Moreover, the contributions of the homogeneous waves largely annul each other by destructive interference, since with $kx \gg 1$ the phase of the waves varies rapidly with α, in the sense that a phase change of π is achieved by only a small change in α.

If we assume that $P(k, \sin\alpha)$ is a smooth, analytical function of α then the method of stationary phase applies on contour C as it stands. Using the concept of phase interference the method asserts that when $kx \gg 1$ only the part of the integration path C, in the vicinity of a saddle point of the exponent ($\alpha = 0$), contributes significantly to the integral.

Consequently an approximation to (6.23) would be

$$P(k,0)\int_C e^{ikx\cos\alpha}\,\mathrm{d}\alpha. \tag{6.24}$$

The expression (6.24) is a multiple of the Hankel function, which does not decay exponentially away from the obstacle. This would be satisfactory only if $P(k,0)=0$ for the correct value of k. However, we have to consider the possibility that the spectrum function has one or more singularities in the complex plane and carry out a more rigurous analysis using the method of steepest descent which does not make *a priori* assumptions about the analyticity of $P(k,\sin\alpha)$.

6.3.2 Near field

The wave vector components in the near field vary with x and y, in contrast with those in the far field, where the solution settled to an asymptotic decaying form. However, guided by numeric results obtained with the BEM program, we carry out a simple analysis of the solution in the near field as follows: let the nearfield propagation vector be

$$\mathbf{k}\sim\boldsymbol{\eta}=(\eta_1,\eta_2). \tag{6.25}$$

Assume that the solution behaves locally as an inhomogeneous wave, then we can approximate ϕ by

$$\phi\sim Ae^{i\Psi(x,y)}, \tag{6.26}$$

We define the components of $\boldsymbol{\eta}$ as follows

$$\eta_1=\frac{\partial\Psi}{\partial x}\,,\eta_2=\frac{\partial\Psi}{\partial y}. \tag{6.27}$$

Differentiating ϕ twice

$$\begin{aligned}\frac{\phi_{xx}}{\phi}&=-\eta_1^2+i\frac{\partial\eta_1}{\partial x},\\ \frac{\phi_{yy}}{\phi}&=-\eta_2^2+i\frac{\partial\eta_2}{\partial y}.\end{aligned} \tag{6.28}$$

Both η_1 and η_2 vary with x and y. If we assume that $\frac{\partial \eta_1}{\partial x}, \frac{\partial \eta_2}{\partial y} \ll k^2$ then

$$\eta_1 \approx \sqrt{-\frac{\phi_{xx}}{\phi}},$$
$$\eta_2 \approx \sqrt{-\frac{\phi_{yy}}{\phi}}. \tag{6.29}$$

We thus use the numeric results for ϕ to obtain an overview of the magnitude of $\boldsymbol{\eta}$ components in the near field. Mapping the magnitude of η_2 across the nearfield gives an overview of the change from real to imaginary, hence from oscillation to decay in different regions of the guide. Examples of this mapping for six modes, are enclosed in Fig. 6.4. To interpret these figures we first note that

$$k^2 = \eta^2 = \eta_1^2 + \eta_2^2, \tag{6.30}$$

then we have two possible situations:

1. $\eta_2 < k$, $\eta_1 \in \mathbb{R}$: both components of the propagation vector are real, hence the solution oscillates in both directions. In our plots this behaviour corresponds to the blue palette.

2. $\eta_2 > k$, $\eta_1 \in \mathbb{C}$: the solution decays in the x direction. This corresponds in our plots to the red palette.

Based on the numeric results and boundary conditions on waveguide and disc at $x = 0$, we propose an approximation to ϕ along $x = 0, |y| > a/d$ as follows

$$\phi(x=0,y) \simeq \gamma(x=0,y) = \begin{cases} A \sin\left[\frac{\pi}{2}\frac{(y-d)}{d-a}\right], & y > a, \\ A \sin\left[\frac{\pi}{2}\frac{(y+d)}{d-a}\right], & y < -a. \end{cases} \tag{6.31}$$

where A is a constant and without loss of generality we will assume for the remainder of this chapter that it has been normalised, so that $A = 1$. Consequently the vector components of $\boldsymbol{\eta}$ are

$$\eta_1 = \sqrt{k^2 - \left(\frac{\pi}{2(d-a)}\right)^2},$$

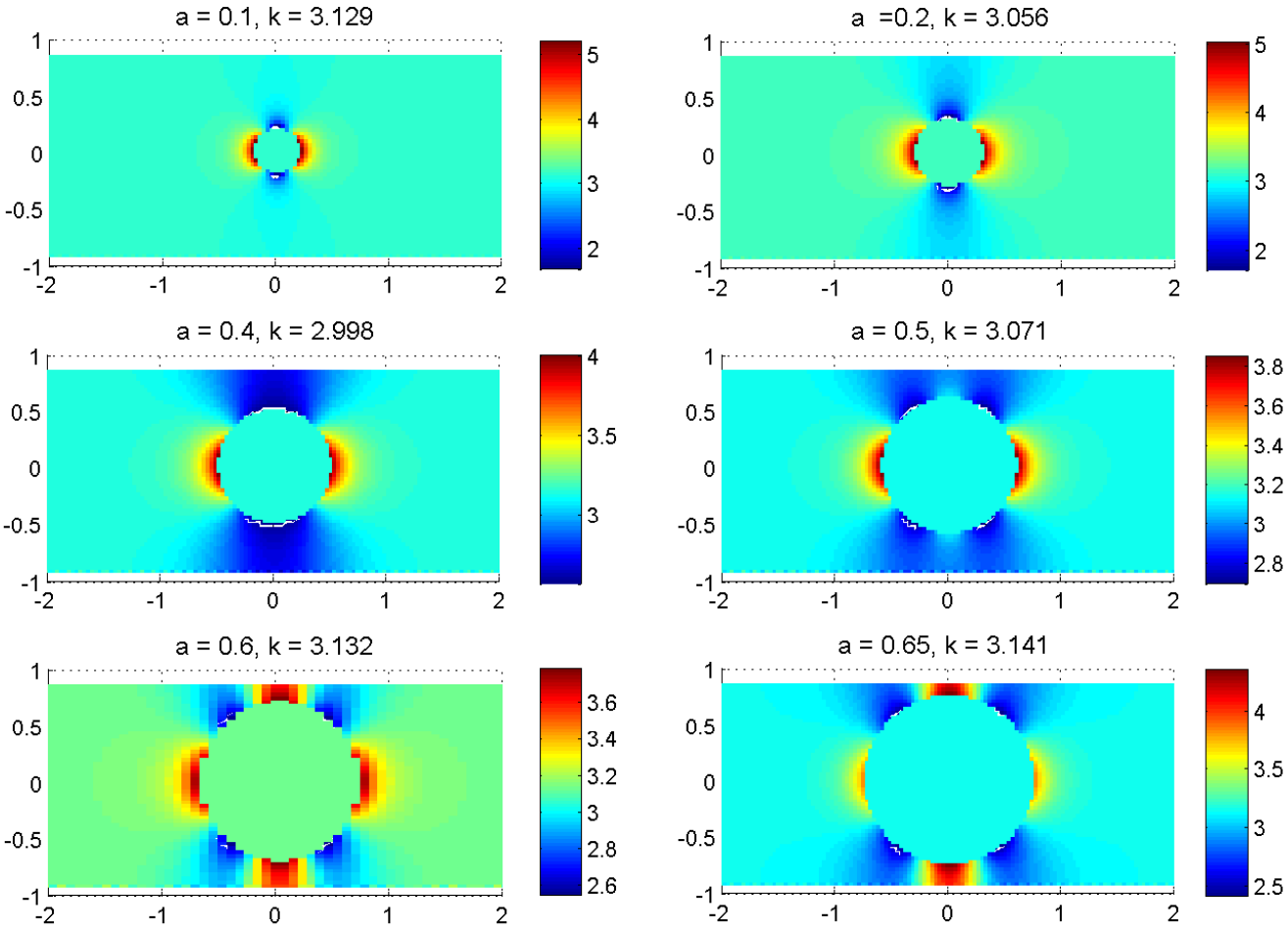

Figure 6.4: The magnitude of the vertical component, η_2, of the propagation vector, in the nearfield of trapped mode solutions for discs of different radii.

$$\eta_2 = \frac{\pi}{2(d-a)}, \tag{6.32}$$

The proposed function satisfies the boundary conditions on both the disc (Neumann) and waveguide (Dirichlet) at $y = 0$. We found an agreement between values for η_1 and η_2 in this region, computed according to (6.28), and illustrated in Fig.6.4, and those calculated according to (6.32). The latter values are enclosed in Table 6.2 for seven cases. This proposed form for ϕ and $\boldsymbol{\eta}$ (6.31 and 6.32 respectively) concurs with the appearance of exponential decay in the centre of the nearfield, in the region between disc and waveguide walls, for trapped modes for discs of radius $0.5 \leq a/d$. Highlighted figures in Table 6.2 show that for a radius such that $0.5 \leq a/d$ the horizontal component exceeds the magnitude of the propagation vector ($\eta_2 > k$) and this gives rise to inhomogeneous waves

in the x direction. We also note that if the components of the wavevector are achieved for a particular value of $\alpha = \alpha_0$ such that

$$\boldsymbol{\eta} = (\eta_1, \eta_2) = \eta(\cos\alpha_0, \sin\alpha_0), \tag{6.33}$$

then for cases where $0.5 \leq a/d$ this particular value of α_0 is imaginary and this tallies with the changes in the profile solution which occur in the near field as the disc radius becomes larger than 0.5 - see Fig. 6.3, i.e. the amplitude of the field decays in the region between the disc and the waveguide walls. We will now use this simple approximation to ϕ on $x = 0$,

a/d	kd	η_2	$\sin\alpha_0$	α_0
0.1	3.1340	1.7453	0.5569	0.5907
0.2	3.0618	1.9635	0.6413	0.6962
0.3	2.9930	2.2440	0.7497	0.8477
0.4	3.0001	2.6180	0.8726	1.0606
0.5	3.0715	3.1416	1.0228	$1.5708 - 0.2132\,\mathrm{i}$
0.6	3.1331	3.9270	1.2534	$1.5708 - 0.6977\,\mathrm{i}$
0.65	3.1414	4.4880	1.4287	$1.5708 - 0.8957\,\mathrm{i}$

Table 6.2: Approximation of magnitude of the vertical component (η_2) of the propagation vector, on the segments $x = 0, a < |y| < d$.

to investigate a suitable choice for $P(k, \sin\alpha)$ so that after carrying out the integration in Eq. (6.18), the result is similar to (6.31). According to (6.18) the solution on $x = 0$ is

$$\phi(x = 0, y) = \int_C P(k, \sin\alpha)\, e^{ik_2 y} \mathrm{d}\alpha = \int_C P(k, \cos\alpha)\, e^{iky\sin\alpha}\, \mathrm{d}\alpha. \tag{6.34}$$

We make the following change of variable

$$\sin\alpha = \lambda, \tag{6.35}$$

and obtain

$$\phi(x = 0, y) = \int_C P(k, \sin\alpha)\, e^{iky\cos\alpha}\, \mathrm{d}\alpha = \int_{-\infty}^{\infty} \frac{P(\lambda)}{\sqrt{1-\lambda^2}} \quad e^{iky\lambda}\ \mathrm{d}\lambda. \tag{6.36}$$

The integration path C now runs along the real axis with λ being a real variable. According to the Fourier theorem, the function $\frac{P(\lambda)}{\sqrt{1-\lambda^2}}$ is defined for all real values of λ such that

$$\frac{P(\lambda)}{\sqrt{1-\lambda^2}} = \frac{k}{2\pi} \int_{-\infty}^{\infty} \phi(y)\, e^{-iky\lambda}\, \mathrm{d}y. \tag{6.37}$$

The expression for $\frac{P(\lambda)}{\sqrt{1-\lambda^2}}$ must be such that the result of (6.36) should be similar to the function $\gamma(x = 0, y)$ which we proposed, based on our numeric results. We propose a spectrum, with simple poles at particular values of α, which when substituted in (6.36) achieve the form of ϕ we prescribed on $x = 0$. Let a particular complex value of λ_0 correspond to a particular value of the vertical component of the wavevector in the nearfield η_2

$$\eta_2 = k \sin \alpha_0 = k\lambda_0. \tag{6.38}$$

We consider the following spectrum function

$$P(\lambda) = \sqrt{1-\lambda^2}\, \frac{e^{-ik\lambda_0 d}}{2\pi i} \left(\frac{1}{\lambda - \lambda_0} + \frac{1}{\lambda + \lambda_0} \right). \tag{6.39}$$

and substitute it in (6.36). First let us consider what happens when integrating the first term in (6.39) above. Assume that λ_0 has a positive imaginary part. Then the path of integration in can be closed by an infinite semicircle, above the real axis if $y > 0$ and below when $y < 0$, without altering the value of the integral. As $\lambda \to \infty$, according to Jordan Lemma, there is no contribution to the integral (6.36) from the semicircular part of the path. Once the path has been closed the value of the integral it can be written down from Cauchy's residue theorem. Proceeding in the same manner with the second term we obtain for (6.36)

$$\phi(x = 0, y) \sim \begin{cases} -e^{ik\lambda_0(y+d)} & \text{for} \quad y < 0, \\ e^{ik\lambda_0(y-d)} & \text{for} \quad y > 0. \end{cases} \tag{6.40}$$

These results need only be expressed in a slightly different way to cater for the case when λ_0 is real. It is then necessary to indent the path of integration in (6.36) so that it avoids the pole at λ_0. Hence, referring back to (6.37) the formal inverse is

$$\frac{P(\lambda)}{\sqrt{1-\lambda^2}} = \frac{k\, e^{-i\eta_2 d}}{2\pi i} \left(\frac{1}{\lambda - \lambda_0} + \frac{1}{\lambda + \lambda_0} \right) = \frac{k\lambda\, e^{-i\eta_2 d}}{\pi i(\lambda^2 - \lambda_0^2)}. \tag{6.41}$$

The plane wave spectrum is then suggested to take the form of a function containing simple poles

$$\frac{k\, e^{-i\eta_2 d}}{2\pi i}\left(\frac{\cos\alpha}{\sin\alpha-\sin\alpha_0}+\frac{\cos\alpha}{\sin\alpha+\sin\alpha_0}\right). \tag{6.42}$$

This gives an useful insight into the type of terms the plane wave spectrum should include and will ensure that the simple functions used to approximate the normal on Γ_- and Γ_+ are appropriate. However, the expression for $P(\sin\alpha)$ is not complete; if we substitute this spectrum function in (6.10), for $x \to \pm\infty$ we obtain a sum of four Fresnel integrals, a result which does not satisfy condition $\phi \to 0$ for any $\pi/2 < kd < \pi$. The approximation (6.31) for ϕ on $x = 0$ factors meaningfully the size of the disc into the spectrum but does not reflect the behaviour of the solution on the boundary of the disc. An additional term which would account for the circular geometry of the obstacle will result in a spectrum which, for a particular frequency, satisfies the required decay condition at infinity.

For the remainder of this chapter we will use the results of our analysis to estimate the integral in (6.17). Based on these observations we choose simple functions to approximate either the potential or its normal on the boundary, and by direct substitution in (6.17) we will obtain a first representation of a trapped mode solution.

6.3.3 Disc integral

In this section we calculate the contribution to the plane wave spectrum coming from the disc integral (6.17) . We use the notation introduced in section (6.1) with the addition of polar coordinates; for a point $Q(x', y')$ on the disc boundary

$$\begin{aligned} x' = r\cos\upsilon, \quad y' = r\sin\upsilon, \\ \upsilon \in [0, 2\pi). \end{aligned} \tag{6.43}$$

From Eq.(6.18)

$$I_{\text{Disc}} = \int\limits_{\partial D} \phi(\mathbf{r}')\frac{\partial}{\partial n}\left(-\frac{iH_0^1(kR)}{4}\right) d\mathbf{r}' = -\frac{i}{4\pi}\int\limits_C e^{i\mathbf{k}\cdot\mathbf{r}}\left[\int\limits_{\partial D}\phi(\mathbf{r}')\frac{\partial}{\partial n}\left(e^{-i\mathbf{k}\cdot\mathbf{r}'}\right) d\mathbf{r}'\right] d\alpha$$

$$= -\frac{i}{4\pi}\int_C e^{i\mathbf{k}\cdot\mathbf{r}}\left[\int_{\partial D}\phi(\mathbf{r}')(-i\mathbf{k}\cdot\hat{\mathbf{r}}')\mathrm{e}^{-\mathbf{ik}\cdot\mathbf{r}'}\mathbf{dr}'\right]d\alpha. \tag{6.44}$$

Until we solve the full problem we can not specify $\phi(\mathbf{x}')$ on the circle. However, based on our numeric solution, an approximation for it, on the segments $\{x = 0, a < y < d\}$ and $\{x = 0, -d < y < -a\}$, is given by the function $\gamma(x = 0, y)$ (6.31) with $\boldsymbol{\eta}$ as in (6.32). Assuming that $a \to 0$ and that the solution is continuous in the region near the disc, the vertical component of ϕ could be locally approximated by (6.31). The horizontal component can also be locally approximated by a simple plane wave hence in the vicinity of the disc we assume that ϕ is

$$\phi \simeq \gamma(x,y) = \begin{cases} \cos\eta_1 x \sin\left[\frac{\pi}{2}\frac{(y-d)}{d-a}\right], & |x| < a,\ a < y, \\ \cos\eta_1 x \sin\left[\frac{\pi}{2}\frac{(y+d)}{d-a}\right], & |x| < a,\ y < -a. \end{cases} \tag{6.45}$$

This particular choice of γ is supported by results obtained using our BEM program - its values calculated along the disc surface agree with $\phi(\mathbf{x})$ computed numerically. To illustrate the similarity, plots of γ and actual values obtained for ϕ, computationally, for two cases ($a/d = 0.2$ and 0.6), are enclosed in Fig.6.5.

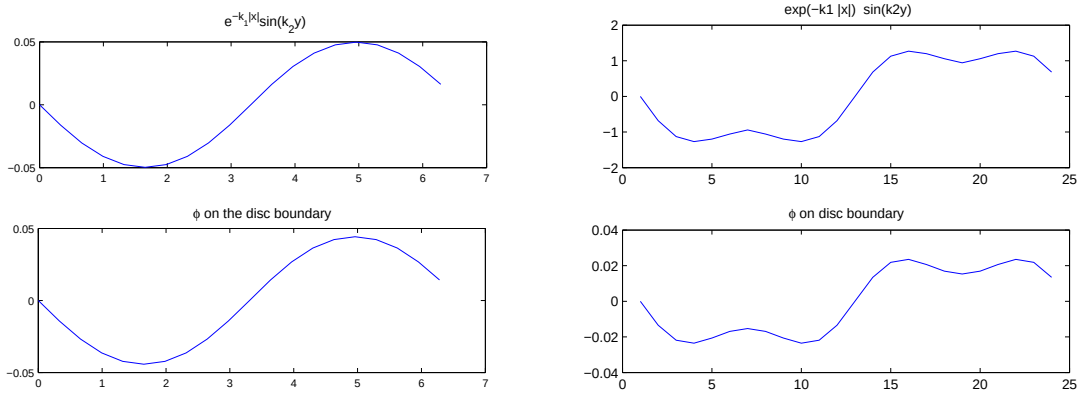

Figure 6.5: Potential computed using the boundary element program and γ values calculated using (6.45), on boundary of two discs ($a = 0.2$ and $a = 0.6$).

The trial function γ is then used as a substitution for $\phi(\mathbf{x}')$ in Eq.(6.44). Calculating the integral is straightforward and details are enclosed in Appendix **??**. The disc integral con-

tribution to the plane wave spectrum is

$$I_{Disc} \sim \frac{i\pi ka}{4} \cos\eta_2 d \sin\alpha_0 \sin\theta \; J_1(2ka) \; H_1^1(kr). \tag{6.46}$$

where a is the disc radius, k is the propagation vector magnitude and trapped mode frequency, α_0 is as defined in (6.33) and J_1 is the Bessel function of first kind and first order. To each disc radius corresponds a particular value α_0 and estimates for these angles are enclosed in Table 6.2.

6.3.4 Waveguide Integral

In this section we calculate the waveguide contribution to the plane wave spectrum function $P(\sin\alpha)$. For this we require a suitable function to describe the normal of ϕ on the waveguide walls. First let us consider the numeric results obtained using our BEM program. As discussed in section (6.3), in the far field the solution tends to a simple exponential mode, with a decay rate $\mu_1 \to \sqrt{(\pi/d)^2 - k^2}$. In Fig. 6.6 plots of $\frac{\partial\phi}{\partial n}$ and $\log\left(\frac{\partial\phi}{\partial n}\right)$ along Γ_- are shown. For $|x| > kd$ the normal on boundaries appears to be an exponential function, with a constant decay rate. It was also established that there is a requirement that $P(\sin\alpha)$ be a function with at least two simple poles, located at specific values of k_2. A simple function can be used to approximate the normal in the far field and obtain the terms prescribed by (6.42). This far field approximation will be continued in the nearfield as well. Let ν be a function which approximates the normal derivative on waveguide walls Γ_- and Γ_+ as follows

$$\Gamma_- : \frac{\partial\phi}{\partial n} = -\frac{\partial\phi}{\partial y} \sim \nu(\mathbf{r}') = \begin{cases} -\mu_2 e^{\mu_1 x'} \cos\mu_2 y' \,, & x' < 0, \\ -\mu_2 e^{-\mu_1 x'} \cos\mu_2 y' \,, & x' > 0, \end{cases} \tag{6.47}$$

$$\Gamma_+ : \frac{\partial\phi}{\partial n} = \frac{\partial\phi}{\partial y} \sim \nu(\mathbf{r}') = \begin{cases} \mu_2 e^{\mu_1 x'} \cos\mu_2 y' \,, & x' < 0, \\ \mu_2 e^{-\mu_1 x'} \cos\mu_2 y' \,, & x' > 0, \end{cases} \tag{6.48}$$

where the propagation vector $\boldsymbol{\mu} = (\mu_1, \mu_2)$ and the particular value of $\alpha = \beta_0$ are as introduced in (6.21). The transition between $\boldsymbol{\eta}$ and $\boldsymbol{\mu}$ is not trivial and we could not model its change with x adequately, hence only the latter wavevector is used in the expression of

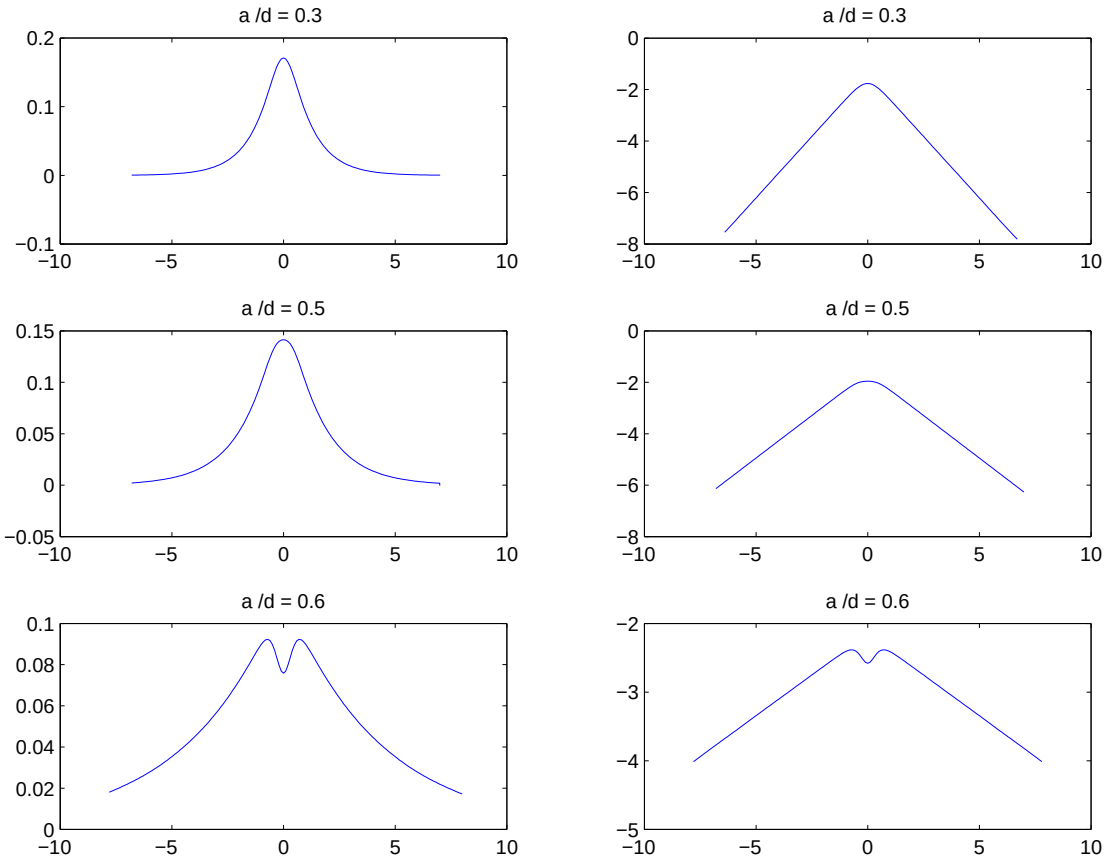

Figure 6.6: Figures on the left side correspond to $\partial\phi/\partial n$ on Γ_-(lower guide wall) obtained using the BEM program. Figures on the right side represent $\log\left(\frac{\partial\phi}{\partial n}\right)$ for the same radii.

ν. We substitute (6.47) and (6.48) in the waveguide integral

$$I_{\text{Waveguide}} = \frac{i}{4\pi}\int_C e^{i\mathbf{k}\cdot\mathbf{r}}\left(\int_{\Gamma_\pm}\frac{\partial\phi(\mathbf{r}')}{\partial n}\,e^{-i\mathbf{k}\cdot\mathbf{r}'}d\mathbf{r}'\right)d\alpha = \int_C\left(I_{\Gamma_-}+I_{\Gamma_+}\right)e^{i\mathbf{k}\cdot\mathbf{r}}d\alpha \qquad (6.49)$$

and obtain

$$\begin{aligned} I_{\Gamma_-} &\sim \int_{\Gamma_-}\nu(\mathbf{r}')\,e^{-i\mathbf{k}\cdot\mathbf{r}'}d\mathbf{r}' = -\mu_2\,\cos\mu_2 d\,e^{ik_2 d}\left(\frac{1}{\mu_1-ik_1}+\frac{1}{\mu_1+ik_1}\right) \\ &= -\frac{2\mu_1\mu_2\cos\mu_2 d\,e^{ik_2 d}}{\mu_1^2+k_1^2}, \end{aligned} \qquad (6.50)$$

$$I_{\Gamma_+} \sim \int_{\Gamma_+} \nu(\mathbf{x}')\, e^{-i\mathbf{k}\cdot\mathbf{r}'} d\mathbf{r}' = -\mu_2\ \cos\mu_2 d\, e^{-ik_2 d} \left(\frac{1}{\mu_1 - ik_1} + \frac{1}{\mu_1 + ik_1} \right)$$
$$= -\frac{2\mu_1\mu_2 \cos\mu_2 d\, e^{-ik_2 d}}{\mu_1^2 + k_1^2}, \tag{6.51}$$

$$I_{\Gamma_-} + I_{\Gamma_+} \sim -\frac{4\mu_1\mu_2 \cos\mu_2 d\ \cos k_2 d}{\mu_1^2 + k_1^2}. \tag{6.52}$$

The total waveguide contribution to the plane wave spectrum is:

$$I_{\text{Waveguide}} \sim -\frac{i}{\pi} \int_C \frac{\mu_1\mu_2 \cos\mu_2 d\ \cos k_2 d}{\mu_1^2 + k_1^2} e^{i\mathbf{k}\cdot\mathbf{r}} d\alpha. \tag{6.53}$$

The wavevector $\boldsymbol{\mu}$ is such that $\mu_2 = \pi/d$ and $k < \pi/d$ hence μ_1 is purely imaginary; therefore according to (6.7)

$$\mu_1^2 = \mu_2^2 - k^2, \tag{6.54}$$

and because $k^2 = \mu^2$

$$\mu_1^2 + k_1^2 = k_2^2 - \mu_2^2, \tag{6.55}$$

which allows us to re-write

$$I_{\text{Waveguide}} \sim -\frac{i\cos\mu_2 d}{2\pi} \int_C \cos k_2 d\ \left(\frac{\mu_1}{k_2 - \mu_2} + \frac{\mu_1}{k_2 + \mu_2} \right) e^{i\mathbf{k}\cdot\mathbf{r}} d\alpha$$
$$= -\frac{i\cos\mu_2 d}{2\pi} \int_C \cos k_2 d \left(\frac{\cos\beta_0}{\sin\beta_0 - \sin\alpha} + \frac{\cos\beta_0}{\sin\beta_0 + \sin\alpha} \right) e^{i\mathbf{k}\cdot\mathbf{r}}\, d\alpha. \tag{6.56}$$

The kernel of the waveguide integral resulted in a series of spectrum terms containing simple poles as prescribed by (6.42). We write compactly

$$I_{\text{Waveguide}} \sim \int_C P_{\text{Waveguide}}(k, \sin\alpha) e^{i\mathbf{k}\cdot\mathbf{r}} d\alpha, \tag{6.57}$$

where $P_{\text{Waveguide}}(\sin\alpha)$ is the waveguide contribution to the plane wave spectrum

$$P_{\text{Waveguide}}(\sin\alpha) = -\frac{i\cos\mu_2 d\ \cos k_2 d}{2\pi}\left(\frac{\cos\beta_0}{\sin\beta_0 - \sin\alpha} + \frac{\cos\beta_0}{\sin\beta_0 + \sin\alpha}\right). \tag{6.58}$$

To calculate this integral we will use the classic method of steepest descent adapted from Clemmow [15]. We first proceed by distorting the original path to pass through a saddle point $\alpha^S = \alpha_R^S + i\alpha_I^S$ - see Fig. 6.7. At the saddle point $\text{Re}(\psi)$ (ψ is as defined in eqn. (3)) attains its maximum value, then it rapidly decays away from the saddle point to $-\infty$. At the same time $\text{Im}(\psi)$ remains constant, on the distorted contour, and equal to its value at the saddle point

$$\text{Im}[\psi(\alpha)] = \text{Im}[\psi(\alpha^s)]. \tag{6.59}$$

If the real and imaginary parts of α are displayed explicitly

$$\alpha = \alpha_R + i\alpha_I \tag{6.60}$$

then the exponential in (6.57) is

$$\psi = ikr\cos(\alpha - \theta) = ikr\cos(\alpha_R - \theta)\cosh\alpha_I + kr\sin(\alpha_R - \theta)\sinh\alpha_I. \tag{6.61}$$

It is necessary for the convergence of the integral that $\sin(\alpha_R - \theta)\sinh\alpha_I$ be negative as $\alpha_I \to \pm\infty$. Consequently the extremes of any path of integration obtained by distorting C must lie in the sectors specified by:

$$\begin{aligned} -\pi + \theta < \alpha_R < 0 \quad &\text{when} \quad \alpha_I > 0, \\ \theta < \alpha_R < \pi + \theta \quad &\text{when} \quad \alpha_I < 0. \end{aligned} \tag{6.62}$$

For a point of interest in the field such that $x > 0$, $\theta \in \left[-\frac{\pi}{2}, \frac{\pi}{2}\right]$, hence the regions allowed for the modification of C are

$$\begin{aligned} -\frac{3\pi}{2} < \alpha_R < 0 \quad &\text{when} \quad \alpha_I > 0, \\ 0 < \alpha_R < \frac{3\pi}{2} \quad &\text{when} \quad \alpha_I < 0. \end{aligned} \tag{6.63}$$

The saddle point of interest, such that the real part of ψ attains a maximum value, is $\alpha^S = \theta$ with $\alpha_R^S = \theta$ and $\alpha_I^S = 0$. To obtain a meaningful approximation to (6.57) the requirement is that when moving away from the saddle point, we follow a path in the complex plane along which the real part of ψ decreases as rapidly as possible and its imaginary part is constant

$$\text{Im}(\psi) = \text{Im}[\psi(\alpha^S = \theta)] = ikr. \tag{6.64}$$

We proceed by distorting the original path of integration C into a new path along which $ikr[1 - \cos(\theta - \alpha)]$ is real. This path is found by applying the requirement in (6.64) to the imaginary part of ψ in 6.61).

$$\cos(\alpha_R - \theta)\cosh\alpha_I = 1. \tag{6.65}$$

For a given θ we find that two paths satisfying (6.65). For our problem we choose the one which passes through $\alpha = \theta$ at an angle $\frac{3\pi}{4}$ - see Fig. 6.7 - and call this modified path $S(\theta)$. Furthermore, (6.65) is equivalent to

$$\sin(\alpha_R - \theta) = -\tanh\alpha_I, \tag{6.66}$$

and when both these conditions, (6.65) and (6.66), are obeyed, Eq. (6.61) states that

$$ikr\cos(\alpha - \theta) = ikr - kr\sinh\alpha_I\tanh\alpha_I. \tag{6.67}$$

We modify our initial contour C to follow $S(\theta)$ where the real part of ψ has its maximum value, zero, at $\alpha = \theta$ and decreases monotonically to $-\infty$ away from the saddle point on either side. It is possible, after distorting the path to $S(\theta)$, to change the variable of integration from α to τ, where

$$ikr\cos(\alpha - \theta) = ikr - kr\tau^2, \tag{6.68}$$

and τ runs through real values from $-\infty$ to ∞. Expression (6.68) is equivalent to

$$\tau = \sqrt{2}e^{\frac{i\pi}{4}}\sin\frac{\alpha - \theta}{2}, \tag{6.69}$$

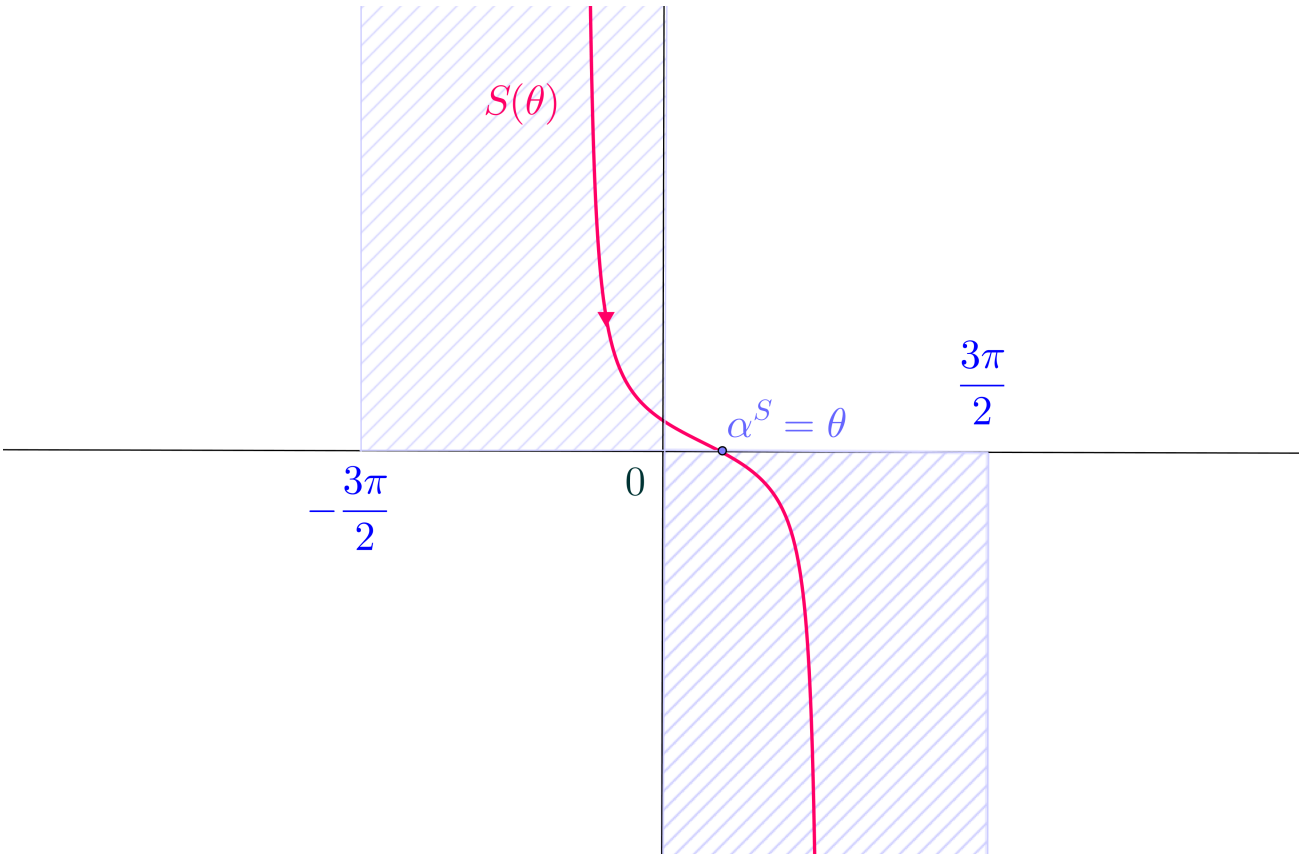

Figure 6.7: Modified C through the saddle point $\alpha^S = \theta$ and allowed regions (shadow) for the convergence of the waveguide integral.

so that

$$\begin{aligned} d\tau =& \frac{e^{\frac{i\pi}{4}}}{\sqrt{2}} \cos\frac{\alpha-\theta}{2}\, d\alpha \\ d\alpha =& \frac{\sqrt{2}\, e^{-\frac{i\pi}{4}}}{\cos\frac{\alpha-\theta}{2}}\, d\tau. \end{aligned} \tag{6.70}$$

and the explicit transformation of the waveguide integral (6.57) is

$$I_{\text{Waveguide}} = \sqrt{2}\, e^{-\frac{i\pi}{4}}\, e^{ikr} \int_{-\infty}^{\infty} \frac{P_{\text{Waveguide}}(k, \sin\alpha)}{\sqrt{1-\frac{i\tau^2}{2}}}\, e^{-kr\tau^2} d\tau. \tag{6.71}$$

This integral is calculated using a method adapted from Clemmow [15]. We omit the calculation here but details of the intermediary steps are included in Appendix C. $P_{\text{Waveguide}}(\sin\alpha)$

contains four simple poles (6.57) each corresponding to an expression involving a Fresnel integral. For the definition of the Fresnel complex integral please refer to eqn. (D.22), Appendix D. Let T_1, T_2, T_3 and T_4 be the four terms in I_{W} (6.57). We obtain the following

$$\begin{aligned} T_1 &= \int_C \frac{i\cos\mu_2 d\ \cos k_2 d}{4\pi} \tan\frac{\alpha-\beta_0}{2}\, e^{ikr\cos(\theta-\alpha)} d\alpha \\ &= \pm 4\sqrt{\pi} e^{i\left(kr-\frac{3\pi}{4}\right)} \frac{i\cos\mu_2 d\ \cos k_2 d}{4\pi} \sin\frac{\alpha-\beta_0}{2}\, F\left[\mp i\sqrt{2kr}\cos\left(\frac{\beta_0-\theta}{2}\right)\right], \end{aligned} \tag{6.72}$$

$$\begin{aligned} T_2 &= \int_C \frac{i\cos\mu_2 d\ \cos k_2 d}{4\pi} \tan\frac{\alpha+\beta_0}{2}\, e^{ikr\cos(\theta+\alpha)} d\alpha \\ &= \pm 4\sqrt{\pi} e^{i\left(kr-\frac{3\pi}{4}\right)} \frac{i\cos\mu_2 d\ \cos k_2 d}{4\pi} \sin\frac{\alpha+\beta_0}{2}\, F\left[\pm i\sqrt{2kr}\cos\left(\frac{\beta_0+\theta}{2}\right)\right], \end{aligned} \tag{6.73}$$

$$\begin{aligned} T_3 &= \int_C \frac{i\cos\mu_2 d\ \cos k_2 d}{4\pi} \cot\frac{\alpha-\beta_0}{2}\, e^{ikr\cos(\theta-\alpha)} d\alpha \\ &= \pm 4\sqrt{\pi} e^{i\left(kr-\frac{3\pi}{4}\right)} \frac{i\cos\mu_2 d\ \cos k_2 d}{4\pi} \cos\frac{\alpha-\beta_0}{2}\, F\left[\mp i\sqrt{2kr}\sin\left(\frac{\beta_0-\theta}{2}\right)\right], \end{aligned} \tag{6.74}$$

$$\begin{aligned} T_4 &= \int_C \frac{i\cos\mu_2 d\ \cos k_2 d}{4\pi} \cot\frac{\alpha+\beta_0}{2}\, e^{ikr\cos(\theta+\alpha)} d\alpha \\ &= \pm 4\sqrt{\pi} e^{i\left(kr-\frac{3\pi}{4}\right)} \frac{i\cos\mu_2 d\ \cos k_2 d}{4\pi} \cos\frac{\alpha+\beta_0}{2}\, F\left[\pm i\sqrt{2kr}\sin\left(\frac{\beta_0+\theta}{2}\right)\right]. \end{aligned} \tag{6.75}$$

To calculate the Helmholtz potential at a point of interest with polar coordinates (r, θ) the initial path C is indented to avoid the simple poles as listed in Table 6.3. The modified path $S(\theta)$ crosses the saddle point $\alpha^s = \theta$ and it will capture these poles or not depending on the θ coordinate. To illustrate this let us consider a field point with $x > 0\ , -\frac{\pi}{2} < \theta < \frac{\pi}{2}$. The relevant saddle-point is at $\alpha^S = \theta$ so allowance must be made for the saddle point lying arbitrarily close to the poles. But $\beta_0 = \sin^{-1}\left(\frac{\mu_2}{k}\right)$, $\mu_2 = \pi$ and $k < \pi/d$ hence $\beta_0 \in \mathbb{C}, \beta_0 = \frac{\pi}{2} - i\xi$ for some $\xi \in \mathbb{R}$. When distorting the initial path of integration C into $S(\theta)$, to allow the approximation of the integral via the steepest descent method, the poles captured are β_0 and $\frac{\pi}{2} - i\xi, -\frac{\pi}{2} + i\xi, \xi \in \mathbb{R}$. Adding the two expressions, for I_{Disc}

Term	Pole
$\sec\left(\frac{\alpha-\beta_0}{2}\right)$	$\alpha = \pi + \beta_0$
$\sec\left(\frac{\alpha_0+\beta_0}{2}\right)$	$\alpha = \pi - \beta_0$
$\mathrm{cosec}\left(\frac{\alpha-\beta_0}{2}\right)$	$\alpha = \beta_0,\ 2\pi + \beta_0$
$\mathrm{cosec}\left(\frac{\alpha+\beta_0}{2}\right)$	$\alpha = -\beta_0, 2\pi - \beta_0$

Table 6.3: Values of α where the path integration must be indented above poles

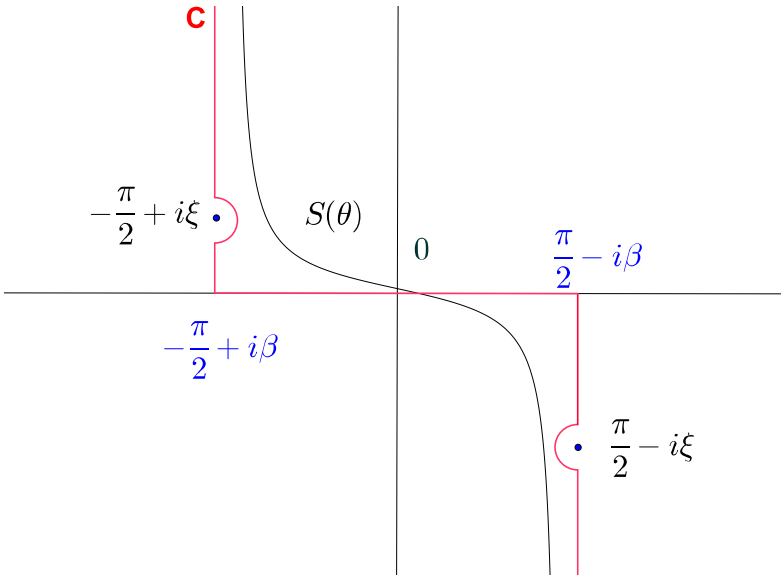

Figure 6.8: Deformed α - contour, $S(\theta)$. Poles are captured or not depending on θ.

and $I_{\text{Waveguide}}$, we obtain an approximation of a trapped mode solution

$$\phi(r,\theta) \approx \frac{i\pi ka\cos\eta_2 d}{4}\sin\alpha_0\sin\theta\ J_1(2ka)\ H_1^1(kr) + \frac{\cos[(k\sin\theta)d]}{\sqrt{\pi}}e^{i\left(kr-\frac{\pi}{4}\right)}$$
$$\left\{\pm\sin\left(\frac{\theta-\beta_0}{2}\right)F\left[\mp i\sqrt{2kr}\cos\left(\frac{\beta_0-\theta}{2}\right)\right]\right.$$
$$\mp\sin\left(\frac{\theta+\beta_0}{2}\right)F\left[\pm i\sqrt{2kr}\cos\left(\frac{\beta_0+\theta}{2}\right)\right]$$
$$\left.\pm\cos\left(\frac{\theta+\beta_0}{2}\right)F\left[\mp i\sqrt{2kr}\sin\left(\frac{\beta_0+\theta}{2}\right)\right]\right.$$

$$\mp \cos\left(\frac{\beta_0-\theta}{2}\right) F\left[\pm i\sqrt{2kr}\sin\left(\frac{\beta_0-\theta}{2}\right)\right]\Bigg\}. \tag{6.76}$$

with the proviso that the sign of each term must be considered for each point in the domain as the integration path is distorted according to the method of steepest descent. Also, the sign of the argument of each Fresnel term must take into account the value of the angle ($\frac{\beta_0\pm\theta}{2}$), and in principle for each point it has to be decided whether each simple pole is captured or not, depending on the position of the point in the field.

The disc integral results in a term involving a Hankel function which reflects the radial symmetry of the obstacle. The waveguide contribution is a series of the Fresnel integrals, commonly found in optics, in particular describing nearfield solutions to problems involving diffraction by infinite screens - which in our problem correspond to the infinite waveguide walls.

As (6.76) is obtained using simple plane wave approximations of the solution and its normal on boundaries, it is not expected to faithfully describe the nearfield potential where the solution has a complex behaviour.

To assess the validity of (6.76) as a trapped mode prediction tool it is necessary to consider its behaviour as $x \to \pm\infty$. The far field behaviour of the Hankel function [1] is given by

$$H_1^1(kr) \approx \sqrt{\frac{2}{\pi kr}}\, e^{i\left(kr-\frac{3\pi}{4}\right)} \tag{6.77}$$

hence I_{Disc} (6.46), as $r \to x \to \pm\infty$, asymptotically behaves like

$$I_{Disc} \approx \frac{1}{2}\sqrt{\frac{\pi}{2}} e^{-\frac{i\pi}{4}} \cos\eta_2 d \sin\alpha_0 \;\sin\theta\; ka\; J_1(2ka)\; \frac{e^{ikr}}{\sqrt{kr}} \tag{6.78}$$

By Clemmow [15] an asymptotic expansion for the complex Fresnel integral

$$F(a) \approx \frac{1}{2ia}\left[1 + \frac{1}{(-2ia^2)} + \frac{1\cdot 3}{(-2ia^2)^2} + \ldots\right] \tag{6.79}$$

can be used when

$$\left|\sqrt{2kr}\cos\left(\frac{\beta_0\pm\theta}{2}\right), \sqrt{2kr}\sin\left(\frac{\beta_0\pm\theta}{2}\right)\right| >> 1. \tag{6.80}$$

For a point in the field such that $\theta \in (-\frac{\pi}{2}, \frac{\pi}{2})$, using the first term of (6.80), the waveguide integral (6.71) is

$$I_{\text{Waveguide}} \approx \frac{\cos[(k\sin\theta)d]\ e^{-\frac{i3\pi}{4}}}{2\sqrt{2\pi}} \left[\cot\left(\frac{\beta_0-\theta}{2}\right) - \cot\left(\frac{\beta_0+\theta}{2}\right) + \tan\left(\frac{\beta_0+\theta}{2}\right) - \tan\left(\frac{\beta_0-\theta}{2}\right)\right] \frac{e^{ikr}}{\sqrt{kr}}. \tag{6.81}$$

We hence obtain an approximation of our solution which is valid as $x \to \infty$

$$\begin{aligned}\phi(\theta) \approx &\left\{ \underbrace{\frac{1}{2}\sqrt{\frac{\pi}{2}} e^{-\frac{i\pi}{4}} \cos\eta_2 d\ \sin\alpha_0\ \sin\theta\ ka\ J_1(2ka)}_{E(D)} + \right. \\ &\left. \underbrace{\frac{\cos[(k\sin\theta)d]\ e^{-\frac{i3\pi}{4}}}{\sqrt{2\pi}} \left[\frac{\cos\beta_0}{\sin\beta_0-\sin\theta} - \frac{\cos\beta_0}{\sin\beta_0+\sin\theta}\right]}_{E(W)} \right\} \frac{e^{ikr}}{\sqrt{kr}} \\ &= E(k)\,\frac{e^{ikr}}{\sqrt{kr}}.\end{aligned} \tag{6.82}$$

Here $E(D), E(W)$ correspond to terms from the disc integral and waveguide integral respectively. The solution obtained depends on $k, a/d$ and the position of the field point. We now check the behaviour of this solution as $x \to \infty$, that is $\theta \to 0$. For $\theta << 1$ we know that

$$\frac{y}{x} = \tan\theta \approx \sin\theta \approx \theta. \tag{6.83}$$

We have for the coefficients in (6.82) above, the following

$$E(D) = \frac{a}{2}\sqrt{\frac{\pi}{2}}\ e^{-\frac{i\pi}{4}} \cos\left[\frac{\pi d}{2(d-a)}\right] \frac{\pi}{2(d-a)} J_1(2ka)\,\frac{y}{x}, \tag{6.84}$$

$$\begin{aligned}E(W) =& \frac{e^{-\frac{i3\pi}{4}}}{\sqrt{2\pi}} \cos\left(\frac{ky}{x}\right) \frac{2\cos\beta_0\sin\theta}{(\sin\beta_0)^2-(\sin\theta)^2} = \frac{2e^{-\frac{i3\pi}{4}}}{\sqrt{2\pi}} \frac{\cos\beta_0}{(\sin\beta_0)^2}\frac{y}{x} \\ =& \frac{2e^{-\frac{i3\pi}{4}}}{\sqrt{2\pi}} \frac{k\sqrt{k^2-(\pi/d)^2}}{(\pi/d)^2} \frac{y}{x}\end{aligned} \tag{6.85}$$

In virtue of (6.83) we discarded the term $(\sin\theta)^2$ in (6.85). We also assumed that $\cos\left(\frac{ky}{x}\right) \approx 1$ for $\theta \to 0$. For a trapped mode the coefficients of the terms of order O(x^{-1}) should cancel out. We now have a complex equation for k depending only on the geometric ratio a/d:

$$\frac{a}{2}\sqrt{\frac{\pi}{2}}\, e^{-\frac{i\pi}{4}} \cos\left[\frac{\pi d}{2(d-a)}\right] \frac{\pi}{2(d-a)} J_1(2ka) + \frac{2e^{-\frac{i3\pi}{4}}}{\sqrt{2\pi}} \frac{k\sqrt{k^2-(\pi/d)^2}}{(\pi/d)^2} = 0. \quad (6.86)$$

We find that for the real and the imaginary part of the equation (6.86) have one, common solution, for each a/d such that $kd < \pi$. These values of k, similar to those obtained for trapped modes, are listed in Table 6.4. In Figure 6.9 we show an example ($a/d = 0.1$) where both the real and imaginary part of $E(k)$ become zero for a particular value of kd. The validity of Eq. (6.82), in the sense that it can correctly predict whether a particular

a/d	**Actual** kd	**Solutions of (6.86)**
0.1	3.1340	3.1415
0.2	3.0618	3.0666
0.3	2.9930	2.9460
0.4	2.9907	2.8922
0.5	3.0715	2.9027
0.6	3.1331	3.1389
0.65	3.1414	N/A

Table 6.4: Comparison of trapped mode frequencies found using our BEM program and solutions of (6.86).

geometry may support a trapped mode, is supported by the following criteria

1. The solution exhibits decay away from the trapping structure, that is $\phi \to 0$ as $\theta \to 0$.

2. The trapped mode frequencies are very similar to those obtained using our BEM program.

3. k varies with the radius of the disc in a specific manner - see Fig. 6.10 below. The pattern followed by the values of k which solve the real and the imaginary parts of (6.86) is similar to that of trapped mode frequencies found computationally: $kd \to \pi$ for $a/d \to 0$, then decreases with the increase of the radius, up to $a/d = 0.34$ where it reaches a minimum value of $kd \approx 2.98$. After this point kd increases and as

$a/d \to 0.67, kd \to \pi$. The behavioural similarity is illustrated by Figure 6.10 which shows side by side the variation of trapped mode frequencies found computationally and the same for the values of kd which solve the real and the imaginary parts of the equation (6.86).

4. A trapped mode exists only for radii such that $0 < a/d < 0.67$. We find that the real and the imaginary parts of (6.86) have a solution only for $0 < a/d < 0.62$; for $a/d > 0.62$ (6.86) does not have a solution in the range $\pi/2 < kd < \pi$.

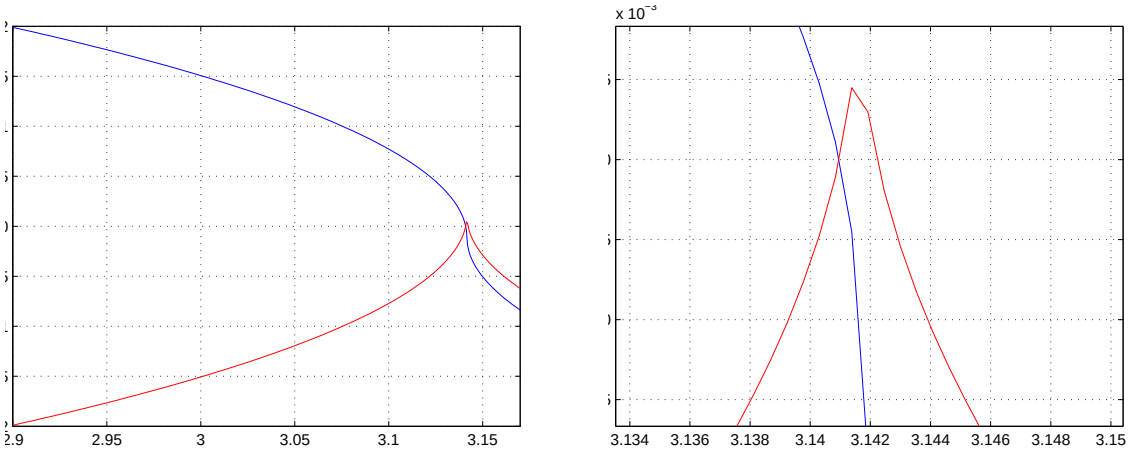

Figure 6.9: Real (blue) and imaginary (red) parts of $E(k)$ for a disc of radius $a/d = 0.1$ and detail of intersection on kd - axis.

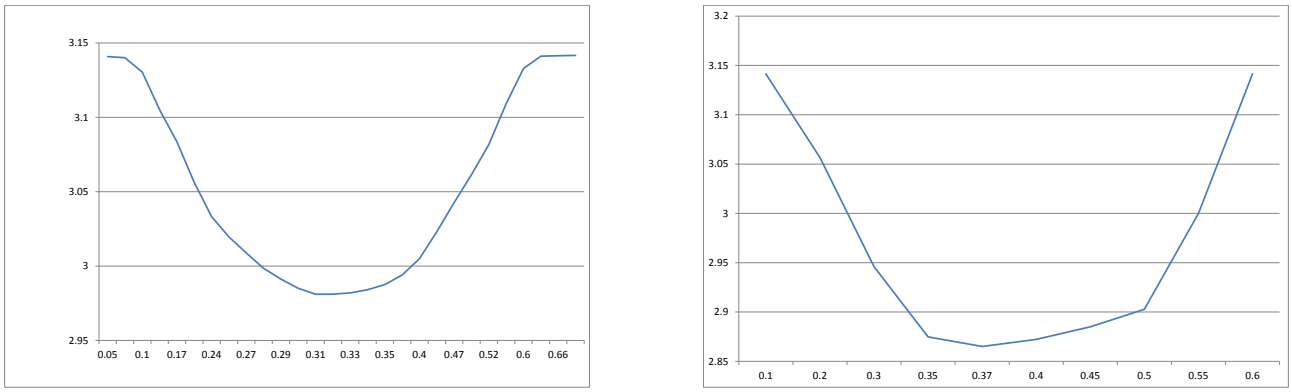

Figure 6.10: Variation of kd with radius of disc a/d for trapped modes found computationally using the boundary element method and values of kd which solve (6.86).

All four criteria listed above are satisfied and we believe that this is a strong endorsement of

the validity of the trapped mode approximation and of the method developed in the sense that it correctly signals the existence of a trapped mode. We also note that the Fresnel integrals are solutions to diffraction problems that are valid in the nearfield, therefore our approximation although not valid near the disc, is adequate for field points located one wavelength away from the origin.

Another test for the validity of this approximation is as follows: for a fixed $|y| < d$ coordinate we plot the solution $\phi(x)$, found numerically with our BEM program. The curve away from the trapping structure is exponentially decaying with absolutely no oscillation in the far field. We call this plot a trapped mode signature. For the same coordinates, (6.73) gives a superposition of oscillating modes and a mode with exponential decay, in both directions, $x \to \pm\infty$. A trapped mode corresponds to an isolated eigenvalue in the continuous spectrum of the relevant operator. For frequencies close to the isolated eigenvalue, we obtain nearly trapped modes, which are perturbations of a trapped mode and appear as superpositions of travelling modes and an exponentially decaying mode. The approximation we obtain with (6.76) is a nearly trapped mode, similar to a highly perturbed trapped mode. The purely exponential decaying mode can only be obtained by calculating exactly the solution for the precise trapped mode frequency. The exponential decay envelope seen in Fig. 6.11 is only present, for a given obstacle, for a particular value of k/d (e.g for $a/d = 0.4$, $kd = 2.8922 = 0.9206\pi$). Plots for both cases, a trapped mode signature and the trapped mode approximation are shown in Fig.(6.11).

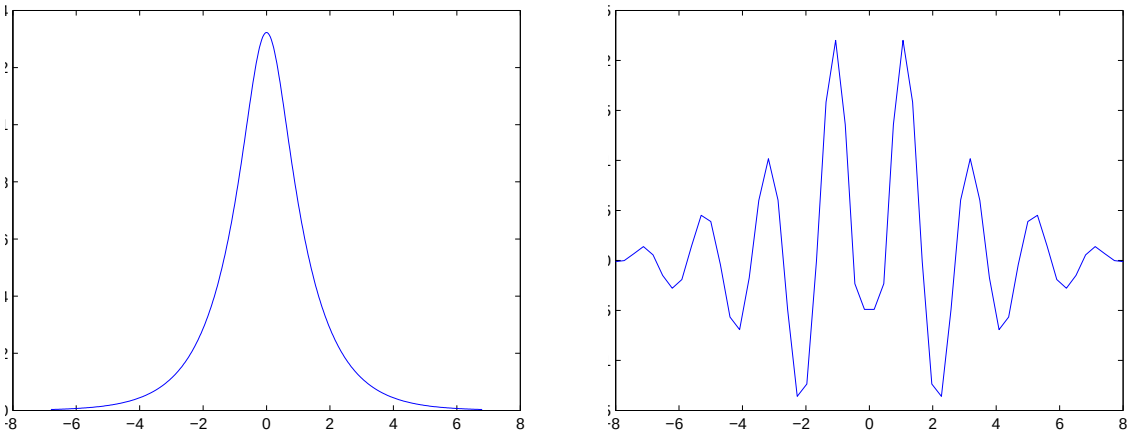

Figure 6.11: Trapped mode signature - ϕ for fixed y coordinate and the nearly trapped mode obtained using (6.73), both cases for a disc of radius $a/d = 0.4$.

6.4 Summary of Chapter

We developed a method which uses simple trigonometric trial functions to investigate whether a trapped mode can be present in a given geometry. Although the approximations are fairly crude this observation in conjunction with the planewave spectrum method was used to obtain a useful approximating treatment by virtue of proceeding from boundary *values* rather than boundary *conditions*.

The plane wave spectrum analysis, as applied here, can be adapted to other trapped mode problems. All the trapped modes we detected have an exponentially decaying part in the far field and an oscillatory nearfield component. The approximation of the solution by a simple decaying mode in the far field applies to all trapped modes in an infinite waveguide, irrespective of the trapping structure. Also, although crude approximations, simple oscillations in the nearfield, with wavelength comensurate with elements of the geometry, can be substituted for the solution in the nearfield and a suitable form for the planewave spectrum may be found.

The results, although not exact for a trapped mode are important as near trapping arises in corresponding finite array of cylinders as shown by Maniar and Newman [47] and Evans and Porter [24]. Maniar and Newman calculated the distribution of forces along a finite array of 100 cylinders at the 'near-trapping' frequency and shown that the force on the middle cylinder is approximately 34 times higher than that on an isolated cylinder force. We also refer to Fig. 11(a) in [24] which shows the free-surface elevation in the plane touching the outside of cylinders in head seas at the near-trapping frequency. The profile is similar to the near trapped mode potential obtained using our approximation and plotted in Fig. 6.11.

Chapter 7

Summary and concluding remarks

7.1 Summary

The thesis has studied trapped modes in waveguides, governed by the two dimensional Helmholtz equation. Our approach to investigating this problem was twofold. Firstly, we developed a numerical method which can be used to study the problem over a wide range of bounded or unbounded 2-D domains. More specifically, based on a boundary integral method we wrote a boundary element program, using Matlab software. The program identifies the eigenmodes and eigenfrequencies which depend on a finite set of parameters, including wave frequency and the domain configuration. We explored various methods of differentiating between real trapped modes and spurious eigenvalues, induced by the truncation of the domain. The most time efficient and reliable method we developed is based on the computation of an energy dissipation index (EDI) for a range of geometric parameters and frequencies. The method relies on the fact that perturbations of trapped modes result in nearly trapped modes, which have a higher radiation loss but much lower than that of a travelling mode. The EDI results for various parameter values provide a good indication of potential candidates for real trapped modes.

Secondly, we carried out an analytical investigation of the trapped modes. Using our detailed numerical results we established general features of trapped mode solutions, common to many geometries. One particular observation was that a good local approximation for the solution on the boundary is provided by simple trigonometric functions. These trial

functions were chosen to fit numerical results and also took into account the local boundary conditions and geometry. We then adapted the planewave spectrum analysis method, developed by Clemmow [15] for various problems in the classical theories of radiation, diffraction and propagation, and applied it to the case of a disc on the centreline of an infinite Dirichlet acoustic waveguide. The approach uses planewaves travelling in diverse directions to build a more elaborate approximate solution, which satisfies certain conditions required for a trapped mode.

We obtained a simple mathematical approximation of a mode which satisfies a set of criteria which is also satisfied by the corresponding trapped mode. From the asymptotic analysis for this solution we obtained an equation for k which depends only on the geometric ratio a/d. This equation has solutions which are very similar to the trapped mode frequencies. Asymptotically, the solution obtained is similar to a nearly trapped mode, which is a perturbation of a genuine trapped mode. The results, although not exact may be useful as near trapping appears in configurations which are approximations of a geometry required for a trapped mode. The general procedure is similar for any shape of the trapping obstacle or the boundary conditions and could be adapted to other geometries.

Using the boundary element program we found additional modes for some geometries already studied and also investigated new structures. We extended the results of Evans and Porter [26] for two intersecting sound-hard discs, in Neumann and Dirichlet waveguides. We studied this geometry in the non-embedded regime for two discs of equal radius and discs of different radii. We also studied this configuration for the next band of frequency values, $\pi < kd < 2\pi$ and found that embedded modes exist for discrete values of the distance between discs and any ratio $a/d \leq 0.4$ for Neumann waveguides and $a/d \leq 0.3$, for Dirichlet waveguides.

We also studied the case of a rectangular cavity of depth h and width $2w$ in a Dirichlet infinite waveguide of width $2d$, for two frequency bands, $0 \leq kd \leq \pi/2$ (non-embedded) and $\pi/2 < kd \leq \pi$ (embedded). For small widths of the cavity, the eigenmode decays slowly with distance x, and the trapped mode is close to the cut-off frequency $\pi/2d$. As $w \to 0$, the solution approaches the non-trapped standing wave solution. Keeping $h/d = 1$ fixed and varying w/d, we found that in the non-embedded regime for $1.2 \leq w$ at least one trapped mode exists for each value of w. As the cavity width is increased additional

modes appear. Embedded trapped modes exist at discrete couples $(h/d, w/d)$. For cavities of dimensions in the range $0 < h/d \leq 6$, $0 < 2w \leq 6$ we found seven modes, listed in Table 5.4. Notably, one geometry with $h/d = 2.2, w/d = 2.9$, supports two x-symmetric trapped modes, at two different frequencies.

We also considered triangular cavities in a Neumann waveguide and the frequency band $0 < kd \leq \pi/2$. As we do not impose any symmetry condition with respect to the centreline of the guide, all modes found are embedded. We checked cavities in the range $0 < h/d < 6$, $0 < 2w/d < 6$ and found five trapped modes for this type of geometry, for discrete couples $(h/d, w/d)$.

To establish whether cavities without corner singularities would still have trapped modes, we looked at a Dirichlet waveguide with a smooth lower boundary, modelled by a Gaussian function. Keeping $h/d = 1$ fixed we checked the frequencies range $0 < kd < \pi/2$ and found that non-embedded trapped modes exist for all w/d and their k-values vary continuously with the geometry. Embedded modes in the higher frequency range, $\pi/2 < kd < \pi$, exist only for discrete pairs $(h/d, w/d)$. Details of two embedded modes we found for this case are in Table 5.5.

The combination of a disc aligned with a cavity increases the affinity of a geometry to trapped mode type resonances. We studied this geometry with Neumann condition on the disc and either Neumann or Dirichlet boundary conditions on the waveguide walls and Neumann condition on the disc. For the Neumann problem we found that trapped modes exist in the band $0 \leq kd \leq \pi$ for discs of all radii and for cavities of specific depth and width. The majority of modes are y-antisymmetric and can be either x-symmetric or antisymmetric. Some modes are neither symmetric nor anti-symmetric with respect to the guide centreline.

We also considered the combination of a disc and a cavity, in Dirichlet or Neumann waveguides, without any (x, y) symmetry. If the disc is removed from the centre of the guide any existing trapped mode will be destroyed. As the separation between the disc and the cavity becomes larger than approximately 2λ, depending on the disc radius and cavity size, nearly trapped modes appear, corresponding to the pure trapped modes for either a single cavity or a single disc in the waveguide. The frequencies are similar but not identical to those corresponding to the pure trapped modes. We did not find any trapped modes for

asymmetric geometries, irrespective of the disc radius and cavity size. This does not exclude the possibility that a trapped mode may exist for a specific combination of geometric parameters, however we were unable to identify such a geometry.

7.2 Possible applications

Possible applications fall into three broad categories: first, the situations where trapped modes are undesirable, as the accumulation of energy can have destructive effects on a structure. Already known examples are constructions supported by large arrays of standing columns (offshore platforms, bridges and proposed designs for floating airports), long tunnels for high speed trains and cavities in quantum waveguides, with application in particle accelerators. Here, the detection of trapped or nearly trapped modes is essential and a simple method to avoid them, where design permits, is to break the symmetry of the configuration.

The second category relates to information about structures which are not directly accessible. Trapped modes are suitable for these applications due to their high localisation and the fact that they are sensitive to environmental changes. A growing body of research is concerned with their use for sensors and non-destructive testing. A part of the energy in a propagating guided wave excites the trapped energy mode through mode conversion and then leaks out [16]. This leak appears as a long-tailed ringing due to a high Q of the trapped mode [53]. Q, the quality factor of an oscillator, is the standard term in physics that describes how efficiently energy is stored rather than lost by a resonator or equivalently the resonant frequency over the bandwidth of the resonance. The resonant frequency and Q of a trapped energy is sensitive to changes in its vibrating region and hence can be used to sense changes in waveguide width, surface condition (roughness and corrosion) and liquid properties (density and viscosity) [53]. Extensive experiments in this regard have been conducted recently at the University of Tokyo [55] to assess the feasibility of remote excitation of trapped energy modes in plates and pipes and its applications to sensors and non-destructive testing. This is of practical interest, because for example pipes are used in many engineering applications, chemical processing and micro-capillaries are used in biomedical applications.

A third category is that of structures where high resonance at a narrow band of frequencies is desired. A rapidly growing area of research is that of trapped modes in metamaterials

i.e. in artificially structured matter with new properties, some with no analogue in naturally available materials. The exotic and often dramatic functionality of most metamaterials is based on the resonant interactions of the metamaterial constituents with the incident electromagnetic radiation and the associated dispersive effects [69]. Hence achieving resonances with high-quality factors is essential in order to make metamaterials performance efficient. However, resonance quality factors demonstrated by conventional metamaterials are often limited to rather small values due to the fact that resonating structural elements suffer significant losses due to radiation. As recent theoretical analysis showed, high-Q resonances involving trapped modes are possible in metamaterials [64]. Fedotov *et al.* reported exceptionally narrow transmission and reflection resonances in planar metamaterials [30]. The appearance of the narrow resonances is attributed to the excitation of, otherwise inaccessible, symmetric trapped modes.

Undoubtedly there are other applications where it is desirable to control the energy input and minimise the radiation loss. A recent discussion with a member of the organisation Cancer Research UK revealed that research is being carried out into the feasibility of using trapped mode frequencies in laser therapy, in order to destroy cancerous cells located behind ribs. The cancerous tissue, which can not be accessed without opening the rib cage, would be the trapping structure and the bones would act as the 'waveguide' structure. We were not able to find any published work on this subject but one can see how such research and applications would be of great interest.

7.3 Further work

The BEM program we developed is flexible and gives reliable results. We found a large number of trapped modes but for all the geometries studied there is scope to investigate whether solutions exist for higher frequency ranges. The number of modes decreases sharply with every cutoff frequency and the presence of additional travelling modes increases computation time for each set of parameters, as they cause more spurious modes. The thee dimensional analogue for this method, possibly with axial symmetry, would also be of great interest, especially given that the great majority of existing results, both analytical and numeric, have been developed for the 2-D problem.

The planewave spectrum analysis method has only been applied to the Dirichlet case. The obvious extension is that of the analogous Neumann problem. Also a simple case to con-

sider would be that of a cavity in either Dirichlet or Neumann waveguide. Further refinements of the choice of trial functions may also be possible.

7.4 Conclusion

The rich catalogue of results obtained with our BEM program leads us to conclude that trapped modes, far from being rare, singular occurrences, are ubiquitous in a wide array of oscillating systems. Both methods we developed, the numerical and analytical, are valid, general and flexible so that they can easily be extended to other cases, which has been the aim of this work.

Trapped modes are an interesting phenomenon, easy to understand intuitively yet difficult to pin down mathematically. They can have varied and surprising profiles. And probably the trapped modes found so far, the implications of this interesting phenomenon and its possible applications are only at the beginning.

Bibliography

[1] M. Abramowitz and I. A. Stegun. *Handbook of Mathematical Functions with Formulas, Graphs, and Mathematical Tables*. Dover Publications, New York, 1972.

[2] D. J. Acheson. *Elementary Fluid Dynamics*. Clarendon Press, Oxford, 2005.

[3] P. Amore, M.Rodriguez, and C. A. Terrero-Escalante. Bound states in open-coupled asymmetrical waveguides and quantum wires. *Journal of Physics A*, 45:105303, 2012.

[4] A. Aslanyan, L. Parnovski, and D. Vassiliev. Complex resonances in acoustic waveguides. *Q.J.Mech. Appl. Math*, 53(2):429–447, 2000.

[5] A. S. Bonnet Bendhia and F. Starling. Guided waves by electromagnetic gratings and nonuniqueness examples for the diffraction problem. *Math. Methods Appl. Sci.*, 17:305338, 1994.

[6] N. R. T. Biggs. Wave trapping in a two-dimensional sound-soft or sound-hard acoustic waveguide of slowly-varying width. *Wave Motion*, 49(1):24–33, 2012.

[7] N. R. T. Biggs and Simon N. Gaulter. Acoustic trapped modes in a three-dimensional waveguide of slowly-varying cross section. *Wave Motion*, 49(1):24–33, 2012.

[8] J. Blank, P. Exner P, and M. Havlek. *Hilbert Space Operators in Quantum Physics*. Springer, Berlin, 2008.

[9] A. J. Burton and G. F. Miller. The application of integral equation methods to the numerical solution of some exterior of some boundary value problems. *Proc. R. Soc. London*, 323:201–210, 1971.

[10] M.A Callan, C.M. Linton, and D.V Evans. Trapped modes in two-dimensional wave-

guides. *J. Fluid Mech*, 229:51–64, 1991.

[11] J. P. Carini, J. T. Londergan, K. Mullen, and D. P. Murdock. Bound states and resonances in waveguides and quantum wires. *Phys. Rev. B*, 46(23):15538 – 15541, 1992.

[12] F. Caspers and T. Scholz. Measurement of trapped modes in perforated waveguides. *Particle accelerators*, 51:251–262, 1996.

[13] M. Aslam Chaudhry and Syed M. Zubair. *On a Class of Incomplete Gamma Functions With Applications*. CRC Press, USA, Boca Raton, Florida, 2002.

[14] J. T. Chen and F. C Wong. Dual formulation of multiple reciprocity method for the acoustic mode of a cavity with a thin partition. *J. Fluid Mech*, 217:75–95, 1998.

[15] P. C. Clemmow. *The Plane Wave Spectrum Representation of Electromagnetic Fields*. Pergamon Press, Oxford, 1966.

[16] P. J. Cobelli, V. Pagneux, A. Maurel, and P. Petijeans. Experimental study on water-wave trapped modes. *J. Fluid Mech*, 666:445–476, 2011.

[17] E.B. Davies and L.Parnovski. Trapped modes in acoustic waveguides. *Q.J.Mech. Appl. Math*, 51:477–492, 1998.

[18] Y. Duan, W. Koch, C.M. Linton, and M. McIver. Complex resonances and trapped modes in ducted domains. *J. Fluid Mech*, 571:119–217, 2007.

[19] C.M. Linton D.V. Evans and F. Ursell. Trapped mode frequencies embedded in the continuous spectrum. *Q.J. Mech. Appl. Math*, 43:253–274, 1993.

[20] D. V. Evans. Edge waves along periodic coastlines. *Q. Jl Mech. Appl. Math.*, 46:642–656, 1991.

[21] D. V. Evans and C. M. Linton. Trapped modes in open channels. *IMA J. Appl. Maths*, 49:45–60, 1991.

[22] D.V. Evans, M. Levitin, and D. Vassiliev. Existence theorems for trapped modes. *J. Fluid Mech*, 261:21–31, 1994.

[23] D.V. Evans and R. Porter. Trapped modes embedded in the continuous spectrum.

Q.J.Mech. Appl. Math, 51:263–274, 1997.

[24] D.V. Evans and R.Porter. Trapping and near-trapping by arrays of cylinders in waves. *Journal of Engineering Mathematics*, 35:331–356, 1998.

[25] D.V. Evans and R.Porter. Rayleigh-Bloch surface waves along periodic gratings and their connection with trapped modes in waveguides. *J. Fluid Mech.*, 386:233–258, 1999.

[26] D.V. Evans and R.Porter. Trapped modes about multiple cylinders in a channel. *J. Fluid Mech.*, 35:149–179, 1999.

[27] D.V. Evans and R.Porter. On the existence of embedded surface waves along arrays of parallel plates. *Q. J. Mech. Appl. Math*, 55(3):481–494, 2002.

[28] D.V. Evans and R.Porter. Embedded Rayleigh - Bloch surface waves along periodic rectangular arrays. *Wave Motion*, 43:29–50, 2005.

[29] P. Exner and P. Seba. Bound states in curved quantum waveguides. *J. Math. Phys*, 30(11):25742580, 1989.

[30] V. A. Fedotov, M. Rose, S. L. Prosvirnin, N. Papasimakis, and N. I. Zheludev. Sharp trapped-mode resonances in planar metamaterials with a broken structural symmetry. *Phys. Rev. Lett.*, 99:147401, 2007.

[31] M. Gennaretti, A. Giordani, and L. Morino. A third-order boundary element method for exterior acoustics with applications to scattering by rigid and elastic shells. *J. Sound Vib*, 225:699–722, 1977.

[32] J. Goldstone and R. L. Jaffe. Bound states in twisting tubes. *Phys. Rev. B*, 45(24):14100–14107, 1992.

[33] D. Gridin, A.T.I. Adamou, and R. Craster. Trapped modes in curved elastic plates. *Proc. R. Soc. Lond. A*, 461:1181–1197, 2005.

[34] D. A. Huntley and A. J Bowen. Field observations of edge waves. *Nature*, pages 349–365, 1973.

[35] S. R. Kuo J. T. Chen, J. H. Lin and S. W. Chyuan. Boundary element analysis for

the helmholtz eigenvalue problems with a multiply connected domain. *Proc. R. Soc. London*, 457:2521–2546, 2001.

[36] F. John. On the motion of floating bodies. *Commun. Pure Appl. Math*, 3:45–10, 1950.

[37] D.S. Jones. The eigenvalues of $\nabla^2 u + \lambda u = 0$ when the boundary conditions are given in semi-infinite domains. *Proc. Camb. Phil. Soc*, 49:668–684, 1953.

[38] J.D. Kaplunov, G.A. Rogerson, and P.E. Tovstik. Localized vibration in elastic structures with slowly varying thickness. *Quart. J. Mech. Appl. Math.*, 58:645–664, 2005.

[39] N. Kuznetsov, V. Maz'ya, and B. Vainberg. *Linear Water Waves*. Cambridge University Press, Cambridge, 2002.

[40] Yuh-Kae Lin, Yueh-Nan Chen, and Der-San Chuu. Bound states of L- or T-shaped quantum wires in inhomogeneous magnetic fields. *Phys. Rev. B*, 64(19):193316, 2001.

[41] C.M. Linton and M. McIver. The existence of Rayleigh-Bloch surface waves. *J. Fluid Mech.*, 470:85–90, 2002.

[42] C.M. Linton, M. McIver, P. McIver, K. Ratcliffe, and J. Zhang. Trapped modes for off-centre structures in guides. *Wave Motion*, 36(1):67–85, 2001.

[43] C.M. Linton and P. McIver. Embedded trapped modes in water waves and acoustics. *Wave Motion*, 45:16–29, 2007.

[44] C.M. Linton and K. Ratcliffe. Bound states in coupled guides. Part II. Three dimensions. *Journal of Mathematical Physics*, 45(4):1380–1393, 2003.

[45] C.M. Linton and K. Ratcliffe. Bound states in coupled guides. Part I.Two dimensions. *Journal of Mathematical Physics*, 45(4):1359–1379, 2003.

[46] D. N. Maksimov and A. F. Sadreev. Bound states in elastic waveguides. *Phys. Rev. E*, 74:016201(6), 2006.

[47] H.D. Maniar and J.N. Newman. Wave diffraction by a long array of cylinders. *J. Fluid Mech*, 339:309–330, 1997.

[48] P. A. Martin. On the null-field equations for the exterior problems of acoustics. *Q. J.*

Mech., 33:385–396, 1980.

[49] M. McIver. An example of non-uniqueness in the two-dimensional linear water wave problem. *J. Fluid Mechanics*, 315:257–266, 1996.

[50] M. McIver. Acoustic wave trapping in one-dimensional axisymmetric arrays. *Q J Mechanics Appl Math*, 64(3):401–414, 2011.

[51] M. McIver, C.M. Linton, P. McIver, and J. Zhang. Trapped modes in two-dimensional waveguides. *Q.J.Mech. Appl. Math*, 54:273–293, 2001.

[52] M. McIver and P. McIver. Trapped modes in an axisymmetric water-wave problem. *Q.J.Mech. Appl. Math*, 50(2):165–178, 1997.

[53] M.Onoe. Remote excitation of trapped energy modes in plates and pipes and its applications to sensors and NDT. *Proc. Frequency Control Symp.*, 15:488–793, 2007.

[54] M.Onoe and R. D. Mindlin. Mathematical theory of vibrations of elastic plates. *Ann. Symp. Freq. Cont*, Proc. 11th, Monmouth, NJ: US Army Signal Engineering Labs.:17–40, 1957.

[55] M.Onoe and T. Suzuki. Experimental study on remote excitation of trapped energy modes of vibration. *Proc. Symp. Ultrasonic Electronics*, 20:3–9, 2007.

[56] P. Morse and H. Feshbach. *Methods of theoretical physics*. McGraw-Hill Book Company, Inc., New York, 1953.

[57] L. G. Althaus A. M. Serenelli O. G. Benvenuto, A. H. Corsico. On mode trapping in pulsating DA white dwarf stars. *Mon. Not. Roy. Astron. Soc.*, 335:480, 2002.

[58] V. Pagneux. Revisiting the edge resonance for lamb waves in a semi-infinite plate. *Acoust. Soc. Am.*, 120 (2):649–656, 2006.

[59] R. Parker. Resonance effects in wake shedding from parallel plates: some experimental observations. *J. Sound Vib.*, 4:62–72, 1966.

[60] R. Parker. Resonance effects in wake shedding from parallel plates: calculation of resonance frequencies. *J. Sound Vib.*, 5:330–343, 1967.

[61] R. Parker and S. Stoneman. The excitation and consequences of acoustic resonances in enclosed fluid flow around solid bodies. *Proc. Inst. Mech. Eng.*, 203:9–19, 1989.

[62] J. Postnova and R. V. Craster. Trapped modes in topographically varying elastic waveguides. *Wave Motion*, 44:205221, 2007.

[63] J. Postnova and R. V. Craster. Trapped modes in elastic plates, ocean and quantum waveguides. *Wave Motion*, 45 (4):565–579, 2008.

[64] S. Prosvirnin and S. Zouhdi. *Complex Media and Metamaterials*. Kluwer Academic Publishers, The Netherlands, 2003.

[65] H. Sakaki. N/a. *Proceedings of the International Symposium on Foundations of Quantum Mechanics in the Light of New Technology*, Physical Society of Japan, Tokyo:94–110, 1984.

[66] L. Schult, D. G. Ravenhall, and H. W. Wyld. Quantum bound states in a classically unbound system of crossed wires. *Phys. Rev. B*, 39:5476–5479, 1989.

[67] E. Shaw. On the resonant vibrations of thick barium titanate disks. *J. Acoust. Soc. Am.*, 28:38–50, 1956.

[68] M. J. Simon and F. Ursell. Uniqueness in linearized two-dimensional water-wave problems. *J. Fluid Mech.*, 148:137–154, 1984.

[69] M. I. Stockman. Criterion for negative refraction with low optical losses from a fundamental principle of causality. *Phys. Rev. Lett.*, 98:177404, 2007.

[70] G. G. Stokes. Report on recent researches in hydrodynamics. *Technical report*, British Association, 1846.

[71] L. N. Trefethen and T. Betcke. Computed eigenmodes of planar regions. *MIMS Print*, 367, 2006.

[72] F. Ursell. Surface waves on deep water in the presence of a submerged cylinder. *Proc. Camb. Phil. Soc*, 46:153–158, 1950.

[73] F. Ursell. Trapping modes in the theory of surface waves. *Proc. Camb. Phil. Soc*, 47:347–358, 1951.

[74] L. A. Weinstein. Open resonators and open waveguides. *Moscow Sovietskoe Radio*, 1966.

[75] D. E. Winget, H. M. van Horn, and C. J. Hansen. The nature of the ZZ Ceti oscillations, Trapped modes in compositionally stratified white dwarfs. *Astrophysical Journal Part 2*, pages 33–36, 1981.

[76] V. Zernov, A. Pichugin, and J. Kaplunov. Eigenvalue of semi-infinite elastic strip. *Proc. R. Soc. Lond.*, A 462:1255–1270, 2006.

Appendix A

New Results - Two discs in an infinite waveguide

Two discs of equal radius on the centreline of an infinite, Neumann waveguide

$a_1/d = a_2/d = 0.2$

c/d	k_1d	k_1d/π	Type	k_2d	k_2d/π	Type
0	1.551038491	0.493709731	Coupled			
0.1	1.529318194	0.486795962				
0.2	1.510278322	0.480735397				
0.3	1.487684878	0.473543697				
0.4	1.464017169	0.466010049				
0.5	1.493432828	0.475373322				
0.6	1.502208861	0.478166813				
0.7	1.510984894	0.480960305				
0.8	1.517871574	0.483152398				
1.6	1.52358481	0.484970973				
2	1.527441353	0.486198546				
2.4	1.530529054	0.48718139				
2.8	1.53306521	0.487988671				
3.2	1.53518849	0.488664531				
3.6	1.536986417	0.489236827				
4	1.539091697	0.489906957				
4.8	1.540502391	0.490355994				
5.2	1.542044881	0.490846983				
5.6	1.542946304	0.491133914				
6	1.543731393	0.491383815				
6.4	1.544458535	0.491615271				
6.8	1.545095595	0.491818053	Separate, symmetric	1.562281028	0.497288333	Separate, anti-symmetric
7	1.54537483	0.491906936		1.561718674	0.497109331	
7.2	1.545667	0.491999936		1.561094809	0.496910749	
7.6	1.546180938	0.492163528		1.560034457	0.496573229	
8	1.546644312	0.492311024		1.559090835	0.496272866	
10	1.548380773	0.492863755		1.55579223	0.49522289	

$a_1/d = a_2/d = 0.3$

c/d	k_1d	k_1d/π	Type	k_2d	k_2d/π	Type
0.1	1.508677075	0.480225705				
0.2	1.408459416	0.448325508	Coupled, symmetric			
0.3	1.350346693	0.429827697				
0.5	1.289916553	0.410592231				
0.6	1.235242504	0.393188981				
0.7	1.324924844	0.42173569				
0.8	1.391666425	0.442980145				
1.2	1.427512843	0.454390388				
1.6	1.445684777	0.460174681				
2	1.458077371	0.464119357				
2.4	1.467021694	0.466966417				
2.8	1.474348663	0.469298658				
3.2	1.479946461	0.471080488	Separate, symmetric	1.554593859	0.494841437	Separate, anti-symmetric
3.6	1.484450871	0.472514283		1.546170137	0.492160089	
4	1.48812562	0.473683989		1.538986397	0.489873439	
4.4	1.491155568	0.474648449		1.533071596	0.487990704	
4.8	1.493674549	0.475450264		1.528271283	0.486462721	
5.2	1.495779984	0.476120443		1.524395959	0.485229169	
5.6	1.497550915	0.476684147		1.521267803	0.484233449	
6	1.499044483	0.477159563		1.518743929	0.483430077	
6.4	1.500307754	0.477561674		1.516702763	0.482780355	
6.8	1.501376804	0.477901962		1.515044385	0.482252478	
7.2	1.502283055	0.47819043		1.513694326	0.481822742	
7.6	1.503051763	0.478435117		1.512591863	0.481471818	
8	1.503704095	0.47864276		1.511688807	0.481184367	
8.4	1.504257829	0.478819019		1.510946879	0.480948204	
8.8	1.504727889	0.478968643		1.510335612	0.480753633	
9.2	1.505126797	0.479095619		1.5098307	0.480592914	
9.6	1.505465055	0.47920329		1.509412684	0.480459856	
10	1.505751479	0.479294461		1.50906592	0.480349478	
10.4	1.506012796	0.479377641		1.508732316	0.480243289	
10.8	1.506209153	0.479440143		1.50854815	0.480184667	
11.2	1.50638402	0.479495805		1.508350176	0.48012165	
11.6	1.506531882	0.479542871		1.508185375	0.480069193	
12	1.506656899	0.479582665		1.508048018	0.480025471	
12.4	1.506762637	0.479616322		1.507933372	0.479988978	
12.8	1.506852085	0.479644794		1.507837503	0.479958462	
13.2	1.506927735	0.479668874		1.507757178	0.479932893	
13.6	1.506991751	0.479689251		1.507689841	0.479911459	
14	1.507045886	0.479706483		1.507633376	0.479893486	
14.4	1.507091584	0.479721029		1.507586028	0.479878415	
14.8	1.507130062	0.479733277		1.507546342	0.479865782	

$a_1/d = a_2/d = 0.4$

c/d	k_1d	k_1d / π	Type	k_2d	k_2d / π	Type
0	1.447831626	0.460858042				
0.8	1.173417604	0.373509551	Coupled, symmetric			
1.2	1.312228528	0.417694337				
1.6	1.352141532	0.430399011				
2	1.376441755	0.438133994				
2.4	1.393247527	0.443483425				
2.8	1.405504832	0.447385037	Separate, symmetric	1.516165438	0.482609319	Separate, anti-symmetric
3.2	1.41472208	0.450318971		1.501277993	0.47787051	
3.6	1.421794408	0.452570158		1.487352602	0.473437931	
4	1.427297071	0.454321706		1.477918455	0.470434955	
4.4	1.43162005	0.45569775		1.470832103	0.468179305	
4.8	1.435038584	0.4567859		1.465502672	0.466482898	
5.2	1.437753284	0.457650014		1.461480374	0.465202564	
5.6	1.439913946	0.458337773		1.458431583	0.464232106	
6	1.441635408	0.45888573		1.456110295	0.463493218	
6.4	1.443006666	0.459322214		1.454336295	0.462928538	
6.8	1.444098015	0.4596696		1.452975532	0.462495395	
7.2	1.444965492	0.459945726		1.451928396	0.462162082	
7.6	1.445654359	0.460164998		1.451120632	0.461904963	
8	1.446200456	0.460338826		1.450495292	0.461705912	
8.4	1.446633334	0.460476615		1.450010002	0.461551439	
8.8	1.446976362	0.460585804		1.449632275	0.461431205	
9.2	1.447248209	0.460672335		1.449337449	0.46133736	
9.6	1.447463766	0.460740949		1.449106895	0.461263972	
10	1.447633026	0.460794826		1.448924696	0.461205977	

$a_1/d = a_2/d = 0.5$

c/d	k_1d	k_1d / π	Type	k_2d	k_2d / π	Type
0	1.393565597	0.443584669				
0.4	1.255639579	0.399681557	Coupled, symmetric			
0.8	1.126254876	0.358497223				
1.2	1.182405309	0.376370419				
1.6	1.259595521	0.400940769				
2	1.299237855	0.413559287				
2.4	1.324637715	0.421644294				
2.8	1.342186976	0.427230385	Separate, symmetric	1.464635612	0.466206905	Separate, anti-symmetric
3.2	1.354792618	0.431242876		1.444974782	0.459948683	
3.6	1.364061655	0.434193295		1.430607611	0.455375481	
4	1.370978622	0.436395029		1.420228039	0.452071568	
4.4	1.376188403	0.438053349		1.412744012	0.449689334	
4.8	1.380134196	0.439309331		1.407335177	0.447967652	
5.2	1.383131552	0.440263417		1.403410174	0.446718288	
5.6	1.38541099	0.440988983		1.400549036	0.445807562	
6	1.38714404	0.441540629		1.398454524	0.445140859	
6.4	1.388460024	0.441959519		1.396915662	0.444651026	
6.8	1.389457355	0.442276978		1.395781809	0.44429011	
7.2	1.390211427	0.442517006		1.394944567	0.444023608	
7.6	1.390816062	0.442709467		1.394365	0.443839126	
8	1.391256953	0.442849807		1.393918822	0.443697104	
8.4	1.391597273	0.442958134		1.393596663	0.443594558	
8.8	1.391862226	0.443042471		1.393365517	0.443520982	
9.2	1.392075519	0.443110364		1.393206822	0.443470468	
9.6	1.392254548	0.44316735		1.393105979	0.443438369	
10	1.392254548	0.44316735		1.393105979	0.443438369	

$a_1/d = a_2/d = 0.6$

c/d	k_1d	k_1d/π	Type	k_2d	k_2d/π	Type
0	1.34975376	0.429638961				
0.2	1.259964517	0.401058224	Coupled, symmetric			
0.4	1.147215438	0.365169162				
0.8	1.09064274	0.347161555				
1.2	1.01064274	0.321696823	Separate, symmetric	1.557509023	0.495769361	Separate, anti-symmetric
1.6	1.168600637	0.371976266		1.526366464	0.485856399	
2	1.231202161	0.391902903		1.489497247	0.474120591	
2.4	1.267396732	0.403423966		1.454501439	0.462981105	
2.8	1.2909574	0.410923542		1.425769678	0.453835523	
3.2	1.307144279	0.416075974		1.404045812	0.446920617	
3.6	1.318606308	0.419724442		1.388288268	0.441904847	
4	1.326869995	0.422354849		1.377067953	0.438333318	
4.4	1.332892134	0.424271751		1.369129699	0.435806499	
4.8	1.337307552	0.425677219		1.363515938	0.434019588	
5.2	1.340555118	0.426710949		1.359536165	0.43275279	
5.6	1.342946923	0.427472283		1.356705145	0.43185165	
6	1.345038699	0.428138114		1.354684222	0.431208372	
6.4	1.346001797	0.428444677		1.353237153	0.430747757	
6.8	1.346951732	0.42874705		1.352198709	0.430417211	
7.2	1.347646913	0.428968332		1.351452541	0.430179699	
7.6	1.348154153	0.429129791		1.350916094	0.430008943	
8	1.348523235	0.429247274		1.350530315	0.429886146	
8.4	1.348791255	0.429332587		1.350252653	0.429797763	
8.8	1.348985456	0.429394403		1.350052078	0.429733918	
9.2	1.349129214	0.429440162		1.349909156	0.429688425	
9.6	1.349232329	0.429472985		1.349802943	0.429654616	
10	1.349309349	0.429497501		1.349726205	0.42963019	

$a_1/d = a_2/d = 0.7$

c/d	k_1d	k_1d / π	Type	k_2d	k_2d / π	Type
0	1.324184354	0.421499985				
0.2	1.27620699	0.406228352	Coupled, symmetric			
0.4	1.208391701	0.384642125				
0.8	1.061830624	0.337990395				
1.2	0.951069099	0.302733989				
1.6	1.060927497	0.337702921	Separate, symmetric	1.497789492	0.476760088	Separate, anti-symmetric
2	1.169739844	0.372338886		1.465312628	0.466422405	
2.4	1.22869358	0.391104399		1.433091206	0.456166032	
2.8	1.253909184	0.399130756		1.404678223	0.44712192	
3.2	1.274593028	0.405714613		1.382037567	0.439915192	
3.6	1.288717375	0.410210522		1.365125602	0.434531959	
4	1.298607773	0.413358726		1.352933015	0.430650947	
4.4	1.305637253	0.415596274		1.346478057	0.428596275	
4.8	1.310676909	0.417200442		1.338212233	0.425965188	
5.2	1.314307377	0.418356053		1.333939397	0.424605105	
5.6	1.316928754	0.419190461		1.330933432	0.423648278	
6	1.31882273	0.419793331		1.328814187	0.422973704	
6.4	1.3203689	0.420285491		1.327316573	0.422496999	
6.8	1.321176483	0.420542552		1.326257522	0.422159894	
7.2	1.321885042	0.420768093		1.325507035	0.421921007	
7.6	1.322393015	0.420929786		1.324975841	0.421751923	
8	1.322756097	0.421045358		1.324600268	0.421632375	
8.4	1.323013541	0.421127305		1.324333725	0.421547531	
8.8	1.323197262	0.421185785		1.324145375	0.421487578	
9.2	1.323327698	0.421227304		1.324011036	0.421444817	
9.6	1.323420361	0.4212568		1.323914173	0.421413984	
10	1.323485786	0.421277625		1.32384313	0.421391371	

$a_1/d = a_2/d = 0.8$

c/d	k_1d	k_1d/π	Type	k_2d	k_2d/π	Type
0	1.324184354	0.421499985				
0.2	1.248278989	0.397338614				
0.4	1.222465209	0.389121852	Separate, symmetric	1.553855546	0.494606425	Separate, anti-symmetric
0.6	1.169508502	0.372265248		1.539432685	0.490015497	
0.8	1.129383379	0.359493054		1.524988137	0.485417665	
1	1.013923974	0.32274127		1.511348467	0.481076033	
1.2	0.845974522	0.269281424		1.498632419	0.477028399	
1.4	0.781909002	0.248888784		1.486589162	0.47319492	
1.6	0.794328775	0.252842111		1.47512193	0.469544796	
1.8	1.027340312	0.327011813		1.463792971	0.465938684	
2	1.107242422	0.352445385		1.452425688	0.462320374	
2.4	1.190130127	0.378829299		1.428827036	0.454808708	
2.8	1.234419566	0.392927033		1.405392167	0.447349175	
3.2	1.261608401	0.401581488		1.384439697	0.440679812	
3.6	1.27945232	0.40726137		1.367386597	0.435251654	
4	1.291618349	0.411133928		1.354381223	0.431111925	
4.4	1.300107337	0.413836051		1.344840815	0.428075126	
4.8	1.306114401	0.415748154		1.337987693	0.425893714	
5.2	1.310401831	0.417112882		1.333114288	0.424342465	
5.6	1.313476934	0.418091716		1.329663033	0.423243899	
6	1.315687663	0.418795411		1.327221209	0.422466644	
6.4	1.317284509	0.419303702		1.325500733	0.421919001	
6.8	1.318430327	0.419668426		1.324280042	0.421530444	
7.2	1.319253205	0.419930356		1.323418084	0.421256075	
7.6	1.319845557	0.420118907		1.322810348	0.421062627	
8	1.320270615	0.420254206		1.322384467	0.420927065	
8.4	1.320577556	0.420351909		1.322088563	0.420832876	
8.8	1.320802372	0.420423469		1.321886349	0.420768509	
9.2	1.320971716	0.420477373		1.321752306	0.420725842	
9.6	1.321105911	0.420520089		1.321669517	0.42069949	
10	1.321220762	0.420556647		1.321627651	0.420686163	

Two discs of different radius on the centerline of an infinite, Neumann waveguide

$a_1/d = 0.3$, $a_2/d = 0.7$

$k_{c1}\,d$ = 1.50867707
$k_{c2}\,d$ = 1.32418435

c/d	k_1d	k_1d/π	Type	k_2d	k_2d/π	Type
0.2	1.323496894	0.421281161				
0.3	1.323508668	0.421284908				
0.4	1.323420655	0.421256893				
0.5	1.295276492	0.412298349				
0.6	1.271724003	0.404801376	Coupled, symmetric, localised around larger disc			
0.7	1.236562292	0.393609082				
0.8	1.200250089	0.382050576				
0.9	1.170958733	0.372726869				
1	1.134286267	0.361053688				
1.2	1.234728953	0.393025513				
1.4	1.262607078	0.401899375				
1.6	1.280296604	0.407530113				
1.8	1.292651503	0.411462791				
2	1.30159264	0.414308836	Separate, symmetric, localised around large disc	1.55819657	0.495988213	Separate, anti-symmetric, localised around small disc
2.4	1.312991402	0.417937166		1.548314517	0.492842665	
2.8	1.319480437	0.420002686		1.539570796	0.490059459	
3.2	1.322458241	0.420950548		1.532667794	0.48786217	
3.6	1.324199665	0.421504859		1.527543841	0.486231169	
4	1.32510927	0.421794395		1.523858651	0.48505814	
4.4	1.325581819	0.421944811		1.521246039	0.484226521	
4.8	1.325826802	0.422022792		1.519403672	0.483640079	
5.2	1.325953748	0.4220632		1.518105773	0.483226946	
5.6	1.326019405	0.422084099		1.517190867	0.482935723	
6	1.326052911	0.422094764		1.5165455	0.482730297	
6.4	1.326068146	0.422099613		1.51609042	0.482585441	
6.8	1.326075647	0.422102001		1.515770319	0.48248355	
7.2	1.326092532	0.422107376		1.515546582	0.482412332	
7.6	1.326125308	0.422117809		1.515392222	0.482363198	
8	1.326080768	0.422103631		1.515288347	0.482330133	
8.4	1.326090764	0.422106813		1.515126058	0.482278475	
8.8	1.326085719	0.422105207		1.515073621	0.482261784	
9.2	1.326086871	0.422105574		1.515041317	0.482251501	
9.6	1.32608557	0.42210516		1.515024609	0.482246183	
10	1.32608278	0.422104272		1.515020248	0.482244795	

Two discs of equal radius on the centerline of an infinite, Dirichlet waveguide

$a_1/d = a_2/d = 0.2$

c/d	k_1d	k_1d/π	Type	k_2d	k_2d/π	Type
0	3.0561657	0.9728078				
0.4	2.8696533	0.9134390	Coupled, symmetric modes			
0.8	2.9751325	0.9470141				
1.2	3.0042589	0.9562853				
1.6	3.0214238	0.9617491				
2	3.0329515	0.9654184	Symmetric modes	3.1248486	0.9946702	Separate, anti-symmetric modes
2.4	3.0411364	0.9680238		3.1094268	0.9897613	
2.8	3.0471421	0.9699355		3.0975929	0.9859944	
3.2	3.0516439	0.9713684		3.0890223	0.9832664	
3.6	3.0550661	0.9724577		3.0828950	0.9813159	
4	3.0576909	0.9732932		3.0785090	0.9799199	
4.4	3.0597149	0.9739375		3.0753512	0.9789147	
4.8	3.0612799	0.9744357		3.0730616	0.9781859	
5.2	3.0624912	0.9748212		3.0713898	0.9776537	
5.6	3.0634285	0.9751196		3.0701615	0.9772628	
6	3.0641530	0.9753502		3.0692540	0.9769739	
6.4	3.0647121	0.9755282		3.0685802	0.9767594	
6.8	3.0651429	0.9756653		3.0680781	0.9765996	
7.2	3.0654742	0.9757707		3.0677025	0.9764800	
7.6	3.0657285	0.9758517		3.0674208	0.9763904	
8	3.0659234	0.9759137		3.0672091	0.9763230	
8.4	3.0660726	0.9759612		3.0670497	0.9762722	
8.8	3.0661865	0.9759975		3.0669295	0.9762340	
9.2	3.0662734	0.9760252		3.0668390	0.9762052	
9.6	3.0663397	0.9760462		3.0667707	0.9761834	
10	3.0663901	0.9760623		3.0667193	0.9761671	

$a_1/d = a_2/d = 0.3$

c/d	k_1d	k_1d/π	Type	k_2d	k_2d/π	Type
0	2.9907554	0.9519870				
0.1	2.9394609	0.9356595	Coupled, symmetric modes			
0.2	2.8668404	0.9125436				
0.3	2.8057705	0.8931045				
0.4	2.7400486	0.8721846				
0.5	2.6592189	0.8464557				
0.7	2.7852560	0.8865745				
0.8	2.8439360	0.9052529				
1.2	2.9081389	0.9256894	Symmetric modes	3.1362458	0.9982981	De-coupled, antisymmetric modes
1.6	2.9400380	0.9358432		3.0998215	0.9867038	
2	2.9595495	0.9420539		3.0670548	0.9762739	
2.4	2.9723821	0.9461386		3.0443969	0.9690616	
2.8	2.9811330	0.9489241		3.0314073	0.9649269	
3.2	2.9872172	0.9508608		3.0200937	0.9613257	
3.6	2.9914884	0.9522203		3.0138963	0.9593530	
4	2.9944982	0.9531784		3.0098313	0.9580591	
4.4	2.9966194	0.9538536		3.0067012	0.9570627	
4.8	2.9981118	0.9543286		3.0053422	0.9566301	
5.2	2.9991589	0.9546619		3.0041337	0.9562454	
5.6	2.9998914	0.9548951		3.0033164	0.9559853	
6	3.0004024	0.9550578		3.0027614	0.9558086	
6.4	3.0007580	0.9551709		3.0023830	0.9556882	
6.8	3.0010049	0.9552495		3.0021244	0.9556059	
7.2	3.0011761	0.9553040		3.0019474	0.9555495	
7.6	3.0012946	0.9553418		3.0018259	0.9555109	
8	3.0013768	0.9553679		3.0017425	0.9554843	
8.4	3.0014337	0.9553860		3.0016852	0.9554661	
8.8	3.0014733	0.9553986		3.0016457	0.9554535	
9.2	3.0015009	0.9554074		3.0016186	0.9554449	
9.6	3.0015205	0.9554137		3.0015999	0.9554389	
10	3.0015347	0.9554182		3.0015871	0.9554349	

$a_1/d = a_2/d = 0.4$

c/d	k_1d	k_1d/π	Type	k_2d	k_2d/π	Type
0	2.9998213	0.9548728				
0.4	2.873801	0.914759	Coupled symmetric modes			
0.8	2.747781	0.874646				
1.2	2.884731	0.918239		3.128299	0.995768	Decoupled, anti-symmetric modes
1.6	2.928180	0.932069		3.098739	0.986359	
2	2.952439	0.939791		3.069600	0.977084	
2.4	2.967716	0.944653		3.047231	0.969964	
2.8	2.977874	0.947887		3.033584	0.965620	
3.2	2.984825	0.950099		3.021425	0.961750	
3.6	2.989655	0.951637		3.014611	0.959581	
4	2.993037	0.952713		3.010107	0.958147	
4.4	2.995410	0.953469		3.007678	0.957374	
4.8	2.997075	0.953999		3.005112	0.956557	
5.2	2.998241	0.954370		3.003766	0.956128	
5.6	2.999055	0.954629		3.002856	0.955839	
6	2.999623	0.954810		3.002238	0.955642	
6.4	3.000018	0.954935		3.001818	0.955508	
6.8	3.000291	0.955022		3.001530	0.955417	
7.2	3.000481	0.955083		3.001334	0.955354	
7.6	3.000612	0.955125		3.001199	0.955311	
8	3.000703	0.955153		3.001107	0.955282	
8.4	3.000766	0.955174		3.001044	0.955262	
8.8	3.000810	0.955187		3.001000	0.955248	
9.2	3.000840	0.955197		3.000970	0.955238	
9.6	3.000862	0.955204		3.000949	0.955232	
10	3.000877	0.955209		3.000935	0.955227	

$a_1/d = a_2/d = 0.5$

c/d	k_1d	k_1d/π	Type	k_2d	k_2d/π	Type
0	3.071451	0.977673				
0.4	3.067872	0.976534				
0.8	2.879437	0.916553				
1.2	2.950033	0.939025		3.139192	0.999236	
1.6	2.999079	0.954637		3.131632	0.996829	
2	3.021638	0.961817		3.123343	0.994191	
2.4	3.035324	0.966174		3.114221	0.991287	
2.8	3.044489	0.969091		3.105358	0.988466	
3.2	3.050969	0.971153		3.097587	0.985993	
3.6	3.055708	0.972662		3.091244	0.983973	
4	3.059252	0.973790		3.086287	0.982396	
4.4	3.061942	0.974647	Symmetric modes	3.082507	0.981193	Decoupled, antisymmetric modes
4.8	3.064004	0.975303		3.079659	0.980286	
5.2	3.065593	0.975809		3.077524	0.979606	
5.6	3.066822	0.976200		3.075925	0.979097	
6	3.067775	0.976503		3.074726	0.978716	
6.4	3.068513	0.976738		3.073826	0.978429	
6.8	3.069086	0.976920		3.073149	0.978214	
7.2	3.069529	0.977061		3.072639	0.978051	
7.6	3.069872	0.977171		3.072252	0.977928	
8	3.070137	0.977255		3.071960	0.977835	
8.4	3.070342	0.977320		3.071738	0.977765	
8.8	3.070500	0.977370		3.071570	0.977711	
9.2	3.070621	0.977409		3.071442	0.977670	
9.6	3.070714	0.977439		3.071345	0.977640	
10	3.070786	0.977461		3.071272	0.977616	

Two discs of different radius on the centerline of an infinite, Dirichlet waveguide

a_1 /d= 0.2
a_2/d = 0.4

c/d	k_1d	k_1d / π	Type	k_2d	k_2d / π	Type
k_{c1}	3.056166	0.972808				
k_{c2}	3.071451	0.977673				
0.4	3.002378	0.955687	Symmetric modes			
0.8	2.923478	0.930572				
1.2	2.987336	0.950899				
1.6	3.012973	0.959059		3.134666	0.997795	De-coupled antisymmetric modes
2	3.028394	0.963968		3.123862	0.994356	
2.4	3.038725	0.967256		3.112335	0.990687	
2.8	3.046027	0.969581		3.102008	0.987400	
3.2	3.051360	0.971278		3.093694	0.984754	
3.6	3.055334	0.972543		3.087360	0.982737	
4	3.058329	0.973497		3.082659	0.981241	
4.4	3.060599	0.974219		3.079216	0.980145	
4.8	3.062868	0.974941		3.076712	0.979348	
5.2	3.063602	0.975175		3.074907	0.978773	
5.6	3.064551	0.975477		3.073621	0.978364	
6	3.065234	0.975694		3.072720	0.978077	
6.4	3.065710	0.975846		3.072105	0.977881	
6.8	3.066029	0.975947		3.071698	0.977752	
7.2	3.066234	0.976013		3.071436	0.977669	
7.6	3.066363	0.976054		3.071273	0.977617	
8	3.066441	0.976078		3.071173	0.977585	
8.4	3.066487	0.976093		3.071113	0.977566	
8.8	3.066515	0.976102		3.071078	0.977554	
9.2	3.066531	0.976107		3.071057	0.977548	
9.6	3.066540	0.976110		3.071044	0.977544	
10	3.066546	0.976112		3.071037	0.977542	

Appendix B

Results - Disc and cavity in an infinite waveguide

B.1 Neumann waveguide

r=0.2

Mode no.	h/d	w/d	kd	kd/π	x-Symmetry
0.2-1	0.4	0.4	1.2956	0.4124	Symmetric
0.2-2	0.5	5.0	1.2948	0.4121	Symmetric
0.2-3	0.8	5.25	1.2293	0.3913	Symmetric
0.2-4	0.8	6.1	1.0734	0.3417	Symmetric
0.2-5	0.8	7.0	1.3244	0.4216	Antisymmetric
0.2-6	2.8	4.8	1.3264	0.4222	Symmetric
0.2-7	3.2	5.5	1.2239	0.3896	Symmetric
0.2-8	3.6	6.1	1.1371	0.3619	Symmetric
0.2-9	3.8	5.5	1.2239	0.3896	Symmetric
0.2-10	4.6	4.2	1.4353	0.4569	Symmetric
0.2-11	5.8	4.2	1.2187	0.3879	Symmetric
0.2-12	5.8	6.4	1.2178	0.3876	Symmetric
0.2-13	5.8	5.4	1.2176	0.3876	Symmetric

Mode 02-2

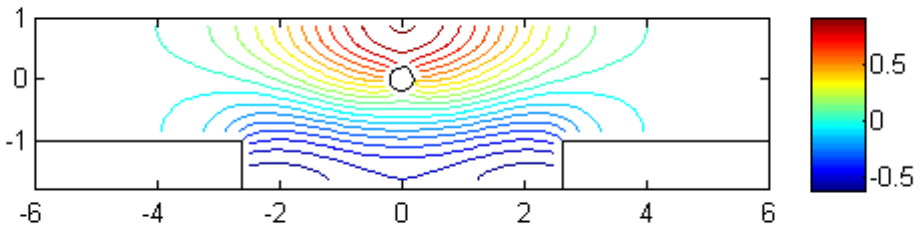

Mode 02-5

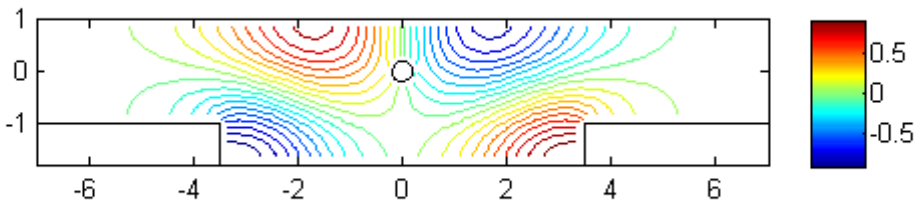

Mode 02-6

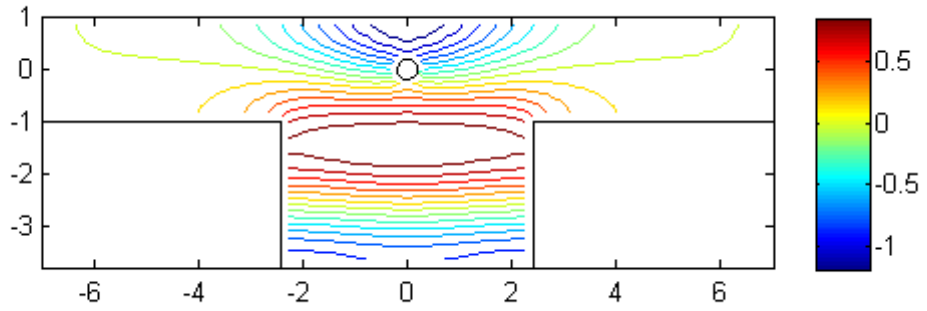

Mode 02-10

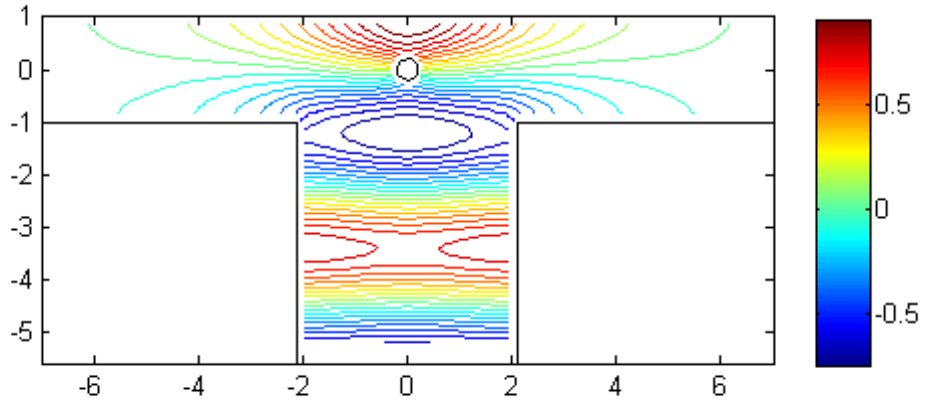

r=0.4

Mode no.	h/d	w/d	kd	kd/π	x-Symmetry
0.4-1	0.8	6.0	1.15662	0.3682	Symm
0.4-2	1.4	6.75	0.98842	0.3146	Symmetric
0.4-3	1	7.0	1.26435	0.4025	Antisymmetric
0.4-4	3.4	6.0	1.14732	0.3652	Symmetric
0.4-5	3.8	6.2	1.09465	0.3484	Symmetric
0.4-6	4.8	4.4	1.36155	0.4334	Antisymmetric
0.4-7	4.2	7.0	1.02482	0.3262	Symmetric
0.4-8	4.6	3.4	1.40248	0.4464	Antisymmetric
0.4-9	5	6.6	1.45577	0.4634	Antisymmetric

Mode 04-1

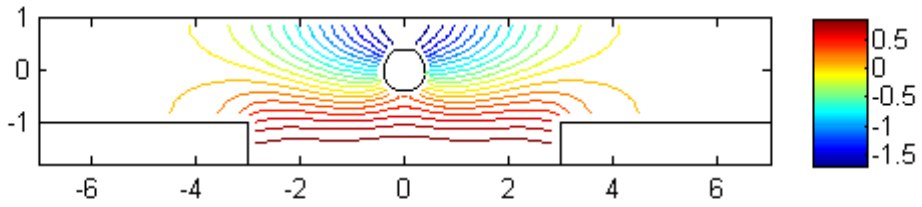

Mode 04-2

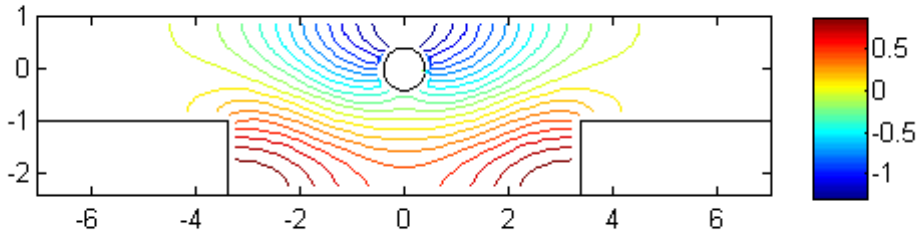

Mode 04-7

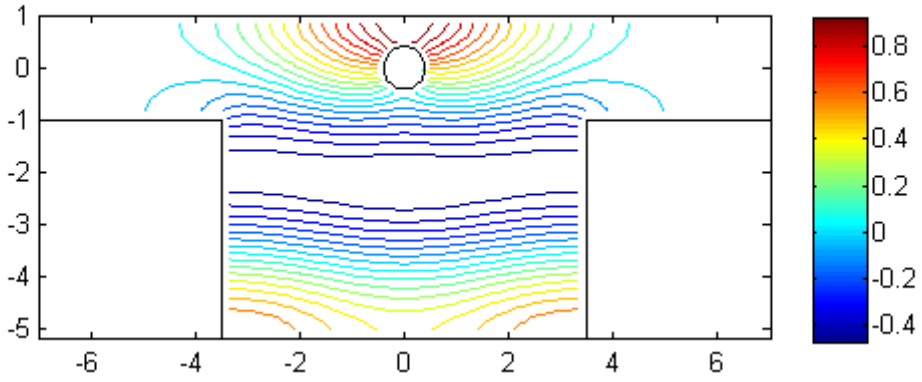

Mode 04-8

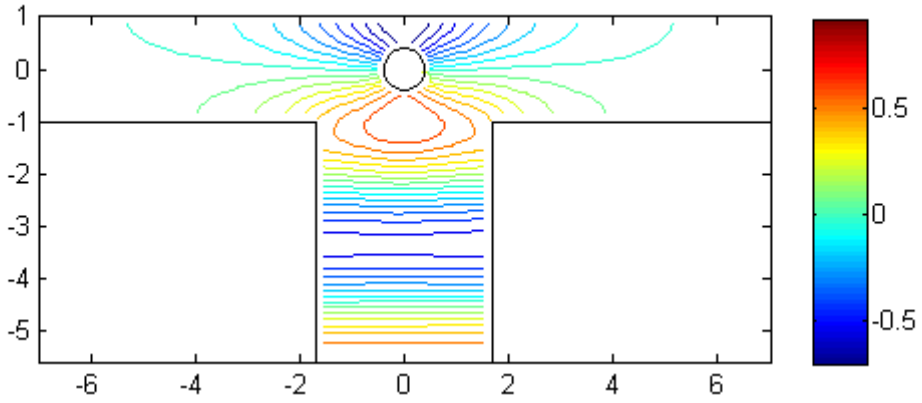

r=0.6

Mode no.	h/d	w/d	kd	kd/π	x-Symmetry
0.6-1	0.6	6.0	1.37107	0.4364	Antisymmetric
0.6-2	0.8	6.5	1.23149	0.3920	Symmetric
0.6-3	2.2	4.5	1.40747	0.4480	Symmetric
0.6-4	2.6	4.5	1.28866	0.4102	Symmetric

Mode 06-1

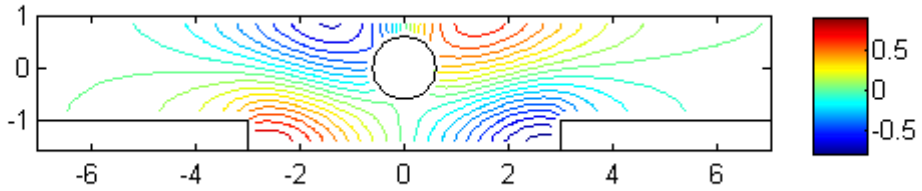

Mode 06-3

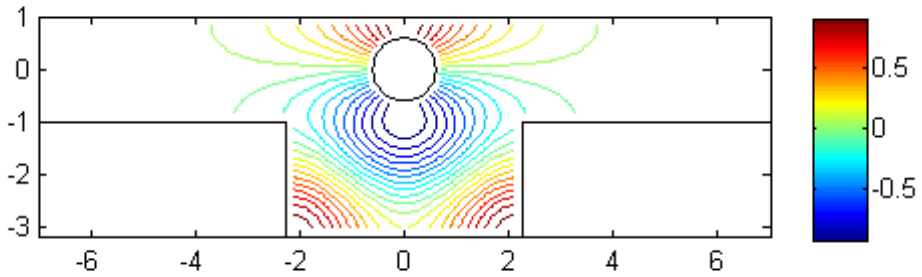

a = 0.8

Mode no.	h/d	w/d	kd	kd/π	x-Symmetry
0.8 -1	0.6	5.75	1.3846	0.4407	Antisymmetric
0.8 -2	2.6	4.5	1.2643	0.4024	Symmetric
0.8 -3	3.6	6.5	1.2309	0.3918	Antisymmetric
0.8 -4	4.8	2	1.3206	0.4204	Symmetric

Mode no. 0.8–3

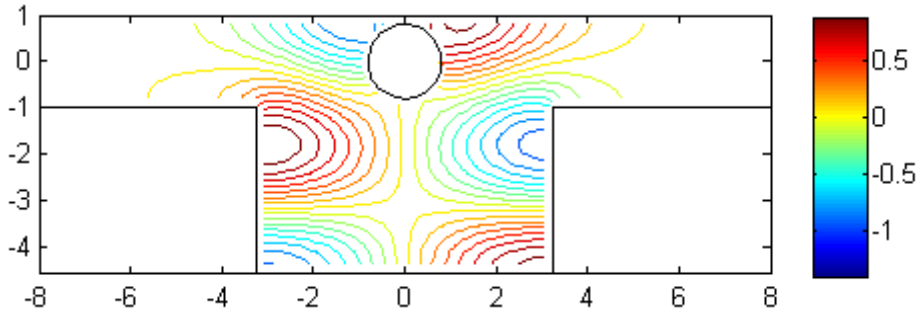

Mode no. 0.8–4

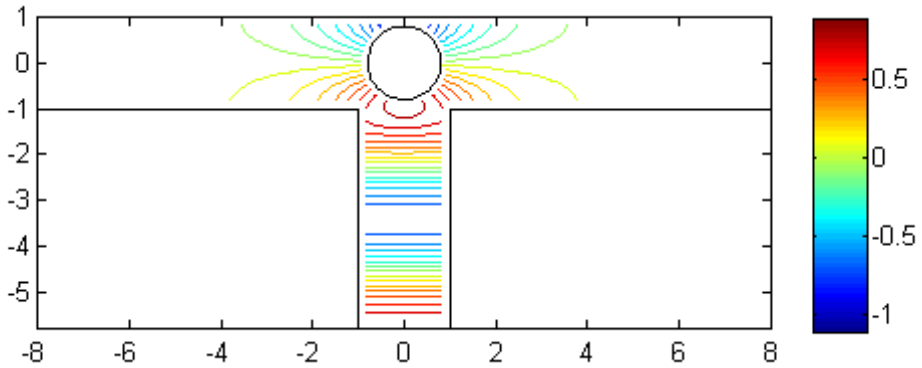

B.2 Dirichlet waveguide

a/d= 0.2

Mode No.	h/d	w/d	kd	kd / π	Type
0.2 - 1	2.0	1.2	3.05274	0.97172	Symmetric
0.2 - 2	2.4	2.9	2.94200	0.93647	Symmetric
0.2 - 3	2.7	1.7	2.83115	0.90118	Symmetric
0.2 - 4	3.6	2.9	2.94046	0.93598	Symmetric
0.2 - 5	3.7	3.6	2.83115	0.90118	Symmetric
0.2 - 6	4.0	1.2	3.05436	0.97223	Symmetric
0.2 - 7	4.0	3.5	2.71868	0.86538	Symmetric

Mode No 0.2 - 1

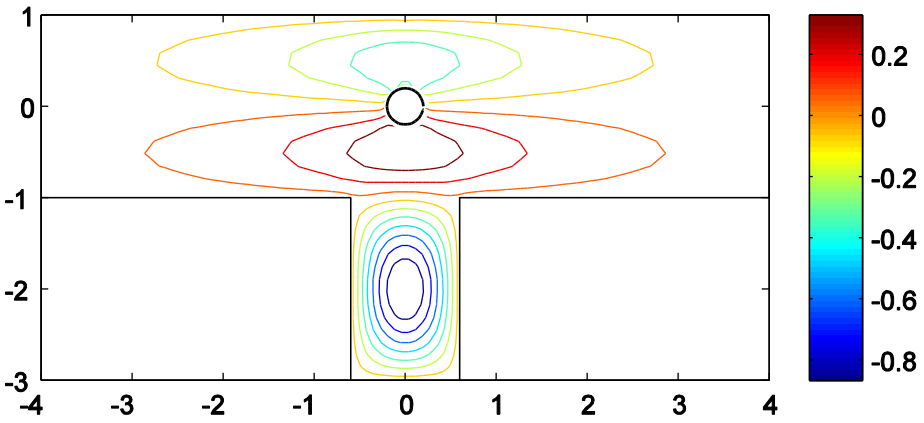

Mode 0.2 - 6

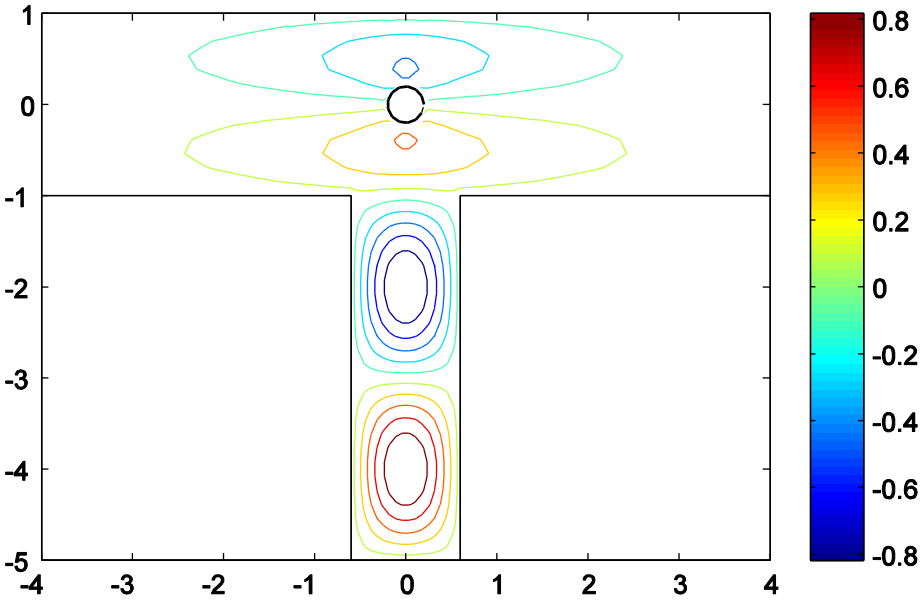

Mode No. 0.2 - 5

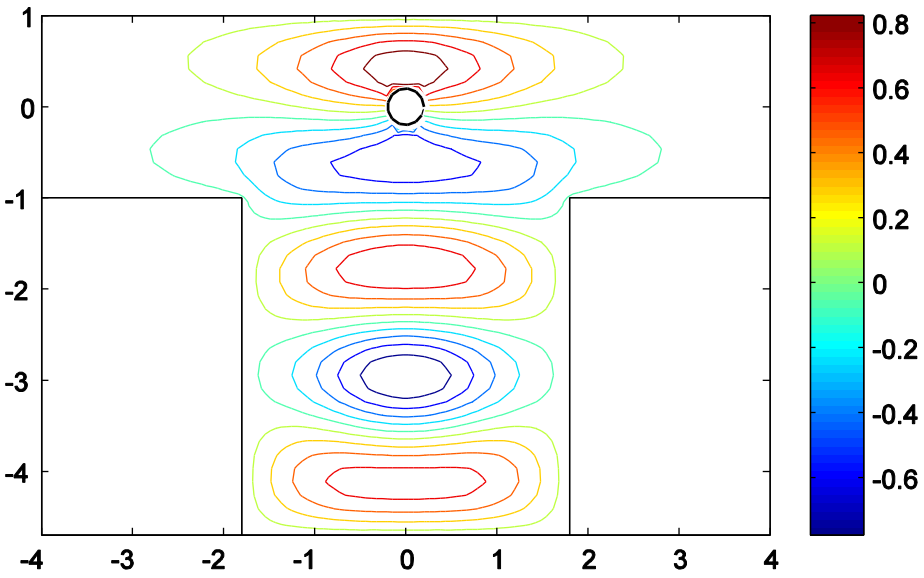

Mode No. 0.2 - 7

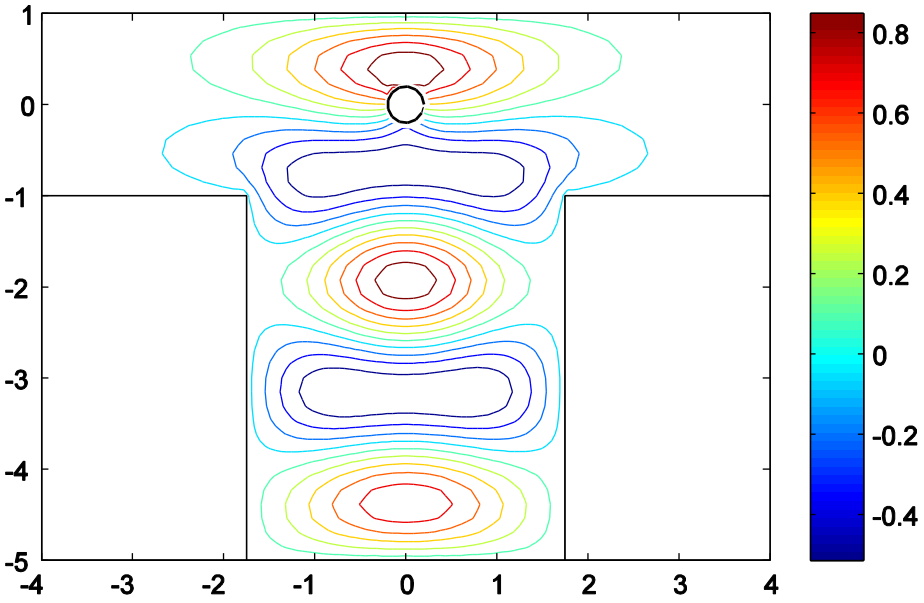

a/d= 0.3

Mode No.	h/d	w/d	kd	kd / π	Type
0.3 - 1	1.2	3.4	2.91233	0.92702	Symmetric
0.3 - 2	1.6	4.0	2.64178	0.84090	Symmetric
0.3 - 3	1.6	3.4	3.04218	0.96836	Antisymmetric
0.3 - 4	1.8	1.3	2.98267	0.94941	Symmetric
0.3 - 5	2.6	1.8	2.98330	0.94961	Symmetric
0.3 - 6	2.2	3.4	2.99660	0.95385	Symmetric
0.3 - 7	2.8	1.6	2.99660	0.95385	Symmetric
0.3 - 8	2.8	3.2	3.07459	0.97867	Anti-symm
0.3 - 9	3	3.8	2.59016	0.82447	Symmetric
0.3 - 10	3	3.6	2.96646	0.94425	Antisymmetric
0.3 - 11	3.2	3.2	3.06215	0.97471	Symmetric
0.3 - 12	3.2	4.2	3.01957	0.96116	Symmetric
0.3 - 13	3.2	4	2.81968	0.89753	Antisymmetric
0.3 - 14	3.2	4	3.02608	0.96323	Symmetric
0.3 - 15	3.2	4.2	3.01957	0.96116	Symmetric
0.3 - 16	3.2	5	2.69225	0.85697	Antisymmetric
0.3 - 17	3.8	4.8	2.49856	0.79532	Antisymmetric
0.3 - 18	4.2	1.6	2.98325	0.94960	Symmetric

Mode No. 0.3 - 2

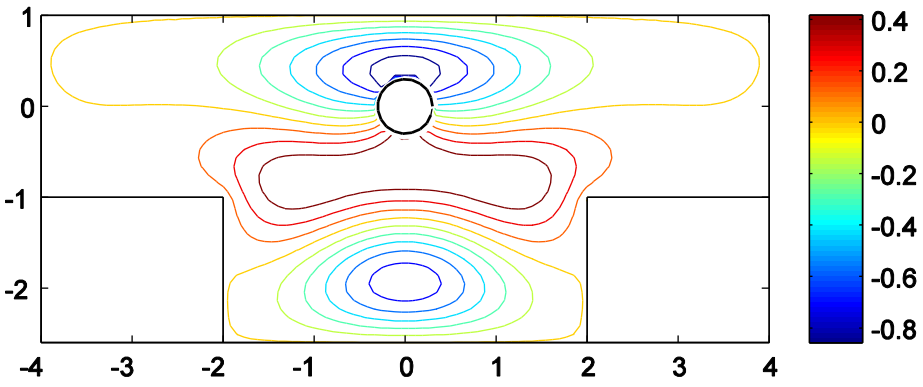

Mode No. 0.3 – 3

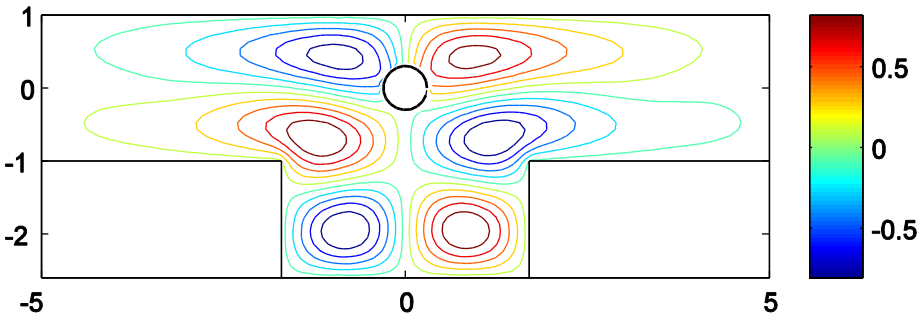

Mode No. 0.3 – 5

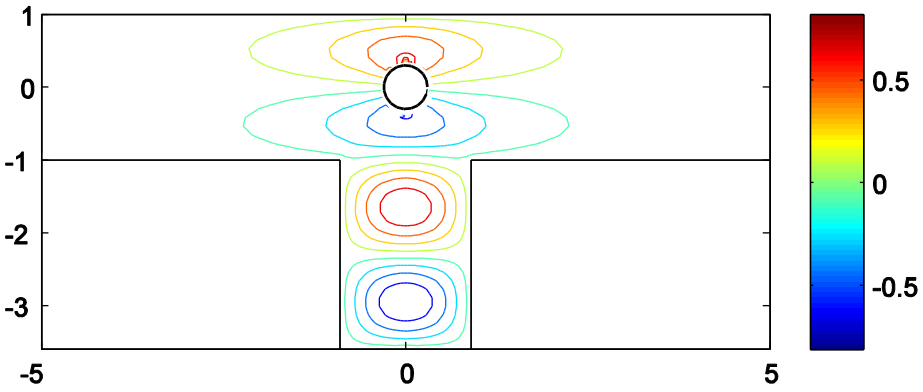

Mode No. 0.3 – 6

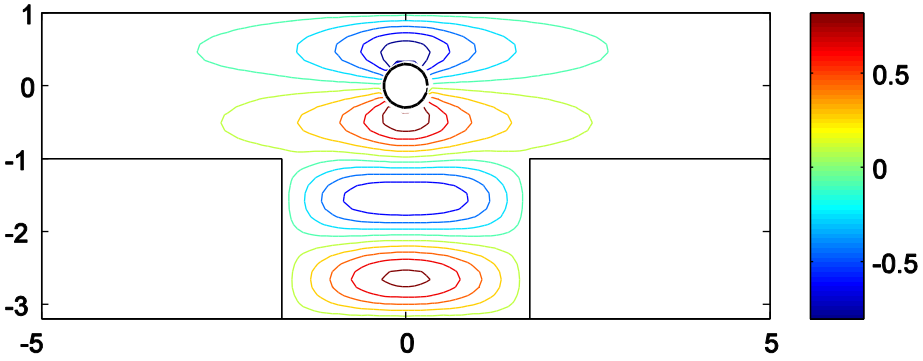

Mode No 0.3 - 11

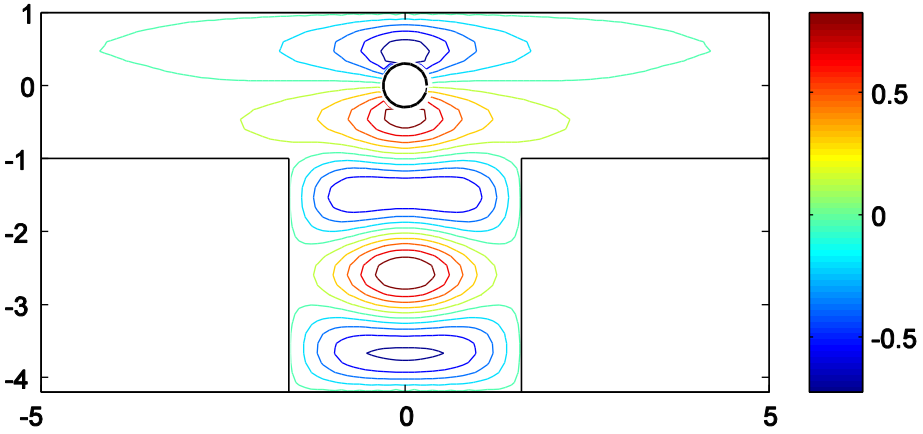

Mode No. 0.3 – 9

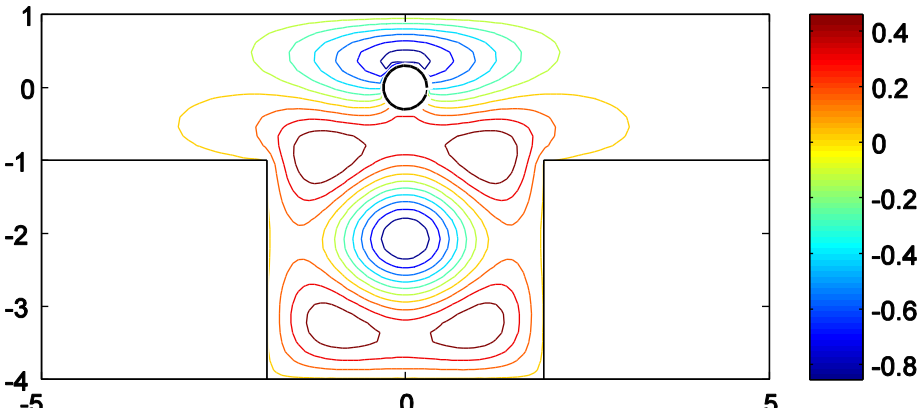

Mode No. 0.3 - 10

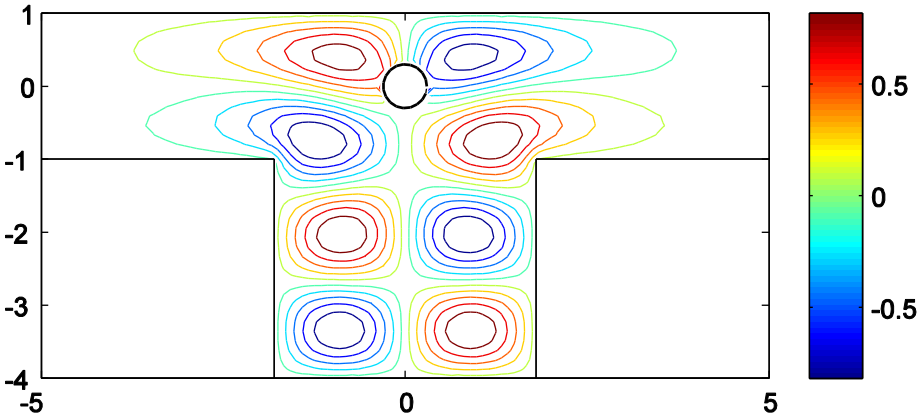

a/d= 0.4

Mode No.	h/d	w/d	kd	kd / π	Type
0.4 - 1	0.4	3.8	2.91181	0.92686	Antisymmetric
0.4 - 2	0.6	4.2	2.72432	0.86718	Antisymmetric
0.4 - 3	0.8	4.8	2.52567	0.80395	Antisymmetric
0.4 - 4	1	3.6	3.09261	0.98441	Symmetric
0.4 - 5	1.4	3	2.64636	0.84236	Symmetric
0.4 - 6	1.4	4	2.75261	0.87618	Symmetric
0.4 - 7	1.8	4	2.83507	0.90243	Antisymmetric
0.4 - 8	2.2	3.6	2.99137	0.95218	Symmetric
0.4 - 9	2.4	4.8	2.46092	0.78333	Antisymmetric
0.4 - 10	3	3.8	2.91729	0.92860	Antisymmetric
0.4 - 11	3	3.8	2.59755	0.82683	Symmetric
0.4 - 12	3.2	1.4	2.98553	0.95033	Symmetric
0.4 - 13	3.2	5	2.46796	0.78558	Symmetric
0.4 - 14	3.2	5	2.69685	0.85843	Antisymmetric
0.4 - 15	3.4	4	2.45937	0.78284	Symmetric
0.4 - 16	3.4	3.8	2.93025	0.93273	Symmetric
0.4 - 17	3.6	2.2	2.98549	0.95031	Symmetric
0.4 - 18	3.8	2	2.95417	0.94034	Symmetric
0.4 - 19	4	4	2.67420	0.85122	Symmetric
0.4 - 20	4.4	4.2	2.53742	0.80769	Symmetric

Mode No. 04 – 3

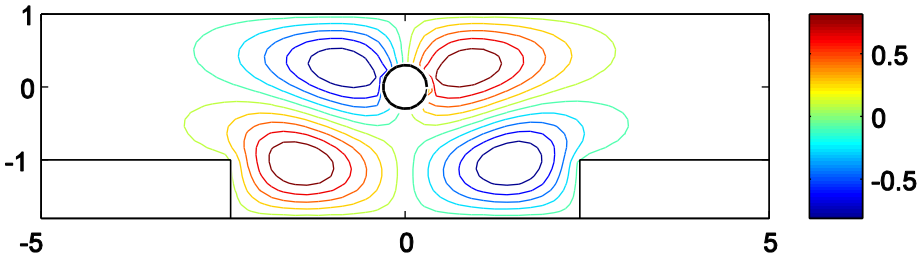

Mode No. 0.4 – 4

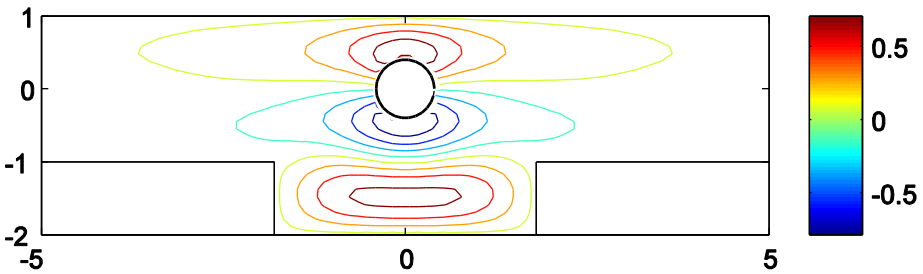

Mode No. 0.4 - 6

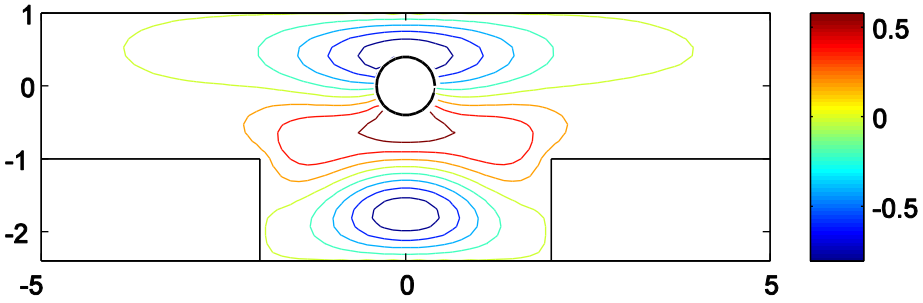

Mode No. 0.4 - 8

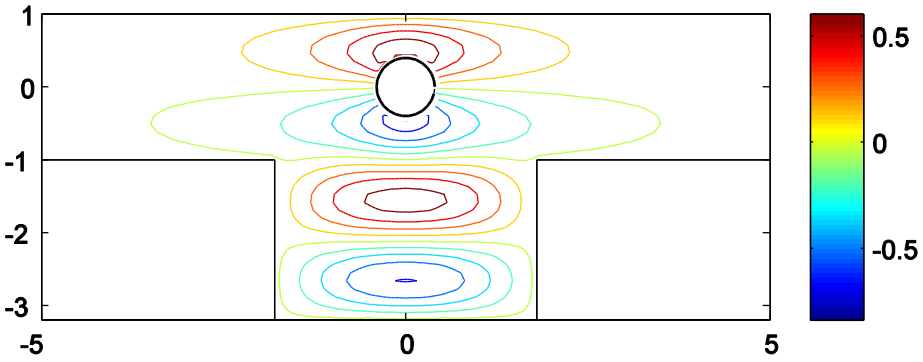

Mode 0.4 – 10

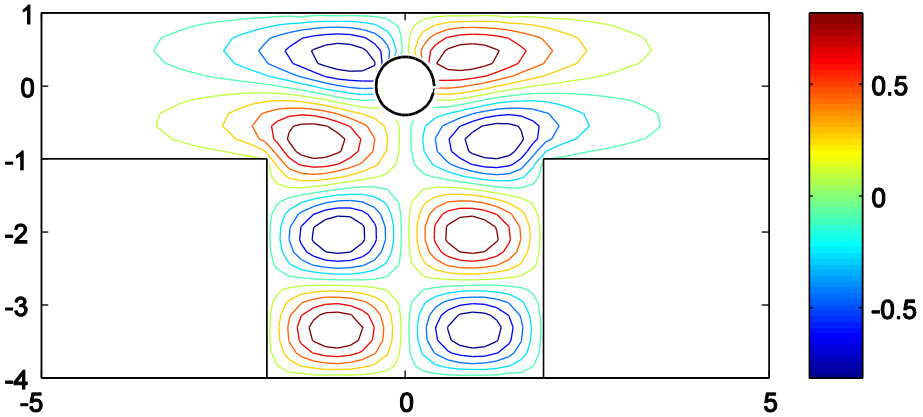

Mode 0.4 - 11

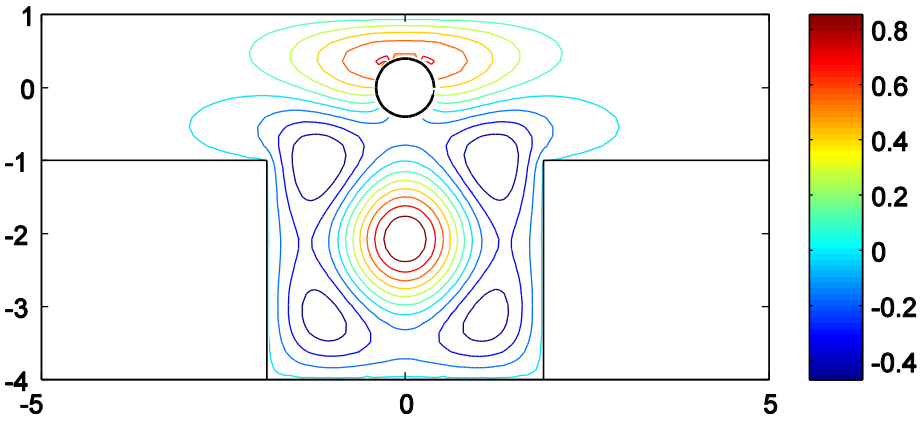

Mode No.0.4 – 16

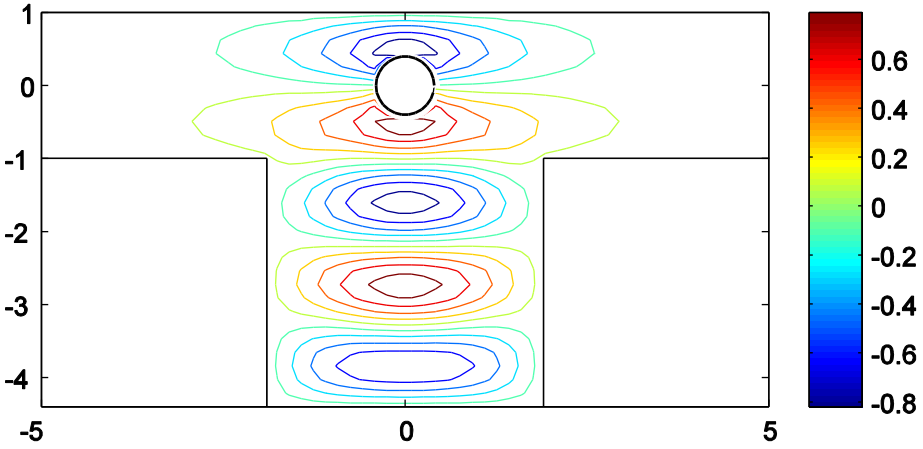

Mode No.0.4 – 20

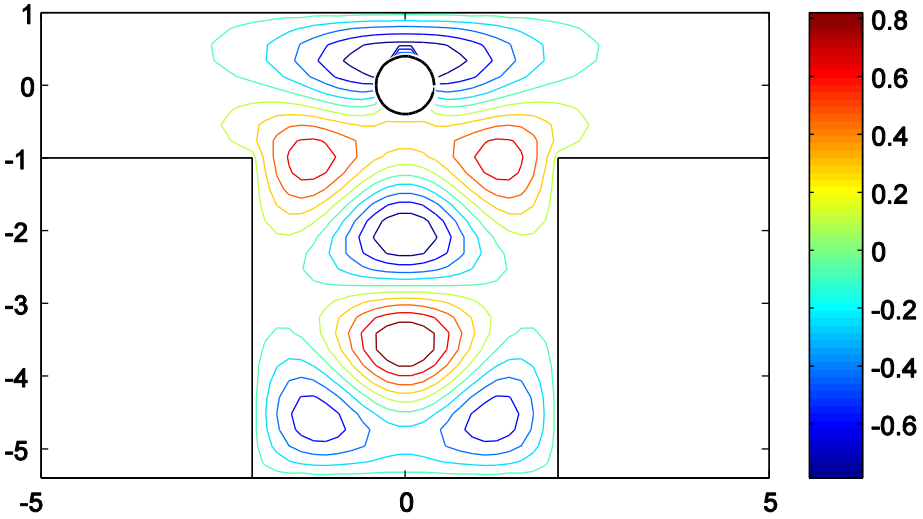

a/d= 0.5

Mode No.	h/d	w/d	kd	kd / π	Type
0.5 - 1	1.2	2	3.05683	0.97302	Symmetric
0.5 - 2	1.6	4	2.91675	0.92843	Antisymmetric
0.5 - 3	3.4	2.6	3.03562	0.96627	Symmetric
0.5 - 4	3.6	4	2.45102	0.78018	Symmetric
0.5 - 5	4	1.2	3.05626	0.97284	Symmetric
0.5 - 6	4	1.6	3.06547	0.97577	Symmetric

Mode No. 0.5 – 1

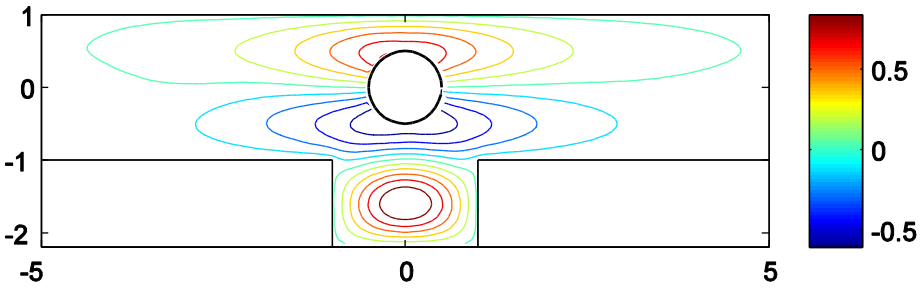

Mode No. 0.5 - 2

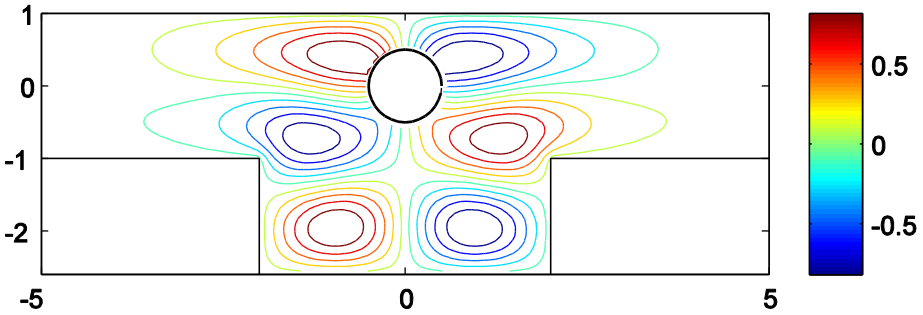

Mode No. 0.5 - 3

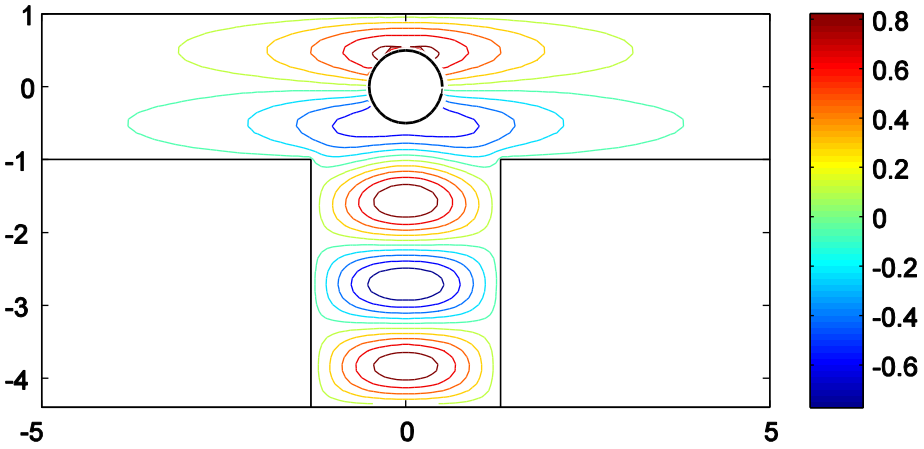

Mode No 0.5 – 4

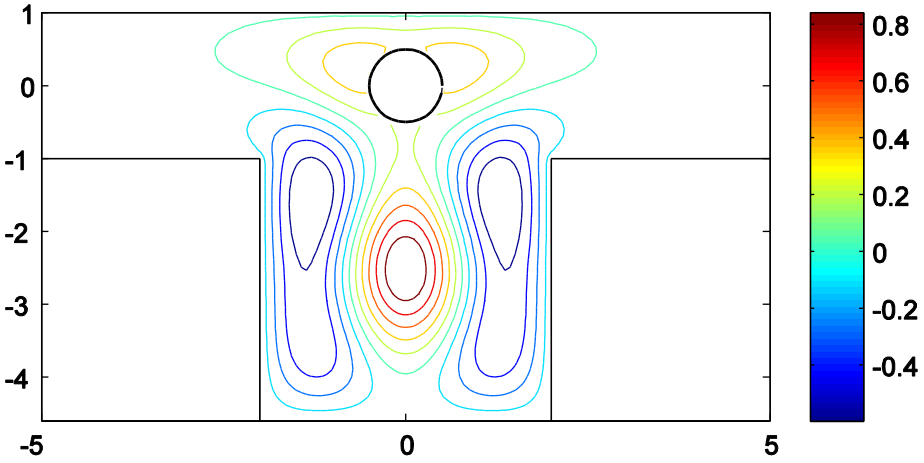

a/d= 0.6

Mode No.	h/d	w/d	kd	kd / π	Type
0.6 - 1	1.8	1.2	3.13480	0.99784	Symmetric
0.6 - 2	2.2	2.8	3.08010	0.98043	Symmetric
0.6 - 3	2.2	4	2.54860	0.81124	Symmetric
0.6 - 4	3.2	3.2	3.11298	0.99089	Symmetric
0.6 - 5	3.2	3.6	2.70943	0.86244	Symmetric
0.6 - 6	3.2	4	3.08229	0.98112	Symmetric
0.6 - 7	3.4	2.2	3.116000	0.99185	Symmetric

Mode 0.6 – 4

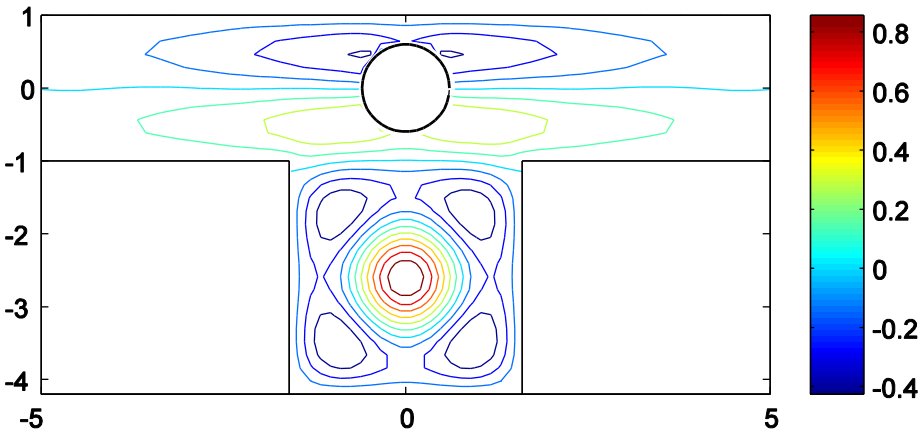

Mode No. 0.6 – 5

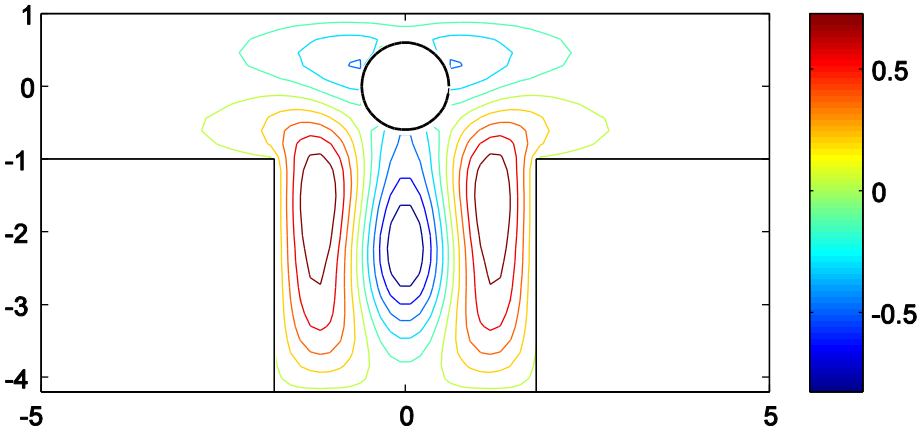

a/d= 0.7

Mode No.	h/d	w/d	kd	kd / π	Type
0.7 - 1	1.0	3	3.094245	0.98493	Symmetric
0.7 - 2	1.2	5	3.072042	0.97786	Antisymmetric
0.7 - 3	1.4	3.6	2.866064	0.91230	Symmetric
0.7 - 4	1.4	4.4	2.969265	0.94515	Antisymmetric
0.7 - 5	2.0	3	3.079549	0.98025	Symmetric
0.7 - 6	2.0	3.2	3.011674	0.95865	Symmetric
0.7 - 7	2.4	4.6	3.056370	0.97287	Antisymmetric
0.7 - 8	2.8	2.9	3.135751	0.99814	Antisymmetric
0.7 - 9	3.0	3.2	2.985512	0.95032	Symmetric
0.7 - 10	3.0	4.4	2.284029	0.72703	Symmetric

Mode No. 0.7 – 1

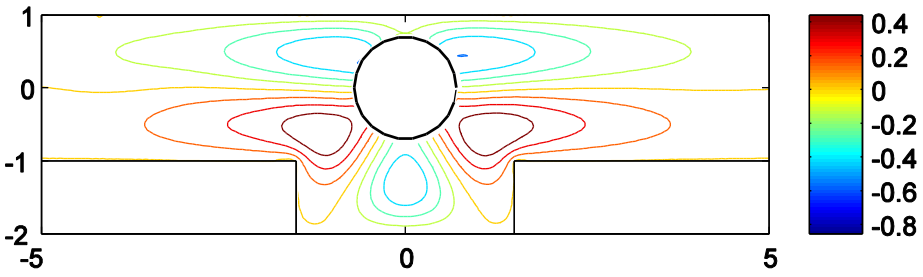

Mode 0.4 – 4

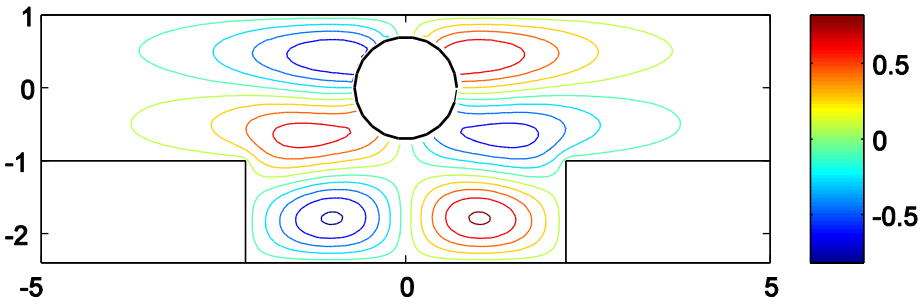

Mode No. 0.7 - 6

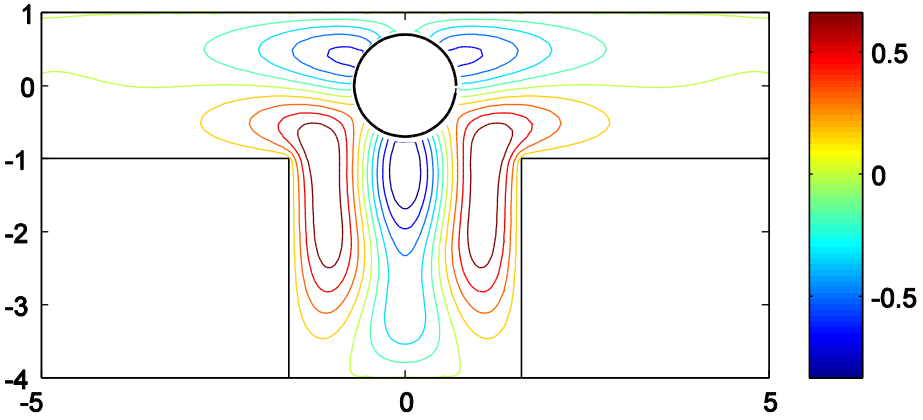

Mode No. 0.7 – 7

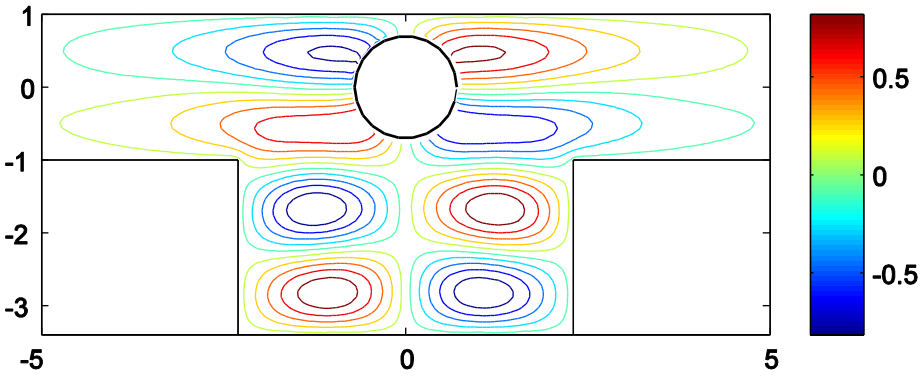

Mode 0.7 – 10

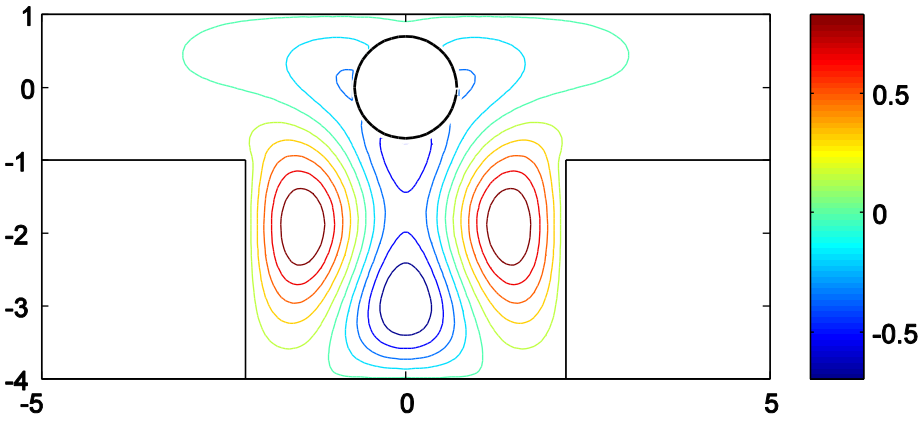

a/d= 0.8

h/d		w/d	kd	kd / π	Type
0.8 - 1	0.8	1.2	3.006279	0.95693	Symmetric
0.8 - 2	1.2	4.4	2.60853	0.83032	Symmetric
0.8 - 3	1.4	5.8	2.90441	0.92450	Antisymmetric
0.8 - 4	1.8	5.2	2.67329	0.85093	Antisymmetric
0.8 - 5	2.8	2	3.00612	0.95688	Symmetric
0.8 - 6	2.8	5.4	3.00583	0.95679	Symmetric
0.8 - 7	3.0	4	2.48272	0.79027	Symmetric
0.8 - 8	3.0	4	2.81717	0.89673	Symmetric

Mode No. 0.8 – 1

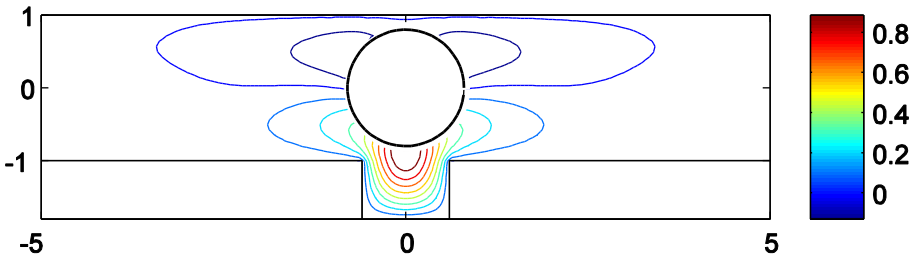

Mode No. 0.8 – 3

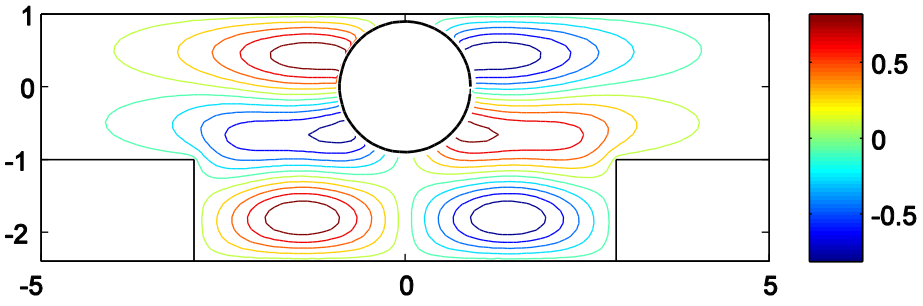

Mode No. 0.8 – 5

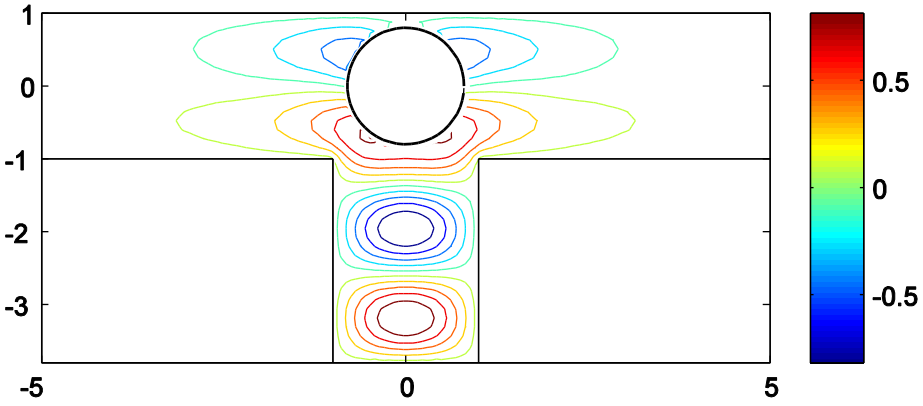

Mode 0.8 – 6

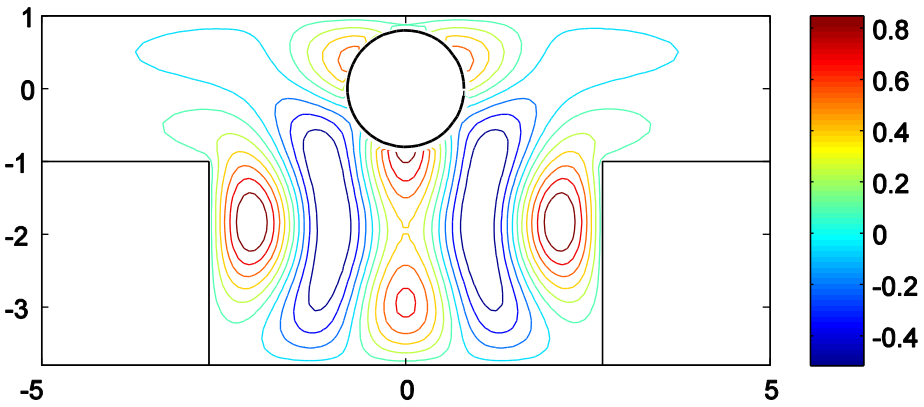

a/d= 0.9

Mode No.		w/d	kd	kd / π	Type
0.9 - 1	1.0	4.8	2.601422	0.82806	Symmetric
0.9 - 2	1.4	5.8	2.889752	0.91984	Antisymmetric
0.9 - 3	1.6	3.6	2.876110	0.91549	Symmetric
0.9 - 4	1.6	5.6	2.160214	0.68762	Symmetric
0.9 - 5	1.8	3.2	2.672035	0.85054	Symmetric
0.9 - 6	1.8	4.6	2.367837	0.75371	Symmetric
0.9 - 7	1.8	5	2.239986	0.71301	Symmetric
0.9 - 8	1.8	5.6	2.085912	0.66397	Symmetric
0.9 - 9	1.8	5.8	2.043547	0.65048	Symmetric
0.9 - 10	2.8	4	2.878430	0.91623	Symmetric
0.9 - 11	2.4	6	2.978324	0.94803	Antisymmetric

Mode No. 0.9 – 3

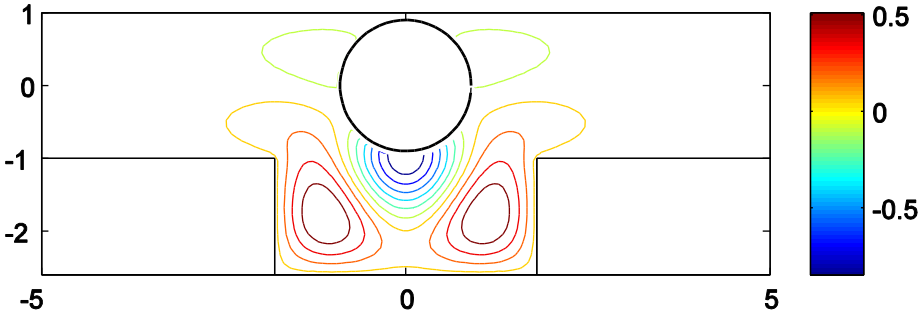

Mode No. 0.9- 5

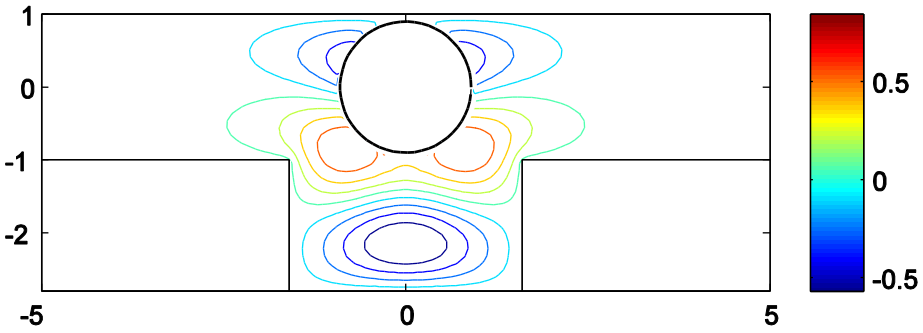

Mode No. 0.9 - 8

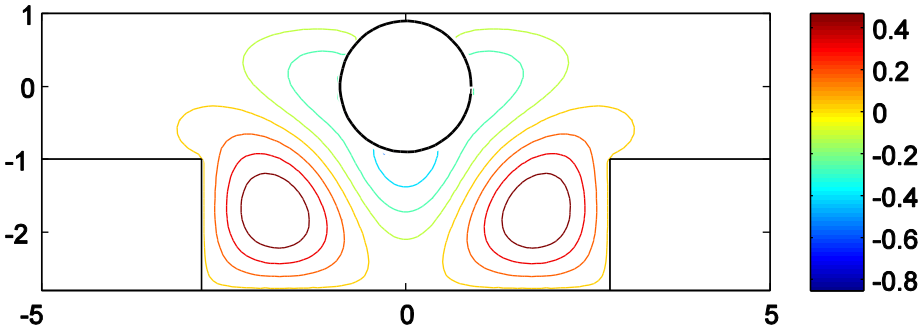

Mode No. 0.8 - 9

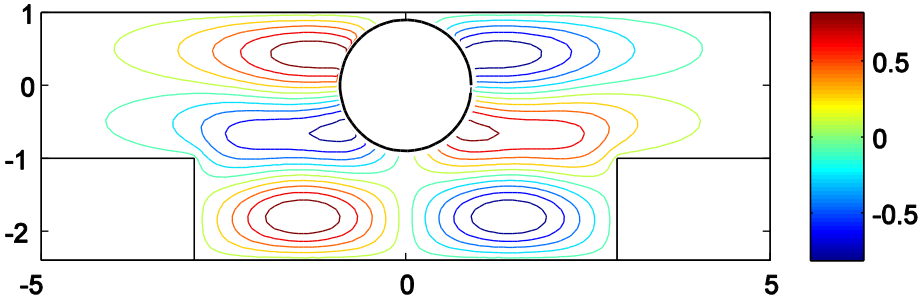

Mode No. 0.9 – 11

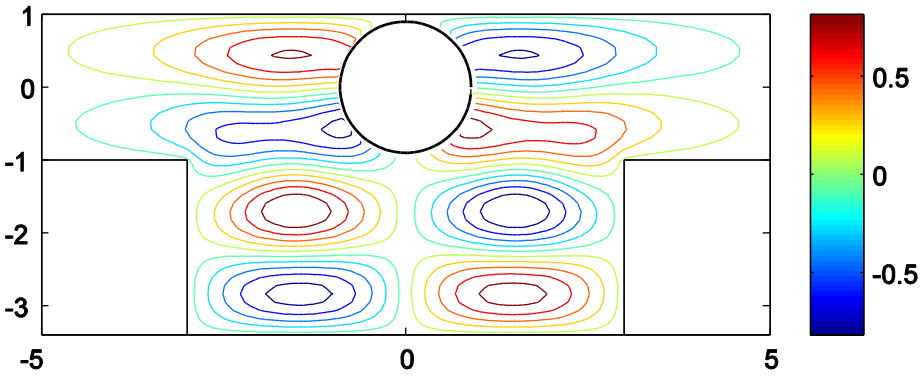

Appendix C

Disc Integral

This section is concerned with resolving the disc integral in (6.17). The notation used is as introduced in section (6.1) and (6.3.3). In expresssion (6.44) change inner integral variables to polar coordinates

$$I_{\text{Disc}} = -\frac{a}{4\pi}\int_C e^{i\mathbf{k}\cdot\mathbf{r}}\left[k\cos\alpha\underbrace{\int_0^{2\pi}\phi(\mathbf{x}')\cos\psi\, e^{-i\mathbf{k}\cdot\mathbf{r}'}\,d\psi}_{D_1} + k\sin\alpha\underbrace{\int_0^{2\pi}\phi(\mathbf{x}')\sin\psi\, e^{-i\mathbf{k}\cdot\mathbf{r}'}\,d\psi}_{D_2}\right]d\alpha$$
$$= -\frac{a}{4\pi}\int_C e^{i\mathbf{k}\cdot\mathbf{r}}\,(k_1D_1 + k_2D_2)\,d\alpha. \tag{C.1}$$

First write the trial function γ (6.31) as

$$\gamma(\mathbf{x}') = \begin{cases} = \frac{e^{i\eta_1 x'}+e^{-i\eta_1 x'}}{2}\cdot\frac{e^{i\eta_2(y'-d)}-e^{-i\eta_2(y'-d)}}{2i}, & y>0, \\ = \frac{e^{i\eta_1 x'}+e^{-i\eta_1 x'}}{2}\cdot\frac{e^{i\eta_2(y'+d)}-e^{-i\eta_2(y'+d)}}{2i}, & y<0. \end{cases} \tag{C.2}$$

and substitute for $\phi(\mathbf{x}')$ in (C.1). D_1, D_2 are then

$$D_1 \sim \frac{\cos\eta_2 d}{4i}\int_0^{2\pi} e^{i[(\eta_1-k_1)x'+(\eta_2-k_2)y']} - e^{i[(\eta_1-k_1)x'+(-\eta_2-k_2)y']}$$
$$+ e^{i[(-\eta_1-k_1)x'+(\eta_2-k_2)y']} - e^{i[(-\eta_1-k_1)x+(-\eta_2-k_2)y']}\,\cos\psi\,d\psi$$

$$= \frac{\cos\eta_2 d}{4i} \sum_{j=1}^{4} \int_0^{2\pi} \epsilon_j \, e^{\alpha_j \cos\psi + \beta_j \sin\psi} \, \cos\psi \; d\psi \tag{C.3}$$

$$\begin{aligned} D_2 \sim \frac{\cos\eta_2 d}{4i} \int_0^{2\pi} & e^{i[(\eta_1 - k_1)x' + (\eta_2 - k_2)y']} - e^{i[(\eta_1 - k_1)x' + (-\eta_2 - k_2)y']} \\ & + e^{i[(-\eta_1 - k_1)x' + (\eta_2 - k_2)y']} - e^{i[(-\eta_1 - k_1)x + (-\eta_2 - k_2)y']} \, \sin\psi \, d\psi \\ = \frac{\cos\eta_2 d}{4i} & \sum_{j=1}^{4} \int_0^{2\pi} \epsilon_j \, e^{\alpha_j \cos\psi + \beta_j \sin\psi} \, \sin\psi \, d\psi \end{aligned} \tag{C.4}$$

where

$$\begin{aligned} \alpha_1 &= ia(\eta_1 - k_1), \quad & \beta_1 &= ia(\eta_2 - k_2) \\ \alpha_2 &= ia(\eta_1 - k_1), \quad & \beta_2 &= ia(-\eta_2 - k_2) \\ \alpha_3 &= ia(-\eta_1 - k_1), \quad & \beta_3 &= ia(\eta_2 - k_2) \\ \alpha_4 &= ia(-\eta_1 - k_1), \quad & \beta_4 &= ia(-\eta_2 - k_2) \end{aligned} \tag{C.5}$$

and

$$\begin{aligned} \epsilon_1 &= \epsilon_3 = +1 \\ \epsilon_2 &= \epsilon_4 = -1 \end{aligned}$$

The integrand is analytic, we move to the complex unit disc $D(0,1)$, i.e. centered at $(x,y) = (0,0)$ with a radius $r = 1$. We make the following substitutions:

$$\begin{aligned} z &= e^{i\psi} \\ d\psi &= \frac{dz}{iz} \end{aligned} \tag{C.6}$$

$$\begin{aligned} \cos\psi &= \frac{1}{2}\left(z + \frac{1}{z}\right) \\ \sin\psi &= \frac{1}{2i}\left(z - \frac{1}{z}\right) \end{aligned} \tag{C.7}$$

(C.8)

With this substitution the exponential in integrand of D_1 and D_2 becomes:

$$\alpha_j \cos\psi + \beta_j \sin\psi = \frac{1}{2}\left(\alpha_j + \frac{\beta_j}{i}\right) z + \frac{1}{2}\left(\alpha_j - \frac{\beta_j}{i}\right)\frac{1}{z} \tag{C.9}$$

Let

$$\tau_j = \frac{1}{2}\left(\alpha_j + \frac{\beta_j}{i}\right) \tag{C.10}$$

$$\lambda_j = \frac{1}{2}\left(\alpha_j - \frac{\beta_j}{i}\right) \tag{C.11}$$

We obtain for D_1:

$$D_1 \sim \frac{\cos\eta_2 d}{8i}\sum_{j=1}^{4}\epsilon_j \int\limits_{D(0,1)} e^{\tau_j z + \frac{\lambda_j}{z}}\left(z + \frac{1}{z}\right)\frac{dz}{iz} \tag{C.12}$$

$$= -\frac{\cos\eta_1 d}{8}\sum_{j=1}^{4}\epsilon_j \left[\int\limits_{D(0,1)}\left(\sum_{m=0}^{\infty}\frac{(\tau_j z)^m}{m!}\right)\left(\sum_{n=0}^{\infty}\frac{\lambda_j^n}{n! z^n}\right)\ dz\right.$$

$$\left. + \int\limits_{D(0,1)}\left(\sum_{p=0}^{\infty}\frac{(\tau_j z)^p}{p!}\right)\left(\sum_{s=0}^{\infty}\frac{\lambda_j^s}{s! z^{s+2}}\right)\ dz\right] \tag{C.13}$$

The integrand is an analytic function of z, except at $z = 0$, and by Cauchy's theorem all terms in the expansion above are zero, except for those where

$$m - n = -1 \quad \text{and} \quad p = s + 1 \tag{C.14}$$

Collect all the residues and obtain for D_1

$$D_1 \sim -\frac{i\pi\cos\eta_2 d}{4}\sum_{j=1}^{4}\epsilon_j(\tau_j + \lambda_j)\sum_{m=0}^{\infty}\frac{(\lambda_j\tau_j)^m}{m!(m+1)!} \tag{C.15}$$

Following the same route we obtain for D_2

$$D_2 \sim -\frac{\pi\cos\eta_2 d}{4}\sum_{j=1}^{4}\epsilon_j(\lambda_j - \tau_j)\sum_{n=0}^{\infty}\frac{(\lambda_j\tau_j)^n}{n!(n+1)!} \tag{C.16}$$

Noting that:

$$\tau_j + \lambda_j = \alpha_j \tag{C.17}$$

$$\lambda_j - \tau_j = i\beta_j \tag{C.18}$$

we have the disc kernel:

$$k_1 D_1 + k_2 D_2 \sim -\frac{i\pi \cos \eta_2 d}{4} \sum_{j=1}^{4} \epsilon_j \left(k_1 \alpha_j + k_2 \beta_j\right) \sum_{m=0}^{\infty} \frac{(\lambda_j \tau_j)^m}{m!(m+1)!} \tag{C.19}$$

We also have for each element of the series expansion above that:

$$\tau_j \lambda_j = \frac{1}{4}(\alpha_j^2 + \beta_j^2) \tag{C.20}$$

Compute for each j:

$$\begin{aligned}
\lambda_1 \tau_1 &= -\frac{a}{2}(\mathbf{k}^2 - \mathbf{k}\cdot\boldsymbol{\eta}) = -\frac{a^2}{4}(\mathbf{k} - \boldsymbol{\eta})^2 \\
\lambda_2 \tau_2 &= -\frac{a}{2}(\mathbf{k}^2 - \mathbf{k}\cdot\bar{\boldsymbol{\eta}}) = -\frac{a^2}{4}(\mathbf{k} - \bar{\boldsymbol{\eta}})^2 \\
\lambda_3 \tau_3 &= -\frac{a}{2}(\mathbf{k}^2 + \mathbf{k}\cdot\bar{\boldsymbol{\eta}}) = -\frac{a^2}{4}(\mathbf{k} + \bar{\boldsymbol{\eta}})^2 \\
\lambda_4 \tau_4 &= -\frac{a}{2}(\mathbf{k}^2 + \mathbf{k}\cdot\boldsymbol{\eta}) = -\frac{a^2}{4}(\mathbf{k} + \boldsymbol{\eta})^2
\end{aligned} \tag{C.21}$$

where we defined:

$$\bar{\boldsymbol{\eta}} = (\eta_1, -\eta_2) \tag{C.22}$$

The identities above are possible because:

$$\mathbf{k}^2 - \mathbf{k} \cdot \boldsymbol{\eta} = k^2 - k_1\eta_1 - k_2\eta_2 \tag{C.23}$$

But $k^2 = \eta^2$ hence

$$\boldsymbol{\eta}^2 - \mathbf{k} \cdot \boldsymbol{\eta} = \eta^2 - k_1\eta_1 - k_2\eta_2 \tag{C.24}$$

$$= k^2 - k_1\eta_1 - k_2\eta_2 \tag{C.25}$$

$$\rightarrow \quad 2(\mathbf{k}^2 - \mathbf{k} \cdot \boldsymbol{\eta}) = (\mathbf{k} - \boldsymbol{\eta})^2 \tag{C.26}$$

We also have that

$$\begin{aligned}
\alpha_1 k_1 + \beta_1 k_2 &= -ia(\mathbf{k}^2 - \boldsymbol{\eta}\cdot\mathbf{k}) = -\frac{ia}{2}(\mathbf{k}-\boldsymbol{\eta})^2 \\
\alpha_2 k_1 + \beta_2 k_2 &= -ia(\mathbf{k}^2 - \bar{\boldsymbol{\eta}}\cdot\mathbf{k}) = -\frac{ia}{2}(\mathbf{k}-\bar{\boldsymbol{\eta}})^2 \\
\alpha_3 k_1 + \beta_3 k_2 &= -ia(\mathbf{k}^2 + \bar{\boldsymbol{\eta}}\cdot\mathbf{k}) = -\frac{ia}{2}(\mathbf{k}+\bar{\boldsymbol{\eta}})^2 \\
\alpha_4 k_1 + \beta_4 k_2 &= -ia(\mathbf{k}^2 - \boldsymbol{\eta}\cdot\mathbf{k}) = -\frac{ia}{2}(\mathbf{k}+\boldsymbol{\eta})^2
\end{aligned} \tag{C.27}$$

Hence

$$k_1 D_1 + k_2 D_2 \sim \frac{i\pi\cos\eta_2 d}{4}\sum_{j=1}^{4}\epsilon_j \sum_{m=0}^{\infty}(-1)^{m+1}\left(\frac{a}{2}\right)^{2m+1}\frac{(\mathbf{k}-\boldsymbol{\eta}^j)^{2m}}{m!(m+1)!} \tag{C.28}$$

where

$$\begin{aligned}
\boldsymbol{\eta}^1 &= \ \ \boldsymbol{\eta} \\
\boldsymbol{\eta}^2 &= \ \ \bar{\boldsymbol{\eta}} \\
\boldsymbol{\eta}^3 &= -\bar{\boldsymbol{\eta}} \\
\boldsymbol{\eta}^4 &= -\boldsymbol{\eta}
\end{aligned} \tag{C.29}$$

We compute the disc contribution to the spectrum:

$$\begin{aligned}
I_{Disc} &\sim -\frac{\cos\eta_2 d}{8}\sum_{j=1}^{4}\epsilon_j \int_C e^{i\mathbf{k}\cdot\mathbf{r}}\sum_{m=0}^{\infty}(-1)^{m+1}\left(\frac{a}{2}\right)^{2(m+1)}\frac{(\mathbf{k}-\boldsymbol{\eta}^j)^{2m+2}}{m!(m+1)!}\ \ d\alpha \\
&= -\frac{\cos\eta_2 d}{8}\sum_{j=1}^{4}\epsilon_j \sum_{m=0}^{\infty}\frac{(-1)^{m+1}}{m!(m+1)!}\left(\frac{a}{2}\right)^{2(m+1)}\int_C e^{i\mathbf{k}\cdot\mathbf{r}}(\mathbf{k}-\boldsymbol{\eta}^j)^{2(m+1)}\ \ d\alpha \\
&= -\frac{\cos\eta_2 d}{8}\sum_{j=1}^{4}\epsilon_j \sum_{m=0}^{\infty}\frac{(-1)^{m+1}}{m!(m+1)!}\left(\frac{a}{2}\right)^{2(m+1)}\int_C e^{i(\mathbf{k}-\boldsymbol{\eta}^j+\boldsymbol{\eta}^j)\cdot\mathbf{r}}(\mathbf{k}-\boldsymbol{\eta}^j)^{2(m+1)}\ \ d\alpha \\
&= -\frac{\cos\eta_2 d}{8}\sum_{j=1}^{4}\epsilon_j \sum_{m=0}^{\infty}\frac{(-1)^{m+1}}{m!(m+1)!}\left(\frac{a}{2}\right)^{2(m+1)}e^{i\boldsymbol{\eta}^j\cdot\mathbf{r}}\int_C e^{i(\mathbf{k}-\boldsymbol{\eta}^j)\cdot\mathbf{r}}(\mathbf{k}-\boldsymbol{\eta}^j)^{2(m+1)}\ \ d\alpha \\
&= -\frac{\cos\eta_2 d}{8}\sum_{j=1}^{4}\epsilon_j \sum_{m=0}^{\infty}\frac{1}{m!(m+1)!}\left(\frac{a}{2}\right)^{2(m+1)}e^{i\boldsymbol{\eta}^j\cdot\mathbf{r}}\int_C \nabla^{2(m+1)}\left[e^{i(\mathbf{k}-\boldsymbol{\eta}^j)\cdot\mathbf{r}}\ \ d\alpha\right]
\end{aligned}$$

$$= -\frac{\cos\eta_2 d}{8}\sum_{j=1}^{4}\epsilon_j\sum_{m=0}^{\infty}\frac{1}{m!(m+1)!}\left(\frac{a}{2}\right)^{2(m+1)} e^{i\boldsymbol{\eta}^j\cdot\mathbf{r}}\ \nabla^{2(m+1)}\left[e^{-i\boldsymbol{\eta}^j\cdot\mathbf{r}}\int_C e^{i\mathbf{k}\cdot\mathbf{r}}\ \ d\alpha\right]$$
$$= -\frac{\cos\eta_2 d}{8}\sum_{j=1}^{4}\epsilon_j\sum_{m=0}^{\infty}\frac{1}{m!(m+1)!}\left(\frac{a}{2}\right)^{2(m+1)} e^{i\boldsymbol{\eta}^j\cdot\mathbf{r}}\ \nabla^{2(m+1)}\left[e^{-i\boldsymbol{\eta}^j\cdot\mathbf{r}}\pi H_0^1(kr)\right] \tag{C.30}$$

We show here the first few terms, for $j=1$, for example:

$$\begin{aligned} m=0:\quad \nabla^2\left[e^{-i\boldsymbol{\eta}^1\cdot\mathbf{r}}\,\pi H_0^1(kr)\right] &= \pi\left(H_0^1(kr)\nabla^2 e^{-i\boldsymbol{\eta}^1\cdot\mathbf{r}} + 2\nabla e^{-i\boldsymbol{\eta}^1\cdot\mathbf{r}}\cdot\nabla H_0^1(kr) + e^{i\boldsymbol{\eta}^1\cdot\mathbf{r}}\nabla^2 H_0^1(kr)\right)\\ &= \pi\left[(i\eta)^2 H_0^1(kr)e^{-i\boldsymbol{\eta}^1\cdot\mathbf{r}} - \frac{2ik}{r}\,\boldsymbol{\eta}^1\cdot\mathbf{r}\ H_1^1(kr)\ e^{-i\boldsymbol{\eta}^1\cdot\mathbf{r}}\right.\\ &\quad \left.-k^2 H_0^1(kr)\,e^{-i\boldsymbol{\eta}^1\cdot\mathbf{r}}\right]\\ &= -2\pi k^2\left[H_0^1(kr) - i\cos(\alpha_0-\theta)\ H_1^1(kr)\right]e^{-i\boldsymbol{\eta}^1\cdot\mathbf{r}} \end{aligned} \tag{C.31}$$

$$m=1:\quad \nabla^4\left[e^{-i\boldsymbol{\eta}^1\cdot\mathbf{r}}\,\pi H_0^1(kr)\right] = 8\pi k^4\left[H_0^1(kr) - i\cos(\alpha_0-\theta)H_1^1(kr)\right]e^{-i\boldsymbol{\eta}^1\cdot\mathbf{r}} \tag{C.32}$$

$$m=2:\quad \nabla^6\left[e^{-i\boldsymbol{\eta}^1\cdot\mathbf{r}}\,\pi H_0^1(kr)\right] = -32\pi k^6\left[H_0^1(kr) - i\cos(\alpha_0-\theta)H_1^1(kr)\right]e^{-i\boldsymbol{\eta}^1\cdot\mathbf{r}} \tag{C.33}$$

By induction we can show that the *m*-th term is:

$$\nabla^{2(m+1)}\left[e^{-i\boldsymbol{\eta}^1\cdot\mathbf{r}}\,\pi H_0^1(kr)\right] \ = (-1)^{m+1}\pi\,2^{2m+1}\,k^{2(m+1)}\left[H_0^1(kr) - i\cos(\alpha_0-\theta)H_1^1(kr)\right]e^{-i\boldsymbol{\eta}^1\cdot\mathbf{r}} \tag{C.34}$$

Adding the contributions for all j we get the disc spectrum:

$$I_{Disc} \sim \frac{i\pi}{4}\cos\eta_2 d\sin\alpha_0\sin\theta\ H_1^1(kr)\sum_{m=0}^{\infty}\frac{(-1)^m(ka)^{2m+2}}{m!(m+1)!} \tag{C.35}$$

But

$$\sum_{m=0}^{\infty}\frac{(-1)^m(ka)^{2m+1}}{m!(m+1)!} = \ J_1(2ka) \tag{C.36}$$

Finally we get the expression for the disc integral as:

$$I_{Disc} \sim \frac{i\pi}{4} \cos\eta_2 d \sin\alpha_0 \sin\theta \; ka \; J_1(2ka) \; H_1^1(kr) \tag{C.37}$$

Appendix D

Waveguide Integral

The waveguide integral is solved using the method of steepest descent and the result obtained is valid for $y \to \pm\infty$. The waveguide integral is (6.56)

$$\begin{aligned} I_{\text{Waveguide}} &\sim -\frac{i\cos\mu_2 d}{2\pi}\int_C \cos k_2 d\,\left(\frac{\mu_1}{k_2-\mu_2}+\frac{\mu_1}{k_2+\mu_2}\right)e^{i\mathbf{k}\cdot\mathbf{r}}d\alpha \\ &= -\frac{i\cos\mu_2 d}{2\pi}\int_C \cos k_2 d\left(\frac{\cos\beta_0}{\sin\beta_0-\sin\alpha}+\frac{\cos\beta_0}{\sin\beta_0+\sin\alpha}\right)e^{i\mathbf{k}\cdot\mathbf{r}}\,d\alpha. \end{aligned} \tag{D.1}$$

Each term in (D.1) is now re-written in a form which allows us to solve this integral using a method developed by Clemmow [15].

$$\begin{aligned} \frac{\cos\beta_0}{\sin\alpha-\sin\beta_0} &= \frac{1}{2}\left(\tan\frac{\alpha+\beta_0}{2}+\cot\frac{\alpha-\beta_0}{2}\right), \\ \frac{\cos\beta_0}{\sin\alpha+\sin\beta_0} &= \frac{1}{2}\left(\tan\frac{\alpha-\beta_0}{2}+\cot\frac{\alpha+\beta_0}{2}\right). \end{aligned} \tag{D.2}$$

First, consider the plane wave representation

$$I(\alpha)=\int_{S(\theta)}\sec\left(\frac{\alpha-\beta_0}{2}\right)e^{ikr\cos(\theta-\alpha)}d\alpha, \tag{D.3}$$

in which the only singularities of the spectrum function in the complex $\alpha-$ plane are simple poles at $\alpha=\pm\beta_0,\ \beta_0+(2n+1)\pi, n=1,2,...$, and the path of integration is distorted from

C to $S(\theta)$ - see Fig. (D.1). With a change of variable from α to $\alpha - \theta$, (D.3) is

$$I(\alpha) = \int_{S(0)} \sec\left(\frac{\alpha - \beta_0 + \theta}{2}\right) e^{ikr\cos\alpha} d\alpha. \tag{D.4}$$

where the path of integration $S(0)$ is that depicted in Fig. (D.1)

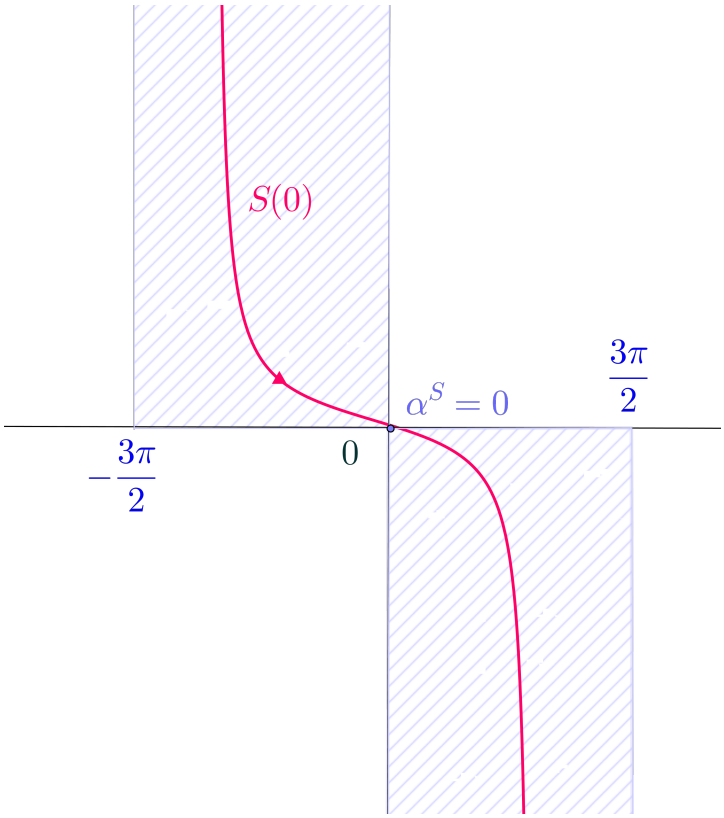

Figure D.1: Integration path $S(0)$

Reversing the sign of α we get

$$I(-\alpha) = \int_{S(0)} \sec\left(\frac{\alpha - \beta_0 + \theta}{2}\right) e^{ikr\cos\alpha} d\alpha \tag{D.5}$$

The addition of (D.4) and (D.5) and division by two puts (D.4) in the form

$$I(\alpha) = 2\cos\left(\frac{\beta_0 - \theta}{2}\right) \int_{S(0)} \frac{\cos(\frac{\alpha}{2})}{\cos\alpha + \cos(\beta_0 - \theta)} e^{ikr\cos\alpha} d\alpha \tag{D.6}$$

The same procedure applied to

$$I(\alpha) = \int_{S(\theta)} \sec\left(\frac{\alpha+\beta_0}{2}\right) e^{ikr\cos(\theta-\alpha)} d\alpha, \tag{D.7}$$

results in

$$2\cos\left(\frac{\beta_0+\theta}{2}\right) \int_{S(0)} \frac{\cos(\frac{\alpha}{2})}{\cos\alpha + \cos(\beta_0+\theta)}\, e^{ikr\cos\alpha} d\alpha. \tag{D.8}$$

For the poles of the spectrum of the form

$$I(\alpha) = \int_{S(\theta)} \operatorname{cosec}\left(\frac{\alpha-\beta_0}{2}\right) e^{ikr\cos(\theta-\alpha)} d\alpha, \tag{D.9}$$

we follow the same change of variable from α to $\alpha-\theta$ we have that

$$I(\alpha) = -I(-\alpha) \tag{D.10}$$

and by addition of $I(\alpha)$ and $-I(\alpha)$ and division by two we get

$$I(\alpha) = 2\sin\left(\frac{\beta_0-\theta}{2}\right) \int_{S(0)} \frac{\cos(\frac{\alpha}{2})}{\cos\alpha - \cos(\beta_0-\theta)}\, e^{ik_0 r\cos\alpha} d\alpha. \tag{D.11}$$

The same routine applied to

$$I(\alpha) = \int_{S(\theta)} \operatorname{cosec}\left(\frac{\alpha+\beta_0}{2}\right) e^{ikr\cos(\theta-\alpha)} d\alpha, \tag{D.12}$$

results in

$$I(\alpha) = 2\sin\left(\frac{\beta_0+\theta}{2}\right) \int_{S(0)} \frac{\cos(\frac{\alpha}{2})}{\cos\alpha - \cos(\beta_0+\theta)}\, e^{ikr\cos\alpha}\, d\alpha. \tag{D.13}$$

Now consider again:

$$2\cos\left(\frac{\beta_0-\theta}{2}\right) \int_{S(0)} \frac{\cos(\frac{\alpha}{2})}{\cos\alpha + \cos(\beta_0-\theta)}\, e^{ikr\cos\alpha}\, d\alpha. \tag{D.14}$$

We make the change of variable from α to τ and by (6.70) the expression (D.6) becomes

$$\begin{aligned} I(\alpha) &= 2e^{\frac{1}{4}i\pi}e^{ikr}\sqrt{2}\cos\frac{\beta_0-\theta}{2}\int_{-\infty}^{\infty}\frac{e^{-k_0r\tau^2}}{i\tau^2+2\cos^2\frac{\beta_0-\theta}{2}}d\tau \\ &= 2e^{-\frac{1}{4}i\pi}e^{ikr}b\int_{-\infty}^{\infty}\frac{e^{-kr\tau^2}}{\tau^2+ib^2}\,d\tau \end{aligned} \tag{D.15}$$

where

$$b = i\sqrt{2}\cos\left(\frac{\beta_0-\theta}{2}\right). \tag{D.16}$$

Integral (D.15) is similar to that in Clemmow [15] and we give here some details for completeness. The integral can be expressed in terms of the complex Fresnel integral. Let

$$I = b\int_{-\infty}^{\infty}\frac{e^{-\chi\tau^2}}{\tau^2+ib^2}\,d\tau, \tag{D.17}$$

where χ is a real positive parameter and we will show that the expression above is also a form of the complex Fresnel integral. Since

$$\begin{aligned} \frac{d}{d\chi}\left(Ie^{-ib^2\chi}\right) &= -\,b\int_{-\infty}^{\infty}e^{-\chi(\tau^2+ib^2)}d\tau, \\ &= -\sqrt{\pi}\,b\,\frac{e^{-ib^2\chi}}{\sqrt{\chi}}, \end{aligned} \tag{D.18}$$

it follows that

$$I = \sqrt{\pi}\,b\,e^{ib^2\chi}\int_{\chi}^{\infty}\frac{e^{ib^2\chi'}}{\sqrt{\chi'}}d\chi', \tag{D.19}$$

the upper limit being determined by the fact that $I\to 0$ as $\chi\to\infty$ ([15]). The transformation $\chi' = \tau^2/b^2$ shows that (D.19) leads to

$$I = 2\sqrt{\pi}e^{ib^2\chi}\int_{b\sqrt{\chi}}^{\infty}e^{-i\tau^2}b\,d\tau = 2\sqrt{\pi}\,F(b\sqrt{\chi}). \tag{D.20}$$

hence

$$b\int_{-\infty}^{\infty}\frac{e^{-\lambda r\tau^2}}{\tau^2+ib^2}d\tau = \pm 2\sqrt{\pi}\,F(\pm b\sqrt{\lambda}). \tag{D.21}$$

where F is the Fresnel complex integral which has the particular form

$$F(a) = e^{ia^2} \int_a^\infty e^{-i\tau^2} d\tau. \tag{D.22}$$

The integral in (D.17) is an odd function of b and the corresponding result for b real and negative is

$$I = 2\sqrt{\pi} F(-b\sqrt{\chi}). \tag{D.23}$$

By analytic continuation, therefore

$$b \int_{-\infty}^{\infty} \frac{e^{-\chi\tau^2}}{\tau^2 + ib^2} d\tau = \pm 2\sqrt{\pi} F(\mp b\sqrt{\chi}), \tag{D.24}$$

where χ is real and positive, and where the upper sign holds for $-\frac{3}{4}\pi < \arg b < \frac{1}{4}\pi$ and the lower sign for $\frac{1}{4}\pi < \arg b < \frac{5}{4}\pi$ [15]. Applying this result to integrals in our problem we get for

$$I(\alpha) = \int_{S(\theta)} \sec\left(\frac{\alpha - \beta_0}{2}\right) e^{ikr\cos(\theta-\alpha)} d\alpha \tag{D.25}$$

$$= \pm\, 4\sqrt{\pi} e^{-\frac{i\pi}{4}} e^{ik_0 r} F\left[\pm i\sqrt{2kr}\cos\left(\frac{\beta_0 - \theta}{2}\right)\right] \tag{D.26}$$

with the upper sign for $\beta_0 - \theta$ between $S(-\pi)$ and $S(\pi)$ and the lower sign otherwise, noting that the expression $\cos\left(\frac{\beta_0 - \theta}{2}\right)$ has period 4π in $\beta_0 - \theta$. We also note that in the argument of the Fresnel integral we have that $\beta_0 = \sin^{-1}\left(\frac{\mu_2}{k}\right)$, $\mu_2 = \pi$ and $k < \pi/d$ hence $\beta_0 \in \mathbb{C}, \beta_0 = \frac{\pi}{2} - i\xi$ for some $\xi \in \mathbb{R}$.

Each term in our waveguide integral (D.1) has a simple pole which can be factored out by writing for example

$$T(\alpha) = \int_C \frac{i\cos\mu_2 d\ \cos k_2 d}{4\pi} \tan\frac{\alpha - \beta_0}{2} e^{ikr\cos(\theta-\alpha)} d\alpha$$

$$= \int_C Q(\cos\alpha) \sec\left(\frac{\alpha - \beta_0}{2}\right) e^{ikr\cos(\theta-\alpha)} d\alpha. \tag{D.27}$$

where $Q(\cos\alpha)$ is

$$\frac{i\cos\mu_2 d\ \cos k_2 d}{4\pi}\sin\left(\frac{\alpha-\beta_0}{2}\right). \tag{D.28}$$

$Q(\cos\alpha)$ has no singularities in the vicinity of the saddle-point so it may be removed from under the integral sign with α equated to θ. Thus we obtain for each term in the waveguide integral the following expression

$$\int_{S(\theta)} Q(\cos\alpha)\sec\left(\frac{\alpha-\beta_0}{2}\right)e^{i\mathbf{k}\cdot\mathbf{r}}d\alpha = \pm\,4\sqrt{\pi}e^{i\left(kr-\frac{3\pi}{4}\right)}Q(\cos\theta)F\left[\mp i\sqrt{2kr}\cos\left(\frac{\beta_0-\theta}{2}\right)\sqrt{2k_0 r}\right], \tag{D.29}$$

$$\int_{S(\theta)} Q(\cos\alpha)\sec\left(\frac{\alpha+\beta_0}{2}\right)e^{i\mathbf{k}\cdot\mathbf{r}}d\alpha = \pm\,4\sqrt{\pi}e^{i\left(kr-\frac{3\pi}{4}\right)}Q(\cos\theta)F\left[\pm i\sqrt{2kr}\cos\left(\frac{\beta_0+\theta}{2}\right)\right], \tag{D.30}$$

$$\int_{S(\theta)} Q(\cos\alpha)\mathrm{cosec}\left(\frac{\alpha-\beta_0}{2}\right)e^{i\mathbf{k}\cdot\mathbf{r}}d\alpha = \pm\,4\sqrt{\pi}e^{i\left(kr-\frac{3\pi}{4}\right)}Q(\cos\theta)F\left[\mp i\sqrt{2kr}\sin\left(\frac{\beta_0-\theta}{2}\right)\right] \tag{D.31}$$

$$\int_{S(\theta)} Q(\cos\alpha)\mathrm{cosec}\left(\frac{\alpha+\alpha_0}{2}\right)e^{i\mathbf{k}\cdot\mathbf{r}}d\alpha = \pm\,4\sqrt{\pi}e^{i\left(kr-\frac{3\pi}{4}\right)}Q(\cos\theta)F\left[\pm i\sqrt{2kr}\sin\left(\frac{\beta_0+\theta}{2}\right)\right] \tag{D.32}$$

Appendix E

Boundary Element Program

We present an example of the boundary element program developed for the case of a Dirichlet waveguide with a cavity and a disc on the centre.

```
%DISC AND SKEW CAVITY IN A DIRICHLET WAVEGUIDE

% The program calculates the energy dissipation for a range of frequencies
[kmin,kmax] and a set of geometric parameters specified by r (disc radius),
hp (cavity height vector) and wp (cavity width vector).

global a  b l X Y d R1 R2 R3 R4 R5 L LNN Alpha Beta W1 W2 W3 W4 N Nc k0 Vmin;
%% Declare global variables for this program
hp =(1:0.2:4); %% cavity height range
wp =(1:0.2:4); %% cavity width range

%% Structure m stores the energy dissipation for each k, hp and wp.
r=0.5;a=16; l=0.1;  Beta=pi; kmin=pi/2;kmax=pi;kp=300;
m =struct('KValues',{},'Energy',{});
 for i=1:length(hp )
     for j=1:length(wp )
         [m(i,j).KValues m(i,j).Energy] =EnergyDissipation(hp (i),hp
(i),wp(j),r,c1,c2,kmin,kmax,kp);
     end
 end
%%
save('m.mat','m','a','l','hp','wp','r','b','kmin','kmax','kp')

%% For each geometry select and display the minimum energy dissipation index
and the correspondent frequency

EnMin=zeros(length(hp),length(wp));
 for i=1:length(hp)
     for j=1:length(wp)
         if isempty(m(i,j).Energy)==1
             EnMin(i,j)=1;
         else
            EnMin(i,j)=min(m(i,j).Energy);
         end
     end
 end
 [ind, e]=min(EnMin);
 %%
index1=1   ;  %
index2=1   ;
h= hp(index1)
w=wp(index2)
[W1 W2 W3 W4 N Nc L LNN Alpha Xc Yc X Y d WX WY]=fBoundary(h,h,w ,r,0,0 );
R1=R(-1); R2=R(-0.5);R3=R(0);  R4=R(0.5);R5=R(1);
 M0=real(M(k0));
           [V0 lambda0]=eig(M0); Lambda=abs(lambda0);
           T= diag(Lambda); [Emin,IndT]=min(T);
           Vmin=V0(:,IndT);
ft=@Phi;
%%
[xp,vp]=VPhi(-(a/2)+0.2,(a/2)-0.2,-0.7,100);figure, plot(xp,vp),grid on
%%  Display trapped mode signature
```

```
function [W1 W2 W3 W4 N Nc L LNN Alpha Xc Yc X Y d WX WY]=
fBoundary(h1,h2,w,r,c1,c2)
%This function calculates the coordinates of points around the boundary.
%The boundary consists of
%a rectangular waveguide with length a, width b, a disc of radius
% a with centre coordinates (c1, c2) and
%a cavity of side heights h1, h2 % and width h2

global  a   b l  ;
Nc=ceil(2*pi*r/l); % No of points around disc
%W1...W4 = Indices of corners of the waveguide
%C1..C4 - Indices of corners of cavity
%l = Length of boundary element
w1=sqrt(((h1-h2)^2)+w^2);  %w1 is the distance betweern C2 and C3 i.e. the
segment at the bottom of the cavity

n1=floor(((a/2)-(w/2))/l);          W1=1+Nc;
n2=floor(h1/l );                    C1=W1+n1;
n3=floor(w1/l) ;                    C2=C1+n2;
n4=floor(h2/l) ;                    C3=C2+n3;
n5=n1;                              C4=C3+n4;
n6=floor(b/l) ;                     W2=C4+n5;
n7=floor(a/l) ;                     W3=W2+n6;
n8=n6  ;                            W4=W3+n7;
N=Nc+n1+n2+n3+n4+n5+n6+n7+n8;                   %Total no of points on the
boundary
Xc=r*double(cos((((0:Nc-1)*2)./Nc)*pi))-c1;     %X coordinates of points on
circle
Yc=r*double(sin((((0:Nc-1)*2)./Nc)*pi))-c2;     %Y coordinates of points on
circle
%The following are vectors with x and y coordinates of points on the
%boundary - taken on each segment going anticlockwise
xstep=l*cos(acos(w/w1));
ystep=l*sin(acos(w/w1));
X1=zeros(1,n1);
for i=1:n1
    X1(i)=-(a/2)+(i-1)*l ;
end
X2=zeros(1,n2);
for i=1:n2
    X2(i)=-w/2;
end
X3=zeros(1,n3);
for i=1:n3
    X3(i)=(-w/2)+(i-1)*xstep ;
end
X4=zeros(1,n4);
for i=1:n4
    X4(i)=w/2 ;
end
X5=zeros(1,n5);
for i=1:n5
    X5(i)=w/2+(i-1)*l ;
end
X6=zeros(1,n6);
for i=1:n6
```

```
    X6(i)=a/2;
end
X7=zeros(1,n7);
for i=1:n7
    X7(i)=(a/2)-(i-1)*l ;
end
X8=zeros(1,n8);
for i=1:n8
    X8(i)=-a/2 ;
end
Y1=zeros(1,n1);
for i=1:n1
    Y1(i)=-b/2;
end
Y2=zeros(1,n2);
for i=1:n2
    Y2(i)=-b/2-(i-1)*l;
end
Y3=zeros(1,n3);
for i=1:n3
    if h1<h2
        Y3(i)=((-b/2)-h1)-ystep*(i-1);
    else
        Y3(i)=(-(b/2))-h1+ystep*(i-1);
    end
end

Y4=zeros(1,n4);
for i=1:n4
    Y4(i)=(-(b/2))-h2 +(i-1)*l;
end
Y5=zeros(1,n5);
for i=1:n5
    Y5(i)=-b/2;
end
Y6=zeros(1,n6);
for i=1:n6
    Y6(i)=(-b/2)+(i-1)*l;
end
Y7=zeros(1,n7);
for i=1:n7
    Y7(i)=b/2;
end
Y8=zeros(1,n8);
for i=1:n8
    Y8(i)=b/2-(i-1)*l;
end
%Waveguide coordinates:
WX=[X1 X2 X3 X4 X5 X6 X7 X8];
WY=[Y1 Y2 Y3 Y4 Y5 Y6 Y7 Y8];
%Domain coordinates
X=[Xc X1 X2 X3 X4 X5 X6 X7 X8];
Y=[Yc Y1 Y2 Y3 Y4 Y5 Y6 Y7 Y8];
L=zeros(N,1);
for i=1:N
    if(i<Nc)
        L(i)=sqrt((X(i+1)-X(i)).^2 +(Y(i+1)-Y(i)).^2);
```

```
    elseif (i==Nc)
         L(i)=sqrt((X(1)-X(i)).^2 +(Y(1)-Y(i)).^2);
    elseif (i>Nc)&&(i<N)
         L(i)=sqrt((X(i+1)-X(i)).^2 +(Y(i+1)-Y(i)).^2);
    else
        L(i)=sqrt((X(Nc+1)-X(i)).^2 +(Y(Nc+1)-Y(i)).^2);
    end
end

Alpha=zeros(N,1);   %Alpha stores the angles in radians between any two
boundary elements
for i=1:N
    if i==1
        Alpha(i)=(2*pi)-acos((((X(i)-X(Nc))^2)+((Y(i)-Y(Nc))^2)+  ((X(i+1)-
X(i))^2)+((Y(i+1)-Y(i))^2 )-(((X(i+1)-X(Nc))^2)+((Y(i+1)-Y(Nc))^2)))/(2*(
sqrt    ((((X(i)-X(Nc))^2)+((Y(i)-Y(Nc))^2)))*   sqrt( (((X(i+1)-
X(i))^2)+((Y(i+1)-Y(i))^2)))   )));
    elseif (i>1)&&(i<Nc)
        Alpha(i)=(2*pi)-acos((((X(i)-X(i-1))^2)+((Y(i)-Y(i-1))^2)+  ((X(i+1)-
X(i))^2)+((Y(i+1)-Y(i))^2 )-(((X(i+1)-X(i-1))^2)+((Y(i+1)-Y(i-1))^2)))/(2*(
sqrt    ((((X(i)-X(i-1))^2)+((Y(i)-Y(i-1))^2)))*   sqrt( (((X(i+1)-
X(i))^2)+((Y(i+1)-Y(i))^2)))   )));
    elseif (i==Nc)
        Alpha(i)=(2*pi)-acos((((X(i)-X(i-1))^2)+((Y(i)-Y(i-1))^2)+  ((X(1)-
X(i))^2)+((Y(1)-Y(i))^2 )-(((X(1)-X(i-1))^2)+((Y(1)-Y(i-1))^2)))/(2*( sqrt
((((X(i)-X(i-1))^2)+((Y(i)-Y(i-1))^2)))*   sqrt( (((X(1)-X(i))^2)+((Y(1)-
Y(i))^2)))   )));
    elseif (i==(Nc+1))
        Alpha(i)=acos((((X(i)-X(N))^2)+((Y(i)-Y(N))^2)+  ((X(i+1)-
X(i))^2)+((Y(i+1)-Y(i))^2 )-(((X(i+1)-X(N))^2)+((Y(i+1)-Y(N))^2)))/(2*( sqrt
((((X(i)-X(N))^2)+((Y(i)-Y(N))^2)))*   sqrt( (((X(i+1)-X(i))^2)+((Y(i+1)-
Y(i))^2)))   )));
    elseif (i<N)&&((Nc+1)<i)
        Alpha(i)=acos((((X(i)-X(i-1))^2)+((Y(i)-Y(i-1))^2)+  ((X(i+1)-
X(i))^2)+((Y(i+1)-Y(i))^2 )-(((X(i+1)-X(i-1))^2)+((Y(i+1)-Y(i-1))^2)))/(2*(
sqrt    ((((X(i)-X(i-1))^2)+((Y(i)-Y(i-1))^2)))*   sqrt( (((X(i+1)-
X(i))^2)+((Y(i+1)-Y(i))^2)))   )));
     elseif (i==N)
        Alpha(i)=acos((((X(i)-X(i-1))^2)+((Y(i)-Y(i-1))^2)+  ((X(Nc+1)-
X(i))^2)+((Y(Nc+1)-Y(i))^2 )-(((X(Nc+1)-X(i-1))^2)+((Y(Nc+1)-Y(i-
1))^2)))/(2*( sqrt    ((((X(i)-X(i-1))^2)+((Y(i)-Y(i-1))^2)))*   sqrt(
(((X(Nc+1)-X(i))^2)+((Y(Nc+1)-Y(i))^2)))   )));
    end
end
Alpha(W1:W2)=0;
Alpha(W3:W4)=0;
d=zeros(N,N);
for i=1:N
    for j=1:N
        if (j<Nc)
            d(i,j)= -(X(j)*Y(j+1)-X(j+1)*Y(j)-X(i)*(Y(j+1)-Y(j))-Y(i)*(X(j)-
X(j+1)));
        elseif (j==Nc)
             d(i,j)= -(X(j)*Y(1)-X(1)*Y(j)-X(i)*(Y(1)-Y(j))-Y(i)*(X(j)-
X(1)));
         elseif (j==N)
```

```
            d(i,j)=X(j)*Y(Nc+1)-X(Nc+1)*Y(j)-X(i)*(Y(Nc+1)-Y(j))-Y(i)*(X(j)-
X(Nc+1));
        else
            d(i,j)=X(j)*Y(j+1)-X(j+1)*Y(j)-X(i)*(Y(j+1)-Y(j))-Y(i)*(X(j)-
X(j+1));

        end
    end
end
LNN=repmat(L',N,1);

%% END OF BOUNDARY FUNCTION

function Matrix=M(k)
%% This   function calculates the integrals for either Phi or its derivatives
at nodal points around the boundary. The matrix has zero determinant for a
trapped mode frequency. The eigenvector corresponding to the zero eigenvalue
stores solves the trapped mode problem.

global    N  Nc d R1 R2 R3 R4 R5   W1 W2 W3 W4  L LNN Alpha Beta;
Matrix= 19*((A(k)+B(k)-(C(k)+D(k)))- diag(Alpha/(2*pi)));
function f1=A(x)
            % Coefficients of Phi(j) i.e. dG/dn on Ej
            %This function computes the first set of coefficients i.e. of
            %(Phi(j) in the linear progression on the boundary element
Phi(j)*(1-psi)
            %+Phi(j+1)*(1+psi) in the Neumann boundary conditions case

        f1= d.* ((x* (((1i)/48)*(((besselh(1,1,(x*R1))) ./R1) +
(3*((besselh(1,1,(x*R2))) ./R2))   + ((besselh(1,1,(x*R3))) ./R3)  +
((besselh(1,1,(x*R4))) ./R4)))));

              for i=1:N
                  f1(i,i)=0;
              end
             f1(:,W1:W2)=0;

             f1(:,W3:W4)=0;
        end

        function f2=B(x)
            % Coefficients of Phi(j+1) i.e. dG/dn calculated on E(j)

            b1 = d.* ((x* (((1i)/48)*(((besselh(1,1,(x*R2))) ./R2) +
((besselh(1,1,(x*R3))) ./R3)    + (3*((besselh(1,1,(x*R4))) ./R4)) +
((besselh(1,1,(x*R5))) ./R5)))));

            ind=find(isnan(b1));
            b1(ind)=0;

            b1(:,W1:((W2)-1))=0;
            b1(:,N)=0;
            b1(:,((W3)-1):((W4)-1))=0;

                b11=b1(:,1:Nc);
```

```
                b12=b1(:,(Nc+1):N);
                b111=circshift(b11,[0,1]);
                b112=circshift(b12,[0,1]);

                f2=[b111,b112];
        end

        function f3= C(x)
            %Coefficients of dPhi / dn
            f3=CNonSingular(x) +Cjj(x) +Cjjminus1(x) ;  %Cjj-1 do not have a
singularity as we use the linearly varying element

                % Disc - Neumann condition:
                  f3(:,1:Nc)=0;

               %Waveguide - Dirichlet condition on boundary element W2 -
               %Phi at node W2 is zero therefore q(W2) on W2 is zero

                f3(:,W2)=0;
                f3(:,W4)=0;         %Same as above for boundary element W4


                f3(:,((W2)+1):((W3)-1))=(- sqrt(Beta^2-
(x^2)))*f3(:,((W2)+1):((W3)-1));
                f3(:,((W4)+1):N)=(- sqrt(Beta^2-(x^2)))*f3(:,((W4)+1):N);
        end
                    function fCNotSing=CNonSingular(x)
                        fCNotSing = LNN.*(((-
1i)/48)*(besselh(0,1,x*R1)+(3*besselh(0,1,x*R2)) +
besselh(0,1,x*R3)+besselh(0,1,x*R4))) ;

                        for l=1:N
                            fCNotSing(l,l)=0;
                        end
%   Coefficients Ajj and Ajj-1 are calculated separately
Ajj have singularities - the source point is collinear with the
point of integration so in this function set them to zero and calculate
using ASing and fAjminus1
                  for n=1:(Nc-1)
                            fCNotSing((n+1),n)=0;
                        end

                        fCNotSing(1,Nc)=0;
                        for n=((Nc+1):(N-1))
                        fCNotSing((n+1),n)=0;
                        end
                        fCNotSing(Nc+1,N)=0;
                    end
                    function CSingular =Cjj(x)

%   This function calculates coefficients on the diagonal resulting from the
integral on the boundary element Bjj.
                        CSingular= diag(c1(x)+c2(x) );
```

```
                    function f1c=c1(x)
                             f1c= ((-1i/96)*(
1.999*GreenSingular((0.0005)*x*L) + 6*GreenSingular(0.25*x *L)
+2*GreenSingular(0.5*x*L) +2* GreenSingular((3/4)*x*L))).*L;
                             end

                    function f2c=c2(x)
                                f2c= L.*((1/(8*pi))*((2*log(x*L))-3));

                             end
                    end
                    function fCjjminusone= Cjjminus1(x)
                    fc1= L.*(((-1i)/48)*(0.0005* besselh(0,1, (0.0005*x*L))+
besselh(0,1, (0.25*x*L))+ besselh(0,1, (0.5*x*L)) +  3*besselh(0,1,
((3/4)*x*L))  + besselh(0,1, (x*L))));

%Must shift coefficients in place for the lower diagonal so split into four
units, shift one to circle around each domain then regroup

                        fc11=diag(fc1(1:Nc));
                        fc12=diag(fc1(Nc+1:N));
                        fc111=circshift(fc11,1);
                        fc112=circshift(fc12,1);
                        c1=zeros(Nc,N-Nc);
                        c2=zeros(N-Nc,Nc);

                        c11=[fc111,c1];
                        c12=[c2,fc112];

                    fCjjminusone=[c11;c12];
                    end
            function f4=D(x)

                %   Coefficients of dPhi/dn

                    fd=DNonSingular(x) +Djj(x) + Djjminus1(x);  %Djj do not
have a singularity - see notes

                    %Disc - Neumann condition:
                     fd(:,1:Nc)=0;
                     fd(:,((W3)-1))=0;
                     fd(:,N)=0;

                    fd(:, W2:((W3)-2))=(-sqrt(Beta^2-(x^2)))* fd(:, W2:((W3)-
2));  %Decay condition at infinity
                    fd(:, W4:(N-1))=(-sqrt(Beta^2-(x^2)))* fd(:, W4:(N-1));
                      %   Dij's are coefficients to Phi(j+1) so need to shift
around each boundary:
                    fd1=fd(:,1:Nc);
                    fd2=fd(:,Nc+1:N);

                    fd11=circshift(fd1,[0,1]);
                    fd12=circshift(fd2,[0,1]);
```

```
                f4=[fd11,fd12];
        end

        function fDNotSing=DNonSingular(y)

                                fDNotSing = LNN.*(((-1i)/48)*
(besselh(0,1,y*R2)+besselh(0,1,y*R3)+(3*besselh(0,1,y*R4))+
besselh(0,1,y*R5)))   ;

                                for l=1:N
                                    fDNotSing(l,l)=0;
                                end

                    %Main diagonal
                                for n=1:N
                                    fDNotSing(n,n)=0;

                                end
                %   Lower diagonal for each structure:

                                for n=1:Nc-1

                                    fDNotSing(n+1,n)=0;

                                end

                                fDNotSing(1,Nc)=0;

                                for n=Nc+1 : N-1

                                    fDNotSing(n+1,n)=0;

                                end


                                fDNotSing(Nc+1,N)=0;
        end

                function DSingular =Djj(x)
                            DSingular= diag(L.*(((-1i)/48)*(0.0005*
besselh(0,1, (0.0005*x*L))+ besselh(0,1, (0.25*x*L))+ besselh(0,1, (0.5*x*L))
+  3*besselh(0,1, ((3/4)*x*L))  + besselh(0,1, (x*L)))));
                end

function fDjjminusone= Djjminus1(x)

                            function f1d=d1(x)
                                f1d=L.* ((((-1i)/96)*(
(1.9999*GreenSingular(0.00005*x*L)) + (6*GreenSingular(0.25*x *L))
+(2*GreenSingular(0.5*x*L)) +(2* GreenSingular((3/4)*x*L)))));
                            end

                            function f2d=d2(x)
                                f2d= L.*(((1/(8*pi))*((2*log(x*L))-3)));
```

```
  end

                              %Create a matrix
                                  fsd1= d1(x)+ d2(x);
%Shift along each structure to place values on lower diagonal

                                  fsd11=diag(fsd1(1:Nc));
                                  fsd12=diag(fsd1(Nc+1:N));

                                  fsd111=circshift(fsd11,1);
                                  fsd112=circshift(fsd12,1);


                                  d01=zeros(Nc,N-Nc);
                                  d02=zeros(N-Nc,Nc);

                                  d11=[fsd111,d01];
                                  d12=[d02,fsd112];

                     fDjjminusone=[d11;d12];

            end

end

% END OF M(k) FUNCTION


function  GS =GreenSingular(y)
GS=(besselh(0,1,y))-(((2i)/pi)*log(y));

% THIS FUNCTION CALCULATES THE ENERGY DISSIPATION FOR A GIVEN VALUE OF K

function [KValue Energy]=EnergyDissipation(h1,h2,w,r,c1,kmin,kmax,kp)
global    a b  l X Y W1 W2 W3 W4  N Nc L LNN Alpha d R1 R2 R3 R4 R5 Beta
Vmin
 [W1 W2 W3 W4 N Nc L LNN Alpha Xc Yc X Y d WX WY]=fBoundary(h1,h2,w,r,c1);
[XPerimeter YPerimeter]=fPerimeter(h1,h2,w,r,c1);
R1=R(-1);
R2=R(-0.5);
R3=R(0);
R4=R(0.5);
R5=R(1);

Points=linspace(kmin, kmax , kp);
RM=zeros(kp,1);
for i=1:kp
    RM(i)=det(real(M(Points(i))));
end
SignRM=sign(RM);
ProductSign=zeros(kp-1,1);
    for i=1:kp-1
        ProductSign(i)=SignRM(i)*SignRM(i+1);
    end
```

```
ZerosofDet=zeros(kp-1,1);
    for j=1:kp-1
        if sign(SignRM(j+1))~=sign(SignRM(j))
            ZerosofDet(j)=fzero('RealDet',[Points(j+1),Points(j)]);
        else
            ZerosofDet(j)=ZerosofDet(j);
        end
    end

KValues=double(nonzeros(ZerosofDet)); %KValues
Energy1=zeros(1,length(KValues));
for i=1:length(KValues)
    Energy1(i)=Phi(KValues(i));
end
[Energy Ind1]=min(Energy1);
KValue=KValues(Ind1);
    function Potential=Phi(k0)


    M0=real(M(k0)); %i.e. find value of k s.t. det(M)=0
    [V0 lambda0]=eig(M0);               %   Calculates the eigenvalues and
eigenvectors of M0
     Lambda=abs(eig(M0)) ;              %   Calculates the eigenvalues of M0
and puts them in a vector column
     [Emin I] =min(Lambda);             %   Calculates value  and index of
the smallest eigenvalue
     Vmin=V0(:,I);

    np=length(XPerimeter);
            PerimeterPotential =zeros(np,1);
                for index2=1:np

PerimeterPotential(index2)=real(sum(Vmin'.*((fA(XPerimeter(index2),YPerimeter
(index2))+fB(XPerimeter(index2),YPerimeter(index2)))-
(fC(XPerimeter(index2),YPerimeter(index2))+fD(XPerimeter(index2),YPerimeter(i
ndex2))))));
                end

    PerimeterEnergy= (sum(PerimeterPotential.^2));



    nx=10;
    ny=10;
    xp1=linspace((-a/2)+0.2,(-a/2)+2,nx);
    xp2=linspace((a/2)-2,(a/2)-0.2,nx);

    xp= [xp1,xp2];
    yp=linspace(-b,b,ny);

    AreaPotential = zeros(2*nx,ny);
    for index5=1:2*nx
        for index6=1:ny

AreaPotential(index5,index6)=real(sum(Vmin'.*((fA(xp(index5),yp(index6))+fB(x
```

```
%DISC AND SKEW CAVITY IN A DIRICHLET WAVEGUIDE

% The program calculates the energy dissipation for a range of frequencies
[kmin,kmax] and a set of geometric parameters specified by r (disc radius),
hp (cavity height vector) and wp (cavity width vector).

global a  b l X Y d R1 R2 R3 R4 R5 L LNN Alpha Beta W1 W2 W3 W4 N Nc k0 Vmin;
%% Declare global variables for this program
hp =(1:0.2:4); %% cavity height range
wp =(1:0.2:4); %% cavity width range

%% Structure m stores the energy dissipation for each k, hp and wp.
r=0.5;a=16; l=0.1;  Beta=pi; kmin=pi/2;kmax=pi;kp=300;
m =struct('KValues',{},'Energy',{});
 for i=1:length(hp )
     for j=1:length(wp )
         [m(i,j).KValues m(i,j).Energy] =EnergyDissipation(hp (i),hp
(i),wp(j),r,c1,c2,kmin,kmax,kp);
     end
 end
%%
save('m.mat','m','a','l','hp','wp','r','b','kmin','kmax','kp')

%% For each geometry select and display the minimum energy dissipation index
and the correspondent frequency

EnMin=zeros(length(hp),length(wp));
 for i=1:length(hp)
     for j=1:length(wp)
         if isempty(m(i,j).Energy)==1
             EnMin(i,j)=1;
         else
            EnMin(i,j)=min(m(i,j).Energy);
         end
     end
 end
 [ind, e]=min(EnMin);
 %%
index1=1   ;  %
index2=1   ;
h= hp(index1)
w=wp(index2)
[W1 W2 W3 W4 N Nc L LNN Alpha Xc Yc X Y d WX WY]=fBoundary(h,h,w ,r,0,0 );
R1=R(-1); R2=R(-0.5);R3=R(0);  R4=R(0.5);R5=R(1);
 M0=real(M(k0));
           [V0 lambda0]=eig(M0); Lambda=abs(lambda0);
           T= diag(Lambda); [Emin,IndT]=min(T);
           Vmin=V0(:,IndT);
ft=@Phi;
%%
[xp,vp]=VPhi(-(a/2)+0.2,(a/2)-0.2,-0.7,100);figure, plot(xp,vp),grid on
%%  Display trapped mode signature
```

```
        b12=b1(Nc+1:N);
        b111=circshift(b11,[0,1]);
        b112=circshift(b12,[0,1]);

      f2=[b111,b112];
    end

 %  C:COEFFICIENTS OF dPhi/dn =q(j)

    function  f3=fC(x,y)
         f3=   L'.*(((-1i)/48)* (((besselh(0,1, k0*Rad(x,y,-1))) +
(3*(besselh(0,1, k0*Rad(x,y,-0.5)))) + (besselh(0,1, k0*Rad(x,y,0))) +
(besselh(0,1, k0*Rad(x,y,0.5))))));

                % Disc - Neumann condition:
                  f3(1:Nc)=0;

                  f3(W2)=0;
                  f3(W4)=0;


                f3(((W2)+1):((W3)-1))=(- sqrt(Beta^2-
(k0^2)))*f3(((W2)+1):((W3)-1));
                f3(((W4)+1):N)=(- sqrt(Beta^2-(k0^2)))*f3(((W4)+1):N);

        end

 %  D:COEFFICIENTS OF dPhi/dn =q(j+1)
    function f4=fD(x,y)
        fd = L'.*(((-1i)/48)* (((besselh(0,1, k0*Rad(x,y,-0.5))) +
(besselh(0,1, k0*Rad(x,y,0))) + (3*(besselh(0,1, k0*Rad(x,y,0.5)))) +
(besselh(0,1, k0*Rad(x,y,1))))));

                    fd(1:Nc)=0;

                    fd(((W3)-1))=0;
                    fd(N)=0;


                    fd(W2:((W3)-2))=(-sqrt(Beta^2-(k0^2)))* fd(W2:((W3)-2));
                    fd(W4:(N-1))=(-sqrt(Beta^2-(k0^2)))* fd(W4:(N-1));


            %   Dij's are coefficients to Phi(j+1) so need to shift around
each boundary:
                    fd1=fd(1:Nc);
                    fd2=fd((Nc+1):N);

                    fd11=circshift(fd1,[0,1]);
                    fd12=circshift(fd2,[0,1]);

                    f4=[fd11,fd12];
```

```
    end

%

            end
end
 %   END OF ENERGY DISSIPATION FUNCTION


function Potential=Phi(x,y)
%   CALCULATES THE POTENTIAL PHI AT AN INTERNAL ARBITRARY POINT x IN THE
DOMAIN
%   Rad is the distance from the arbitrary point x to points on the
%   boundary elments
%   As the point is in the interior of the domain, not on the boundary,
%   there are no singularities

global  W1 W2 W3 W4   L N Nc  Beta k0 Vmin ; % V0 is the eigenvector
corresponding to lambda0, it is in the nullspace of M(k0). See Phi1 for
solutions with eigenvector for k1
Potential =  real(sum(Vmin'.* ((fA(x,y)+fB(x,y))-(fC(x,y) + fD(x,y)))));

%   A:- COEFFICIENTS of Phi(j)
    function f1=fA(x,y)
            f1=(dfun(x,y)).*(((k0*(1i/48))* (((besselh(1,1, k0*Rad(x,y,-
1))).(Rad(x,y,-1))) +(3*((besselh(1,1, k0*Rad(x,y,-0.5))).(Rad(x,y,-
0.5))))+((besselh(1,1, k0*Rad(x,y,0))).(Rad(x,y,0)))+((besselh(1,1,
k0*Rad(x,y,0.5))).(Rad(x,y,0.5))))));
            f1(W1:W2)=0;

            f1(W3:W4)=0;
    end


%   B:COEFFICIENTS of Phi(j+1)

    function f2=fB(x,y)
      b1=(dfun(x,y)).*(((k0*(1i/48))* (((besselh(1,1, k0*Rad(x,y,-
0.5))).(Rad(x,y,-0.5))) +((besselh(1,1,
k0*Rad(x,y,0))).(Rad(x,y,0)))+(3*((besselh(1,1,
k0*Rad(x,y,0.5))).(Rad(x,y,0.5))))+((besselh(1,1,
k0*Rad(x,y,1))).(Rad(x,y,1))))));

        ind=find(isnan(b1));
        b1(ind)=0;

        b1(W1:((W2)-1))=0;
        b1(N)=0;
        b1(((W3)-1):((W4)-1))=0;

        b11=b1(1:Nc);
        b12=b1(Nc+1:N);
        b111=circshift(b11,[0,1]);
        b112=circshift(b12,[0,1]);
```

```
      f2=[b111,b112];

    end


 %  C:COEFFICIENTS OF dPhi/dn =q(j)
    function  f3=fC(x,y)
         f3=   L'.*(((-1i)/48)* (((besselh(0,1, k0*Rad(x,y,-1))) +
(3*(besselh(0,1, k0*Rad(x,y,-0.5)))) + (besselh(0,1, k0*Rad(x,y,0))) +
(besselh(0,1, k0*Rad(x,y,0.5))))));
                % Disc - Neumann condition:
                  f3(1:Nc)=0;
                  f3(W2)=0;
                  f3(W4)=0;
                f3(((W2)+1):((W3)-1))=(- sqrt(Beta^2-
(k0^2)))*f3(((W2)+1):((W3)-1));
                f3(((W4)+1):N)=(- sqrt(Beta^2-(k0^2)))*f3(((W4)+1):N);

        end
%  D:COEFFICIENTS OF dPhi/dn =q(j+1)

    function f4=fD(x,y)
        fd = L'.*(((-1i)/48)* (((besselh(0,1, k0*Rad(x,y,-0.5))) +
(besselh(0,1, k0*Rad(x,y,0))) + (3*(besselh(0,1, k0*Rad(x,y,0.5)))) +
(besselh(0,1, k0*Rad(x,y,1))))));

                    fd(1:Nc)=0;
                    fd(((W3)-1))=0;
                    fd(N)=0;
                    fd(W2:((W3)-2))=(-sqrt(Beta^2-(k0^2)))* fd(W2:((W3)-2));
                    fd(W4:(N-1))=(-sqrt(Beta^2-(k0^2)))* fd(W4:(N-1));

%   Dij's are coefficients to Phi(j+1) so need to shift around each boundary:
                    fd1=fd(1:Nc);
                    fd2=fd((Nc+1):N);

                    fd11=circshift(fd1,[0,1]);
                    fd12=circshift(fd2,[0,1]);

                    f4=[fd11,fd12];

    end

end

function  R =R(z)
 %   Function used to calculate elements with local coordinates
   global N Nc X Y;
   R=zeros(N,N);


for i =1:N
```

```
    for j=1:N
        if (j==Nc)
          R(i,j)=sqrt (((X(j)*(0.5*(1-z))+X(1)*(0.5*(1+z))-X(i))^2) +
((Y(j)*(0.5*(1-z))+Y(1)*(0.5*(1+z))-Y(i))^2) );
         elseif (j==N)
              R(i,j)= sqrt (((X(j)*(0.5*(1-z))+X(Nc+1)*(0.5*(1+z))-X(i))^2) +
((Y(j)*(0.5*(1-z))+Y(Nc+1)*(0.5*(1+z))-Y(i))^2));
          else
             R(i,j)= sqrt (((X(j)*(0.5*(1-z))+X(j+1)*(0.5*(1+z))-X(i))^2) +
((Y(j)*(0.5*(1-z))+Y(j+1)*(0.5*(1+z))-Y(i))^2));
        end
    end
end
```